Topological phases of periodically driven crystals

Michel Fruchart

Numéro National de Thèse : 2016LYSEN025

THÈSE de DOCTORAT DE L'UNIVERSITÉ DE LYON
opérée par
l'École Normale Supérieure de Lyon

École Doctorale N°52
Physique et Astrophysique de Lyon
Discipline : physique

Soutenue publiquement le cinq octobre 2016 par

Michel FRUCHART

Topological phases of periodically driven crystals

Phases topologiques dans les cristaux soumis à un forçage périodique

Devant le jury composé de :

Jean Dalibard, Professeur, Collège de France	Examinateur
Benoît Douçot, Directeur de recherche, LPTHE	Examinateur
Mark O. Goerbig, Directeur de recherche, LPS Orsay	Rapporteur
Karyn Le Hur, Directrice de recherche, CPHT	Examinateur
Gianluca Panati, Professeur, Università di Roma	Examinateur
Mark S. Rudner, Professeur, Niels Bohr Institute	Rapporteur
David Carpentier, Directeur de recherche, LPENSL	Directeur de thèse
Krzysztof Gawędzki, Directeur de recherche, LPENSL	Codirecteur de thèse

Chapter 1

Introduction

1 General introduction

The study of physical phenomena usually involves local observables or correlations between local quantities. In some instances however, certain "global" quantities which do not depend on the details of the local description are required. In solid state physics, topological tools were first used to study defects in an ordered phase [Mer79]. Such an ordered phase of matter is characterized by an order parameter, and topological defects appear as particular configurations of the order parameter field with singularities. As an example, consider a two-dimensional film of superfluid ^{4}He, which is described by a complex order parameter field $\psi(x) = \psi_0(x)\,\mathrm{e}^{\mathrm{i}\theta(x)}$ characterizing the breaking of $U(1)$ symmetry. An example of defect associated with such a $U(1)$ order parameter in two dimensions is a vortex, where the order parameter ψ vanishes. The circulation around this defect is an integer called the topological charge of the vortex. It measures how many time the phase $\theta(x)$ winds along a curve surrounding the vortex. The topological charge is not sensitive to the precise configuration of the order parameter field: it is left invariant by smooth modifications of the order parameter field inside the region encircled by the curve. This is the reason why it is referred to as a topological quantity.

In general, topology is concerned with global properties which are invariant under a certain kind of transformations, like smooth deformations. Such global properties may distinguish objects which look locally similar, or gather objects which look different at first sight. The usual example of such a global property is the number of holes (or *genus* g) of a two-dimensional surface (see figures 1.1 and 1.2). For example, a sphere has no hole, whereas a torus has one hole: it is not possible to smoothly deform a sphere into a torus. To make the notion of topologically equivalent objects precise, it is necessary to specify what are the allowed transformations: for the sake of this introduction, we will only rely on an intuitive picture. Imagine that objects are made of modeling clay: allowed transformations consist in deforming the clay without drastic modification like tearing it or gluing two parts together. Hence, a coffee cup has a handle, so it corresponds to a genus 1 surface, which can be deformed into a torus without such drastic modification. This topological classification explains, for example, why a genus 1 donut tastes different than a genus 3 pretzel.

The topological character of vortices provides them with a robustness (against smooth deformations of the configuration of the order parameter) which allows to

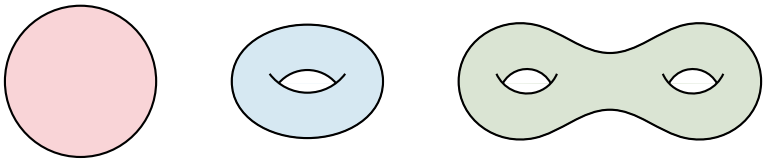

Figure 1.1: Genus of some 2D surfaces. The genus g of a closed 2D surface essentially counts the number of "holes" or "handles" in the surface. A sphere has no hole (genus 0), a torus has one hole (genus 1), and so on. If fact, any orientable closed surface (two-dimensional manifold) is homeomorphic to a connected sum of g tori. It is related to the Euler characteristic of the surface $\chi = 2 - 2g$, an homological invariant which can be computed as the integrated local curvature through the Chern-Gauss-Bonnet theorem.

treat them as independent objects, behaving similarly to electric charges: as one would expect, two vortices with opposite topological charges can annihilate when they meet, and a vortex with charge $+2$ can break down into two vortices with charge $+1$, and so on, leading to a very fruitful analogy. In the case of defects, topological methods are used to characterize different configurations of a given ordered phase. It happens that topology may also serve a completely different purpose and distinguish different phases of matter in a situation where their symmetries are the same and no order parameter can be used to differentiate between them. This is the case of topological phases of matter like the quantum Hall effect, that we shall discuss in the next section.

1.1 The quantum Hall effect

We wish to focus on a particular application of topology in condensed matter, which started with the discovery of the quantum Hall effect by von Klitzing, Dorda and Pepper [KDP80] in 1980, the topological nature of which was soon recognized by TKNN (Thouless, Kohmoto, Nightingale and den Nijs) [TKNN82] and Avron, Seiler and Simon [ASS83; Sim83]. This discovery opened a new field in condensed matter and beyond. The interest in the quantum Hall effect comes from multiple points of view. First, there is a fundamental interest, both from theoreticians and experimentalists. The integer quantum Hall effect is the first example of a phase of matter escaping the Landau paradigm, as it is not associated with a local order parameter. Moreover, it is described by a beautiful theory which connects relatively modern mathematical constructs to experimentally realizable situations. Third, there is a practical interest from metrology, as the integer quantum Hall effect (IQHE) provides an extremely precise and reproducible measure of the fundamental constant e^2/h, with a relative uncertainty lower than 10^{-9}, which is used as an electrical resistance standard [WK11; JJ06]. Besides, the IQHE and its derivatives (like the fractional quantum Hall effect) are now used as a platform for the fundamental study of quantum mechanics (in particular of the decoherence) in the field of electronic quantum optics [BFPB13] and to develop quantum computation [Kit03; NSSF08; JOPS10].

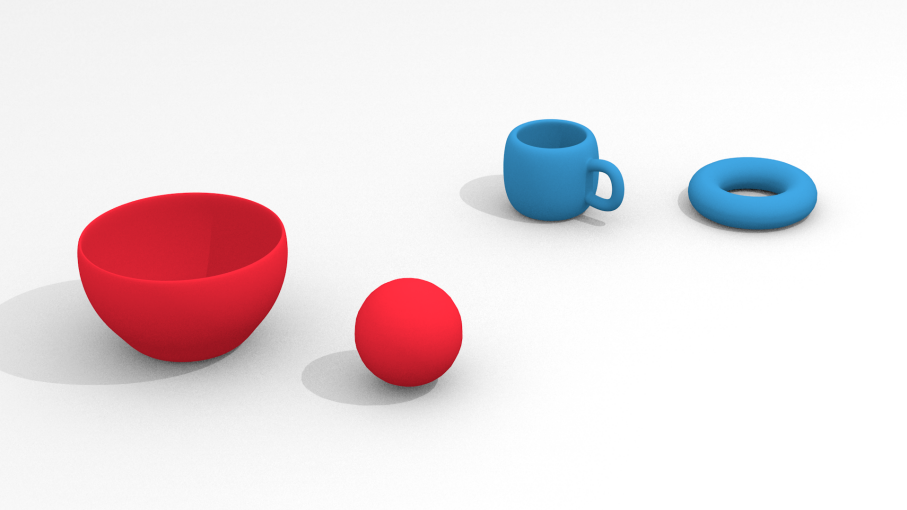

Figure 1.2: Topology of 2D surfaces. A bowl and a sphere have genus $g = 0$. A coffee cup and a torus have genus $g = 1$.

First, we shall review the "classical" Hall effect. When a two-dimensional electron gas is submitted to a transverse magnetic field B, the in-plane current density J and electric field E are related in linear response by

$$J_\mu = \sigma_{\mu\nu} E_\nu \tag{1.1}$$

where σ is the 2×2 conductivity tensor. Within the semiclassical Drude theory (see e.g. [Pot07])

$$\sigma = \frac{\sigma_0}{1 + (\omega_c \tau)^2} \begin{pmatrix} 1 & \omega_c \tau \\ -\omega_c \tau & 1 \end{pmatrix} \tag{1.2}$$

where

$$\sigma_0 = \frac{n e^2 \tau}{m^*} \tag{1.3}$$

is the conductivity at zero magnetic field,

$$\omega_c = \frac{eB}{m^*} \tag{1.4}$$

is the cyclotron pulsation, proportional to the magnetic field, n is the electron density, τ is a relaxation time (a characteristic time for the relaxation to equilibrium, essentially due to collision processes), m^* the effective mass of the electrons and e the fundamental charge. When the magnetic field is strong enough or the relaxation time is large enough so that $\omega_c \tau \gg 1$, the diagonal components σ_{xx} and σ_{yy} can be neglected with respect to the antidiagonal components $\sigma_{xy} = -\sigma_{yx}$; in this case, the Hall conductance can be approximated as $\sigma_{xy} = \frac{e^2}{h} \nu$ where we have defined the dimensionless parameter $\nu = hn/eB$. Experimentally, the different components of the conductivity tensor are usually probed in a Hall bar setup, see figure 1.3, which enables to escape issues due to contact resistances and to probe both the longitudinal and

Hall conductances (in two dimensions, conductances and conductivities are related through a dimensionless geometric factor (when the conductivity tensor is uniform in the sample), which is in fact 1 in the case of the Hall conductance [Goe11]).

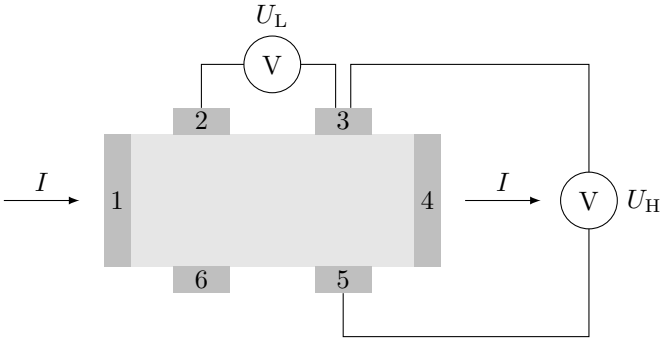

Figure 1.3: Hall bar setup. In the Hall bar setup, a current I is driven through the sample by terminals 1 and 4. In the meantime, the longitudinal tension U_L between e.g. leads 2 and 3 is measured, as well as the transverse tension U_H between e.g. leads 3 and 5. The longitudinal and Hall resistances are obtained by $R_\mathrm{L} = U_\mathrm{L}/I$ and $R_\mathrm{H} = U_\mathrm{H}/I$.

A surprising behavior, called the quantum Hall effect, happens when a weakly disordered electron gas is put in a high magnetic field at low temperature (when $\hbar\omega_\mathrm{c} \gg k_\mathrm{B}T$): in 1980, von Klitzing, Dorda and Pepper [KDP80] observed that the Hall conductance σ_{xy} against the inverse magnetic field $1/B$ displays plateaus, where the value of σ_{xy} is quantized with an extremely high precision to integer multiples of e^2/h, i.e.

$$\sigma_{xy} = \frac{e^2}{h}\,\tilde{\nu} \qquad \text{with } \tilde{\nu} \in \mathbb{Z}. \tag{1.5}$$

The integer $\tilde{\nu}$ is the quantity $\nu = hn/eB$ rounded to the nearest integer, and the Hall conductance σ_{xy} jumps from one plateau to another. The transitions between plateaus are accompanied by a peak in the longitudinal conductance σ_{xx}, which vanishes otherwise, as represented on figure 1.4. Experimentally, it is usual to measure the Hall resistivity ρ_{xy} as well as the longitudinal resistivity ρ_{xx}, components of the resistivity tensor $\rho = \sigma^{-1}$. This is for example the case in figure 1.5. To connect both points of view, notice that as long as σ_{xy} is nonvanishing (so when $B \neq 0$), $\rho_{xx} = 0$ iff $\sigma_{xx} = 0$. Moreover, when σ_{xx} (or ρ_{xx}) vanishes, then $\rho_{xy} = -1/\sigma_{xy}$ so whenever one is quantized, the other is too. The quantized value of σ_{xy} is a universal property: it is not altered by the precise geometry of the system, nor by the impurities and disorder, and it is the same, to great precision, in various systems like semiconductor-oxide interface in MOSFET, semiconductor heterojunctions, or graphene. This universality and this invariance against perturbations are a clue that the quantized Hall conductance may be related to a topological invariant. It turns out that it is indeed the case, and that the quantity $\tilde{\nu}$ is a topological invariant of the ground state of the system, the "first Chern number associated to the Fermi projector" (see chapter 2).

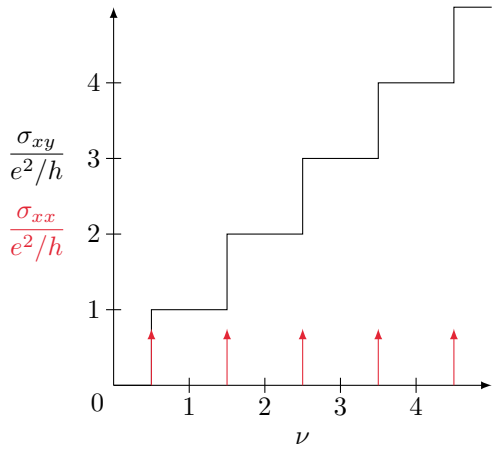

Figure 1.4: Simplified view of the quantum Hall effect. In an idealized picture, there are quantized plateaus of Hall conductance around integer values $\tilde{\nu} \in \mathbb{Z}$ of the dimensionless $\nu = hn/eB$, on which the Hall conductance is equal to $\tilde{\nu}e^2/h$. An abrupt transition happens at half-integer values of ν. The longitudinal conductivity vanishes, except at the transitions between plateaus, where it takes very large values.

To describe the two-dimensional electron gas where the IQHE takes places, a simplified description neglecting interactions between electrons is sufficient, so we focus on the one-particle description. The Landau Hamiltonian describing an two-dimensional electron in a constant magnetic field B is

$$H = \frac{1}{2m^*}(P + eA)^2 = \frac{1}{2m^*}\Pi^2 \tag{1.6}$$

where P is the momentum operator, A the vector potential and $\Pi = P + eA$. It can be written as an harmonic oscillator Hamiltonian

$$H = \hbar\omega_c \left(a^\dagger a + \frac{1}{2}\right) \quad \text{where} \quad a^\dagger = \frac{1}{\sqrt{2\hbar eB}}\left(\Pi_x + \mathrm{i}\Pi_y\right) \tag{1.7}$$

with $[a, a^\dagger] = \mathrm{Id}$. Its spectrum is therefore

$$E_n = \hbar\omega_c \left(n + \frac{1}{2}\right). \tag{1.8}$$

Each energy E_n is strongly degenerate, as there are $N_A = A/(2\pi\ell_B^2)$ states with energy E_n in an area A, where $\ell_B = \sqrt{\hbar/eB}$ is the magnetic length. The set of all degenerate states with energy E_n is called the nth Landau level, or nth Landau band when it is broadened by disorder.

Landau levels are in several ways similar to energy bands in an insulating crystal. They are separated from each other by energy gaps, and contain a large number of states. In a system with disorder, it is possible to set the chemical potential in a gap between Landau levels: in this situation, the system resembles a band insulator.

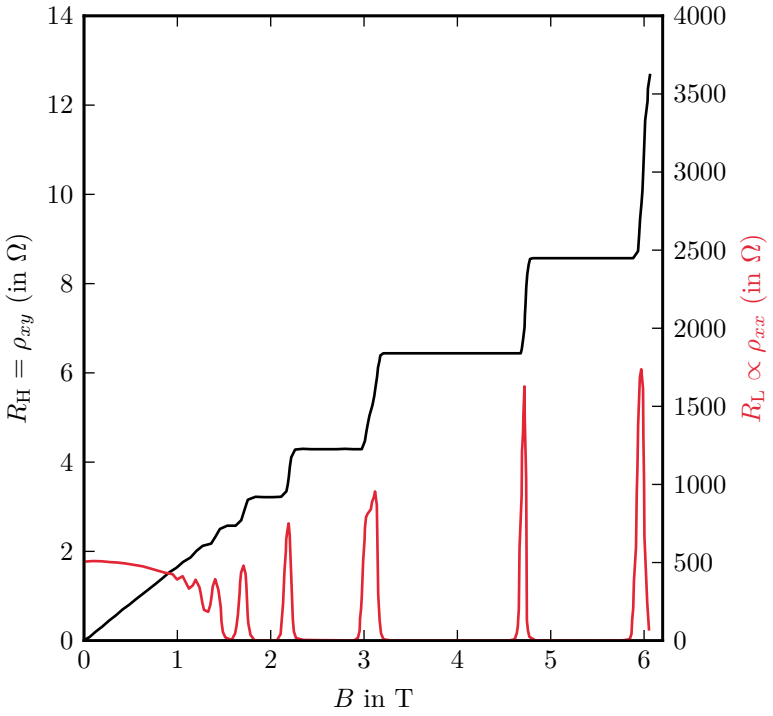

Figure 1.5: Hall and longitudinal resistances in the quantum Hall effect. Experimental curves of the Hall resistance (in black) and of the longitudinal resistance (in red) in a GaAs-AlGaAs heterostructure as a function of the magnetic field, at 8 mK. Adapted from [Kli86].

However, this insulator has peculiar properties, which may be illustrated in a semi-classical picture (see figure 1.6): in a strong enough magnetic field, states in a Landau level drift along equipotential lines of the confinement and disorder potentials. In the bulk, the system is an insulator: an electron is confined to a closed orbit and cannot carry current. However, at the edge, electrons may move along the interface, which leads to a global motion. In other words, at the boundary, the confinement potential bends the otherwise flat Landau bands, so the Landau levels that are below the chemical potential in the bulk are forced to cross it near the edge. There are conducting states confined near to the boundary of the sample: the unidirectional edge states. The boundary of the system is therefore a one-dimensional metal. The edge modes are chiral (or unidirectional): for example, they may go from the left to the right, but not the other way around. This chiral behavior may be understood semi-classically as stemming from skipping cyclotron orbits near the edge [Büt88a] (see figure 1.6). As a consequence, there are no available states to backscatter to, even in presence of impurities: the edge states may be deformed in presence of a rough edge or impurities, but will still move in the same direction without dissipation. The

existence of such robust chiral edge states can be tracked down as stemming from the nontrivial topology of the states in the bulk. An energy band is a well-defined object, described by a set of dispersion relations and the corresponding eigenstates (or if we only keep essential informations, by an energy range and a spectral projector, as we will see later). As such, it can have a nontrivial topology, encoded in the eigenstates. In the same way as closed surfaces have a certain number g of holes, an energy band may have nontrivial topological properties, encoded (in this case) in their first Chern number C_1. A trivial band, e.g. obtained in a tight-binding model with vanishing tunneling terms, has Chern number zero. This is also the case of the energy bands of usual materials, like air of vacuum. In contrast, a Landau band has a nonzero Chern number. This topological property is preserved as long as a band is well-defined, that is to say, separated from all other bands. When a gap closes and two bands touch each other, they can exchange their topological properties; for example, two (sub)bands with opposite Chern numbers can be transformed into two trivial bands when they touch (so the total Chern number of the two bands is conserved). Otherwise, the topological properties of bands are robust to perturbations. In particular, this explains the robustness of the "topologically protected" edge states. The number of edge states is given by the number of Landau bands under the Fermi level, an observation which can be generalized as follows: the number of edge states is equal to the total Chern number of the band(s) below the Fermi level. In transport measurements, the Hall current is carried by the edge states, each of which happens to contribute as e^2/h to the Hall conductance [Büt88a], which means that $\tilde{\nu} = C_1$ in equation (1.5); the topological nature of this quantity explains the extremely precise quantization of the Hall plateaus. (I refer the reader to standard reviews [PKG90; DP08; CJOD99; Goe11; DPR06] for more details on the IQHE.)

The quantum Hall effect is the first example of a more general family of phenomena called *topological insulators*, a key feature of which is the appearance of *topologically protected edge states* at their boundaries due to the existence of a nontrivial topology of the bulk bands. This general principle is called the bulk-boundary correspondence: whenever the bulk is nontrivial, topologically protected edge states appear at the boundary of a finite sample, and conversely, topologically protected edge states are due to a nontrivial topology of bulk bands[(1)].

A disordered electron gas under a strong magnetic field has the disadvantage of not being easily cast into the framework of Bloch theory. On the one hand, the magnetic field requires to consider a supercell (for rational values on the dimensionless magnetic flux), which depends on the magnitude of the field; in a very strong magnetic field, this leads to the beautiful but complex physics of the Harper-Hofstadter butterfly [Har55; Hof76]. On the other hand, a disordered system lacks translation invariance and can therefore not be described within Bloch theory, yet disorder plays a essential role in the quantum Hall effect: the quantum mechanics of a two-dimensional electron gas under strong magnetic field without any disorder leads to a completely standard classical Hall effect. A coherent understanding of the topological nature of the quantum Hall

[(1)] In fact, when a symmetry is necessary to define the bulk invariant (see later), and in the right space dimension, it may be possible to have a gapped boundary instead of a gapless boundary provided the symmetry is broken at the interface, a situation first recognized by Ezawa, Tanaka and Nagaosa [ETN13].

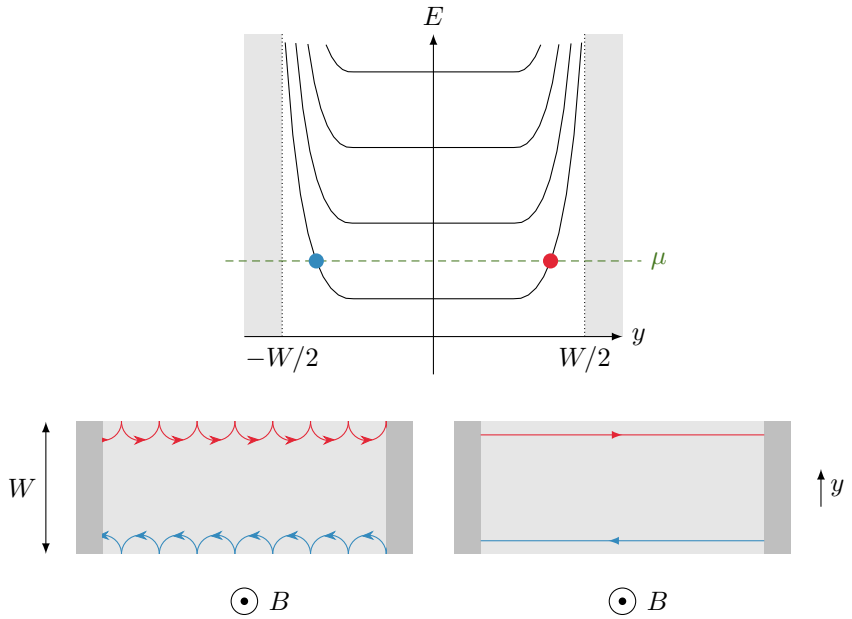

Figure 1.6: Skipping orbits and edge state picture. A finite sample may be modeled by a confinement potential which bends the Landau level near the boundary (here at $y = \pm W/2$). As a consequence, even if the system is a bulk insulator with a chemical potential fixed between two Landau levels, there will be metallic states crossing the chemical potential near the boundary (in blue and red), corresponding to edge states. Such edge states may be pictorially represented as cyclotron orbits bouncing on the interfaces, which induces a chiral motion. The resulting chiral edge states, which are a common property of IQHE and Chern (Bloch) insulators, are represented in the rightmost picture.

effect requires to take into account disorder from the beginning, and defining the topological invariants requires the framework of noncommutative geometry [BEB94], a beautiful but conceptually and technically advanced tool. It is however possible to understand key features of IQHE (and more generally of topological insulators) in the framework of band theory. Haldane [Hal88] was the first to discover an example of a model implemented on a lattice, without net magnetic field (so that the full lattice periodicity is retained, and Bloch theory is applicable), which exhibit the same topological properties as the quantum Hall effect. Such systems, now called Chern insulators, are easier to study theoretically, an advantage which has allowed a series of extensions, among which

– the inclusion of symmetries in the description: symmetries add constraints which allow for different topological properties;
– the extension to other domains of physics: it was recognized that there may be analogues of the quantum Hall effect in ^{3}He as soon as 1988 by Volovik [Vol88a], then in photonic crystals by Haldane and Raghu [HR08; RH08] in 2005); now, it is understood that analogues of IQHE and of derivatives with other symmetries may

arise in all systems which support waves (optics, acoustics, mechanics, cold atoms, and so on);
– the possibility to induce topological properties through e.g. interactions [RQHZ08], dissipation [RL09; ZRPL15; DRBZ11; BBKR13; BD15; RLL16], or an external driving (see later).

This list does not aim at completeness, but highlights the three main directions that I believe are intersecting in this thesis.

The framework of topological Bloch band theory is the following: one associates to a translation-invariant system a Bloch Hamiltonian $H(k)$, where k is a reciprocal vector living on the Brillouin zone, which is in fact a torus as k is only defined modulo reciprocal lattice vectors. The spectrum of $H(k)$ provides a band structure described by energy levels $E_i(k)$, which may exhibit spectral gaps. In this case, a spectral projector family $P(k)$ describes the eigenstates of the band between two gaps. For example, a two-by-two Bloch Hamiltonian has eigenstates $\psi_\pm(k)$ with energies $E_\pm(k)$; if $E_+(k) > \mu > E_-(k)$, we define $P_\pm(k) = |\psi_\pm(k)\rangle\langle\psi_\pm(k)|$. It is possible to associate topological invariants (like the first Chern number) to the projector family P which do not change even if H is modified as long as the gap does not close.

Now, let us consider a boundary between two topologically inequivalent insulators: the system is trivial on the left of the boundary whereas it is nontrivial on the right. Away from the boundary, the system is not aware of the existence of an interface, so it is a bulk insulator which can be describe as if it were infinite, and (topological) Bloch theory can be applied. Near the boundary, this description may break down, but let us accept to use a position-dependent Bloch Hamiltonian, parametrized by the distance to the interface: in order to pass from a trivial to a nontrivial insulator, there must be a position near the interface where the gap closes (so the topological invariants cannot be defined), leading to metallic edges. It is possible to make this description partially rigorous through the use of Green functions, a method pioneered by Volovik [Vol88a] and significantly expanded by Gurarie and Essin [Gur11; EG11]. This method was also extended [RLBL13; NR15] to the case of periodically driven (Floquet) topological phases.

1.2 Symmetries and topological insulators

The study of quantum Hall effects was an established subfield of condensed matter when a breakthrough was achieved by Kane and Mele in 2005 [KM05a; KM05b]. They proposed a "time-reversal invariant version" of the IQHE (breaking time-reversal invariance is a crucial ingredient of IQHE/Chern insulators), which they called "quantum spin Hall effect" (QSHE). Here, the crucial ingredients appear to be a band inversion near a symmetric point of the Brillouin zone and a strong spin-orbit coupling, which effectively generate a momentum- and spin-dependent magnetic field. A year later, Bernevig, Hughes and Zhang [BHZ06] proposed an experimental realization in HgTe-CdTe quantum wells, which was experimentally achieved the following year by König and collaborators [KWBR07], in Molenkamp group (see figure 1.7). It was discovered by Fu, Kane and Mele [FKM07], Roy [Roy09], Moore and Balents [MB07], that the time-reversal invariant topological insulator or QSHE has an equivalent in three dimensions, which was soon to be experimentally observed in $Bi_{1-x}Sb_x$ by

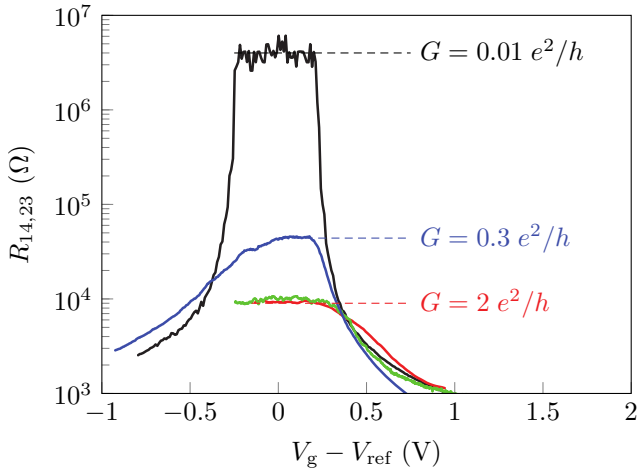

Figure 1.7: Transport signature of topological edge states in the QSHE in HgTe quantum wells. Longitudinal four-terminal resistance $R_{14,23}$ with respect to the gate voltage $V_g - V_{ref}$ in a trivial (black curve) and in topological (red, green and blue curves) HgTe-CdTe quantum well, at 30 mK. In the topological situation (when there is a band inversion), $R_{14,23}$ reaches a quantized value of 2 e^2/h, as expected from the Landauer-Büttiker formalism applied to the edge state transport (except in the blue curve, corresponding to a larger sample where the conductance is reduced by inelastic processes causing backscattering). In the trivial situation (black curve), the resistance is very high in the gap, which is the expected behavior of a conventional insulator. Adapted from [KWBR07]. Reprinted with permission from AAAS.

Hsieh and collaborators [HQWX08] in Hasan group with angle-resolved photoemission spectroscopy (ARPES) measurements. They observed the signature of surface states: a Dirac dispersion relation of surface electrons for energies in the bulk gap of the material, as predicted by the topological band theory. Several other materials with a nontrivial 3D Kane-Mele topology were subsequently discovered, among which Bi_2Se_3; we reproduce in figure 1.8 an experimental ARPES spectrum of the topological surface states of this material from [XQHW09].

In a time-reversal invariant (TRI) electronic system, it is not possible to have a nontrivial Chern insulator. Time-reversal is represented as an antiunitary operator Θ, with $\Theta^2 = -\mathrm{Id}$ for particles with half-integer spin. In a time-reversal invariant system, the Bloch Hamiltonian respects $\Theta H(k)\Theta^{-1} = H(-k)$, so any eigenstate $\psi(k)$ of $H(k)$, has a *Kramers partner* $\Theta\psi(k)$ which is an eigenstate of $H(-k)$. The contribution of Kramers partners in the Chern insulator topology are opposite and cancel out. As was shown by Kane and Mele, however, it is possible to somehow overcome this cancellation by defining a finer invariant, characterizing the topology of TRI systems. The simplest way to understand the Kane-Mele topology is probably through its most striking physical consequence, in terms of edge states. While Chern insulators have characteristic chiral edge states on the boundary, Kane-Mele insulators exhibit helical edge states, which are essentially a Kramers pair of chiral edge states with

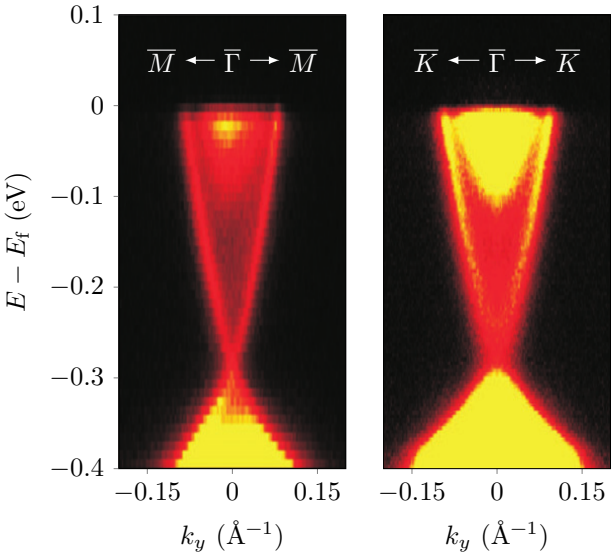

Figure 1.8: ARPES signature of topological surface states in Bi_2Se_3. ARPES spectrum of 2D surface electronic band dispersion of the three-dimensional time-reversal invariant topological insulator Bi_2Se_3 (111) near the Γ point, along the $\overline{\Gamma} - \overline{M}$ (left) and $\overline{\Gamma} - \overline{K}$ (right) cuts of the surface Brillouin zone. This data proves the existence of surface states with linear dispersion in the bulk gap of Bi_2Se_3. Adapted from [XQHW09]. Reprinted by permission from Macmillan Publishers Ltd, Nature Physics, copyright 2009.

opposite chiralities (see figure 1.9). As the counter-propagating edge states form a Kramers pair, backscattering from an edge state to its counter-propagating partner is not allowed. As long as time-reversal invariance (with $\Theta^2 = -\mathrm{Id}$) is not broken, in space dimensions $d = 2$ and 3, a topological quantity called the *Kane-Mele invariant* $\mathrm{KM} \in \mathbb{Z}_2$ (associated to the valence band) can be defined. In terms of the edge states, it means that one Kramers pair of edge state is topologically distinct from no edge state, but that two Kramers pairs of edge states are topologically equivalent to no edge state, as backscattering is allowed in this case (this is why $\mathrm{KM} \in \mathbb{Z}_2$). In fact, the Kane-Mele invariant can be defined without starting from a situation where spin is conserved, and it is even possible to conceive a toy model with only spin-non-conserving terms which is time-reversal invariant and topologically nontrivial from the point of view of Kane-Mele topology.

A particular example may be helpful to illustrate what happens: when spin is conserved, it is possible to associate first Chern numbers $C_{\uparrow\downarrow}$ to each spin species. In a time-reversal invariant system, $C_\uparrow = -C_\downarrow$. When $C_\uparrow = -C_\downarrow = 1$, a Chern insulating phase occurs for each spin species, giving rise in a finite sample to a Kramers pair of a right-handed edge state with spin up associated to a left-moving edge state with

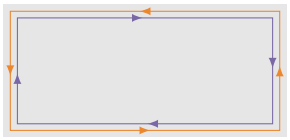

Figure 1.9: Edge states of a Kane-Mele insulator. In a Kane-Mele insulator (also called QSHE state), there are two counter-propagating helical edge states which form a Kramers pair on each interface. As a consequence, backscattering from an edge state to its counter-propagating partner is not allowed.

spin down. In this situation, the Kane-Mele invariant simplifies into

$$\mathrm{KM} = \frac{C_\uparrow - C_\downarrow}{2} \text{ mod. } 2 = C_\uparrow \text{ mod. } 2. \tag{1.9}$$

If we start from this situation and turn on time-reversal invariant spin-flip perturbations, spin is no more conserved. Hence, neither $C_\uparrow$ nor $C_\downarrow$ remain well-defined. However, the Kane-Mele invariant KM remains well-defined and does not change as long as the gap separating the valence band from the conduction band remains open (and time-reversal invariance is preserved).

Kane and Mele discovery (along with the discovery of graphene in 2004) focused the attention of the condensed matter community on topological physics, and a huge volume of results have been produced (or rediscovered ...) since then (good reviews include [Lud15; CTSR15; HK10; QZ11; BLD16]). It was realized that (i) there are systems analogous to IQHE in other dimension than $d = 2$ and (ii) symmetries give rise to different/finer topological invariants, which led to express known phenomena such as domain walls in the Su-Schrieffer-Heeger model of polyacetylene [SSH79] or unpaired Majorana fermions in the Kitaev chain [Kit01] in the language of topological insulators, and to conceive and realize new kinds of topological insulators.

A milestone in the topic of topological phases was achieved by Schnyder, Ryu, Furusaki and Ludwig [SRFL08; SRFL09; RSFL10] and Kitaev [Kit09], who developed a classification of topological phases according to their non-spatial symmetries, leading to the so-called "periodic table of topological insulators". The main idea is that there are three fundamental symmetries which act only on the internal degrees of freedom (locally on space), which are time-reversal Θ, charge conjugation C (also called particle-hole symmetry) and chiral symmetry Γ (which is related to Θ and C by $\Gamma = \Theta C$ if they are defined, possibly up to a phase). Time-reversal and charge-conjugation Θ and C are antiunitary operators which can square to $+\mathrm{Id}$ or $-\mathrm{Id}$, whereas Γ is unitary (but is not a unitarily implemented symmetry as it anticommutes with the Hamiltonian). There are ten ways to combine all the possible symmetries of a one-particle Hamiltonian H, which are called *symmetry classes* (they were already discovered by Altland and Zirnbauer in the context of disordered systems [AZ97], and related to Cartan symmetric spaces). For example, the Hamiltonian may have no such symmetry at all: it is said to be in class A, and examples in two dimensions are the IQHE and Chern insulators. Another possibility is that H is time-reversal invariant with a time-reversal operator squaring to $-\mathrm{Id}$, but there are no charge conjugation symmetry and no chiral symmetry: then H is in class AII, this

is the case of Kane-Mele insulators. Different approaches were developed to obtain this classification: Schnyder, Ryu, Furusaki and Ludwig [SRFL08; SRFL09; RSFL10] used an approach based on the (lack of) Anderson localization of the low-energy Dirac edge states of a topological insulator, whereas the K-theoretic approach developed by Kitaev [Kit09] focuses on the classification of equivalent bulk Hamiltonians. The agreement of the results of both approaches is not a trivial fact, and is the core of bulk-boundary correspondence. Another point of view on this classification based on anomalies has emerged from the study of the electromagnetic response of the quantum Hall effect, and more generally of the study of gauge fields coupled to topological insulator [RML12]. Spatial/crystallographic symmetries (which are unitary realized) also constrain and enrich the possible topological properties, but in a less robust way: the bulk-boundary correspondence in this case is only valid for boundaries which are invariant under the relevant symmetry, at least on average. Despite a lot of activity, partially reviewed in [CTSR15] (see also the more recent papers [WL16; SSG15; DL16]) a full classification of these refined topological phases is, to the knowledge of the author, not yet achieved.

1.3 Topological phases outside solid-state physics

Linear waves propagating in a spatially periodic structure are described within Bloch theory by dispersion relations $\omega(k)$ which organize in a band structure, in analogy with electrons in a crystal. Hence, they can support topological invariants and host topological edge states in a finite sample, provided there may be phase interferences between the waves and the relevant phase structure can be engineered in the medium. As a nontrivial topology manifests itself in particular geometrical phase patterns, which are at the origin of edge states, this is is not a surprise: geometrical phases (Pancharatnam–Berry phases [Pan56; Ber84] and Hannay angles [Han85]) were known to appear in classical systems as well as in quantum systems [CJ04]. Such behavior was predicted (and often observed) in a variety of systems, including mechanical systems [PP09; BJKP11; KL13; CUV14; VUG14; PCV15; SH15; NKRV15], acoustic waves [YGSL15; KFMA15; FKA15; XMYS15], light and electromagnetic waves [HR08; RH08; WCJS09; HDLT11; KMTK12; FYF12; RZPL13; HMFM13; LJS14; MGFV16; CJNM16], optomechanical systems [PBSM15], cold atoms [JMDL14; ALSA14; AALB13; MSKB13], linear electrical circuits [NOSS15; AGJ15] and (bio)chemical reaction networks [MV16]. This set of investigations has a considerable importance, as it was understood (and confirmed experimentally) that the topological properties of a Bloch band structure and the corresponding edge states are essentially wave properties which may be found in all domains of physics, raising considerable interest in the domain, with fascinating fundamental discoveries as well as promising forthcoming applications.

1.3.1 Electromagnetic waves: photonic crystals in the optical and microwave domains

A fruitful analogy between optical and electronic systems [HL90; JJWM11] started to emerge in the '80s, especially after the conceptualization of the notion of photonic crystals [Yab87; Joh87], characterized by a photonic band structure which can have photonic band gaps, in analogy with electronic band structures. The main idea [JJWM11; NL14] is that the dynamical Maxwell equations can be cast to the form of a Schrödinger equation

$$\mathrm{i}\partial_t \psi = M\psi \tag{1.10}$$

where the Maxwell operator M and the electromagnetic field ψ are defined as

$$\psi = \begin{pmatrix} E \\ H \end{pmatrix} \qquad \text{and} \qquad M = \begin{pmatrix} \varepsilon & 0 \\ 0 & \mu \end{pmatrix}^{-1} \begin{pmatrix} 0 & \mathrm{i}\,\mathrm{curl} \\ -\mathrm{i}\,\mathrm{curl} & 0 \end{pmatrix}. \tag{1.11}$$

Here, E and H are, respectively, the mesoscopic electric and magnetic vector fields, ε and μ are, respectively, the local dielectric permittivity and magnetic permeability tensors, which describe the response of the material where the electromagnetic field propagates. They are assumed to be independent of time, but may vary in space. In bi-anisotropic and bi-isotropic materials like optically active media, the Maxwell operator also has diagonal components. In absence of sources, the two other Maxwell equations yield the constraints $\mathrm{div}(\mu H) = 0$ and $\mathrm{div}(\varepsilon E) = 0$. Squaring the Maxwell-Schrödinger equation leads to the second-order wave equation

$$(\partial_t^2 + M^2)\psi = 0 \tag{1.12}$$

where the evolutions of the electric and magnetic fields are decoupled. In a photonic crystal, the permittivity and permeability $\varepsilon(x)$ and $\mu(x)$ depend periodically on space. A Fourier transform can be applied to reduce the Maxwell operator M into a family of Bloch Maxwell operators $M(k)$, where k is the quasimomentum, the eigenvalues of which give the dispersion relation $\omega_n(k)$ of the photonic crystal.

Haldane and Raghu [HR08; RH08] realized in 2005 that it is be possible to induce topologically nontrivial bands in such a gapped photonic crystal if time-reversal symmetry is broken through Faraday rotation in a gyromagnetic medium where μ is not a symmetric tensor[(2)]. This idea was experimentally confirmed [WCJS09] by Wang, Chong, Joannopoulos and Soljačić, who observed unidirectional electromagnetic modes immune to backscattering. They used a lattice of ferrite rods with a radius of the order of the centimeter submitted to a magnetic field to realize a topologically nontrivial photonic crystal in the microwave regime. With scattering measurements using two antennas and a network analyzer, which basically sends and receives microwave light to measure the scattering matrix, they demonstrated the existence of non-reciprocal (or chiral) modes located near the edge, in agreement with theoretical predictions, see figures 1.11 and 1.10. By adding a metallic obstacle, they also showed the robustness of this topological chiral edge state.

[(2)] Usually, the permeability and permittivity are symmetric tensors. However, in an external magnetic field B_0, the tensors ϵ and μ may fail to be symmetric: in this case, the medium is said to be *gyrotropic*. The reversal of magnetic field transposes the tensors, as $\epsilon(-B_0) = \epsilon^T(B_0)$ and $\mu(-B_0) = \mu^T(B_0)$. When only μ (resp. ε) is concerned, the material is said to be *gyromagnetic* (resp. *gyroelectric*).

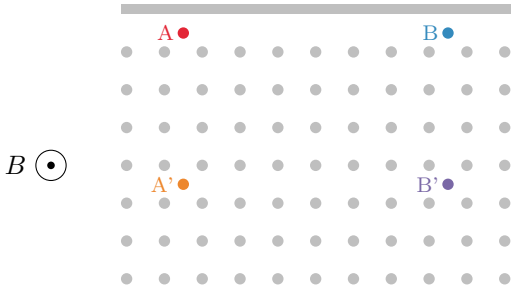

Figure 1.10: Photonic crystal with an edge and probe antennas. The photonic crystal used by [WCJS09] is composed of ferrimagnetic rods put in a magnetic field. An interface is realized by a metal wall, which plays the same role that an interface with vacuum in electronic systems (air or vacuum would allow radiation loss). Two antennas are used to measure the backward and forward transmissions of microwave light in the photonic crystal. Either the bulk (with antenna A' and B') or the edge (with antenna A and B) can be probed this way (see figure 1.11). This allowed Wang and collaborators [WCJS09] to demonstrate the existence of non-reciprocal (or chiral) modes located near the edge, in agreement with the theoretical predictions.

An important amount of theoretical and experimental investigations followed this work; a recent review is [LJS14]. From the fundamental point of view, the classification of photonic topological insulators was studied by De Nittis and Lein [NL14]. Microwave systems like the one used by Wang and collaborators were also employed to experimentally realize the merging of Dirac cones [BKMM13] and to observe weak topological effects [BKMM14] in artificial graphene. At microwave wavelength, a network analyzer allows to probe the phase structure of eigenstates, which is particularly interesting to probe topological phases. This kind of scattering experiment was carried out by Hu et al. [HPWP15] in a system of optical ring resonators [LC13] described as a Chalker-Coddington-like [CC88; HC96] directed scattering network [PC14; TD15].

Another branch of development of this field is particularly relevant here. For visible light, the gyrotropic effects are usually very small, so the extension of the method used by Wang et al. [WCJS09] seems to be experimentally challenging. A way to circumvent this difficulty was proposed and experimentally realized by Rechtsman and collaborators [RZPL13], who used helical waveguides arranged on an two-dimensional lattice to realize a two-dimensional Floquet topological insulator. In their setup, the spatial direction along which light propagates (along the waveguides) does not play the same role as the two orthogonal directions, so the system is better described by a specialization of the dynamical Maxwell equations. Such waveguides are obtained by illuminating a glass like silica with ultrashort laser pulses, which slightly modify the refraction index from its initial value n_0 to a spatially dependent $n_0 + \delta n(x)$. This allows to produce well-controlled waveguides for visible light. In the paraxial approximation where light essentially propagates along the waveguide axis z, the Helmholtz equation governing the spatial part ϕ of a monochromatic electromagnetic

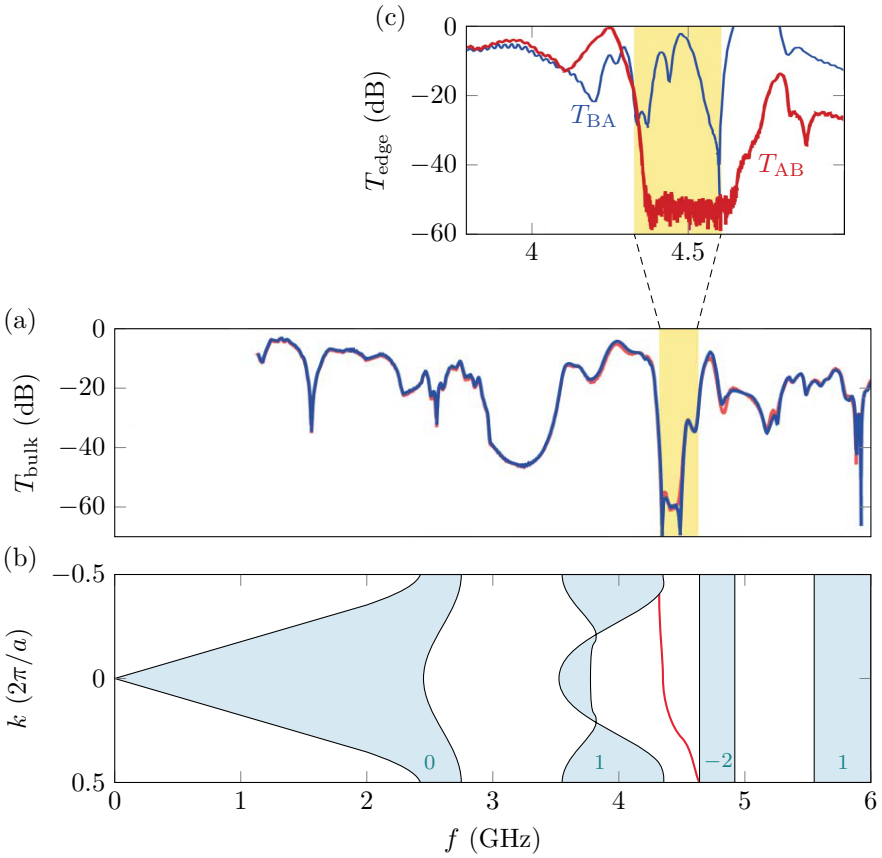

Figure 1.11: Scattering signature of chiral photonic edge states. The (projected) photonic band structure for transverse magnetic modes $f(k)$ sketched in (b) of the photonic crystal designed by [WCJS09] exhibits topological gaps, supporting topological edge states (in red). A signature of such edge states is obtained by carrying out scattering measurements: in the bulk (a), the transmission is reciprocal, as there is no significant discrepancy between the forwards transmission (in blue) and backwards transmission (in red). (c) In contrast, on the edge, the backwards transmission is much smaller than the forwards transmission. In the band structure (b), the first Chern numbers of bands are indicated as blue integers. They are compatible with the existence of the red edge state. An additional edge state should appear in the gap separating the two bands with largest frequencies; however, [WCJS09] explain that such bands have ill-defined band-edges due to a large absorption near the ferromagnetic resonance, which is probably the reason why this additional edge mode is not indicated. Adapted from [WCJS09]. Reprinted by permission from Macmillan Publishers Ltd, Nature, copyright 2009.

field $\psi(t,x) = \phi(x)\mathrm{e}^{-\mathrm{i}\omega t}$ at frequency ω takes the form

$$\mathrm{i}\partial_z\phi = -\frac{1}{2k_0}\nabla_\perp^2\phi - \frac{k_0\delta n}{n_0}\phi \tag{1.13}$$

where $\nabla_\perp = \partial_x^2 + \partial_y^2$, $k_0 = 2\pi n_0/\lambda$, and $\lambda = 2\pi c/\omega$ is the vacuum wavelength of the radiation. The propagation of light along such a waveguide is similar to an evolution in time, with time t is replaced by the distance of propagation z along the waveguide axis. The equation of propagation is similar to the Schrödinger equation where the space-dependent refraction index plays the role of a potential (see e.g. [Lon09; SN10] for details). For example, when two such waveguides are sufficiently close to each other, they can exchange light by evanescent coupling: as a consequence, light initially sent into one waveguide will oscillate between the two waveguides, in a process similar to the Rabi oscillations. Hence, on the one hand, and as long as waveguides are not too strongly coupled, it is possible to describe an arrangement of parallel waveguides by a coupled-mode theory analogous to the tight-binding approximation in solid-sate physics (see e.g. [YY06; SN10]). On the other hand, the helical form of the waveguides can be taken into account in this tight-binding-like description as a periodic modulation of the coupled-mode/tight-binding parameters in the direction of propagation (see e.g. [Lon09; SN10]). The equations of propagation are therefore formally equivalent to the equation of evolution of a tight-binding Hamiltonian periodically modulated in time. A sinusoidal modulation of the waveguide mimics the interaction of an electron with a linearly polarized electric field. The helical waveguides used by Rechtsman and collaborators correspond to a circular polarization. They indeed observed, for the right set of parameters, a chiral propagation of light on the edge of the system, even when defects are added.

1.3.2 Mechanical waves: phonons in bead-spring lattices

Following the seminal work of Prodan and collaborators [PP09; BJKP11] who identified topological phonon modes in systems inspired from biology, Kane and Lubensky [KL13] developed a framework to characterize the topological properties of beads and spring systems, in analogy with electronic systems. In particular, they provided a (physically) precise statement of the bulk-boundary correspondence in mechanical lattices. In such a mechanical lattice, beads connected to each other by Hookean springs are positioned in a spatially periodic fashion. The harmonic oscillations about the equilibrium positions are decomposed into phonon modes. As the system is spatially periodic, the phonon spectrum organizes into Bloch bands $\omega_i(k)$, where k is the quasimomentum, and an isolated Bloch band can be topologically nontrivial. The mechanical lattice possesses two kinds of degrees of freedom: the displacements of the beads and the extensions of the bonds, defined with respect to the equilibrium configuration. There is a geometrical relation between the displacements u_i and the extensions e_m, contained in the *rigidity matrix* R defined by

$$e_m = R_{mi}u_i. \tag{1.14}$$

Similarly, the geometrical relation between the tensions T_m of the bonds and the forces F_i on the beads is contained in the *equilibrium matrix* $Q \equiv R^T$ such that

$$F_i = Q_{im}T_m. \tag{1.15}$$

Concerning the dynamics, the tension T_m on a Hookean bond is related to its extension by $T_m = -K_m e_m$, and the force F_i on a bead is given by Newton's law $F_i = M_i \ddot{u}_i$. When all stiffnesses and masses are equal, $K_m = K$ and $M_i = M$, it is convenient to define $\omega_0 = \sqrt{K/M}$, and the equation of motion reads

$$\mathrm{i}\frac{\mathrm{d}}{\mathrm{d}t}\psi = \mathcal{H}\psi \tag{1.16}$$

where

$$\mathcal{H} = \omega_0 \begin{pmatrix} 0 & Q \\ Q^T & 0 \end{pmatrix} \qquad \text{and} \qquad \psi = \begin{pmatrix} \dot{u} \\ -\mathrm{i}\omega_0 e \end{pmatrix}. \tag{1.17}$$

Again, the Fourier transform can be used to make use of the spatial periodicity of the system, which gives a family of matrix Bloch Hamiltonians $\mathcal{H}(k)$. When this family of Bloch Hamiltonians is gapped, topological invariants can be computed in the usual way. A gap at zero frequency in the excitation spectrum is only possible when the lattice is *isostatic*, i.e. when the number of constraints (due to bonds) is equal to the number of degrees of freedom of the beads and in this case a structural symmetry (a chiral symmetry in the language of topological insulators) visible in the block-antidiagonal structure of $\mathcal{H}$ can be used to protect topological phases. A generalized Hamiltonian framework to describe (topological) mechanical systems, not specialized to beads and springs, as well as a classification of such phases (both at zero and nonzero frequency) were recently developed by Süsstrunk and Huber [SH16] in a very clear paper.

Kane and Lubensky proposed a mechanical analogue of the Su-Schrieffer-Heeger model of polyacetylene, which was experimentally realized by Chen et al. [CUV14]. Outside of phase transitions, the bulk is insulating, which means that there are no modes at zero frequency. In a mechanical system with bonds of very large stiffness (e.g. if springs are replaced by plastic rods), no motion is possible. At the interface between two topologically distinct mechanical insulators, however, there is a robust zero-frequency mode, so a motion is possible only through such topological boundary modes (see figure 1.12). The motion is not infinitesimal, however, as a nonlinear soliton coupled to the domain wall separating the two topologically distinct phases can propagate along the chain [CUV14; VUG14], a behavior reminiscent of what happens in polyacetylene [JR76].

Another experimental realization of a mechanical topological system is due to Nash and collaborators [NKRV15], who used a lattice of coupled gyroscopes to create a two-dimensional mechanical metamaterial with chiral edge states (an analogue of the Haldane model). I encourage the reader to look at their videos. Here, again, a time-periodic motion is used to induce a topological phase.

1.4 Inducing topological properties through a time-periodic excitation

We have already mentioned that a time-periodic modulation (or its equivalent in paraxial propagation) can be used to induce topological properties in photonic and mechanical systems. This was only realized after it was proposed to use light to control topological phases in the solid state, a task which appeared to be experimentally

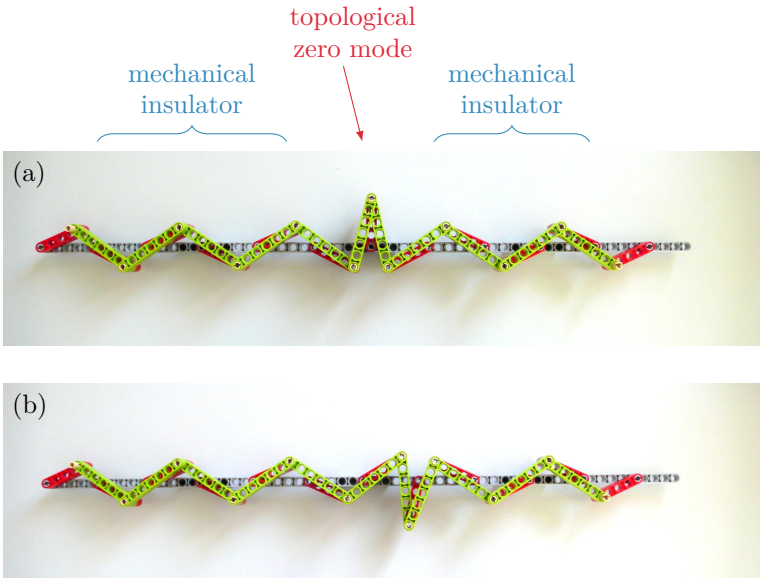

Figure 1.12: Mechanical topological insulator in LEGO. A LEGO version of the mechanical SSH model designed by Vitelli et al. [VUG14]. The two insulating phases correspond to the red rods pointing to the left or to the right of their pinning point. In such phases, nothing can move (at zero frequency). At the interface between two topologically distinct phases, in contrast, there is a zero-frequency degree of freedom, corresponding to a free motion. If we push a little the green or red rods near the interface, the domain wall can move, e.g. from (a) to (b), and can propagate all along the system.

challenging. The idea of inducing a topological transition through an excitation periodic in time, e.g. by shining light on a sheet of graphene, was proposed in 2009 by Oka and Aoki [OA09]. They were quickly followed by Inoue and Tanaka [IT10] and Lindner, Refael and Galitski [LRG11] who proposed the idea of a "Floquet topological insulator" where a quantum spin Hall effect is induced by light. Similar ideas were already (theoretically) developed in the beginning of the 2000s in cold atom systems; the state of the field in 2007 is reviewed in [LSAD07].

As a first approximation, a (Bloch) Hamiltonian $H_0(k)$ subject to a time-dependent perturbation $W(t) = W(t+T)$ periodic in time can be replaced by a time-independent "effective Hamiltonian" which captures the long-time stroboscopic dynamics of the system after an integer number of time periods (i.e. at times nT, with $n \in \mathbb{Z}$). For a monochromatic perturbation

$$W(t) = W_1(k)\mathrm{e}^{\mathrm{i}\omega t} + W_{-1}(k)\mathrm{e}^{-\mathrm{i}\omega t} \tag{1.18}$$

this effective Hamiltonian is, at first order,

$$H^{\mathrm{eff}}(k) = H_0(k) + \frac{1}{\omega}[W_1(k), W_{-1}(k)] + O\left(\frac{1}{\omega^2}\right). \tag{1.19}$$

Starting from a critical phase with Dirac cones (such as graphene), it is possible to induce topological properties provided the sign of the masses at the different Dirac points can be controlled. It is the case for the coupling with an electromagnetic wave in graphene, which induces opposite masses in the two valleys [OA09; IT10]; similarly, in the setup used by [RZPL13], the helical waveguides precisely mimic the coupling with a circularly polarized light. To give an intuition of what happens, we will focus on the low energy Hamiltonian near a single Dirac cone

$$H_0(q) = q_x\sigma_x + q_y\sigma_y \tag{1.20}$$

and take the simple perturbation $W_1 = W/4\,(\sigma_x + \mathrm{i}\sigma_y)$ and $W_{-1} = W_1^\dagger$. We obtain

$$H^{\text{eff}}(q) = q_x\sigma_x + q_y\sigma_y + \frac{W^2}{\omega}\sigma_z + \text{higher order terms.} \tag{1.21}$$

It is therefore possible to gap the Dirac point with a mass depending on W. In graphene, the perturbation due to a circularly polarized light is either W_1 or $W_1^\dagger$ depending on the valley, so the masses $\pm W^2/\omega$ on both valleys are indeed opposite. A simpler perturbation identical on both valley may also induce topological properties, but at higher order in perturbation.

At first sight, the time-independent effective Hamiltonian H^{eff} is enough to understand this kind of topological periodically driven systems: the driving field can yield a topologically nontrivial H^{eff} from a trivial unperturbed Hamiltonian H_0. In fact, the meaning of this effective Hamiltonian has to be made precise. In a driven system, energy is no more conserved, as it is exchanged with the driving field. However, the time periodicity of the driving ensures that energy is only exchanged in quanta of $\hbar\omega$ (where ω is the driving angular frequency), so the quantity

$$\varepsilon = E \bmod \hbar\omega \tag{1.22}$$

called *quasi-energy* is still conserved. Hence a periodically driven system is characterized by a quasi-energy spectrum (and the corresponding eigenstates) instead of an energy spectrum. This quasi-energy spectrum appears as the spectrum of the effective Hamiltonian H^{eff} or, up to exponentiation, as the spectrum on the circle of the evolution operator after one period, $U(T) = \mathrm{e}^{-\mathrm{i}TH^{\text{eff}}}$, which is often called the Floquet operator. As a consequence, quasi-energies are essentially phases (periodic quantities) which are organized on a circle, see figure 1.13. The Floquet operator $U(T)$ is well-defined, but the effective Hamiltonian is not uniquely defined: a choice of the branch cut for the complex logarithm is required. The periodicity of quasi-energy seems to be innocuous. Instead of energy bands in the spectrum of a Hamiltonian, quasi-energy bands appear in the spectrum of the Floquet operator $U(T)$, and we could expect to describe the topology of periodically driven systems in the same way as static phases, through the topology of the quasi-energy bands. It turns out that such out-of-equilibrium phases display richer topological features than equilibrium phases: a system where all band invariants vanish may still exhibit topological properties, in the so-called "anomalous" topological phases. This peculiar property of periodically driven systems which was first observed by Kitagawa et al. [KBRD10], soon thereafter was observed in optical experiments [KBFR12]) and understood in 2013 by Rudner, Lindner, Berg, and Levin [RLBL13]. They developed a new framework to

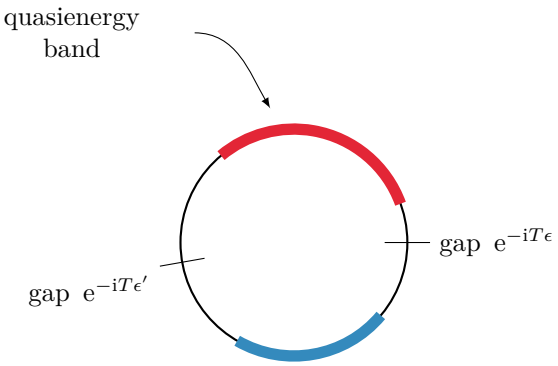

Figure 1.13: A quasi-energy spectrum. The spectrum of the unitary evolution operator after one period $U(T)$ is called the quasi-energy spectrum, and it organizes the unit circle $U(1)$. As in static systems, the quasi-energy spectrum of a crystal is composed of bands (there are two bands in this example, in blue and in red) separated by gaps.

fully describe the topological properties of the unitary evolution of a two-dimensional periodically driven system without specific symmetry, which correctly accounts for the existence of chiral edge states at the boundary of a finite sample. The key to understand such anomalous phases turns out to be the periodicity of the quasi-energy spectrum. In an equilibrium system with two energy bands, there may be edge states in the bulk gap, located between the two bands[(3)]. In a Floquet system with two quasi-energy bands, there are *two* bulk gaps, each of which may host edge states in a finite system, as pictured in figure 1.14. Naturally, this observation generalizes to more than two bands. In fermionic systems, the periodicity of quasi-energy also highlights the question of the thermodynamic filling of quasi-energy bands: there is no "bottom of the band" to start filling from. It is therefore not reasonable to expect a unique behavior essentially independent of the driving fields, baths and reservoirs to which the system is connected.

The framework developed by Rudner et al. [RLBL13] consists in defining *gap invariants* which are directly related (equal) to the number of edge states (counted with chirality) that would fill the corresponding bulk gap in a finite system with boundaries. This point of view is particularly adapted to situations where it is possible to probe the response of the system at a fixed quasi-energy, for example through scattering experiments, without having to rely on a particular filling. This is the case in several classical systems (a beautiful experiment in photonic crystals is found in [SLIY15]). In contrast, topological phases are usually understood as stemming from the topology of the ground state, a fruitful point of view which was extended to interacting phases like FQHE and led to the notion of *topological order* introduced

[(3)] To put both situations in a single form, we can consider that a constant Hamiltonian is in fact periodic, with a period T small enough so that $T\sigma(H) \subset]-\pi, \pi[$, i.e. so that the band structure laid on the circle does not overlap with itself. In this situation, the energy "gaps" going from the top of the upper band to $+\infty$ and from the bottom of the lower band to $-\infty$ correspond to the quasi-energy gap near $e^{\pm i\pi} = -1$, which therefore contain no edge state.

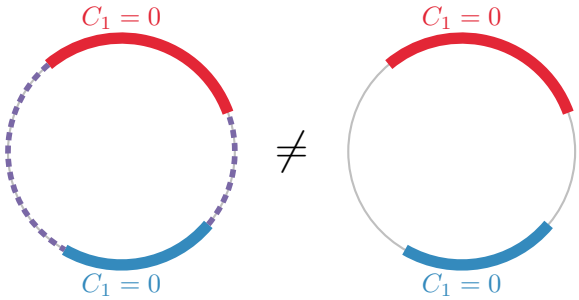

Figure 1.14: Anomalous and trivial systems. Quasi-energy spectra of two systems with edges, which share the same bulk dispersion (red and blue bands) but have different bulk topological properties, manifesting themselves in different edge dispersion (in dashed purple). Despite this difference, both systems have the same bulk band invariants (first Chern numbers C_1), which are not sufficient to fully characterize the system [RLBL13].

by Xiao-Gang Wen [Wen90]. A number of developments were carried out in this direction, in particular to classify symmetry protected topological phases (SPT, a particular formalization of what we call "topological insulators" here) through the ground states of gapped Hamiltonians with group cohomology [CGLW13; GW14; CGLW12; Wit16]. In the case of topological periodically driven systems, there are several reasons why this description may not be fully relevant: (i) in an anomalous phases, the topological invariants associated to a band always vanish and yet the system exhibits topological properties manifesting themselves as edge states in a finite system; (ii) the ground state is not well-defined, as the filling of Floquet bands is not unambiguous, and depends in a crucial way in the details of the coupling to the environment.

The idea of inducing topological properties through a time-periodic driving, and, therefore, the peculiar properties of Floquet topological phases, are of fundamental interest. Beyond this fundamental interest, Floquet topological phases provide a convenient way to realize topological phases outside of solid state physics. In cold atoms, the idea of using periodically driven lattices in order to control the tunneling matrix elements is already well-established, and I refer the reader to recent reviews [Hol15; GD14] for more details. In particular, controlling tunneling amplitudes allows to create artificial gauge fields [HTCÖ12]. An obvious application of this kind of technique is the simulation of topological insulators: let us mention the experimental realizations of the Haldane model [JMDL14], the Harper-Hofstadter Hamiltonian [ALSA14; AALB13; MSKB13]). More or less independently, as we have seen, the same ideas were also used to design and realize topological phases (i) in mechanical systems: experimentally with a lattice of gyroscopes connected by springs [NKRV15], and theoretically with gyroscopes [WLB15] and in a rotating frame [WLZ15; KH15], and (ii) with light [KBFR12; RZPL13], where the periodic evolution in time is replaced by a periodic modulation in the $(d+1)$th dimension of real space along which propagation occurs. All in all, I believe that periodically driven systems (and the correspond-

ing synthetic gauge fields) are an important tool to extend the notion of topological insulator outside of the initial scope where it was discovered.

Finally, the framework developed to study periodically driven phases, which also applies to undriven phases, may serve as a platform for a better understanding of topological phases. For example, the topological edge states in an anomalous system are (or at least seem to be) of the same nature that standard edge states. Yet, anomalous systems are not related to a band invariant: this deviation from standard behavior can serve as a tool to probe the limits of usual characterizations of topological states, and to extend them in a setting which may be better suited to be generalized to systems outside the scope of condensed matter.

1.4.1 Topological Floquet phases in electronic systems

To realize topological Floquet phases in a solid state context appears to be challenging. Floquet theory is a high-frequency approach, meaningful when the driving is fast with respect to the characteristic time scales of the undriven system. In this very high frequency regime, the system essentially feels an effective static potential. In contrast, the opposite limit is the slow adiabatic driving where the state of the system essentially follows the instantaneous eigenstates of the time-dependent Hamiltonian. Starting from a very high frequency limit, interesting physical behaviors typically occur when the frequency becomes comparable with the natural timescale of the undriven system. However, there are several issues which arise when frequency is "too low": first, at low frequency, the initial energy bands are folded a lot of times on the circle, and opening a sizable gap seems difficult. At even lower frequencies, the quasi-energy spectrum becomes meaningless, the perturbative expansions break down, and Floquet theory is no longer helpful. Hence, in order to have meaningful and interesting results, the bandwidth should be comparable to (or at least of the order of) the driving frequency. For example, the bandwidth of graphene is approximately $6t$ where $t \approx 3\,\mathrm{eV}$, so we may expect that the order of magnitude of the relevant radiation frequency should be in the far ultraviolet range, $f \sim 6t/h \sim 1 \times 10^{15}\,\mathrm{Hz}$. Such kind of ionizing radiation will damage the system. This problem is even worse as in order to get a sizable Floquet band gap, a very high light intensity would be required at such frequencies, e.g. obtained with a laser. If light is introduced through minimal coupling $p \to p - eA$ in a Dirac Hamiltonian $H(p) = v_\mathrm{F} p \cdot \sigma$, the gap is of order of [CPRT11]

$$\Delta \sim \frac{\alpha v_\mathrm{F}^2 I}{\omega^3} \tag{1.23}$$

where $I \sim c\,\varepsilon_0\,\omega^2 A^2$ is the intensity of the laser beam, in $\mathrm{W} \cdot \mathrm{m}^{-2}$ (see e.g. [Pas16]), and $\alpha \approx 1/137$ is the fine structure constant. With the previously calculated angular frequency $\omega \sim 1 \times 10^{16}\,\mathrm{rad} \cdot \mathrm{s}^{-1}$, a gap of 10 meV would require $I \sim 1 \times 10^{17}\,\mathrm{W} \cdot \mathrm{m}^{-2}$ with $v_\mathrm{F} \sim 1 \times 10^6\,\mathrm{m} \cdot \mathrm{s}^{-1}$ in graphene. Such a high laser intensity would probably have deleterious effects on the stability of the graphene sheet, be it only heating. Several proposals have slightly more optimistic estimations of both the driving frequency and the laser intensity required [CPRT11; UPTB14; PUBT14; QGS16], but they seem to be out of experimental reach for now. Despite this disappointing order of magnitudes, there is still hope, as Floquet states were unambiguously detected in Gedik group by Mahmood and collaborators [MCAG16] (following previous works

[WSJG13]), who used time-resolved pump-probe angle-resolved photoemission spectroscopy (Tr-ARPES) on surface states of the topological insulator Bi_2Se_3 to induce Floquet states with the pump light and observe them with the probe light. In particular, they were able to distinguish the contribution of Volkov states (which are in this case Floquet states for the free electrons outside, but close to the surface of the system) and Bloch-Floquet states of the crystal, see figure 1.15. To give an order of magnitude, the pump light that was used to induce Floquet states was in the infrared range, with $\omega \sim 10^{14}\,\mathrm{Hz}$ and $I \sim 10^{12}\,\mathrm{W}^2 \cdot \mathrm{m}^{-1}$. Even if it is still far from the realization of Floquet topological phases, this work is particularly promising as it proves that it is indeed possible to induce Floquet states in a crystal, at least for a short time (approximately one picosecond).

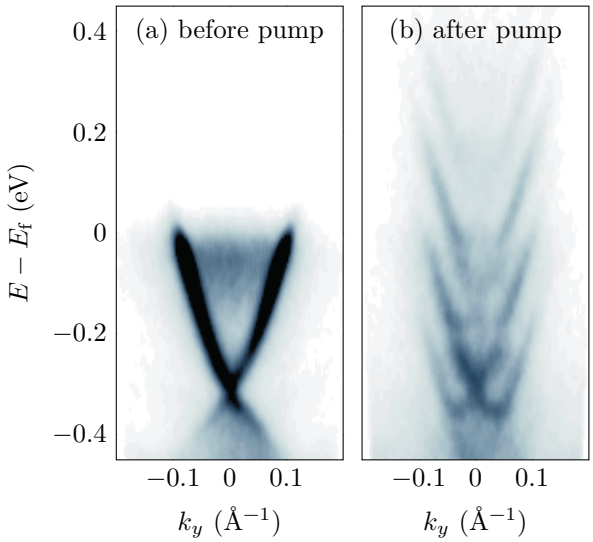

Figure 1.15: Tr-ARPES signature of Bloch-Floquet states. Time-resolved ARPES spectra from [MCAG16] exhibiting Bloch-Floquet states. (a) Before any strong excitation, ARPES enables to observe a Dirac cone at the surface of Bi_2Se_3 as well as bulk bands. (b) After the pump pulse excited the sample, several "replica" (or "sidebands") of the original Dirac cone are observed in the time-resolved ARPES spectrum, translated by multiples of the energy $\hbar\omega \simeq 0.16\,\mathrm{eV}$, where ω is the angular frequency of the pump light. Avoided crossing gaps can be observed between the Floquet sidebands. In this spectrum, there is a mixture of contributions from Floquet and Volkov states (they should lead to the same signature), but Mahmood et al. were able to prove that Bloch-Floquet states indeed exist in the crystal. Adapted from [MCAG16]. Reprinted by permission from Macmillan Publishers Ltd, Nature Physics, copyright 2016.

Even when (if?) the difficulties of realizing topological Floquet states in a solid state setting are overcome, the issue of filling quasi-energy states will still need to be either addressed or avoided. In such an out-of-equilibrium driven system, a source of dissipation is essential if we hope to reach a non-equilibrium steady-state (NESS) which may be described by an effective unitary evolution [TOA09; BDP15; DOM14; DOM15], as the driving field acts as a source of energy. An important question in this

context is how the band structure is filled in the stationary regime [SBLR15; INC15; LDM14], as long-time physical observables such as transport or response properties are determined by the steady-state.

In the following, we will assume that a stationary regime is reached, and we won't focus on the thermodynamics (filling) but on the dynamical structure (evolution operator and effective Hamiltonian) of the system. This is not a problem as the topological properties of a band structure is independent of its filling. In this context however, we will try to avoid the word "insulator" (especially in "Floquet insulator") to refer to gapped driven systems as long as the filling of quasi-energy bands is not specified.

2 Aim of this work

2.1 Topology of systems under a time-periodic excitation

The first proposals for inducing topological states in periodically driven systems were carried out in a situation with no symmetry at all (in class A) by Oka and Aoki [OA09] and Inoue and Tanaka [IT10] (similar ideas were also present in the cold atoms literature, in particular with proposals to realize artificial gauge fields). A year later, Lindner, Refael and Galitski [LRG11] proposed a similar idea for systems with fermionic time-reversal invariance (in class AII, like Kane-Mele insulators). The same year, Jiang and collaborators [JKAA11] proposed to use a periodic driving to induce Majorana fermions in a 1D chain with particle-hole symmetry (in class D). In the same time, Kitagawa and collaborators [KRBD10; KBRD10] took a first step towards the topological classification of periodically driven systems. A breakthrough came from Rudner, Lindner, Berg, Levin in 2013 [RLBL13], who realized that the invariants characterizing equilibrium systems are not sufficient to completely characterize periodically driven systems, and developed a framework to fully describe two-dimensional systems without symmetries (in class A). Due to the importance of symmetries in topological systems, a generalization of this framework to other symmetries classes is crucial. Using different methods, Asbóth, Tarasinski, and Delplace [ATD14] defined an invariant for periodically driven 1D chiral systems (in class AIII, like the SSH model). One of the aims of this thesis was to define such an invariant for fermionic-time-reversal invariant systems (in class AII, like the Kane-Mele insulators), a goal that was realized in the same framework that Rudner and collaborators. I also reinterpreted Asbóth's et al. results in the same framework, and extended the definition of the Floquet invariants to all dimensions for complex classes (A and AIII). The central object in this approach is the unitary evolution operator $U(t,k)$. When the spectrum of the Floquet operator $U(T,k)$ (the quasi-energy spectrum) possesses gaps, it is possible to define periodized versions of the evolution operator $V_\varepsilon(t,k) = V_\varepsilon(t+T,k)$, which crucially depend on choice of the gap ε in the quasi-energy spectrum. In class A, homotopy theory defines a bulk topological invariant from the unitary map V_ε: its winding (or degree)

$$W_\varepsilon[U] = \deg(V_\varepsilon) \in \mathbb{Z} \tag{1.24}$$

which counts the chiral edge states in the bulk gap ε that appear in a finite sample [RLBL13]. This is a **gap invariant**, in contrast with e.g. Chern invariants, which are **band invariants**, as they characterize (quasi-)energy bands. There is a relation between them: the difference between W's in two different gaps gives the Chern number of the quasi-energy band in between,

$$W_{\varepsilon'}[U] - W_{\varepsilon}[U] = C_1[P_{\varepsilon,\varepsilon'}]. \tag{1.25}$$

I extended this definition to any even dimension d, where the $(d/2)$-th Chern invariant appears [Fru16]. In class AII, when time-reversal symmetry $\Theta^2 = -\mathrm{Id}$ is present, that is when

$$\Theta H(t,k)\Theta^{-1} = H(-t,-k) \tag{1.26}$$

then $W_\varepsilon[U]$ always vanishes in two dimensions, a behavior reminiscent of the vanishing of the first Chern number in this situation. However, in $d = 2, 3$ it is possible to define another invariant

$$K_\varepsilon[U] \in \mathbb{Z}_2 \tag{1.27}$$

which counts the helical edge states in the bulk gap ε that appear in a finite sample [CDFG15b]. It is a $\mathbb{Z}_2$-valued index, as the Kane-Mele invariant. Similarly, the difference of K's for two gaps gives the Kane-Mele invariant of the corresponding band

$$K_{\varepsilon'}[U] - K_{\varepsilon}[U] = \mathrm{KM}[P_{\varepsilon,\varepsilon'}]. \tag{1.28}$$

In class AIII, when chiral symmetry is present, that is

$$\Gamma H(t,k)\Gamma^{-1} = H(-t,k) \tag{1.29}$$

there is a constraint on the *chiral gaps* $\varepsilon = 0$ and π (also called *real gaps*), which implies the vanishing of $W_{0/\pi}[U]$ in even dimension. In all odd dimensions, W is not defined, but it is possible to define chiral gap invariants for the chiral gaps,

$$G_\varepsilon[U] \in \mathbb{Z} \qquad (\varepsilon = 0 \text{ or } \pi) \tag{1.30}$$

and again, their difference is the usual chiral band invariant [Fru16].

It is conjectured that this structure is general, and arises for all Cartan-Altland-Zirnbauer classes. All known topological insulators (or superconductors) should be characterized by gap invariants, which naturally extend to periodically driven phases. Evidence in this direction are the works of Nathan and Rudner [NR15] and Roy and Harper [RH16]. In the chapter 4 of this work, I show that the bulk invariants W and G characterize all $\mathbb{Z}$ classes of the periodic table of topological insulators; notably, the constraints put on such invariants by antiunitary symmetries enable to recover a large part of the periodic table (without the $\mathbb{Z}_2$ invariants).

It would be particularly interesting to observe topological Floquet states in a solid state setup. As I already mentioned, it is also quite challenging. The natural probe in electronic condensed matter system is transport measurements, which proved to be particularly adapted to the study of topological states in the quantum Hall effects [Büt88a] as well as in the Kane-Mele insulators [RBBM09; Büt09]. We expect to observe an analogue of the quantization of the conductance in the periodically driven

system, even if it is not completely obvious that it should happen. Transport in topological periodically driven systems was already studied theoretically in several setups [KOBF11; GFAA11; KS13; TPBU14; FP16]. I used time-resolved numerical simulations to study the transport properties of such a Floquet topological insulator. We indeed find that the stationary time-averaged differential conductance turns out to be quantized in a topological bulk gap [FDWW16], in a situation where transport remains ballistic, and where dissipation is dominated by the coupling to the metallic leads. Moreover, the three-terminal conductances allow to probe the chiral nature of the edge states.

3 Organization of this thesis and related publications

During my thesis, I contributed to several peer-review articles.

1. *An Introduction to Topological Insulators*,
   Michel Fruchart, David Carpentier
   Comptes Rendus Physique 14 (2013) 779-815
   doi:10.1016/j.crhy.2013.09.013, arXiv:1310.0255
   This review article aims at providing a simple and self-contained introduction to Chern and Kane-Mele topological insulators.
2. *Parallel Transport and Band Theory in Crystals*,
   Michel Fruchart, David Carpentier, Krzysztof Gawędzki
   EPL 106, 60002 (2014)
   doi:10.1209/0295-5075/106/60002, arXiv:1403.2836
   In non-Bravais crystals, the definition of the matrix Bloch Hamiltonian is not unique: there are several inequivalent ways to represent the Hamiltonian operator as a k-dependent matrix. Correspondingly (but independently) there are several inequivalent choices of *parallel transport*, and therefore of Berry *curvatures*. This is surprising, as the Berry curvature (as opposed to the Berry connection) is gauge-invariant, and therefore generally understood as a physical quantity. In this paper, we show that there is a particular "canonical" Berry curvature which is independent of the choice of the fundamental domain for the crystal, directly related to the position operator, and which respects the symmetries of the crystal. Notably, this canonical Berry curvature is *not* periodic in reciprocal space. As this topic does not naturally fit the subject of this thesis, I will not expose it in details.
3. *Topological index for periodically driven time-reversal invariant 2D systems*,
   David Carpentier, Pierre Delplace, Michel Fruchart, Krzysztof Gawędzki
   Phys. Rev. Lett. 114, 106806 (2015)
   doi:10.1103/PhysRevLett.114.106806, arXiv:1407.7747
   This paper defines a topological invariant for periodically driven systems with fermionic time-reversal invariance (in class AII) in two dimensions, i.e. the extension of the Kane-Mele invariant to Floquet systems. Its contents are discussed in details in section 3.4 of chapter 4, page 152.
4. *Construction and properties of a topological index for periodically driven time-reversal invariant 2D crystals*,
   David Carpentier, Pierre Delplace, Michel Fruchart, Krzysztof Gawędzki, Clément

Tauber
Nuclear Physics B 896 (2015) 779-834
doi:10.1016/j.nuclphysb.2015.05.009, arXiv:1503.04157
This is a supporting paper supporting the previous one, containing proofs of our claims. To avoid an useless repetition of technical topics, I will not include them in this thesis, and the reader seeking proofs and details on the construction of the index K is directed to this work.

5. *Probing (topological) Floquet states through DC transport*,
Michel Fruchart, Pierre Delplace, Joseph Weston, Xavier Waintal, David Carpentier
Physica E 75 (2016) 287-294
doi:10.1016/j.physe.2015.09.035, arXiv:1507.00152
Transport measurements are the archetypal way of probing topological edge states. In this work, we use time-resolved numerical simulations to probe the transport properties of (topological) Floquet states in a regime where we expected to understand the results, with the aim of setting the ground for more dicey explorations. Despite encouraging results, it turns out that even the simple regime is not fully understood. This topic is exposed in details in chapter 5, page 165.

6. *Complex classes of periodically driven topological lattice systems*,
Michel Fruchart, Phys. Rev. B 93, 115429 (2016)
doi:10.1103/PhysRevB.93.115429, arXiv:1511.06755. This paper extends previous works to cast in a single framework known topological invariants for complex CAZ classes A and AIII, and to extend them to any relevant dimension. Notably, a 3D chiral invariant for Floquet systems is defined. Its contents are discussed in details in sections 3.2 and 3.3 of chapter 4, respectively at pages 126 and 143.

7. Anomalous topological directed scattering networks
Pierre Delplace, Michel Fruchart, Clément Tauber
in preparation.
Directed scattering network models like the Chalker-Coddington model [CC88; HC96] are described by evolution operators expressed in terms of scattering matrices. Chong and collaborators [PC14] identified them as a "static" realization of Floquet phases, more precisely of "discrete time quantum walks" (DTQW). In particular, they were the first to observe experimentally an anomalous Floquet phases (with vanishing band invariants) in such a system [HPWP15; GGSY16]. This paper is devoted to the equivalence on two rather different points of view on such systems. In the formulation of Ho and Chalker [HC96], appear both the one-step evolution operator of the directed network and a two-step Floquet/DTQW-like formulation used by Chong and collaborators. In the first point of view, which focuses on the full stack of degrees of freedom, the directed nature of the network model gives rise to a "structure constraint" which is at the origin of the topology. The second point of view, which *halves* the number of degrees of freedom to adhere closely to the analogy with a DTQW is only permitted by the existence of this structure constraint. In addition to the always present structure constraint, we also identify an additional pseudo-symmetry without equivalent in Hamiltonian systems, which is associated to a quasi-energy rotation. This symmetry can force a vanishing band invariant (first Chern number) despite the explicit time-reversal symmetry breaking. This work is preparation at the time of writing this thesis.

This thesis is organized as follows.

- A general introduction (you are reading it) starts on page 3.
- A rather technical chapter 2, starting on page 33 briefly reviews the topology of vector bundles.
- The chapter 3, starting on page 57 gives a review of the usual equilibrium topological insulators and their classification.
- The chapter 4, starting on page 109 is the main part of this work, and is devoted to the topology of periodically-driven/Floquet systems, in particular in presence of symmetries.
- Finally, the chapter 5, starting on page 165, is another important part of this work, and is devoted to transport signatures of (topological) Floquet states.
- Additionally, a french summary of this thesis, which is essentially a tranlsation of the current introduction, is available at page 199.

Chapter 2

Vector bundles and their topology

In this chapter, we introduce several mathematical objects required for a precise theoretical description of topological insulators. I will briefly introduce the notion of bundles, in particular vector bundles, and quickly review the key features of their topological classification. In a next chapter, we will see that band theory allows to describe the energy bands of a crystal in terms of vector bundles, which may or not be topologically nontrivial, which corresponds to trivial or nontrivial topological insulators. In the following, maps will always be supposed to be continuous unless explicitly mentioned, and as smooth as necessary when a differential structure is assumed.

1 Vector bundles

The following section is devoted to introducing the notion of bundles. To give a general idea, suppose that we want to define F-valued functions on a manifold M. Typically, this is what happens when we consider a vector field over M, in which case F is a vector space. Locally, fields are functions from M to F. Globally, however, it happens that in order to describe physical phenomena, it is crucial to be able to allow fields to have a *global twist*, which allows them to feel the topologically nontrivial nature of the base manifold (in particular, band theory is naturally formulated in the language of vector bundles describing Bloch states, and the topological properties of a band structure are consequences of their global twist). Bundles provide such a global structure, which is not captured in a local description.

1.1 Pictorial introduction

Consider a simple planet, a sphere standing still in empty space, with a very thin layer of atmosphere. Wind on this planet is mostly horizontal, because the layer is so thin it can be considered as two-dimensional and we can neglect ascending and descending flows. There is a velocity field $\vec{v}(p)$ defined at any point p of the surface of the planet which gives the direction of the wind, which is therefore "horizontal". That means that $\vec{v}(p) \cdot \vec{u}_r(p) = 0$ with spherical unit vectors $(\vec{u}_r, \vec{u}_\theta, \vec{u}_\phi)$ at any point p of the sphere. In fact, the set of such horizontal vectors forms a vector space

$$T_p = \left\{ \vec{w} \in \mathbb{R}^3 \mid w \cdot \vec{u}_r(p) = 0 \right\} \tag{2.1}$$

called the *tangent space* at point p of the surface of our planet (and vectors inside are called *tangent vectors* at p, which means they are horizontal). Notice that the velocity at point p does not live in the same vector space than the velocity at point q. This may seem surprising, but is not when we realize that a horizontal vector at p is not horizontal at q (see figure 2.1b), simply because $\vec{u}_r(p) \neq \vec{u}_r(q)$. All spaces T_p are isomorphic to the plane $\mathbb{R}^2$, but they are not identical (this is quite obvious if we look at how they are embedded into the whole space $\mathbb{R}^3$). We can put together this collection of vector spaces (one over each point of the surface) in a disjoint union

$$T = \bigsqcup_{p \in S^2} T_p = \bigcup_{p \in S^2} \{(p, w) \mid w \in T_p\} \subset \mathbb{R}^3 \times \mathbb{R}^3 \tag{2.2}$$

which simply means that we gather all possible velocities w in all possible vector spaces T_p, but we remember over which point p of the surface w is supposed to be, so we can recover it later thanks to a *projection map* π which gives the position $p = \pi(t)$ corresponding to an element $t = (p, w) \in T$. In fact, we can recover the whole vector space T_p (which is called *fiber over* p) as $T_p = \pi^{-1}(p)$. The disjoint union T along with the projection map $\pi : T \to S^2$ is said to be a *bundle* over S^2 with typical fiber $\mathbb{R}^2$. The wind velocity field over the planet is a map $p \mapsto v(p)$ going from S^2 to T, with $v(p) \in T_p$. In the language of bundles, v is a *section* of the bundle T.

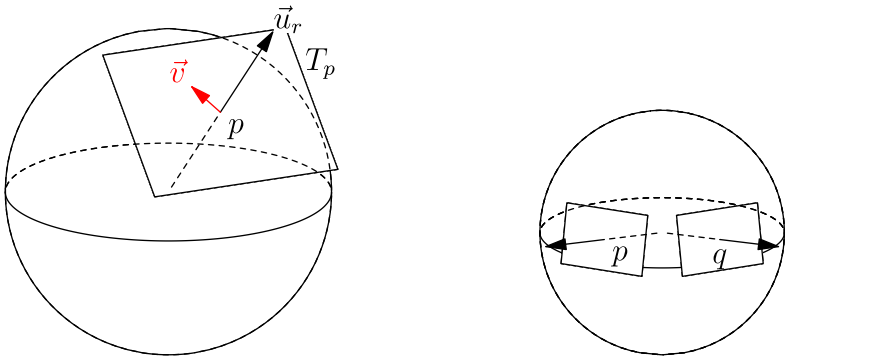

(a) A planet and one of its tangent planes. **(b) Tangent planes at two different points.**

Figure 2.1: Tangent bundle of the 2-sphere.

Finally, as we have seen, velocities are different points live in different fibers, so we cannot compare them, or add them. Neither can we differentiate the velocity field. In order to extend this kind of operations in a meaningful way, we need to introduce an additional structure called a *parallel transport*, which essentially specifies a particular way to move a vector along a path on the planet. In a "flat" space like the plane, the parallel transport of a vector leaves it unchanged. On the other hand the parallel transport on the sphere must ensure that the transported vector remains horizontal, and this is only possible if it is modified in a particular way.

A final note: this example is slightly misleading because it illustrates bundles on the tangent bundle of a manifold, and also because everything is naturally embedded in the three-dimensional space (so we can see what happens). (It is also misleading

from a meteorological point of view, see e.g. [Mor13].) First, the manifold needs not to be embedded in a larger-dimensional space. Second, the fibers are not necessarily geometrically related to the manifold (e.g. tangent or orthogonal), neither is the parallel transport specification[(1)]. For example, we could replace the tangent planes by a copy of the group $U(1)$ representing all possible dephasings of a wavefunction (instead of all possible wind velocities), and define a parallel transport by specifying the electromagnetic field strength $F_{\mu\nu}$ (as in Wu and Yang's version of the Dirac monopole bundle [WY75]).

1.2 Vector bundles

After this slightly misleading example, we will introduce (vector) bundles more formally. My principal references are the review of Eguchi, Gilkey and Hanson [EGH80] aimed at (high-energy) physicists, Steenrod's classical textbook [Ste51] and the more recent textbooks of Hatcher [Hat03b] and Husemöller [Hus93].

1.2.1 Fiber bundles

A **fiber bundle** consists of three objects: two topological spaces, the **total space** E and the **base space** M, a continuous **projection map**

$$\pi : E \to M \tag{2.3}$$

and a space F called the **fiber** (see figure 2.2). The set

$$E_x = \pi^{-1}(x) \tag{2.4}$$

is called the **fiber over the point** x **of** M, and is required to be homeomorphic to F. A local triviality condition is imposed to the projection map: for each point $x \in M$ there is an open neighborhood U of x and a homeomorphism $\phi : U \times F \to \pi^{-1}(U)$ commuting with the projection π in the following sense: $\pi \mid_U \circ \phi = \tilde{\pi}$, where $\tilde{\pi} : U \times F \to F$ is the projection on U (that only means that for $(x, f) \in U \times F$, $\pi(\phi(x, f)) = x$). Maps $U \times F \to \pi^{-1}(U)$ are called **local trivializations**. Hence, E looks locally like the cartesian product $M \times F$. The bundle is called **trivial** if this also holds globally, i.e. if E and $M \times F$ are isomorphic. When it is not the case, the vector bundle is said to be **nontrivial**, or *twisted*.

A bundle (E', π', M') is a **subbundle** of (E, π, M) if E' is a subspace of E, and projections agree $\pi' = \pi \mid_{E'} : E' \to M'$. In the following, we will implicitly assume that $M' = M$ when dealing with subbundles.

A **bundle morphism** between (E, π, M) and (E', π', M') is a pair of map $u : E \to E'$ and $f : M \to M'$ such that $\pi' \circ u = f \circ \pi$, that is, the fiber over $x \in M$ is carried

[(1)] A common but maybe misleading approach to motivate topological phases is to draw a parallel between the curvature of a manifold and the Berry curvature of a vector bundle. Integrating these quantities over the manifold yields respectively the Euler characteristic (directly related to the genus) of the surface, and the first Chern number of the vector bundle. This analogy is enlightening when we realize that the (affine) curvature of the manifold is in fact the curvature of the connection of its tangent bundle. On the other hand, the curvature of the base manifold is irrelevant in the case e.g. of the Berry curvature.

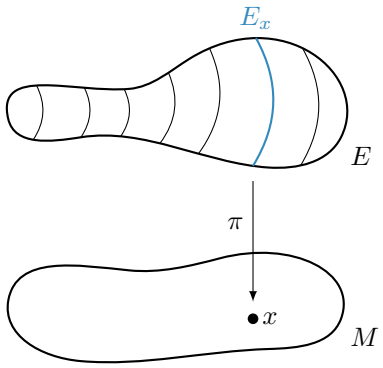

Figure 2.2: Schematic view of a bundle. Over each point x of the base manifold M, there is a fiber E_x (here, the fiber E_x over x is drawn in blue). A projection map π is defined over the whole bundle E, which sends all elements of the fiber E_x back to the base point x, so E_x is the inverse image of x by π.

over $f(x) \in M'$ by u. When there is a bundle morphism (u', f') with $u' : E' \to E$ and $f' : M' \to M$ such that (i) $f' \circ f = \mathrm{id}_{M'}$ and $f \circ f' = \mathrm{id}_M$ and (ii) $u' \circ u = \mathrm{id}_{E'}$ and $u \circ u' = \mathrm{id}_E$, then (u, f) (and (u', f')) is a **bundle isomorphism**, and (E, π, M) and (E', π', M) are said to be **isomorphic**.

A **section** of a bundle consists of assigning a preferred point $s(x) \in E_x$ to each point x of (a part of) the base space M. A **global section** of a fiber bundle E is a smooth map $s : M \to E$ such that $\pi \circ s = \mathrm{id}_M$. A **local section** on an open set $U \subset M$ is a map $s : U \to E$ such that $\pi \circ s = \mathrm{id}_U$. Sections can, for example, represent a field configuration. Local sections always exist, even in nontrivial bundles, but this is not always the case of global sections.

Given a map $f : A \to B$ between from two manifolds A and B and a bundle $\pi : E \to B$ over B, we can construct a bundle E' over A by "pulling back" fibers through f, that is, the fiber of E' over $a \in A$ is defined as a copy of the fiber of E over $f(a) \in B$ (see figure 2.3). Then, there exist a bundle $\pi' : E' \to A$ and a map $f' : E' \to E$ taking the fiber F'_a of E' over each point $a \in A$ isomorphically onto the fiber $F_{f(a)}$ of E over $f(a)$; this bundle is called the **pullback bundle of E by f**. It is usually written as f^*E.

1.2.2 Vector bundles

A special case of fiber bundles which we shall use extensively are vector bundles. A bundle whose typical fiber is a finite-dimensional vector space $F = V$, and whose local trivializations $U \times F \to \pi^{-1}(U)$ are linear is called a **vector bundle**. The dimension or *rank* of the bundle is defined as the dimension of a fiber. Sections inherit the vector space structure: if s and s' are two sections and f a smooth function on M, then $fs + s'$, define pointwise as $(fs + s')(x) = f(x)s(x) + s'(x)$ is also a section. As such, the set $\Gamma(E)$ of sections of E is a vector space under pointwise operations. The *zero section* $s(x) = 0$ for any $x \in M$ always exists, so vector bundles always have a global section. However, non-vanishing global sections do not always exist. In fact,

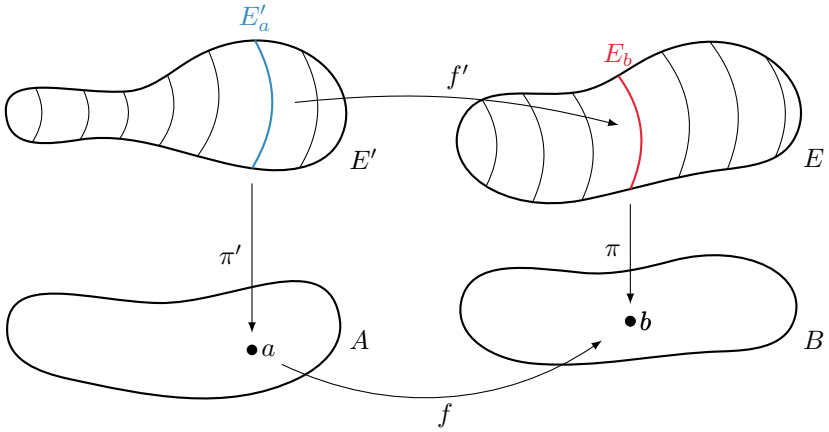

Figure 2.3: Schematic view of a pullback bundle. A map f going from the manifold A to the manifold B enables to "pull back" bundles in the reverse direction. From a bundle E over B, a new bundle $E' = f^*E$ over A is defined by assigning to a points a of A the fiber of E over $f(a)$.

a n-dimensional vector bundle (i.e. of rank n) is trivial iff it has a **frame**, that is a collection of n global sections which form a basis of the fiber over each point [Hat03b]. On the contrary, the *obstruction* to define a frame will signal a nontrivial topology of a vector bundle.

Starting from one (or several) vector bundles on the same base space, we can use usual linear constructions on the fibers to obtain new vector bundles. For example, the direct sum $V \oplus W$ is defined pointwise, with $(V \oplus W)_x = V_x \oplus W_x$. Similarly, the tensor product $V \otimes W$, the exterior product $V \wedge W$ of fibers are naturally extended to vector bundles (on the same base space). Notably, the bundle with maximal exterior power, with fiber $\Lambda^n V = V \wedge \overset{n}{\cdots} \wedge V$, is called the *determinant line bundle* (a *line bundle* is a one-dimensional vector bundle), and the bundle with typical fiber V^* (the dual vector space of V) is called the dual bundle.

It is always useful to have a scalar product at one's disposal when working on vector spaces. Given a complex vector bundle E, an **Hermitian structure** $h : E \to M$ is an Hermitian scalar product h_x on each fiber E_x which depends smoothly on x. More precisely, it is a positive-definite section $h \in \Gamma(\overline{E}^* \otimes E)$, which may be represented on local trivialization by Hermitian matrix-valued functions. A complex vector bundle equipped with an Hermitian structure is called a **Hermitian vector bundle**. We will assume vector bundles to have an Hermitian structure as soon as needed, e.g. when formula include scalar products or when adjoint operators are used.

We have seen that bundles locally look like direct products. In fact, it is possible to glue such local descriptions to reconstruct the bundle. Consider a good open cover $(U_i)_i$ of M. By definition there exist an isomorphism $\phi_i : U_i \times F \to \pi^{-1}(U_i)$ for each U_i; this is why we say that the fiber bundle *locally* looks like a direct product. In a given neighborhood U_i, local sections can be represented by usual maps $U_i \to F$. But

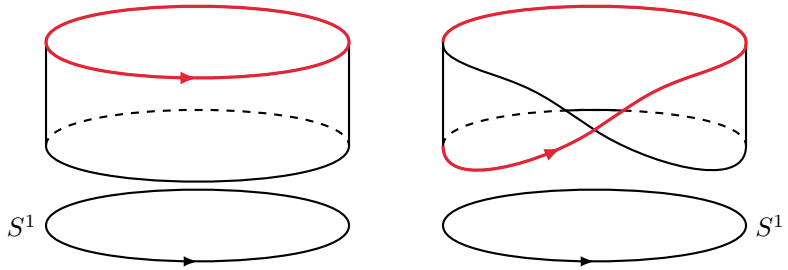

Figure 2.4: A cylinder bundle and a Möbius bundle. A cylinder (left) is a trivial bundle (with no twist), whereas a Möbius strip (right) is a nontrivial bundle (with twist). Here, we have used the typical fiber $F = [-1, 1]$ instead of $\mathbb{R}$ to get an easier object to draw. Attempts to construct a never vanishing section (successful for the cylinder, unsuccessful for the Möbius strip) are represented in red.

we need a way to go from a neighborhood to another: on the overlap $(U_i \cap U_j) \times F$, we define the **transition function**

$$\phi_{ij} = \phi_i^{-1} \phi_j. \tag{2.5}$$

Transition functions are assumed to belong to a group G of transformations of the fiber space F called the **structure group** of the bundle, which is $G = \mathrm{GL}(V)$ for vector bundles. They satisfy the so-called **cocycle conditions**,

$$\phi_{ii} = \mathrm{id} \qquad \text{and} \qquad \phi_{ij}\phi_{jk} = \phi_{ik} \tag{2.6}$$

on the intersection $U_i \cap U_j \cap U_k$ of three overlapping neighborhoods. In fact, a set of transition functions (satisfying the cocycle conditions) completely determines the bundle [Ste51, § 3].

1.2.3 Example: the Möbius bundle

To provide an intuitive picture of nontrivial bundles, let us consider a simple example: the Möbius bundle. Let the base manifold M be the circle S^1, parameterized by the angle θ. We cover it with the open sets (see also figure 2.5)

$$\begin{aligned} U_1 &= (0 - \epsilon, \pi/3 + \epsilon) \\ U_2 &= (\pi/3 - \epsilon, 2\pi/3 + \epsilon). \\ U_3 &= (2\pi/3 - \epsilon, 2\pi + \epsilon) \end{aligned} \tag{2.7}$$

(We used three open sets to avoid a non-connected intersection $U_1 \cap U_2$.) Take the typical fiber to be the line $F = \mathbb{R}$, and the structure group to be $\mathrm{GL}(\mathbb{R})$ (so we can have a vector bundle). To construct the bundle, we have to glue together the three pieces $U_i \times F$ with coordinates (θ, f_i) by specifying transition functions. In general, the transition function t_{ij} is of the form $f \mapsto \alpha f$ with $\alpha \in \mathbb{R}^* \simeq \mathrm{GL}(\mathbb{R})$. Here, we will consider two possible sets of transition functions. First, set

$$t_{12} = t_{23} = t_{31} = f \mapsto f. \tag{2.8}$$

In this case, the bundle is a trivial bundle (not twisted), which is in fact a cylinder (see figure 2.4) Another possibility is to take

$$t_{12} = t_{23} = f \mapsto f \quad \text{and} \quad t_{31} = f \mapsto -f. \tag{2.9}$$

In this case, the bundle is not trivial (it is twisted) ! It is the Möbius bundle (see figure 2.4).

Indeed, it is not possible to find a never-vanishing global section of the Möbius bundle. Intuitively, if it were so, it would be possible to make it constant, by dividing by the norm, so let us consider a constant global section. After one full turn from a starting position θ, we have crossed two transition functions $t \mapsto t$ and one transition function $t \mapsto -t$ so $s(\theta + 2\pi) = -s(\theta)$, and hence s vanishes. This illustrates the more general obstruction to define a frame of global sections in a nontrivial vector bundle.

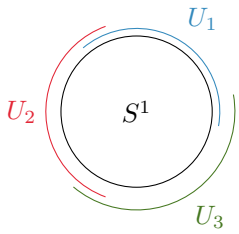

Figure 2.5: Schematic view of the open covering of the circle. Three overlapping open sets U_i are used to cover the circle S^1.

1.3 Connections on vector bundles

Vectors living in different fibers cannot be compared (e.g. added or subtracted) directly. A particular structure called a *connection* is required to do so, and in particular to extend the notion of derivatives and differential operators on fields over a manifold (i.e. on sections of a bundle over this manifold) . In the following, we consider a smooth vector bundle E of rank n with fiber F over a smooth differentiable manifold M. Let $\Gamma(E)$ be the space of (smooth) sections of E. We recall the reader that $T(M)$ is the tangent bundle to M and that $T^*(M)$ is its cotangent bundle, and $\Lambda^q T^*(M)$ its q^{th} power. The *space of E-valued q-forms on M* (or in other words, of q-forms with value in the vector bundle E) is the space of sections of $\Lambda^q T^*(M) \otimes E$

$$\Omega^q(M, E) = \Gamma(\Lambda^q T^*(M) \otimes E). \tag{2.10}$$

When $E = E_0$ is the trivial line bundle, then $\Omega^q(M) = \Omega^q(M, E_0)$ is simply the space of q-forms on M. In this case, the exterior derivative d provides a map $\mathrm{d} : \Omega^q(M) \to \Omega^{q+1}(M)$. We now aim at defining an equivalent to the exterior derivative in the case of a generic vector bundle, that is, an operator

$$\Omega^q(M, E) \to \Omega^{q+1}(M, E). \tag{2.11}$$

A **connection** on the smooth vector bundle E over M is a complex linear map

$$\nabla : \Omega^0(M, E) \equiv \Gamma(E) \to \Gamma(T^*(M) \otimes E) \equiv \Omega^1(M, E) \tag{2.12}$$

such that

$$\nabla(fs) = f\nabla(s) + \mathrm{d}f \otimes s \tag{2.13}$$

for a smooth function $f \in \Omega^0(M)$ and a section $s \in \Omega^0(M, E)$. If we have such a map, there is a unique extension to a linear map

$$\nabla : \Omega^q(M, E) \to \Omega^{q+1}(M, E) \tag{2.14}$$

such that

$$\nabla(\alpha \otimes s) = \mathrm{d}\alpha \otimes s + (-1)^{|\alpha|}\, \alpha \wedge \nabla s \tag{2.15}$$

for all $|\alpha|$-forms $\alpha \in \Omega^{|\alpha|}(M)$ on M and all F-valued $(q-|\alpha|)$-forms $s \in \Omega^{q-|\alpha|}(M, E)$. We will also call *connection* this extension.

On a Hermitian vector bundle, the connection should be required to preserve the Hermitian structure, namely to satisfy $\mathrm{d}h(s, s') = h(\nabla s, s') + h(s, \nabla s')$; such a connection is a **unitary connection**.

There is also a unique 2-form $K \in \Omega^2(M, \mathrm{End}(E))$ called the **curvature form** of the connection such that

$$\nabla^2 s = \nabla(\nabla(s)) = Ks \tag{2.16}$$

for all $s \in \Omega^q(M, E)$.

Locally, E has a basis of local sections $e_1, \ldots, e_n$ so we can write

$$\nabla e_i = \sum_j A_{ji} \otimes e_j \tag{2.17}$$

where $A_{ji} \in \Omega^1(M)$ are 1-forms on M. The $\mathrm{End}(E)$-valued 1-form A is called the (local!) **connection form**, and we have (locally)

$$\nabla s = (\mathrm{d} + A)s. \tag{2.18}$$

When a Hermitian structure is available (e_i are then assumed to be orthonormal) the connection form is

$$A_{ij} = \langle e_i, \nabla e_j \rangle\,. \tag{2.19}$$

The curvature is then given by

$$\nabla^2 e_i = \sum_j K_{ji} \otimes e_j \tag{2.20}$$

where K is a $\mathrm{End}(E)$-valued 2-form called the *curvature form*,

$$K = \mathrm{d}A - A \wedge A. \tag{2.21}$$

(that is, $K_{ij} = \mathrm{d}A_{ij} - A_{ik} \wedge A_{kj}$). The curvature form K is globally defined, and does not depend on the choice of the local trivialization.

A related notion is the *covariant derivative* along a vector field $X \in \Gamma(T(M))$, which takes a section $s \in \Gamma(E)$ and gives back another section $\nabla_X s \in T(E)$, defined as

$$\nabla_X s = \langle \nabla s, X \rangle . \tag{2.22}$$

The connection is decomposed over covariant derivatives along local coordinates as

$$\nabla s = \nabla_{\partial/\partial x^\mu}(s) \mathrm{d}x^\mu. \tag{2.23}$$

1.3.1 Projected connections on vector bundles

Consider a trivial bundle $E = M \times \mathbb{C}^n$ with the trivial connection $\nabla = \mathrm{d}$. A family of orthogonal projectors P over the base manifold M is associated with a subbundle E' of E with fiber $P(x)\mathbb{C}^n$ over $x \in M$. This defines a **projected connection**

$$\nabla^P = P\nabla = P\mathrm{d} \tag{2.24}$$

and its curvature is

$$K^P = P\mathrm{d}P \wedge \mathrm{d}P. \tag{2.25}$$

Particularly noticeable is the fact that even if ∇ is flat, ∇^P may not be.

The Berry connection in quantum mechanics is an example of projected connection, where the projectors implement the adiabatic constraint.

2 Another mathematical preliminary: topology

Mathematicians are often concerned with details. Topology is a somehow paradoxical branch of mathematics which is devoted to rigorously ignore details, and rather to focus on the global properties of certain objects, like a space or a map, which are not sensitive to the specific features of the object. Crucially, such properties are left invariant by continuous deformations of the objects they characterize, and as such, are known as *topological invariants*. In the best cases, such topological invariants fully characterize a class of objects defined up to smooth transformations. *Homotopy theory* is the most natural framework to define such topological properties, but although very easy to define, the objects in homotopy theory are generally very difficult to compute. Yet, it serves as a ground for computationally simpler but weaker theories like homology, cohomology and K-theory.

The reader may refer to [Hat03a] and [DFN85; Spa94; Uni13] for details and in [GBL08] for the big picture.

2.1 Homotopy

Two continuous maps $f_0 : X \to Y$ and $f_1 : X \to Y$ (where X and Y are smooth manifolds) are said to be **homotopically equivalent** or simply *homotopic* if there is a continuous map (called *homotopy*)

$$F : [0, 1] \times X \to Y \tag{2.26}$$

such that $F(0,x) = f_0(x)$ and $F(1,x) = f_1(x)$ for all $x \in X$. If f_0 and f_1 are smooth, it is always possible to assume that F is smooth too. Homotopy is an equivalence relation, written $f_0 \overset{\text{hom.}}{\sim} f_1$, which defines **homotopy classes**. The set of homotopy classes of maps $X \to Y$ is usually written $[X,Y]$. Note that a homotopy class always has a smooth representative, a fact which is useful to compute the homotopy class of a given map. A map equivalent to any constant map is said to be **null-homotopic**.

Two spaces X and Y are said to be **homotopically equivalent** or of the same **homotopy type**, if there are two maps $f : X \to Y$ and $g : Y \to X$ such that $f \circ g$ is homotopic to id_Y and $g \circ f$ is homotopic to id_X. Indeed, isomorphic spaces are of the same homotopy type. If X and X' (resp. Y and Y') are of the same homotopy type, then $[X,Y] \simeq [X',Y']$.

A particular attention was given to homotopy classes from the spheres (i.e. with $X = S^n$), which form a group. The **n-th homotopy group** of a manifold Y is defined as $\pi_n(Y) = [S^n, Y]$ (note that a precise definition requires the choice of a basepoint). The 0-th homotopy group $\pi_0(Y)$ lists the connected components of Y; the first homotopy group $\pi_1(Y)$ is called the **fundamental group** of Y, and describes the classes of equivalence of *closed loops* in Y. For example, $\pi_1(\mathbb{R}^2) \simeq \{1\}$ is the trivial group, because all loops on the plane are contractible to a point. On the other hand, if we remove the origin, so $Y = \mathbb{R}^2 \backslash \{0\}$, then we obtain $\pi_1(\mathbb{R}^2 \backslash \{0\}) \simeq \mathbb{Z}$, according to the number of times the loop winds around the origin (with a sign to distinguish clockwise and anticlockwise loops), see figure 2.6. As $\mathbb{R}^2 \backslash \{0\}$ and S^1 are of the same homotopy type, this illustrates that the fundamental group of the circle is $\pi_1(S^1) \simeq \mathbb{Z}$. To determine the homotopy group of spheres $\pi_p(S^q)$ is a surprisingly complicated problem. Although low-dimensional ones were indeed computed, and that there is a regularity in the so-called *stable range* when $2q \geq p+2$, all homotopy groups of spheres are not known.

2.2 Topology of vector bundles

The next section focuses on the topology of vector bundles: we want to know when two vector bundles are essentially the same. This question is motivated by considerations of physics: vector bundles are good descriptions of particular features of certain physical systems (e.g. the bands in Bloch theory), and a drastic difference between two such systems is expected to have observable physical consequences (it turns out to be the case). We focus on complex vector bundles which appear in Bloch theory. Very similar constructions appear in the study of real vector bundles and principal bundles. The interested reader is directed to the references [EGH80; Ste51; Hat03b; Hus93]. On K-theory, see [Hat03b; Kar08; Par08] for more details and [RLL00] for the operator version.

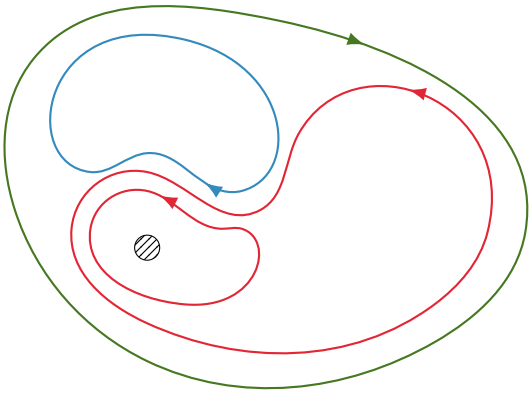

Figure 2.6: Loops on the punctured plane and their homotopy classes. The punctured plane is obtained by removing a point (or for the sake of the illustration, a hatched disk) from the plane $\mathbb{R}^2$. Several oriented paths are drawn, colored according to their homotopy class. The blue loop corresponds to a null-homotopic map, and can therefore be contracted to a point. The red loops are homotopic. However, they are not homotopic to the green loop, as their orientations are opposite. In contrast, on the full plane (without the hatched disk), all those loops would be homotopic.

2.2.1 Homotopy and the classification of vector bundles

A natural question, which will gain an important physical meaning later, is whether two vector bundles are isomorphic. In fact, given a base manifold M, we can ask what are the different possible vector bundles over M. Naturally, two vector bundles cannot be isomorphic if the fibers have not the same dimension, so we are led to consider the set $\mathrm{Vect}_{\mathbb{C}}(M, n)$ of *isomorphism classes* of n-dimensional (complex) vector bundles over M. The same results also hold when replacing all $\mathbb{C}$ with $\mathbb{R}$ and $\mathbb{C}$-linearity with $\mathbb{R}$-linearity, but we will mainly be concerned with complex vector bundles in the following.

The main idea is to replace the classification of vector bundles over M by the classification of maps from M to a particular manifold, for which the tools of homotopy theory are available. Two fundamental results allow for this reformulation:

- First, there is a relation between homotopy of maps and isomorphisms of vector bundles. Consider a vector bundle $E \to M$ and two homotopic maps $f : N \to M$ and $g : N \to M$. Then the pullback bundles f^*E and g^*E are isomorphic.
- Second, every vector bundle can be seen as the pullback bundle of a certain "universal bundle". The idea is that the base manifold of the universal bundle is made of all possible (finite-dimensional) vector spaces, and the fiber over a vector space *is* this vector space.

A consequence of the first point is that a homotopy equivalence between manifolds $f : N \to M$ induces a bijection $f^* : \mathrm{Vect}(M, n) \to \mathrm{Vect}(N, n)$. In particular, every vector bundle over a contractible base space is trivial.

The second point is made more precise in the following. First, we must define

the "universal bundle" from which we can pull back every other vector bundle. To do so, we first define its base manifold, which is called the *classifying space*. In the case of vector bundles, the classifying space is called the *Grassmannian* $\mathrm{Gr}_n(\mathbb{C}^k)$ (for $n \leq k$) as the set if all n-dimensional vector subspaces of $\mathbb{C}^k$. For example (and in the real case to simplify visualization) $\mathrm{Gr}_1(\mathbb{R}^2)$ is the set of all lines passing through the origin in the plane $\mathbb{R}^2$. The inclusions $\mathbb{C}^k \subset \mathbb{C}^{k+1} \subset \cdots$ give inclusions $\mathrm{Gr}_n(\mathbb{C}^k) \subset \mathrm{Gr}_n(\mathbb{C}^{k+1}) \subset \cdots$, so we can consider the limit

$$\mathrm{Gr}_n(\infty, \mathbb{C}) = \bigcup_k \mathrm{Gr}_n(k, \mathbb{C}) \tag{2.27}$$

which is essentially the set of all n-dimensional vector spaces. There are canonical n-dimensional vector bundles over $\mathrm{Gr}_n(k, \mathbb{C})$ and $\mathrm{Gr}_n(\infty, \mathbb{C})$, defined as

$$E_n^G(k, \mathbb{C}) = \left\{(x, v) \in \mathrm{Gr}_n(k, \mathbb{C}) \times \mathbb{C}^k\right\} \tag{2.28}$$

and again, due to natural inclusions,

$$E_n^G(\infty, \mathbb{C}) = \bigcup_k E_n^G(k, \mathbb{C}). \tag{2.29}$$

The vector bundle $E_n^G(\infty, \mathbb{C}) \to \mathrm{Gr}_n(\infty, \mathbb{C})$ is called the *universal bundle*. It was constructed in order to somehow contain all vector bundles of rank n, in the following sense: the map

$$\begin{aligned} [M, \mathrm{Gr}_n(\infty)] &\to \mathrm{Vect}(M, n) \\ [f] &\to f^* E_n^G(\infty) \end{aligned} \tag{2.30}$$

is a bijection. Hence, every vector bundle of rank n over M can be seen as a pullback bundle of the universal bundle by some map $f : M \to \mathrm{Gr}_n(\infty)$.

The sad conclusion of this construction is that generally, it is not technically possible to compute the homotopy classes $[M, \mathrm{Gr}_n(\infty)]$. As a consequence, more tools are necessary.

- First, objects called "characteristic classes" enable to explicitly compute invariants that partially characterize the topology of vector bundles. As their name indicate, the topological invariants are the same for equivalent vector bundles, but they may not be sufficient to completely characterize them. In particular, characteristic classes are cohomological objects that allow to explicitly compute those invariants as integrals of differential forms.
- Second, a weaker notion of equivalence between vector bundles, called "stable equivalence", allows to make the problem tractable, and results in what is called K-theory. The classes of stably equivalent vector bundles over a compact manifold M turns out to be a group, called the (reduced) K-group of M.

2.2.2 Characteristic classes

A nontrivial vector bundle is characterized by an obstruction to extend a local product structure to a global product structure, and in particular to find a global frame. When such a bundle is equipped with a connection ∇, we expect that the connection (and

in particular its curvature) will somehow keep track of this obstruction, as it prevents from parallel transporting a basis everywhere in a coherent way. *Characteristic classes* are quantities constructed from the curvature of the connection which turn out to depend only on the bundle (hence their name), and to (almost) provide a measure of how much it is impossible to find a global frame. In the following, we will focus on complex vector bundles, for which the characteristic classes are called "Chern classes", but a similar construction is possible also for real vector bundles.

Consider a differentiable vector bundle $E \to M$ of rank n, equipped with a connection ∇ with curvature form K. An *invariant polynomial* P is a polynomial which is invariant under the action of a group. Here, the structure group $\mathrm{GL}(k,\mathbb{C})$ acts through its adjoint action on the curvature form K at transitions between different trivializations, so we consider invariant polynomials such that $P(g^{-1}Xg) = P(X)$ for any $X \in M_k(\mathbb{C})$ and $g \in \mathrm{GL}(k,\mathbb{C})$. Invariant polynomials of the curvature form $P(K)$ are closed differential forms which turn out to depend only on the isomorphism class of E; in this sense, they are topologically invariant.

A particular invariant polynomial is the *total Chern form*, defined as

$$c(K) = \det\left(\mathrm{Id} + \frac{\mathrm{i}}{2\pi}K\right) \in H^*(M,\mathbb{R}). \tag{2.31}$$

It is expanded into homogeneous polynomials $c_j(K) \in H^{2j}(M,\mathbb{R})$ called the *jth Chern forms* as

$$c(K) = \mathrm{Id} + c_1(K) + c_2(K) + \cdots \tag{2.32}$$

with the lowest order terms

$$c_0(K) = 1 \quad c_1(K) = \frac{\mathrm{i}}{2\pi}\operatorname{tr} K \quad c_2(K) = \frac{1}{8\pi^2}\operatorname{tr}(K\wedge K) - (\operatorname{tr} K)\wedge(\operatorname{tr} K), \text{ etc.} \tag{2.33}$$

All $c_j(K)$ with $2j > \dim M$ vanish, so $c(K)$ is a finite sum.

The jth Chern form $c_j(K)$ is closed, $\mathrm{d}c_j(K) = 0$, and therefore defines a $(2j)$-th cohomology class, the *jth Chern class* $c_j(E) \in H^{2j}(M,\mathbb{R})$, which actually does not depend on the choice of the connection on E (if K and K' are the curvatures of two connections ∇ and ∇' on E, the difference $c_j(K) - c_j(K')$ is exact, so it disappears in cohomology). They are all collected into the *total Chern class* $c(E) \in H^{\mathrm{even}}(M,\mathbb{R})$.

The total Chern class "commutes" with pullbacks, given a map $f : N \to M$, the Chern class of the pullback bundle f^*E is given by the pullback $c(f^*E) = f^*c(E)$, and it factorizes on direct sums, that is[(2)] $c(E_1 \oplus E_2) = c(E_1) \wedge c(E_2)$.

The Chern class $c(E)$ only depends on the isomorphism class of E. In this sense, it is a *topological invariant*: if two bundles have different Chern classes, then they are not isomorphic. Equivalently, two isomorphic bundles share the same Chern class. However, the converse is in general not true, and two non-isomorphic bundles may share the same Chern class. More precisely, Chern classes are the primary obstruction to find global non-vanishing sections. Namely, if E has m linearly independent

[(2)] This identity is more precisely written as $c(E_1 \oplus E_2) = c(E_1) \smile c(E_2)$ where the cup product $\smile$ is defined on cohomology classes as $c = [\phi]$ and $c' = [\phi']$, $c \smile c' = [\phi \wedge \phi']$.

sections, then the last m Chern classes vanish. More precisely, besides $c_0(E) = 1$ which obviously never vanishes, we have the following properties.

- If $E \simeq M \times \mathbb{C}^n$ (so it is trivializable), then all $c_j(E) = 0$ for $j = 1, \dots, n$.
- If $E \simeq E' \oplus T_m$ where $T_m \to M$ is a trivial bundle of rank m, then $c_j(E) = 0$ for $j = n - m + 1, \dots, n$.

When they are well-normalized, the Chern forms are actually of integer class, $c_j(K) \in H^{2j}(M, \mathbb{Z})$, which means that their integral over any $2j$-cycle of M is an integer (which is a more concrete kind of topological invariant). If the base space M is a compact oriented, $2m$-dimensional manifold, one can form several $2m$-forms from the Chern forms $c_j(K)$ (by choosing a partition $j_1 + j_2 + \cdots + j_k = m$ of m and taking the product $c_{j_1}(K) \wedge \cdots \wedge c_{j_k}(K)$) and integrate them over M: the resulting numbers are integers (due to the fact that c_j belong to integer cohomology class) called *Chern numbers* of the bundle [MS74; Kha16; AI98].

All jth Chern classes are indeed invariant polynomials, and any invariant polynomial of the curvature form $P(K)$ can be expressed in terms of the $c_j(K)$. We will be particularly interested in another invariant polynomial, which gives rise to another set of useful differential forms. The *total Chern character* is defined as the closed form

$$\mathrm{ch}(K) = \mathrm{tr}\left[\exp\left(\frac{\mathrm{i}}{2\pi}K\right)\right]. \tag{2.34}$$

It is expanded as

$$\mathrm{ch}(K) = \sum_j \mathrm{ch}_j(K) \tag{2.35}$$

where $\mathrm{ch}_j(K)$ is the *jth Chern character*

$$\mathrm{ch}_j(K) = \frac{1}{j!}\left(\frac{\mathrm{i}}{2\pi}\right)^j \mathrm{tr}\left(K^j\right) \tag{2.36}$$

where $K^j = K \wedge \cdots \wedge K$ is an exterior power. Again, $\mathrm{ch}_j(K) = 0$ if $2j > \dim M$. As we said, the Chern characters can be expressed in terms of the Chern forms, with [AI98]

$$\mathrm{ch}_0 = n \qquad \mathrm{ch}_1 = c_1 \qquad \mathrm{ch}_2 = \frac{1}{2}\left(c_1^2 - 2c_2\right), \text{ etc.} \tag{2.37}$$

The Chern class behaves well for direct sums, but not for tensor products. The Chern character behaves well for both, as

$$\mathrm{ch}(E \oplus E') = \mathrm{ch}(E) + \mathrm{ch}(E') \qquad \text{and} \qquad \mathrm{ch}(E \otimes E') = \mathrm{ch}(E) \wedge \mathrm{ch}(E'). \tag{2.38}$$

2.2.3 K-theory

We will first motivate K-theory from a physical point of view, following [Kit09]. As we shall see in the section 1.1 on Bloch theory, page 57, energy bands of a solid are represented by possibly nontrivial subbundles of a trivial Bloch bundle. In condensed matter, all models are effective descriptions at low-energy to some extent. Hence, we reasonably expect the properties of a system to be unchanged if a completely

independent trivial band is added to its description, e.g. accounting for high energy excitations. For topological properties, this reasonable assumption[3] is not always satisfied: a strictly two-band system can be topologically nontrivial, but become trivial when a third (trivial and unrelated) band is added to the description. In other words, the two Hamiltonians

$$H \qquad \text{and} \qquad H \oplus E_\infty \mathrm{Id} = \begin{pmatrix} H & 0 \\ 0 & E_\infty \end{pmatrix} \tag{2.39}$$

may not be topologically equivalent. K-theory provides a slightly weaker notion of topological equivalence which gets rid of this kind of possibility.

From a slightly more mathematical point of view, the isomorphism classes of vector bundles are not "stable". That means that it is possible that two vector bundles E and E' which are not isomorphic, $E \not\simeq E'$, become isomorphic when added to another vector bundle F, that is, $E \oplus F \simeq E' \oplus F$. This kind of irregular behavior happens when the dimension of the fiber is too small to be typical. The idea of K-theory is to define a notion of "stable equivalence" between vector bundles which gets rid of this kind of pathology so that E and E' are stably equivalent. The main advantage of this approach is that it forgets enough things so that the set of stable equivalence classes i) becomes an abelian group and ii) can actually be computed in nontrivial cases.

More precisely, two vector bundles E and E' are said to be *stably equivalent*, written $E \overset{\text{st.}}{\sim} E'$, when there are integers r and s such that

$$E \oplus I_r \simeq E' \oplus I_s, \tag{2.40}$$

where I_k is the trivial vector bundles of rank k on M. When it is possible to have $r = s$, E and E' are said to be *stably isomorphic*, written $E \overset{\text{st.}}{\simeq} E'$. When M is a compact manifold, the set $\widetilde{\mathrm{K}}^0(M)$ of stable equivalence classes forms an abelian group with respect to the direct sum $\oplus$ (for each bundle E, there exists a bundle E' such that $E \oplus E'$ is trivial, which provides an inverse), called the *reduced K-theory* of M.

The reduced K-group does not take the rank of the bundle into account, as $I_r \overset{\text{st.}}{\sim} I_s$, so we define the *K-theory* of M as the set $\mathrm{K}^0(M)$ of formal difference of bundles $E - E'$ (see them as couples $E - E' = (E, E')$) with the equivalence relation

$$E_1 - E_1' = E_2 - E_2' \quad \text{iff} \quad E_1 \oplus E_2 \overset{\text{st.}}{\simeq} E_1' \oplus E_2' \tag{2.41}$$

For compact M, $\mathrm{K}^0(M)$ is an abelian group with the addition defined as

$$(E_1 - E_1') + (E_2 - E_2') = (E_1 \oplus E_2) - (E_1' \oplus E_2') \tag{2.42}$$

[3] Is this assumption really reasonable? Several topological insulators based on unstable homotopy groups were studied, starting with the so-called Hopf topological insulators [MRW08] (based on $\pi_3(S^2) \simeq \mathbb{Z}$, which is characterized by the Hopf invariant). See also [KZ15]. It is not clear to the author of this thesis whether this kind of unstable nontrivial topology may or not survive experimental realization.

and the equivalence class of $E - E$ (for any E) as the zero element[4].

Indeed, the reduced K-theory $\widetilde{\mathrm{K}}^0(M)$ can be recovered from the full K-theory $\mathrm{K}^0(M)$ by forgetting all informations about the rank of the bundles. There is an exact sequence

$$0 \longrightarrow \mathbb{Z} \longrightarrow \mathrm{K}^0(M) \longrightarrow \widetilde{\mathrm{K}}^0(M) \longrightarrow 0 \tag{2.43}$$

where the first arrow is induced by the projection of M onto a point P, $\mathbb{Z} \simeq K^0(P) \to K^0(M)$ (the K-theory of a point only keeps track of the rank of the bundle, as there is nothing else to do) and the second one is the natural homomorphism $\mathrm{K}^0(M) \to \widetilde{\mathrm{K}}^0(M)$ sending $E - I_r$ to the stable equivalence class of E. The choice of a base point $x_0 \in M$ induces a canonical splitting so that $\widetilde{\mathrm{K}}^0(M)$ is the kernel of $\mathrm{K}^0(M) \to \mathrm{K}^0(\{x_0\})$ and

$$\mathrm{K}^0(M) \simeq \mathbb{Z} \oplus \widetilde{\mathrm{K}}^0(M). \tag{2.44}$$

Finally, the Chern character ch induces an isomorphism

$$\mathrm{K}^0(M) \otimes \mathbb{R} \xrightarrow{\simeq} H^{\mathrm{even}}(M, \mathbb{R}) \tag{2.45}$$

between the torsion-free part[5] of the K-theory of M and the even cohomology of M (the tensoring with $\mathbb{R}$ removes the torsion part of K^0, and we could replace $\mathbb{R}$ by $\mathbb{C}$ or $\mathbb{Q}$ with the same effect). This isomorphism means that we may use differential forms (the Chern character forms) to actually compute the stable isomorphism class of a vector bundle, at least when $\mathrm{K}^0(M)$ has no torsion.

2.2.4 Another point of view on K-theory

Instead of focusing on vector bundles over M, we will concentrate on families of projectors on M. The two points of view are equivalent, because a vector bundle can be associated to any projector family, and conversely, a projector family to any vector bundle.

Given an abelian monoid[6] $(V, +, e)$, the *Grothendieck group* of V is

$$G(V) = V \times V / \overset{\mathrm{Gr.}}{\sim} \tag{2.46}$$

where

$$(v_1, v_2) \overset{\mathrm{Gr.}}{\sim} (u_1, u_2) \qquad \text{when} \qquad \exists\, w \in V \text{ s.t. } v_1 + u_2 + w = u_1 + v_2 + w. \tag{2.47}$$

[4] This method is called the Grothendieck construction, see later.

[5] Consider an (additive) abelian group G the *torsion subgroup* of G is the group $\mathrm{Tor}(G) = \{g \in G \mid ng = 0 \text{ for some nonzero integer } n\}$ of finite order elements. The group is has no torsion when $\mathrm{Tor}(G)$ is reduced to $\{0\}$. In any case, the quotient $G/\mathrm{Tor}(G)$ has no torsion, and tensoring with a divisible group D (like $(\mathbb{Q}, +)$ or $(\mathbb{R}, +)$) removes torsion, as $G \oplus D \cong G/\mathrm{Tor}(G) \oplus D$.

[6] A monoid $(M, \cdot, e)$ is a set M with a binary operation $\cdot : M \times M \to M$ and a neutral element $e \in M$ such that the binary operation is associative, $(a \cdot b) \cdot c = a \cdot (b \cdot c)$ and the neutral element satisfies $e \cdot a = a = a \cdot e$ for all $a \in M$. It is abelian if $a \cdot b = b \cdot a$ for all $a, b \in M$, and in this case the binary operation is preferentially written $+$. Standard examples include the natural numbers $(\mathbb{N}, +, 0)$ (where $\mathbb{N}$ includes 0) with the addition and the positive integers $(\mathbb{N}^*, \times, 1)$ with the multiplication.

It is a group with neutral element $[(v,v)] = [(e,e)]$ and the sum

$$[(v_1,v_2)] + [(u_1,u_2)] = [(u_1+v_1, u_2+v_2)] \tag{2.48}$$

for which

$$[(v_1,v_2)] = -[(v_2,v_1)]. \tag{2.49}$$

A familiar example is the construction of all integers $a-b=(a,b)$ from the non-negative integers with equivalence relation $a-b \overset{\text{Gr.}}{\sim} c-d$ iff $a+d=c+b$.

Let $\mathcal{P}_n(M)$ represent continuous families of $n\times n$ matrix orthogonal projectors over M, that is

$$\mathcal{P}_n(M) = \left\{ P\in C^0(M, M_n(\mathbb{C})) \mid P(x)^2 = P(x) = P^\dagger(x) \text{ for } x\in M \right\}. \tag{2.50}$$

There is an obvious inclusion $\mathcal{P}_n \hookrightarrow \mathcal{P}_{n+1}$ which send p to $p\oplus 0$, so we can take the ascending union

$$\mathcal{P}_\infty(M) = \bigcup_n \mathcal{P}_n(M). \tag{2.51}$$

Two elements $p,q\in\mathcal{P}_\infty(M)$ are said to be homotopic in $\mathcal{P}_\infty(M)$, written $p \overset{\text{hom.}}{\sim} q$, if there is a sufficiently large $\mathcal{P}_n(M)\ni p,q$ where they are homotopic.

The K-group $\mathrm{K}^0(M)$ is

$$\mathrm{K}^0(M) = G(\mathcal{P}_\infty/\overset{\text{hom.}}{\sim}). \tag{2.52}$$

In other words, it represents stable equivalence classes of projector maps on M, which is consistent with the vector bundle picture.

The same game can be played with unitary maps $\mathcal{U}_n(M)$ (except the inclusion is now given by $u\mapsto u\oplus 1$) and we define the K-group $\mathrm{K}^1(M)$ as

$$\mathrm{K}^1(M) = \mathcal{U}_\infty/\overset{\text{hom.}}{\sim} \tag{2.53}$$

which represents stable equivalence classes of unitary maps on M.

As we have seen in the previous section for the group K^0, we can compute the torsion free part of K-theory from cohomology through the Chern isomorphisms

$$\begin{aligned} \mathrm{K}^0(M)\otimes_{\mathbb{Z}}\mathbb{R} &\simeq H^{\text{even}}(M,\mathbb{R}) \\ \mathrm{K}^1(M)\otimes_{\mathbb{Z}}\mathbb{R} &\simeq H^{\text{odd}}(M,\mathbb{R}). \end{aligned} \tag{2.54}$$

We have seen that the first one is realized by the Chern character (2.35). When the vector bundle at hand is defined by a family of projector $P\in\mathcal{P}_n(M)$ (by setting the fiber over $x\in M$ to be $P(x)\mathbb{C}^n$), the **(even) Chern character form associated to** P is expressed in terms of the corresponding projected connection (2.25) as

$$\mathrm{ch}(P) = \sum_n \mathrm{ch}_n(P) = \sum_{n\geq 0} \frac{1}{n!}\left(\frac{\mathrm{i}}{2\pi}\right)^n \mathrm{tr}\left[P(\mathrm{d}P)^{2n}\right] \tag{2.55}$$

where $(\mathrm{d}P)^{2n} = \mathrm{d}P \wedge \overset{2n}{\cdots} \wedge \mathrm{d}P$.

Following [ASSS89], we define the corresponding **n-th Chern invariant** associated to the closed $2n$-dimensional submanifold X of M as the period

$$C_n(P, X) = \int_X \mathrm{ch}_n(P). \tag{2.56}$$

The Chern invariants are in general not equal to the Chern numbers defined above (so we did not use the same name), though they are related through equation (2.37). However, the first Chern invariant C_1 and the first Chern number $\tilde{C}_1$ are the same, and it is common to call it that way.

In the case of unitary maps $U \in \mathcal{U}(M)$, the Chern isomorphism is realized by the *odd Chern character associated to* U, defined as [Par08, p. 197] (see also [Get93; TWZ13]))

$$\widetilde{\mathrm{ch}}(U) = \sum_{n\geq 0} \widetilde{\mathrm{ch}}_n(U) = \sum_n (-1)^n \frac{n!}{(2n+1)!} \left(\frac{\mathrm{i}}{2\pi}\right)^{n+1} \mathrm{tr}\left[(U^{-1}\mathrm{d}U)^{2n+1}\right]. \tag{2.57}$$

The homogeneous forms $\widetilde{\mathrm{ch}}_n(U)$ are called the *odd Chern forms*. We have

$$\widetilde{\mathrm{ch}}(U) + \widetilde{\mathrm{ch}}(U^{-1}) = 0. \tag{2.58}$$

We then define the **n-th winding number** (or **degree**, or **odd Chern invariant**) of U associated to the closed $(2n+1)$-dimensional submanifold X of M as the period

$$W_n(U, X) = \int_X \widetilde{\mathrm{ch}}_n(U). \tag{2.59}$$

When X is a spherical cycle, this winding number is guaranteed to be an integer [BS78]. Note that if D is a diffeomorphism on the manifold X, then $W_n(U \circ D, X) = \pm W_n(U, X)$ where the positive (negative) sign applies if D is an orientation-preserving (orientation reversing) diffeomorphism.

The winding number essentially counts the number of times the map V winds around nontrivial $(2n+1)$-cycles in $U(N)$. For instance, in the case of $d = 0$ (so $n = 0$)

$$\deg(V) = \frac{\mathrm{i}}{2\pi} \int \mathrm{tr}(V^{-1}(\varphi)V'(\varphi))\,\mathrm{d}\varphi \tag{2.60}$$

so the map $S^1 \to U(1)$ defined by $f(\varphi) = 1$ has no winding, whereas the map defined by $g(\varphi) = \mathrm{e}^{-\mathrm{i}\varphi}$ has a winding $\deg(g) = 1$.

The odd Chern character can in fact be defined for any invertible family $G : M \to \mathrm{GL}(n)$ [Get93]. Now, by polar decomposition, G can always be written as

$$G(x) = U(x)H(x) \tag{2.61}$$

for $x \in M$, where $U : M \to U(n)$ is a unitary family and where $H : M \to \mathrm{HPD}(n)$ is a family of Hermitian positive definite matrices. As $\mathrm{HPD}(n)$ is a star domain, there is an homotopy defined by

$$H_s(x) = s\mathrm{Id} + (1-s)H(x) \tag{2.62}$$

from H to the constant map Id, with $H_s(x) \in \mathrm{HPD}(n)$ for all $s \in [0,1]$ and all $x \in M$. This gives an homotopy defined by

$$G_s(x) = U(x)H(x) \tag{2.63}$$

from $G_0 = G$ to $G_1 = U$, so we can deform the invertible map G to a unitary map U with the same winding.

Notice that what we quickly sketched is topological K-theory, which is defined through vector bundles. A noncommutative analogue is operator K-theory, which is based on C^*-algebra (see [RLL00]). The topological K-theory of M is recovered as the operator K-theory of continuous functions on M as $\mathrm{K}^q(M) \simeq \mathrm{K}_q(C(M))$, but it is possible to consider more general C^*-algebra, for example covering disordered systems: see e.g. [PS16] and [Kel15].

2.3 Example: vector bundles over a sphere

We will consider the very simple example of vector bundles over the 2-sphere S^2. This example is motivated by the fact that (gapped) Bloch Hamiltonians (see section 1) in space dimension d are closely related to vector (sub)bundles over S^d (which is called the Poincaré-Bloch sphere in the case $d = 2$). We will see in the next chapter that when weak topological invariants vanish, it is possible to replace the Brillouin torus by a sphere to describe the strong invariants as stemming from a nontrivial topology of vector bundles over the sphere.

2.3.1 A nontrivial vector bundle

Starting from the trivial vector bundle $E = S^2 \times \mathbb{C}^2$, we will split it into two nontrivial bundles $E_\pm$ by constructing projection operators $P_\pm : E \to E_\pm$.

First embed S^2 into $\mathbb{R}^3$ with coordinates (x_1, x_2, x_3) as the surface

$$S^2 \simeq \left\{ x \in \mathbb{R}^3 \mid x^2 \equiv \sum x_i^2 = 1 \right\}. \tag{2.64}$$

It will be convenient to use spherical coordinates

$$x \simeq \begin{pmatrix} x_1 \\ x_2 \\ x_3 \end{pmatrix} = \begin{pmatrix} \sin\theta\, \cos\phi \\ \sin\theta\, \sin\phi \\ \cos\theta \end{pmatrix}. \tag{2.65}$$

The trivial vector bundle E is endowed with a natural connection $\nabla = \mathrm{d}$ defined by

$$\langle e_i(x), \nabla s(x) \rangle = \mathrm{d} \langle e_i(x), s(x) \rangle. \tag{2.66}$$

for a constant frame $(e_i)_i$ and a section s. Notice that this definition does not depend on the choice of the *constant* frame of global sections. It is flat, $\nabla^2 = 0$ due to $\mathrm{d}^2 = 0$.

Define the matrix (in fact a section of the endomorphism bundle $\mathrm{End}(E) = E \otimes E^*$)

$$H(x) = \sum_i x_i \sigma_i = \begin{pmatrix} x_3 & x_1 - \mathrm{i}x_2 \\ x_1 + \mathrm{i}x_2 & -x_3 \end{pmatrix} \tag{2.67}$$

where σ_i are Pauli matrices (see appendix A, page 54). (As the name suggests, this matrix will later be related to a Hamiltonian.)

Observe that $H^2(x) = \mathrm{Id}$ (as $x \in S^2$), so the eigenvalues of $H(x)$ are either ± 1. Projectors

$$P_\pm(x) = \frac{1}{2}\left(\mathrm{Id} \pm H(x)\right) \tag{2.68}$$

on the corresponding eigenspaces allow to define two subbundles of E, namely $E_\pm$ with fiber $P_\pm(x)\mathbb{C}^2$ over $x \in S^2$. Indeed, $E = E_+ \oplus E_-$. A *projected connection* $\nabla_\pm$ may be defined on $E_\pm$ by

$$\nabla_\pm = P_\pm \nabla. \tag{2.69}$$

Its curvature is given by

$$K_\pm = \nabla_\pm^2 = P_\pm \mathrm{d}P_\pm \wedge \mathrm{d}P_\pm. \tag{2.70}$$

We can use equation (2.68) and the explicit[7] expression (2.67) of H to compute its trace as

$$\mathrm{tr}(K_\pm) = \pm\frac{\mathrm{i}}{4}\epsilon^{ijk} x_i \mathrm{d}x_j \wedge \mathrm{d}x_k = \pm\frac{\mathrm{i}}{2}\mathrm{vol}_{S^2} \tag{2.71}$$

where vol_{S^2} is the (unnormalized) volume form on S^2.

For concreteness, focus on the "valence bundle" E_- and we set $P = P_-$, $K = K_-$. As S^2 is a 2-manifold, its is characterized by only one Chern invariant (which is also the first Chern number)

$$C_1 = \frac{\mathrm{i}}{2\pi}\int_{S^2} \mathrm{tr}\, K = \frac{1}{4\pi}\int_{S^2} \mathrm{vol}_{S^2} = 1, \tag{2.72}$$

so we conclude that the bundle E_- is nontrivial!

2.3.2 Another look at the same problem: connection forms and transition functions

To gain an understanding of what happens, it may be useful to look at a local picture. Eigenstates of $H(x)$ are, up to a phase,

$$|\psi_+(\theta,\phi)\rangle = \begin{pmatrix} \cos\frac{\theta}{2} \\ \sin\frac{\theta}{2}\mathrm{e}^{\mathrm{i}\phi} \end{pmatrix} \qquad \text{and} \qquad |\psi_-(\theta,\phi)\rangle = \begin{pmatrix} -\sin\frac{\theta}{2} \\ \cos\frac{\theta}{2}\mathrm{e}^{\mathrm{i}\phi} \end{pmatrix}. \tag{2.73}$$

In the following, we will focus on the "filled" state $|\psi_-\rangle$ and the corresponding subbundle E_- for concreteness.

The vector $|\psi_-\rangle$ has an ill-defined phase in the limit $\theta \to 0$. Indeed, we may change the global phase of the vector, but it would only move the singularity: there is an obstruction to define $|\psi_-\rangle$ on the whole sphere due to the nonvanishing first Chern number. Let us therefore consider an open cover of the sphere composed of two overlapping hemispheres U_N and U_S (see figure 2.7). Their intersection is homotopic to the equator of the sphere which is a circle, $\mathcal{C} = U_\mathrm{N} \cap U_\mathrm{S} \simeq S^1$, and can be viewed

[7] Even more explicitly with coordinates $(x_1, x_2, x_2) = (x, y, z)$, we have $\mathrm{tr}(K_\pm) = \pm(\mathrm{i}/2)(x\mathrm{d}y \wedge \mathrm{d}z + y\mathrm{d}z \wedge \mathrm{d}x + z\mathrm{d}x \wedge \mathrm{d}y)$.

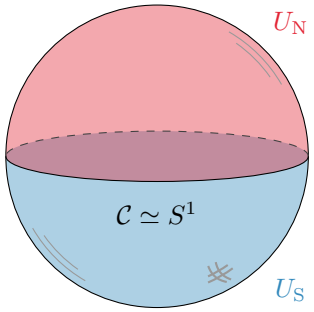

Figure 2.7: Open covering of the 2-sphere.

as the boundary $\mathcal{C} = \partial U_{\mathrm{N}} = -\partial U_{\mathrm{S}}$ (they have opposite orientations). We define a local frame of E_- on each hemisphere by

$$|\psi_-^{\mathrm{S}}(\theta,\phi)\rangle = \begin{pmatrix} -\sin\frac{\theta}{2} \\ \cos\frac{\theta}{2}\mathrm{e}^{\mathrm{i}\phi} \end{pmatrix} \qquad \text{and} \qquad |\psi_-^{\mathrm{N}}(\theta,\phi)\rangle = \begin{pmatrix} -\mathrm{e}^{-\mathrm{i}\phi}\sin\frac{\theta}{2} \\ \cos\frac{\theta}{2} \end{pmatrix} \tag{2.74}$$

so $|\psi_-^{\mathrm{N/S}}\rangle$ is well defined on $U_{\mathrm{N/S}}$. The transition function from the trivialization on U_{N} to the one on U_{S} is a phase change on the equator $\mathcal{C}$ given by the map $t_{\mathrm{NS}} : \mathcal{C} \to U(1)$ defined by

$$t_{\mathrm{NS}}(\phi) = \mathrm{e}^{-\mathrm{i}\phi}. \tag{2.75}$$

On the southern hemisphere U_{S}, we have a frame of eigenstates $(\psi_+^{\mathrm{S}}, \psi_-^{\mathrm{S}})$. In this basis, the projector $P_- \simeq \mathrm{diag}(0,1)$ is obviously diagonal so the projected connection is fully defined by the application of (2.19) which yields

$$A = A^{\mathrm{S}} = A_-^{\mathrm{S}} = \langle \psi_-^{\mathrm{S}}, \mathrm{d}\psi_-^{\mathrm{S}} \rangle \tag{2.76}$$

and the curvature is

$$K = \mathrm{d}A - A \wedge A = \mathrm{d}A \tag{2.77}$$

as A is only a 1×1 matrix (so $K = \mathrm{tr}\, K$ and $A = \mathrm{tr}A$). Therefore, the connection form is

$$A = \mathrm{i}\cos^2\left(\frac{\theta}{2}\right)\mathrm{d}\phi \tag{2.78}$$

and the curvature is

$$K = \mathrm{d}A = -\frac{\mathrm{i}}{2}\sin\theta \mathrm{d}\theta \wedge \mathrm{d}\phi. \tag{2.79}$$

The same game can be played on the northern hemisphere, giving a connection form A_-^{N}. On the intersection between the hemispheres, both connection forms are related by the transition function by

$$\mathrm{tr}A_-^{\mathrm{N}} = \mathrm{tr}A_-^{\mathrm{S}} + \mathrm{tr}\left[t_{\mathrm{NS}}^{-1}\mathrm{d}t_{\mathrm{NS}}\right] \tag{2.80}$$

so in our case

$$A_-^{\mathrm{N}} = A_-^{\mathrm{S}} - \mathrm{id}\phi \tag{2.81}$$

so as expected the curvature does not depend on the choice of the local trivialization.

In order to highlight its interpretation as an obstruction to define eigenvectors on the whole sphere, we now express the first Chern number as the winding number of the transition function t_{NS}. Indeed,

$$C_1 = \frac{\mathrm{i}}{2\pi}\int_{S^2} \mathrm{tr}\, K = \frac{\mathrm{i}}{2\pi}\left(\int_{U_{\mathrm{N}}} \mathrm{tr}\, K + \int_{U_{\mathrm{S}}} \mathrm{tr}\, K\right). \tag{2.82}$$

On each open set $U_{\mathrm{N/S}}$, we have $\mathrm{tr}\, K = \mathrm{d}\mathrm{tr} A_-^{\mathrm{N/S}}$ so we have

$$C_1 = \frac{\mathrm{i}}{2\pi}\left(\int_{\partial U_{\mathrm{N}}} \mathrm{tr} A_-^{\mathrm{N}} + \int_{\partial U_{\mathrm{S}}} \mathrm{tr} A_-^{\mathrm{S}}\right) = \frac{\mathrm{i}}{2\pi}\int_{\partial U_{\mathrm{N}}} (\mathrm{tr} A_-^{\mathrm{N}} - \mathrm{tr} A_-^{\mathrm{S}}) \tag{2.83}$$

(remind that the boundaries of the two hemispheres are the same, but with opposite orientations). Using equation (2.81),

$$C_1 = \frac{\mathrm{i}}{2\pi}\int_{S^2} \mathrm{tr}\, K = \frac{\mathrm{i}}{2\pi}\int_{\partial U_{\mathrm{N}}} \mathrm{tr}\left[t_{\mathrm{NS}}^{-1}\mathrm{d}t_{\mathrm{NS}}\right] \tag{2.84}$$

The last integral is readily computed as

$$C_1 = \frac{\mathrm{i}}{2\pi}\int_{S^1} (-\mathrm{id}\phi) = 1 \tag{2.85}$$

as we already knew.

2.3.3 A higher-dimensional generalization

It would be a shame not to mention that this construction generalizes to the bundle $S^d \times \mathbb{C}^{2^\ell}$, by replacing Pauli matrices by a set of d generalized Dirac matrices $(\Gamma_0, \dots, \Gamma_n)$, which are $2^\ell \times 2^\ell$ Hermitian matrices obeying

$$\Gamma_i\Gamma_j + \Gamma_j\Gamma_i = 2\delta_{ij}\mathrm{Id} \qquad \text{and} \qquad \Gamma_0\Gamma_1\cdots\Gamma_d = \mathrm{i}^\ell\mathrm{Id}. \tag{2.86}$$

In fact, nearly nothing changes, except in the expressions in terms of coordinates, and in the explicit expression of the curvature which generalizes to [EGH80]

$$\mathrm{tr}(K_\pm) = \pm\frac{d!\,(2\mathrm{i})^\ell}{2^{d+1}}\,\mathrm{vol}_{S^d}. \tag{2.87}$$

Appendix A – Pauli matrices

A.1 Definition

We define Pauli matrices

$$\sigma_1 = \sigma_x = \begin{pmatrix} 0 & 1 \\ 1 & 0 \end{pmatrix} \qquad \sigma_2 = \sigma_y = \begin{pmatrix} 0 & -\mathrm{i} \\ \mathrm{i} & 0 \end{pmatrix} \qquad \sigma_3 = \sigma_z = \begin{pmatrix} 1 & 0 \\ 0 & -1 \end{pmatrix}. \tag{2.88}$$

They are often supplemented with the identity $\sigma_0 = \mathrm{Id}$. A common convention consists of using Latin indices $i, j, \dots$ starting from 1 to exclude the identity, and Greek indices $\mu, \nu, \dots$ starting from 0 to include it.

A.2 General properties

Pauli matrices are traceless, with determinant -1,

$$\mathrm{tr}(\sigma_i) = 0 \qquad \text{and} \qquad \det(\sigma_i) = -1. \tag{2.89}$$

They are involutive,

$$\sigma_i^2 = \mathrm{Id}. \tag{2.90}$$

A.3 Commutation and anticommutation rules

Pauli matrices obey the commutation rules

$$[\sigma_i, \sigma_j] = 2\mathrm{i}\,\varepsilon_{ijk}\sigma_k. \tag{2.91}$$

As a consequence, when correctly normalized, they form a representation of $\mathfrak{su}(2)$, and

$$\mathfrak{su}(2) = \mathrm{span}_{\mathbb{R}}\left(\frac{\mathrm{i}\sigma_1}{2}, \frac{\mathrm{i}\sigma_2}{2}, \frac{\mathrm{i}\sigma_3}{2}\right). \tag{2.92}$$

Furthermore, they generate the Clifford algebra Cl_3, as

$$\{\sigma_i, \sigma_j\} = 2\delta ij\mathrm{Id}. \tag{2.93}$$

The two previous relations give the product of two Pauli matrices as

$$\sigma_i\sigma_j = \delta ij\mathrm{Id} + \mathrm{i}\,\varepsilon_{ijk}\sigma_k. \tag{2.94}$$

A.4 Pauli matrices as a basis of two-by-two Hermitian matrices

Together with the identity $\sigma_0 = \mathrm{Id}$, Pauli matrices form a basis of the *real* vector space of two-by-two Hermitian matrices (and a basis of the *complex* vector space of all two-by-two matrices if the coefficients are allowed to be complex). This basis is orthonormal for the scalar product

$$\langle A, B\rangle = \frac{1}{2}\mathrm{tr}(AB) \tag{2.95}$$

so any two-by-two Hermitian matrix is decomposed as

$$M = \sum_\mu \langle\sigma_\mu, M\rangle\,\sigma_\mu. \tag{2.96}$$

In such a decomposition, the components can be cast into a "Pauli vector" $\vec{m} = (m_1, m_2, m_3)$ (and if needed in a "Pauli 4-vector" $m^\mu = (m_0, m_1, m_2, m_3)$) so that we can symbolically write the decomposition as

$$M = m_0\mathrm{Id} + \vec{m}\cdot\vec{\sigma} = m^\mu\sigma_\mu. \tag{2.97}$$

where $\vec{\sigma} = (\sigma_1, \sigma_2, \sigma_3)$.

A.5 Combination of Pauli vectors

The matrix product of two-by-two matrices induces a composition law for Pauli (quadri)vectors through the identity

$$(a^\mu \sigma_\mu)(b^\nu \sigma_\nu) = c^\rho \sigma_\rho \tag{2.98}$$

with

$$c^\rho = \begin{pmatrix} a_0 b_0 + \vec{a} \cdot \vec{b} \\ a_0 \vec{b} + b_0 \vec{a} + \mathrm{i}\, \vec{a} \times \vec{b} \end{pmatrix} \tag{2.99}$$

where $\times$ is the cross-product of $\mathbb{C}^3$-vectors. A more simple version of this equation is often useful,

$$(\vec{a} \cdot \sigma)(\vec{b} \cdot \sigma) = \vec{a} \cdot \vec{b}\, \mathrm{Id} + \mathrm{i}(\vec{a} \times \vec{b}) \cdot \sigma. \tag{2.100}$$

A.6 Exponential of Pauli matrices

For a *normalized* vector n and a real θ,

$$\exp(\mathrm{i}\theta \vec{n} \cdot \vec{\sigma}) = \cos\theta\, \mathrm{Id} + \mathrm{i} \sin\theta\, \vec{n} \cdot \vec{\sigma} \tag{2.101}$$

Chapter 3

Topological insulators and topological phases

This chapter is devoted to a (partial and biased) review of topological insulators, in a way which prepares for the core of this work, devoted to the topology of crystals under a time-periodic perturbation. In a first time, I will remind the reader of the Bloch theory of waves in periodic media in a way that highlights its underlying mathematical structure: a band, in Bloch theory, is described by a spectral projector over an energy range, and this defines a complex vector bundle, which may or not be topologically trivial. This possibility leads to the notion of topological insulators, which are reviewed in a second part.

1 Band theory

1.1 Bloch theory

The description of electrons in a crystalline solid rely on the fundamental assumption that they evolve in a fixed background of nuclei lying on a spatially periodic lattice (the crystal), giving rise to a spatially periodic attractive potential. This separation between nuclear and electronic degrees of freedom is known as the Born-Oppenheimer approximation. In a real material, a handful of deviations from this ideal description arise (due to e.g. defects and impurities), but they are usually treated as a perturbation of the crystalline solid. This is because the description of an ideal periodic material is enormously simplified by the so-called *Bloch decomposition*. We will describe it from two complementary points of view. The aim of Bloch decomposition is to use the discrete translational invariance of the Hamiltonian to block-diagonalize it as much as possible. A full translational invariance would ensure the conservation of the momentum; in such a system, plane waves with fixed momentum are eigenstates of the evolution, and any state of the system can be decomposed as a superposition of such plane waves. In a system with only discrete translational invariance such as a crystal, momentum is no more conserved; yet the *quasi-momentum*, defined as the momentum modulo a reciprocal lattice vector, is still conserved. The corresponding eigenstates of the evolution are called *Bloch waves*, which are simply plane waves with an additional spatial modulation on small spatial scales (on the level of the unit cell of the crystal).

In all this work, we will make use of the so-called *tight-binding approximation* to describe the (valence) electrons of the crystal. Its main idea is to fix the position of atoms on a lattice and to then allow electrons to tunnel from (the atomic orbital of) one atom to another, usually a neighbor or a next-neighbor, through what is called a hopping process. It is obvious that this description is artificial, effective, and unsatisfactory as the sharing of electrons is the main reason why the crystal holds together and therefore the main cause of the positioning of atoms on a lattice, although this was arbitrarily fixed by the theoretician from the beginning. Yet, tight binding models are incredibly useful in order to understand complicated features of electrons in solids (such as the topological phases this work deals with), because they allow to focus on the relevant degrees of freedom (the electrons), and because although they do not enable to realize ab-initio prediction, they can still be, as an effective model, related to experimental situations.

As we have seen, tight-binding models are effective in essence, so it is perfectly reasonable to only include relevant degrees of freedom; for example, when describing graphene, only the out-of-plane $2\,\mathrm{p_z}$ atomic orbitals are included. Other internal degrees of freedom such as spin can also be included if needed. Not all crystals are Bravais lattices: for example, the honeycomb lattice of graphene has a triangular Bravais lattice with two sublattices (equivalently, two sites per unit cell) usually called A and B. After the Bloch decomposition, those sublattice degrees of freedom are more or less on the same footing as genuine internal degrees of freedom, so we will gather them as a whole and let N be their count. Indeed, Bloch decomposition is particularly useful in a tight-binding setting, because after having block-diagonalized the translational degrees of freedom, one is left with a (family of) $N \times N$ matrix Hamiltonian(s), N being, as we previously stated, the number of degrees of freedom inside a unit cell. Matrices being considerably easier to deal with than functions, this simplification is really helpful.

We will now rephrase this inside a standard mathematical framework. A classical mathematical reference for Bloch-Floquet theory of Schrödinger operators with periodic potentials is the chapter XIII.16 of [RS78]. For more solid-state physics oriented references, see Ziman's excellent book [Zim79] as well as Marder's more recent textbook [Mar15].

We first need to introduce the notion of a fundamental domain. Given a set X and a group G acting on it, we can define an equivalence relation by $x \sim y$ whenever $y = g \cdot x$, for $x, y \in X$ and $g \in G$. The set of all equivalence classes is then the **quotient** X/G. A **fundamental domain** for a group action of G on X is a choice of exactly one representative for each equivalence class; or alternatively one of the numerous possible ways to embed X/G in X. Formally, it is a subset $\mathcal{F} \subset X$ such that $\cup_{g\in G}\, g \cdot \mathcal{F} = X$ and that $\cap_{g\in G}\, g \cdot \mathcal{F}$ has no interior.

We consider atoms arranged on a **crystal** $\mathcal{C}$, a discrete subset of the d-dimensional Euclidean space $\mathbb{E}^d$ representing the locations of atoms. The periodicity of the crystal is taken into account by the fact that it is acted upon by a Bravais lattice $\Gamma \subset \mathbb{R}^d$ of discrete translations, $\Gamma \simeq \mathbb{Z}^d$ (as groups). For non-Bravais crystals, there are $m = |\mathcal{C}/\Gamma|$ classes of translationally equivalent points of $\mathcal{C}$ called **sublattices** (for example, the hexagonal lattice of graphene has two sublattices). The Bravais lattice

is composed of vectors connecting sites of the same sublattice. The set of sublattices $\mathcal{C}/\Gamma$ may be represented by a **unit cell** $\mathcal{F} \subset \mathcal{C}$, which has one point in each sublattice, i.e. it is a fundamental domain for the action of the translation group Γ on $\mathcal{C}$. A translation of $\mathcal{F}$ by a Bravais vector is also a possible choice for a unit cell but when there are several sublattices, i.e. $m > 1$, then there are choices of $\mathcal{F}$ that are not related in this way (one can e.g. take representatives for the different sublattices arbitrarily far from each other).

Along with the translational degrees of freedom, one may consider a finite number n of internal degrees of freedom, e.g. different orbitals or the spin of electrons, represented as a finite-dimensional complex vector space V, with $\dim(V) = n$, equipped with a scalar product $\langle \cdot, \cdot \rangle_V$. The Hilbert space of crystalline states is then the space $\mathcal{H} = \ell^2(\mathcal{C}, V)$ of V-valued square-summable functions on $\mathcal{C}$ with the scalar product

$$\langle \psi | \chi \rangle = \sum_{x \in \mathcal{C}} \langle \psi(x) | \chi(x) \rangle_V . \tag{3.1}$$

We now want to use the discrete translations to decompose the Hilbert space $\mathcal{H}$ into a direct sum of fixed quasi-momentum components; as we will see, the translational invariance of the Hamiltonian will ensure that it is block-diagonalized by this decomposition.

Remember that the crystal is embedded in the Euclidean space $\mathbb{E}^d$. Translations in $\mathbb{E}^d$ live in its translation vector space $T \simeq \mathbb{R}^d$. The dual vector space $T^* \simeq \mathrm{Hom}(T, \mathbb{R}) \simeq \mathbb{R}^d$ is the set of **reciprocal vectors**, which are in fact linear forms in disguise: a reciprocal vector $k \in T^*$ is in fact a linear map $\chi_k : v \mapsto k \cdot v$ for $v \in T$. The translation of states $\psi \in \mathcal{H}$ by a vector $\gamma \in \Gamma \subset T$ of the Bravais lattice is defined by the unitary **translation operator** T_γ such that $T_\gamma \psi(x) = \psi(x - \gamma)$ for $x \in \mathcal{C}$. Operators T_γ define a representation of the translation group Γ in $\mathcal{H}$ which may be decomposed into irreducible components. As the translation group Γ is abelian, its irreducible representations are its characters (which are one-dimensional),

$$\chi_k : \gamma \mapsto \mathrm{e}^{\mathrm{i}k \cdot \gamma} \tag{3.2}$$

where $k \in T^*$ is a reciprocal vector. Let us now define the **reciprocal lattice** $\Gamma^* = \mathrm{Hom}(\Gamma, \mathbb{Z})$ (composed of **reciprocal lattice vectors** $G \in T^*$ with $G \cdot \gamma \in 2\pi\mathbb{Z}$) and notice that $\mathrm{e}^{\mathrm{i}k \cdot \gamma} = \mathrm{e}^{\mathrm{i}(k+G) \cdot \gamma}$ for $G \in \Gamma^*$. Hence, the characters of Γ form a group, the *Pontryagin dual* $\hat{\Gamma}$ of Γ, which is also a d-dimensional torus called the **Brillouin torus**:

$$\mathrm{BZ} \equiv \hat{\Gamma} \equiv T^*/\Gamma^* \simeq \mathbb{T}^d. \tag{3.3}$$

The elements $\overline{k} \in \mathrm{BZ}$ are called **quasi-momenta**, and we will follow a longstanding tradition of careless physicists and identify them with any of their lifts k (or $k + G$) in T^*. A choice of a fundamental domain $\mathcal{F}^* \subset T^*$ to represent the Brillouin torus is called a **Brillouin zone** (usually, it is a *Wigner-Seitz cell*, also called a *Voronoi cell*, defined as the closure of the set of all points in T^* which are closer to some $v \in \Gamma^*$ than to any other point of Γ^*, the most common choice being the *first Brillouin zone* where v is the origin).

The decomposition of $\mathcal{H}$ into irreducible components is realized by the Fourier transform $\psi \mapsto \widehat{\psi}$, where

$$\widehat{\psi}(k,x) = \sum_{\gamma\in\Gamma} \mathrm{e}^{-\mathrm{i}k\cdot\gamma}\psi(x-\gamma). \tag{3.4}$$

Note that $\widehat{\psi}(k) = \widehat{\psi}(k+G)$ and

$$\widehat{\psi}(k,x-\gamma) = \mathrm{e}^{\mathrm{i}k\cdot\gamma}\widehat{\psi}(k,x) \tag{3.5}$$

so that $(\widehat{T_\gamma\psi})(k,x) = \mathrm{e}^{\mathrm{i}k\cdot\gamma}\,\widehat{\psi}(k,x)$. This property defines the **Bloch functions** on $\mathcal{C}$ with quasi-momentum k, which for fixed k form a finite-dimensional **Bloch space**

$$\mathcal{H}(k) = \left\{\psi\in\mathcal{H} \mid \psi(x-\gamma) = \mathrm{e}^{\mathrm{i}k\cdot\gamma}\psi(x) \text{ for } \gamma\in\Gamma\right\} = \mathcal{H}(k+G) \tag{3.6}$$

that may be equipped with the scalar product

$$\langle\varphi(k) \mid \chi(k)\rangle_k = \sum_{x\in\mathcal{C}/\Gamma} \overline{\varphi(k,x)}\chi(k,x). \tag{3.7}$$

Bloch spaces $\mathcal{H}(k)$ are defined canonically for each k, without any further choices. As a Bloch function is determined by its values on a unit cell $\mathcal{F}\subset\mathcal{C}$, their dimension is $\dim(\mathcal{H}(k)) = (\mathrm{card}\mathcal{F})\times(\dim V) = m\times n = N$.

Geometrically, the collection of vector spaces $\mathcal{H}(k)$ forms a complex N-dimensional vector bundle $\mathcal{H}$ over the Brillouin torus BZ that we shall call the **Bloch bundle**, and we will see that it is trivializable. Spaces $\mathcal{H}(k)$ are the fibers of $\mathcal{H}$ and their scalar product equips $\mathcal{H}$ with a Hermitian structure. Sections of $\mathcal{H}$ are maps $k\mapsto\varphi(k)\in\mathcal{H}(k)$, and they are smooth if functions $k\mapsto\varphi(k,x)$ are smooth for all x. The Fourier transform (3.4) realizes an isomorphism between $\mathcal{H}$ and the space of square-integrable sections $k\mapsto\widehat{\psi}(k)$ of the Bloch bundle $\mathcal{H}$ over BZ which preserves the norm, as stated by the Plancherel formula

$$\|\psi\|^2 = \frac{1}{|\mathrm{BZ}|}\int_{\mathrm{BZ}} \|\widehat{\psi}(k)\|_k^2 \mathrm{d}k \tag{3.8}$$

where $|\mathrm{BZ}|$ is the volume of BZ (which can be computed as the volume of a Brillouin zone embedded in the Euclidean space). Its inverse is given by the normalized integral of $\widehat{\psi}(k,x)$ over the Brillouin torus

$$\psi(x) = \frac{1}{|\mathrm{BZ}|}\int_{\mathrm{BZ}} \widehat{\psi}(k,x)\,\mathrm{d}k. \tag{3.9}$$

As we previously stated, the Bloch bundle may be trivialized (yet not in a canonical way), which will enable us to represent operators on $\mathcal{H}$ as families of matrices over the Brillouin torus. A trivialization of $\mathcal{H}$ is a family of smooth sections $k\mapsto e^i(k)$, $i=1,\dots,N$, defined over BZ (i.e. with $e^i(k) = e^i(k+G)$), which for each k form an orthonormal basis (a *frame*) of $\mathcal{H}(k)$.

Let $(v_1, \dots, v_n)$ be a basis of V. An example of trivialization of $\mathcal{H}$ is provided by the Fourier transforms of functions $\phi_{i,j} \in \ell^2(\mathcal{C}, V)$ defined by

$$\phi_{(i,j)}(x) = \delta_{x,x_i} v_j \tag{3.10}$$

concentrated at points $x_i \in \mathcal{F}$ of a fixed unit cell $\mathcal{F} \subset \mathcal{C}$. We shall denote by $e_I^{\mathcal{F}}(k)$ for $(i,j) = I$ the corresponding vectors in $\mathcal{H}(k)$,

$$e_{(i,j)}^{\mathcal{F}}(k) = \sum_{\gamma \in \Gamma} \mathrm{e}^{-\mathrm{i}k\cdot\gamma} \phi_{(i,j)}(x-\gamma). \tag{3.11}$$

Bloch functions decompose on this frame as

$$\varphi = \sum_I \varphi_I e_I^{\mathcal{F}} \qquad \text{where} \qquad \varphi_I(k) = \langle e_I^{\mathcal{F}}(k) \mid \phi(k) \rangle_k . \tag{3.12}$$

The trivialization of $\mathcal{H}$ defined this way depends on the choice of the fundamental domain $\mathcal{F}$. If $\mathcal{F}'$ is another unit cell then $x_i' = x_i + \gamma_i$ with $\gamma_i \in \Gamma$ for an appropriate numbering of its points so that

$$\delta_{x,x_i'} = T_{\gamma_i} \delta_{x,x_i} \tag{3.13}$$

and consequently

$$e_{(i,j)}^{\mathcal{F}'}(k) = \mathrm{e}^{\mathrm{i}k\cdot\gamma_i} e_{(i,j)}^{\mathcal{F}}(k). \tag{3.14}$$

For convenience, in the following we will treat the composite index $I = (i,j)$ as a number running from 1 to N. Each trivialization permits to identify the Bloch bundle $\mathcal{H}$ with the trivial bundle $\mathrm{BZ} \times \mathbb{C}^N$.

To sum up, Bloch decomposition amounts to use the Fourier transform to define a Bloch bundle

$$\mathcal{H} = \bigoplus_{k \in \mathrm{BZ}} \mathcal{H}(k) \tag{3.15}$$

where BZ is the Brillouin torus and $\mathcal{H}(k)$ are N-dimensional complex vector spaces, so that the Hilbert space $\mathcal{H}$ is isomorphic the set of sections of a (trivializable) vector bundle $\mathcal{H} \to \mathrm{BZ}$ over the Brillouin torus,

$$\mathcal{H} \simeq \Gamma(\mathcal{H}). \tag{3.16}$$

Now consider a tight-binding Hamiltonian on $\mathcal{C}$, that is an Hermitian operator

$$H = \sum_{x,y \in \mathcal{C}} h(x,y) \, |x\rangle\langle y| \in \mathrm{End}(\mathcal{H}) \tag{3.17}$$

where $|x\rangle$ represents a state with a localized wave function $\xi \mapsto \delta_{\xi,x}$, and where $h(x,y) \in \mathrm{End}(V)$ with $h(x,y)^\dagger = h(y,x)$ so that $H^\dagger = H$ is Hermitian. Assume that this Hamiltonian is translation invariant with respect to Bravais lattice translations, that is $T_\gamma H T_\gamma^{-1} = H$, or explicitly

$$h(x+\gamma, y+\gamma) = h(x,y) \tag{3.18}$$

for a translation $\gamma \in \Gamma$. Then, H maps Bloch functions into Bloch functions: if ψ is an element of $\mathcal{H}(k)$, so $\psi(k, x-\gamma) = \mathrm{e}^{\mathrm{i}k\cdot\gamma}$, then

$$(H\psi(k))(x) = \sum_{y\in\mathcal{C}} h(x,y)\psi(k,y) \tag{3.19}$$

is also an element of $\mathcal{H}(k)$ (the Hamiltonian fibers over the Brillouin torus), and that defines **Bloch Hamiltonians** $H(k) = H(k+G)$ acting on $\mathcal{H}(k)$, which decompose H along (3.15) as

$$H = \bigoplus_{k\in\mathrm{BZ}} H(k). \tag{3.20}$$

This equation may be understood as the continuous version of a decomposition of H into block-diagonal form, corresponding to the identification of conserved quantities due to symmetries. This is already a huge simplifications as Bloch Hamiltonians act on finite-dimensional vector spaces. The last step consists in representing those operators as matrices by choosing a frame of sections $k \mapsto e_i(k)$, $i = 1, \dots, N$ of the Bloch bundle to define the promised $N \times N$ Bloch Hamiltonian matrices as

$$H_{ij}(k) = \langle e_i(k) \mid H \mid e_j(k)\rangle\,. \tag{3.21}$$

We already know a frame of smooth global sections defined over the whole Brillouin torus, maps $k \mapsto e_I^{\mathcal{F}}(k)$ defined through the Fourier transform, which define Bloch Hamiltonians $H^{\mathcal{F}}(k)$.

For example, let us take $V = \mathbb{C}$ and $\mathcal{F} = \{x_1, \dots, x_m\}$, so the Bloch Hamiltonian (in basis $e^{\mathcal{F}}$) is a $m \times m$ matrix. Let us write $|x_1\rangle_{\mathrm{B}}$ the corresponding basis vectors[(1)] in $\mathbb{C}^m$. A typical tight-binding element is $|x\rangle\langle y|$, with $x, y \in \mathcal{C}$. Points on the crystal are decomposed as e.g. $x = \gamma_x + [x]$ where $\gamma_x \in \Gamma$ and $[x] \in \mathcal{F}$ (same for y), so to obtain the Bloch Hamiltonian, we simply have to replace

$$|x\rangle\langle y| \longrightarrow \mathrm{e}^{-\mathrm{i}k\cdot(\gamma_y-\gamma_x)}\,|[x]\rangle_{\mathrm{B}}\langle[y]|_{\mathrm{B}}\,. \tag{3.22}$$

To give an even more simple example, in a one-dimensional system with $m = 1$, we simply replace $|x\rangle\langle x+1|$ with $\mathrm{e}^{-\mathrm{i}k}$, $|x+1\rangle\langle x|$ with $\mathrm{e}^{+\mathrm{i}k}$, $|x\rangle\langle x+2|$ with $\mathrm{e}^{-2\mathrm{i}k}$, and so on.

1.1.1 An alternative picture

Bloch functions can also be seen as Γ-periodic functions on $\mathcal{C}$ modulated by a Bloch phase: this is the usual formulation of Bloch theorem, which states that a wavefunction $\psi_k(x)$ can be written as the product of a periodic function $u_k(x) = u_k(x+\gamma)$ and of a phase factor $\mathrm{e}^{-\mathrm{i}k\cdot x}$, that is $\psi_k(x) = \mathrm{e}^{-\mathrm{i}k\cdot x}u_k(x)$. We will make this statement precise in the following, and show that the Bloch bundle can be identified with the quotient

$$\frac{T^* \times \ell^2(\mathcal{C}/\Gamma)}{\Gamma^*} \simeq \mathcal{H} \tag{3.23}$$

where T^* is the set of reciprocal vectors, $\ell^2(\mathcal{C}/\Gamma)$ are Γ-periodic functions on $\mathcal{C}$ and Γ^* is the reciprocal lattice. To do so in a meaningful way, we will need to allow the

(1) For example, we can take $|x_1\rangle_{\mathrm{B}} = (1, 0, \dots, 0)$, $|x_2\rangle_{\mathrm{B}} = (0, 1, 0, \dots, 0)$, etc.

quasi-momentum to live in the whole reciprocal space $T^* \simeq \mathbb{R}^d$ and only at the end to identify k with $k+G$.

First, Γ-periodic functions on $\mathcal{C}$ are maps u satisfying $u(x) = T_\gamma u(x)$. They form the vector space $\ell^2(\mathcal{C}/\Gamma)$. This being said, we can define the trivial bundle

$$\mathcal{B} = T^* \times \ell^2(\mathcal{C}/\Gamma) \tag{3.24}$$

with typical element (k, u). From a section $k \mapsto u(k)$ of this trivial bundle, where $u(k, x) = u(k, x+\gamma)$, one can define

$$\psi(k, x) = \mathrm{e}^{-\mathrm{i}k\cdot(x-x_0)} u(k, x) \tag{3.25}$$

where $x_0 \in \mathbb{E}^d$ is a fixed origin in the Euclidean space, needed to get a vector $x - x_0 \in T$, where T is the translation vector space, out of $x \in \mathcal{C} \subset \mathbb{E}^d$. Thus ψ is a section of the Bloch bundle. By construction, $\psi(k, x-\gamma) = \mathrm{e}^{\mathrm{i}k\cdot\gamma}\psi(k, x)$ so $\psi(k) \in \mathcal{H}(k) \equiv \mathcal{H}(k+G)$ but we also need $\psi(k+G, x) = \psi(k)$ which is not necessarily true. It is for sections $k \mapsto u(k)$ such that

$$u(k+G, x) = \mathrm{e}^{\mathrm{i}G\cdot(x-x_0)} u(k, x). \tag{3.26}$$

In order to impose this relation, we define an equivalence relation between elements of the bundle $\mathcal{B}$: the previous equation can be interpreted as an action of the reciprocal lattice Γ^* on periodic functions, so we now have an action of Γ^* on $\mathcal{B}$ defined by

$$(k, u) \mapsto (k+G, x \mapsto \mathrm{e}^{\mathrm{i}G\cdot(x-x_0)} u(x)) \tag{3.27}$$

for $G \in \Gamma^*$. Dividing $\mathcal{B}$ by this action gives a bundle on BZ with fiber $\mathcal{H}(k)$, i.e. the Bloch bundle.

Starting from a frame of sections of $\mathcal{B}$

$$\tilde{b}_{(i,j)}(k, x) = \sum_{\gamma\in\Gamma} T_\gamma \delta_{x,x_i} v_j = \sum_{\gamma\in\Gamma} \delta_{x-\gamma,x_i} v_j \tag{3.28}$$

for $x_i \in \mathcal{F}$ and $v_j \in V$, we define functions

$$\tilde{e}^{x_0}_{(i,j)}(k, x) = \mathrm{e}^{-\mathrm{i}k(x-x_0)} \tilde{b}_{(i,j)}(k, x) = \mathrm{e}^{-\mathrm{i}k(x-x_0)} \sum_{\gamma\in\Gamma} \delta_{x-\gamma,x_i} v_j. \tag{3.29}$$

They naturally provide *local* sections of the Bloch bundle, but not global sections as $\tilde{e}^{x_0}_I(k) \neq \tilde{e}^{x_0}_I(k+G)$ (they are however identified in the quotient).

1.1.2 Different Bloch Hamiltonians

Sections $\tilde{e}^{x_0}_I$ obtained from $\mathcal{B}$ therefore allow to define a family of Bloch matrix Hamiltonian, which will however not be defined on the Brillouin torus, but rather on the whole plane T^*. The choice of the Bloch Hamiltonian can have no impact on the physical observables: it is an arbitrary choice of basis which enables to represent operators as matrices. For example, the energy spectrum of $H^{\mathcal{F}}(k)$ is the same as the one of $\tilde{H}(k)$. On the other hand, particular choices can prove to be more useful in

discussing a particular property. In order to study topological properties, it is more convenient to have a periodic Bloch Hamiltonian, so we will work with $H^{\mathcal{F}}(k)$ which will be shortened as $H(k)$ in the following (but we should keep in mind that it depends on the unit cell). In certain situations, it appears that the *non-periodic* Bloch Hamiltonian $\tilde{H}(k)$ is more convenient. I partially explored this issue in [FCG14]. Following the observations of Bena and Montambaux [BM09] and Fuchs, Piéchon, Goerbig and Montambaux [FPGM10] on graphene-like systems, we observed that there is an almost canonical choice of parallel transport on the Bloch bundles, which gives rise to a canonical Berry curvature when projected on a band [FCG14]. The corresponding projected (Berry) connection is directly related to the position operator, as discovered by Blount in 1962 [Blo62]. Other choices of parallel transport may be related to the position operator, but in a more complicated fashion. The non-periodic matrix Bloch Hamiltonian happens to be directly related to such objects, as the frame used to define it is parallel transported by the (almost) canonical connection. It is therefore not surprising to find the non-periodic Bloch Hamiltonian more convenient to work with in situations where the position operator appears, for example when the system is subjected to an external electric field, a situation first considered by Zak [Zak68; Zak89], leading to a distinction between a Bloch-Floquet transform and a Zak-Bloch-Floquet transform [PST03], which are closely related to the objects we defined. Observables more easily described with the later choice seem to arise in Stückelberg interferometry of Bloch states [LFM15] and in Friedel oscillations [DK16]. Although the non-periodic Bloch Hamiltonian is convenient as it is naturally related to the canonical curvature, it is still possible to choose another frame to define matrix families representing operators. Expressing simple quantities in such a basis would be unnecessarily complicated, but possible. As it is outside of its scope, I will not discuss this matter any further in this thesis.

1.1.3 Example: graphene

To illustrate Bloch theory on a simple example (and also to prepare for the Haldane model that we shall study in section 2.1), consider the tight-binding model of graphene [Wal47; CGPN09]. Here, the crystal $\mathcal{C}$ is a hexagonal lattice (also called honeycomb lattice). The Bravais lattice Γ is composed of integer linear combinations of the lattice vectors

$$a_1 = \frac{a}{2}\begin{pmatrix} 3 \\ \sqrt{3} \end{pmatrix} \qquad \text{and} \qquad a_2 = \frac{a}{2}\begin{pmatrix} 3 \\ -\sqrt{3} \end{pmatrix}, \tag{3.30}$$

that is

$$\Gamma \simeq \left\{ i a_1 + j a_2 \mid (i,j) \in \mathbb{Z}^2 \right\}. \tag{3.31}$$

We also define the nearest neighbor vectors

$$\delta_1 = \frac{a}{2}\begin{pmatrix} 1 \\ \sqrt{3} \end{pmatrix}, \qquad \delta_2 = \frac{a}{2}\begin{pmatrix} 1 \\ -\sqrt{3} \end{pmatrix} \qquad \text{and} \qquad \delta_3 = \frac{a}{2}\begin{pmatrix} -2 \\ 0 \end{pmatrix}. \tag{3.32}$$

A choice of fundamental domain for the graphene lattice, illustrated on figure 3.1a, is

$$\mathcal{F} = \{x_0, x_0 + \delta_3\} \tag{3.33}$$

where $x_0 \in \mathbb{E}^2$ is an (arbitrary) origin of the Euclidean plane. Here, we choose to take $x_0 \in \mathcal{C}$ for simplicity, but this is not mandatory (another possible choice of

fundamental domain is $\mathcal{F}' = \{x_0 - \delta_3/2, x_0 + \delta_3/2\}$, for example). The crystal $\mathcal{C}$ is obtained by the action of Γ on $\mathcal{F}$, that is

$$\mathcal{C} = \Gamma\mathcal{F} = \left\{x_0 + ia_1 + ja_2 \mid (i,j) \in \mathbb{Z}^2\right\} \cup \left\{x_0 + \delta_3 + ia_1 + ja_2 \mid (i,j) \in \mathbb{Z}^2\right\}. \quad (3.34)$$

The crystal is composed of two subsets, each coming from a single point in $\mathcal{F}$. The first set will be called sublattice A, and the second sublattice B. This is illustrated on figure 3.1a. Notice that another choice of fundamental domain, e.g. with δ_2 instead of δ_3, would give the same crystal. The reciprocal lattice Γ^* is generated by vectors

$$a_1^* = \frac{2\pi}{3a}\begin{pmatrix}1\\\sqrt{3}\end{pmatrix} \qquad \text{and} \qquad a_2^* = \frac{2\pi}{3a}\begin{pmatrix}1\\-\sqrt{3}\end{pmatrix} \quad (3.35)$$

(which were chosen so that $a_i^* \cdot a_j = 2\pi\delta_{ij}$), that is

$$\Gamma^* \simeq \left\{ia_1^* + ja_2^* \mid (i,j) \in \mathbb{Z}^2\right\}. \quad (3.36)$$

The first Brillouin zone (see figure 3.1) is an hexagon with corners $(K, K - K', -K', -K, K' - K, K')$ where

$$K = \frac{2\pi}{3\sqrt{3}a}\begin{pmatrix}\sqrt{3}\\1\end{pmatrix} \qquad \text{and} \qquad K' = \frac{2\pi}{3\sqrt{3}a}\begin{pmatrix}\sqrt{3}\\-1\end{pmatrix} \quad (3.37)$$

are the so-called K points, also called Dirac points in graphene.

In this example (and in the Haldane model), we consider spinless electrons: the full Hamiltonian of the electronic problem factorizes as the product $H_{\text{tot}} = H_{\text{orbital}} \otimes H_{\text{spin}}$ of an orbital part of a spin part. In this example, as well as in the Haldane model, the spin Hamiltonian is simply the identify $H_{\text{spin}} = \text{Id}$ (the spinless picture is actually valid as long as H_{spin} do not depend on space, so the Bloch Hamiltonian also factorizes as $H_{\text{tot}}(k) = H_{\text{orbital}}(k) \otimes H_{\text{spin}}(k)$ where $H_{\text{spin}}(k)$ is a constant matrix not depending on k). Hence, it is possible to only keep the orbital part.

When there are no internal degrees of freedom (e.g. because they were factored out, which is the case here for spinless electrons), a tight-binding Hamiltonian can be written in the form

$$H = \sum_{x,y \in \mathcal{C}} h_{x,y} \left|x\right\rangle\left\langle y\right| \quad (3.38)$$

where $|x\rangle$ represents a state with a localized wave function (approximated on the crystal by) $\xi \mapsto \delta_{\xi,x}$, and where $h_{x,y} = \overline{h_{y,x}}$ so H is Hermitian. It is generally assumed that $h_{x,y}$ vanishes for a large enough $|x-y|$. Here, we introduce both nearest-neighbors and second-nearest-neighbors couplings leading to the Hamiltonian

$$H = t \sum_{\langle x,y\rangle} \left|x\right\rangle\left\langle y\right| + t' \sum_{\langle x,y\rangle_2} \left|x\right\rangle\left\langle y\right| + \sum_{x \in \mathcal{C}} M_x \left|x\right\rangle\left\langle x\right| \quad (3.39)$$

where $\langle x, y\rangle_j$ means that the sum runs on j^{th} nearest neighbors pairs (all of them, but without repetitions), with $j = 1$ when omitted. We also introduce a staggered potential

$$M_x = \begin{cases} +M & \text{when } x \in A \\ -M & \text{when } x \in B \end{cases} \quad (3.40)$$

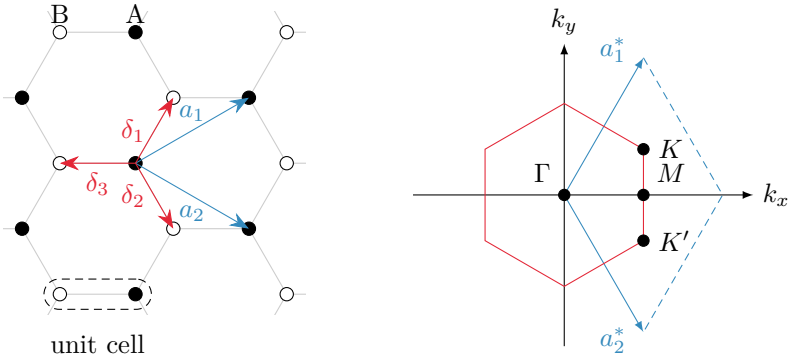

(a) Crystal. **(b) Reciprocal lattice.**

Figure 3.1: Graphene and its reciprocal lattice. The hexagonal lattice (also called honeycomb lattice) of graphene is constituted of two sublattices A and B, located (with our choice of fundamental cell) at 0 and δ_3 respectively. Vectors δ_i (in red) connect nearest neighbors. The Bravais lattice of the crystal is a triangular lattice of primitive vectors a_1 and a_2 (in blue). This corresponds to a triangular reciprocal lattice with primitive vectors a_1^* and a_2^* (in blue). Two possible fundamental domains for the Brillouin torus (or Brillouin zones) are proposed: a blue rhombus and a red hexagon. The red hexagon represents the first Brillouin zone (composed of points that are closer to the origin than they are of any other reciprocal lattice points); particularly noticeable points of the first Brillouin zone are the origin, usually called the Gamma point Γ (not to be confused with the Bravais lattice), the two inequivalent K points K and K', which are the Dirac points in the gapless case, and the three inequivalent M points at the centers of the edges. (Equivalent points are equal up to a reciprocal lattice translation.)

inducing an asymmetry between sublattices A and B, which will be required to open a gap in the band structure; $M = 0$ in pristine graphene, but it is possible to open a gap in its band structure, e.g. by growing it on a well-chosen substrate [ZGFF07] (see also [Nov07]), and the model with $M \neq 0$ also describes boron nitride [Sem84].

To obtain Bloch Hamiltonians, we need frames of sections of the Bloch bundle. With the ones defined in the previous section 1.1, we can compute the two kinds of Bloch Hamiltonians,

$$H_{ij}^{\mathcal{F}}(k) = \langle e_i^{\mathcal{F}}(k)|H|e_j^{\mathcal{F}}(k)\rangle = H_{ij}^{\mathcal{F}}(k+G) \tag{3.41}$$

which depends on the unit cell $\mathcal{F}$ and is k-periodic, and

$$\tilde{H}_{ij}(k) = \langle \tilde{e}_i^{x_0}(k)|H|\tilde{e}_j^{x_0}(k)\rangle \neq H_{ij}(k+G) \tag{3.42}$$

which does actually not depend on x_0, but is not k-periodic[(2)]. Both Bloch Hamiltonians can be written in the form

$$H^{\mathcal{F}}(k) = \begin{pmatrix} +M & \overline{g^{\mathcal{F}}(k)} \\ g^{\mathcal{F}}(k) & -M \end{pmatrix} \qquad \text{and} \qquad \tilde{H}(k) = \begin{pmatrix} +M & \overline{\tilde{g}(k)} \\ \tilde{g}(k) & -M \end{pmatrix} \tag{3.43}$$

[(2)] In fact, we work with $k \in T^*$ in this case, and the quotient by Γ^* is yet to be taken.

For our choice of fundamental domain (3.33) and $t' = 0$, we have

$$g^{\mathcal{F}}(k) = t\left(1 + \mathrm{e}^{\mathrm{i}k\cdot a_1} + \mathrm{e}^{\mathrm{i}k\cdot a_2}\right) \tag{3.44}$$

and

$$\tilde{g}(k) = t\left(\mathrm{e}^{\mathrm{i}k\cdot \delta_1} + \mathrm{e}^{\mathrm{i}k\cdot \delta_2} + \mathrm{e}^{\mathrm{i}k\cdot \delta_3}\right). \tag{3.45}$$

When second nearest neighbors couplings (which will be essential in part 2.1) are present, $t' \neq 0$, the term

$$t'\left(\mathrm{e}^{\mathrm{i}k\cdot a_1} + \mathrm{e}^{\mathrm{i}k\cdot a_2} + \mathrm{e}^{-\mathrm{i}k\cdot a_1} + \mathrm{e}^{-\mathrm{i}k\cdot a_2} + \mathrm{e}^{\mathrm{i}k\cdot (a_1-a_2)} + \mathrm{e}^{\mathrm{i}k\cdot (a_2-a_1)}\right)\mathrm{Id} \tag{3.46}$$

is added to either or $H^{\mathcal{F}}(k)$ or $\tilde{H}(k)$ (it is the same in both cases as hoppings connect the same sublattice).

1.1.4 Example: the SSH model

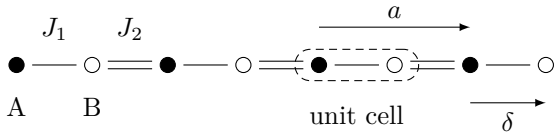

Figure 3.2: Lattice of the SSH model.

The SSH model [SSH79] was developed by Su, Schrieffer and Heeger to describe *trans*-polyacetylene (or polyethyne, $(C_2H_2)_n$). If we were to build a linear polymer composed of CH chunks, the most simple way to associate them is the most symmetric configuration represented on figure 3.3 (b). However, it happens that this configuration is not the most stable, and it is energetically preferable to slightly move the atoms to alternate short and long bonds: in other words, there is a dimerization of the molecule due to the coupling of the electronic modes with phonons, a phenomenon called Peierls instability. There are two equivalent possibilities for atoms to dimerize, represented on figure 3.3 (c) and (d). A crucial point is that the lattice (not only the distribution of electrons) is deformed from the initial, fully delocalized (and physically irrelevant) system, as illustrated on figure 3.4. As long as the atoms are confined in a plane, the two ground states (c) and (d) are inequivalent (they are however related e.g. by reflection symmetry). As a consequence, the lattice is not Bravais, and there are two kinds of inequivalent carbon atoms, collected into two sublattices that we will call A and B. A long bond (usually represented as a simple bond) corresponds to a lower hopping term than a short (double) bond. See [BCM92; HKSS88] for more detailed reviews.

For a fixed configuration of the atom positions, the (low energy) electronic properties of polyacetylene are described by a one-dimensional tight-binding model with two sublattices A and B (see figure 3.2), the SSH model introduced by Su, Schrieffer and Heeger. Here, the one-dimensional Bravais lattice is simply

$$\Gamma = \langle a \rangle \simeq \mathbb{Z} \tag{3.47}$$

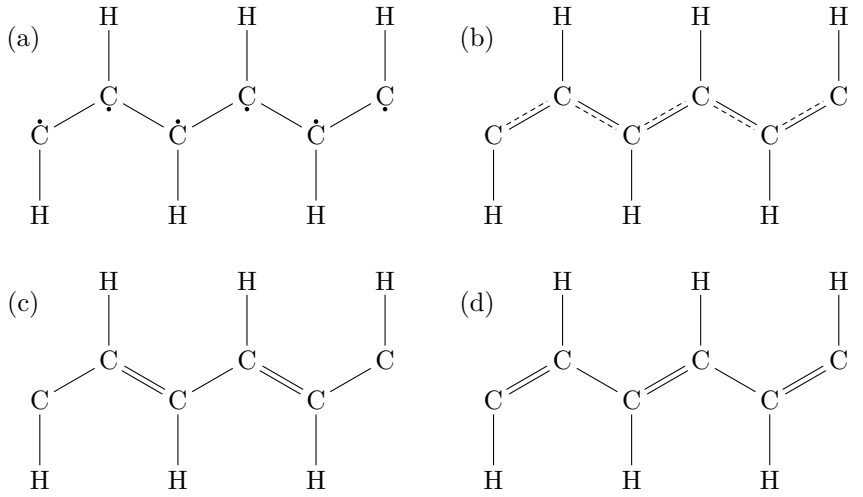

Figure 3.3: Polyacetylene. Polyacetylene, or more precisely *trans*-polyacetylene is a linear polymer. Naively, assembling C_2H_2 units into the polymer $(C_2H_2)_n$ could be done (a) by putting radicals on carbon atoms or better, (b) by delocalizing the unpaired electrons on the whole molecule. If carbon atoms were fixed, it would be the more stable solution. However, the coupling with phonon (i.e. deformations of the lattice, which allows carbon atoms to move) favors energetically the two dimerized configurations (c) and (d), so there is a spontaneous symmetry breaking leading to the system we are used to.

where a is a one-dimensional vector, see figure 3.2), and a choice of fundamental domain is

$$\mathcal{F} = \{x_0, x_0 + \delta\} \tag{3.48}$$

corresponding to sublattices A and B respectively (see figure 3.2). It is described by the Hamiltonian

$$H = \sum_{\gamma \in \Gamma} J_1 \left|x_0 + \gamma\right\rangle \left\langle x_0 + \gamma + \delta\right| + J_2 \left|x_0 + \gamma\right\rangle \left\langle x_0 + \gamma + 1 + \delta\right| + \text{h.c.}. \tag{3.49}$$

where the sum runs on the Bravais lattice $\Gamma \simeq \mathbb{Z}$, and $|x\rangle$ represents a state localized at point $x \in \mathcal{C}$. It is very convenient to shorten notations a little to write this Hamiltonian as

$$H = \sum_{x \in \Gamma} J_1 \left|x, A\right\rangle \left\langle x, B\right| + J_2 \left|x, A\right\rangle \left\langle x + 1, B\right| + \text{h.c.} \tag{3.50}$$

where x_0 was removed and x represents both a point of the crystal and a Bravais lattice vector so e.g. $|\gamma, B\rangle$ in fact means $|x_0 + \gamma + \delta\rangle$. This corresponds to the Bloch Hamiltonian

$$H(k) = (J_1 + J_2 \cos(k))\sigma_1 + J_2 \sin(k)\sigma_2 \tag{3.51}$$

where σ_i are the Pauli matrices in the basis of sublattices A and B.

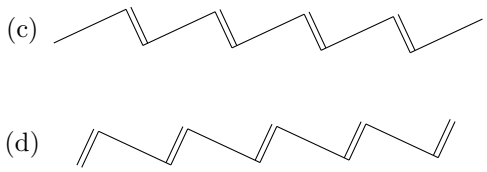

Figure 3.4: Exaggerated picture of the deformation of *trans*-polyacetylene. The two stable configurations of *trans*-polyacetylene represented in figure 3.3 (c,d) are not equivalent, at least as long as the molecule is confined on the plane, as it is clearly seen when the deformed lattice is represented. Here, the deformation is exaggerated for clarity; in real polyacetylene, its order of magnitude is less that 3 %.

1.1.5 Time-dependent Bloch Hamiltonians and evolution operators

In the main part of this thesis, we will be concerned with tight-binding Hamiltonians which depend on time. We will focus on the simple case where the underlying lattice does not depend on time. In this case, the Bloch decomposition is simply done at fixed time. From a time-dependent tight-binding Hamiltonian $H(t)$, we obtain a time-dependent Bloch Hamiltonian $H(t,k)$, which is defined by extending (3.21) as

$$H_{ij}(t,k) = \langle e_i(k) \mid H(t) \mid e_j(k) \rangle \,. \tag{3.52}$$

It is a smooth function of time when $H(t)$ is. In the case where the lattice depends on time, it may be possible to capture the physics through an effective description on a fixed lattice, through a modulation of the hopping parameters. In certain cases, e.g. when the topology of the lattice changes, such an effective description will break down, but we will not consider this kind of situations.

The evolution operator of the system is defined as the solution of the differential equation

$$\mathrm{i}\hbar\dot{U} = HU \tag{3.53}$$

where $\dot{U}$ represents the time derivative of U, with initial condition $U(0) = \mathrm{Id}$. In a spatially periodic system, there is a family of matrix Bloch evolution operators $U(t,k)$ which are similarly defined from the Bloch Hamiltonians by

$$\mathrm{i}\hbar\dot{U}_{ij}(t,k) = H_{ij}(t,k)U_{ij}(t,k). \tag{3.54}$$

Physically, the evolution happens separately in each fixed k subspace thanks to momentum conservation, as we assume that the evolution does not alter space periodicity. Alternatively,

$$U_{ij}(t,k) = \langle e_i(k) \mid U(t) \mid e_j(k) \rangle \,. \tag{3.55}$$

(A similar definition may indeed be applied to all operators commuting with space translations.) When the Hamiltonian does not depend on time, there is a simple expression for the evolution operator as $U(t) = \mathrm{e}^{-\mathrm{i}/\hbar t H}$, and for its Bloch version,

$$U(t,k) = \exp\left(-\frac{\mathrm{i}}{\hbar}\, tH(k)\right). \tag{3.56}$$

When the Hamiltonian does depend on time, however, the evolution operator is a time-ordered exponential, which is in general impossible to compute analytically. However, it may be numerically evaluated in a simple way by discretizing the infinite product

$$U(t,k) = \lim_{\delta t/t \to 0} \prod_{n=0}^{[t/\delta t]} \exp\left(-\frac{\mathrm{i}}{\hbar}\,\delta t\, H(n\delta t, k)\right) \tag{3.57}$$

with a small but finite δt. Notice that the product is time-ordered with $n = 0$ being on the right, so

$$\prod_{n=0}^{N} f(n) = f(N)\cdot f(N-1)\cdots f(n)\cdots f(1)\cdot f(0) \tag{3.58}$$

with

$$f(n) = \exp\left(-\frac{\mathrm{i}}{\hbar}\,\delta t\, H(n\delta t, k)\right). \tag{3.59}$$

1.2 Energy bands

Each Bloch Hamiltonian is a hermitian operator with a discrete, real spectrum $\mathcal{S}(k) = (E_i(k))_{1\le i\le r} \subset \mathbb{R}$ with $E_1(k) \le \cdots \le E_r(k)$. Energy eigenvalues $E_i(k)$ are associated with eigenvectors $\psi_i(k)$. Energies E_i are well-defined and piecewise smooth; eigenvectors are defined up to a choice of phase (or a unitary transformation when there are degeneracies). Maps $k \mapsto E_i(k)$ are usually called *energy bands*, but we will also use this name to denote the corresponding wave function. It may happen that a certain value of energy E separates two energy bands, that is, there may be some i such that $E_i(k)$ is always smaller than E and $E_{i+1}(k)$ is always greater, or, more formally,

$$\max_k E_i(k) < E < \min_k E_{i+1}(k). \tag{3.60}$$

In this case, the band structure has a **band gap** at energy E, and we define the **gap width** (or simply *gap*) $E_{\mathrm{gap}} = \min_k E_{i+1}(k) - \max_k E_i(k)$.

A band structure may have a *local gap* when $E_i(k) < \min_k E_{i+1}(k)$, but fail to satisfy condition (3.60): in this case, the band structure is *not* considered to be gapped.

We will treat as a whole the set of energy bands $E < E_i, \ldots, E_j < E'$ comprised between two band gaps E and E'; this object will also be called an *energy band*. It is convenient to represent it as a *spectral projector* over the range $]E, E'[$ [ASSS89],

$$P_{E,E'}(k) = \sum_{\substack{i \text{ s.t.} \\ E<E_i<E'}} |\psi_i(k)\rangle\langle\psi_i(k)| = \frac{1}{2\pi\mathrm{i}} \int_{\mathcal{C}} \frac{\mathrm{d}z}{z - H(k)} \tag{3.61}$$

where the contour $\mathcal{C}$ encircles the band in the complex z plane (see figure 3.5). Spectral projectors define *spectral bundles* over the Brillouin torus, with fiber $P_{E,E'}(k)\mathbb{C}^r$ over k, so each energy band (separated from others bands by gaps) corresponds to a subbundle of the Bloch bundle. As we shall see, the band subbundles may be nontrivial, leading to topological properties.

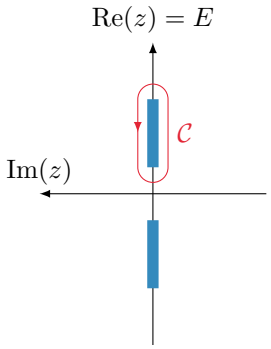

Figure 3.5: Complex contour defining a spectral projector.

1.2.1 Example: two-by-two matrices

Both of the examples that we considered happen to yield 2×2 matrices as Bloch Hamiltonians: 2×2 matrices provide enough structure to describe all two-band crossings, and therefore to construct minimal and sufficient low-energy effective models for the corresponding phenomena. In this paragraph, we shall consider a generic 2×2 Hamiltonian and diagonalize it; the results of this (easy) computation can readily be applied both to graphene and to the SSH model.

Consider the most general 2×2 Hamiltonian

$$H^\sigma(h) = h_\mu \sigma_\mu = h_0 \mathrm{Id} + \vec{h} \cdot \vec{\sigma} \tag{3.62}$$

where[3] h_μ are real parameters and σ_i are Pauli matrices (see appendix A, page 54); we may also use the notation $h_x = h_1$, $\sigma_x = \sigma_1$, $h_y = h_2$, etc. and $\vec{h} = (h_1, h_2, h_3)$. More explicitly,

$$H^\sigma(h) = h_0 \mathrm{Id} + h_1 \sigma_1 + h_2 \sigma_2 + h_3 \sigma_3. \tag{3.63}$$

When $h_0 = 0$, the eigenvalues of $H^\sigma(h)$ are

$$E^\sigma_\pm(h) = \pm \sqrt{h_1^2 + h_2^2 + h_3^3} = \pm \| \vec{h} \|. \tag{3.64}$$

and the corresponding normalized eigenvectors are

$$|\psi^\sigma_\pm(h)\rangle = \frac{1}{\sqrt{2E^\sigma_\pm(E^\sigma_\pm + h_z)}} \begin{pmatrix} h_z + E^\sigma_\pm \\ h_x + \mathrm{i} h_y \end{pmatrix}. \tag{3.65}$$

In the following we will always consider $h_0 = 0$. When it is not the case, the eigenvalues become $h_0 + E^\sigma_\pm(h)$, and the eigenvectors are indeed not modified.

The spectrum of $H^\sigma(h)$ is gapped as long as $\vec{h} \neq 0$, and in this case, the spectral projectors on positive/negative energies (corresponding to conduction/valence bands)

[3] We use the standard convention of Greek indices starting at 0 and Latin indices starting at 1.

are

$$P^\sigma_\pm(h) = |\psi^\sigma_\pm\rangle\langle\psi^\sigma_\pm| = \frac{1}{2E^\sigma_\pm(E^\sigma_\pm + h_z)} \begin{pmatrix} (E^\sigma_\pm + h_z)^2 & (E^\sigma_\pm + h_z)(h_x - \mathrm{i}h_y) \\ (E^\sigma_\pm + h_z)(h_x + \mathrm{i}h_y) & (E^\sigma_\pm)^2 - h_z^2 \end{pmatrix}. \tag{3.66}$$

As we discussed in section 2.3, page 51, the eigenvectors cannot be smoothly defined for all values of $h \neq 0$, and this obstruction is at the root of nontrivial topological properties. In contrast, the projectors are smoothly defined for all values of $h \neq 0$.

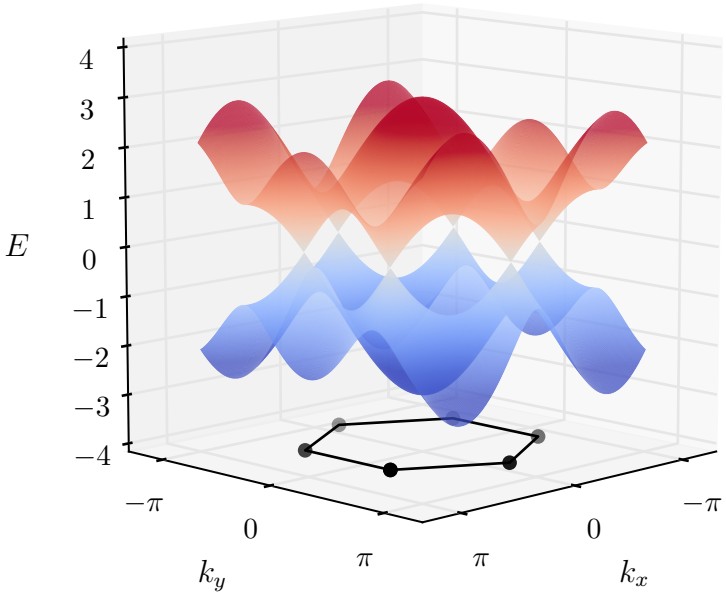

Figure 3.6: Dispersion relation of graphene. Dispersion relation of the simplified tight-binding description of graphene with $t = 1$, over a square slightly larger than the first Brillouin zone (black hexagon). Linear gap closing (Dirac cones) happen at the K points (black dots), two of which are inequivalent.

Example: graphene (continued) Graphene is not a gapped system. Instead, it is a semimetal, as one can see on figure 3.6 representing its dispersion relation (where linear crossings between the conduction and the valence band are especially noticeable; they occur at the so-called *Dirac points* $\pm K$ on the Brillouin zone). However, as we discussed in paragraph 1.1.3, it is possible to induce a gap (or in high-energy physics language, a *mass*) in graphene, which gives rise to the dispersion relation

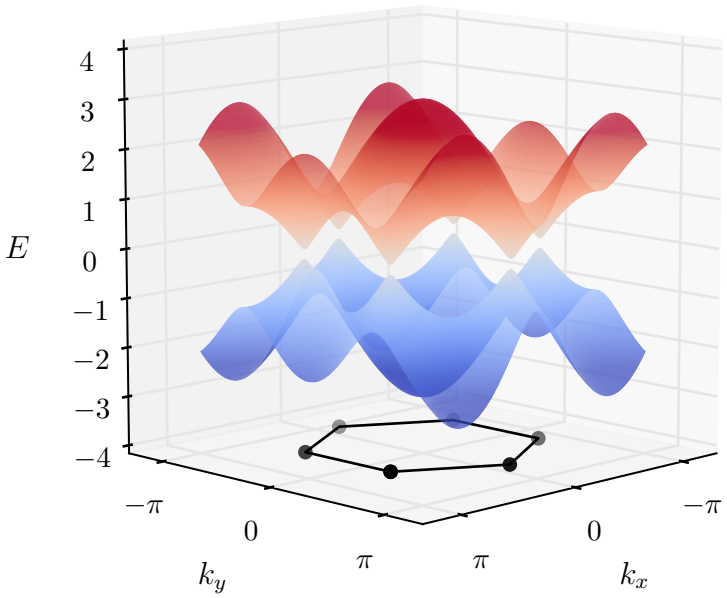

Figure 3.7: Dispersion relation of gapped graphene. Here, the Dirac cones of figure 3.6 are now gapped, due to a mass term $m = 0.1$, so the system is fully gapped. A zoom of the dispersion relation near the Dirac points is found on figure 3.8.

of figure 3.7. The dispersion relation is qualitatively modified only near the Dirac points, as we can see on figure 3.8. In the massive case, the valence and conduction bands are unambiguously defined on the whole Brillouin zone, and one can define the corresponding projectors.

The Hamiltonian $H^{\mathcal{F}} = H$ of equation 3.43 with $t' = 0$ can be written as

$$H(k) = t(1 + \cos(k \cdot a_1) + \cos(k \cdot a_2))\sigma_x + t(\sin(k \cdot a_1) + \sin(k \cdot a_2))\sigma_y + m\sigma_z, \quad (3.67)$$

corresponding to a Pauli vector $h = \vec{h}(k)$, where

$$\vec{h}(k) = \begin{pmatrix} t(1 + \cos(k \cdot a_1) + \cos(k \cdot a_2)) \\ t(\sin(k \cdot a_1) + \sin(k \cdot a_2)) \\ m \end{pmatrix}. \quad (3.68)$$

In particular, the spectrum of graphene is given by

$$(h^* E^{\sigma}_{\pm})(k) = \pm\sqrt{m^2 + 3t^2\left[1 + \frac{2}{3}\big(\cos(k \cdot a_1) + \cos(k \cdot a_2) + \cos(k \cdot (a_1 - a_2))\big)\right]}.$$

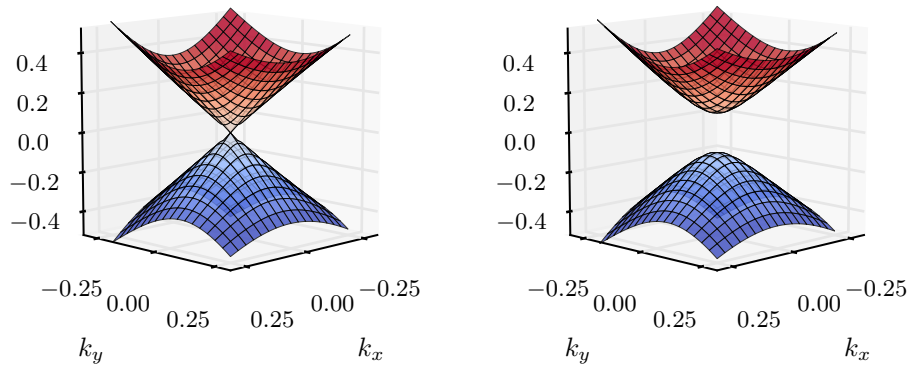

(a) gapless case. **(b) gapped case.**

Figure 3.8: Zoom of the dispersion relation near a Dirac point. Zooms near the K point of the dispersion relations of graphene ((a), figure 3.6) and gapped graphene ((b), figure 3.7) are presented.

When it is gapped (i.e. as long as $m \neq 0$), the projectors $h^* P^\sigma_\pm$ are well-defined, and can be readily computed.

A 2×2 Bloch Hamiltonian $H(k)$ can always be written as

$$H(k) = h_\mu(k)\sigma_\mu = H^\sigma(h(k)) \tag{3.69}$$

or in other words, $H = h^* H^\sigma \equiv H^\sigma \circ h$ where the star represents the pullback operation (defined by this relation). Notice that here $h : \mathrm{BZ} \to \mathbb{R}^3$ is a map from the Brillouin torus to $\mathbb{R}^3$, and not a point of $\mathbb{R}^3$ like in e.g. equation (3.62). We can directly use the preceding: eigenvectors, energies and projectors of H are $h^*\psi^\sigma_\pm$, $h^* E^\sigma_\pm$ and $h^* P^\sigma_\pm$. When $k \mapsto h(k)$ is a smooth map, then $h^* E^\sigma_{pm}$ and $h^* P^\sigma_\pm$ are too, but this is not always the case of the eigenstates $h^*\psi_\pm$: it may happen that it is impossible to define smooth maps $h^*\psi^\sigma_\pm$ on the whole Brillouin torus. In fact, as we shall see in section 2, this obstruction is a direct consequence of a topologically nontrivial insulator.

1.3 Electrons in a solid and the Pauli principle

In a solid state setting, we are concerned about a chunk of material at equilibrium, near zero temperature: the temperature scale of electrons in a solid is set by the Fermi temperature which is on the order of $1 \times 10^5\,\mathrm{K}$, which is huge with respect to room temperature. As a consequence, the fact that temperature is in fact not exactly zero can be treated as a perturbative correction. In such a system, there are many electrons (say N), and the Hilbert space is the N^{th} antisymmetric tensor product of the single-

particle Hilbert space. When interactions between electrons can be neglected[4], the fundamental state of the many-body system is readily obtained from the spectrum of the one-body system. As electrons are fermionic particles, they must obey the Pauli exclusion principle, which states that two (or more) or them cannot share the same one-particle state. As a consequence, the fundamental state at zero temperature is obtained by *filling* one-body eigenstates starting from the lowest energy (the bottom of the bands) until we run out of electrons. The energy of the highest occupied one-particle state (at zero temperature) is called the Fermi energy E_F; all states with energy below E_F are occupied (and constitute the so called *Fermi sea*) and all states above E_F are empty. This description gives a good picture of what happens, but it is not really robust: what happens at nonzero temperature? or when the system is open? To answer those questions, it is better to introduce a purely thermodynamical quantity, the **chemical potential** μ of the system[5]. At equilibrium, the electrons are distributed according to the Fermi-Dirac distribution

$$n_\mathrm{FD}(E) = \frac{1}{\mathrm{e}^{\beta(E-\mu)}+1} \tag{3.70}$$

where $\beta = 1/k_\mathrm{B}T$ is the inverse temperature, giving the population of a state with energy E. This implicitly defines μ. Alternatively (but equivalently), the chemical potential can be defined as a derivative of the appropriate thermodynamic function, e.g.

$$\mu = \left.\frac{\partial G}{\partial N}\right|_{T,P} = \left.\frac{\partial U}{\partial N}\right|_{S,V}. \tag{3.71}$$

Physically, the chemical potential is interpreted as the energy required to add an electron to the system, or equivalently as the Lagrange multiplier associated to the particle number conservation. With such a thermodynamic definition, we find that a zero temperature, the chemical potential lies exactly at the middle of the energies of the highest filled and the lowest empty states. In particular, when there is a gap between a filled band and an empty one (i.e. in an insulator), the chemical potential lies in the middle of this gap. On the other hand, when there is no gap (in a metal), the Fermi energy and the chemical potential coincide at zero temperature. The thermodynamic definitions (3.71) assume that the system is closed, that is, electrons cannot enter or leave the system. This is not always the case: the chemical potential can also be controlled by the environment, in particular in transport experiments where the system may be connected to electronic reservoirs and may be placed under a gate (in which case μ is fixed as a thermodynamic variable, and not N). When the chemical potential is inside a gap in the band structure, the system is called an *insulator*; it is principally characterized by its gap E_gap (see figure 3.9). In other situations, when the chemical potential crosses a band, the system is a usually a *metal* (see figure 3.9), except in the very special situation where the density of states vanishes at the Fermi level: in this case, the system is a *semimetal*.

[4] Another case is when interactions can be taken into account in a mean field approach, but then we start from the mean-field one-particle Hamiltonian.

[5] The chemical potential includes contributions from external field, e.g. qV for an electric potential V or mgh to take gravity into account. In the former case, μ may also be called an electrochemical potential.

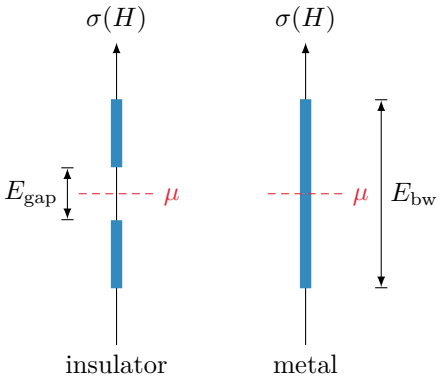

Figure 3.9: Metal and insulator.

This classification comes first from transport properties, which are spectacularly different in metals and insulators. In both cases, in the absence of any external field, the ground state does not carry any current. In a metal, it is possible to excite an electron from just below the Fermi level to just above it, a change which costs an very small amount of energy per electron, that can be provided e.g. by an electric field. The electron-hole pair that is created by this process can carry current, a characteristic of metals, which are good electrical conductors. In an insulator however, it is not possible to create such a low energy excitation: a minimal energy E_{gap} is required to create an electron pair, and this energy is huge (see later), so it cannot be provided by the electric field of a tension source. As a consequence, the system is not able to carry an electrical current, in other words it is an electrical insulator[(6)]. At zero temperature, the gap controls whether the system is insulating or not: we can estimate the order of magnitude of the electric field needed to induce Landau-Zener tunnelling between bands, which is negligible as long as $eE/k_{\text{F}} \ll E_{\text{gap}}\sqrt{E_{\text{gap}}/E_{\text{F}}}$ [Mar15]. Taking typical values of $E_{\text{F}} = 10\,\text{eV}$, $k_{\text{F}} = 1\,\text{Å}$, and $E_{\text{gap}} = 0.1\,\text{eV}$, we find that the electric field has to be comparable with $1 \times 10^6\,\text{V}\cdot\text{cm}^{-1}$ to induce Zener breakdown. In practice, electrical breakdown usually occurs below this limit, due to a variety of other mechanisms due to interfaces, defects, temperature, etc. Besides, at finite temperature, the thermal filling of the conduction band can induce a density of charge carriers sufficient to carry a macroscopic current even when there is a gap: this is the case of semiconductors. As we shall see in the following parts of this work, transport measurements are a key source of information about mesoscopic systems.

In an insulator (at zero temperature), the band gap separates the filled **valence band** from the empty **conduction band**. Let the *valence projector* $P_{\text{v}}(k)$ be the (spectral) projector on states of the valence band. We also define a *conduction projector* $P_{\text{c}}(k) = \text{Id} - P_{\text{v}}(k)$. Maps $k \mapsto P_{\text{v/c}}(k)$ are always well-defined as long as the gap is open (thanks to equation (3.61)), even if there are obstructions to the existence of globally defined wave functions on the Brillouin zone (we shall see in section 2 that

(6) This description breaks down when our assumptions are not satisfied, e.g. when electrons are interacting (in Mott insulators) or when the system is no longer a periodic crystal (in Anderson insulators).

it can happen, and in fact is a signature of the nontrivial topology of the band). The corresponding vector bundles over the Brillouin torus are naturally called the *valence bundle* and the *conduction bundle*.

For example, in gapped graphene, when the chemical potential lies in the gap, the lowest band in the valence band, and the highest one is the conduction band; so we have $P_{\mathrm{v}} = h^* P_-^\sigma$ and $P_{\mathrm{c}} = h^* P_+^\sigma$. In terms of the geometrical objects, the valence bundle, for instance, has fiber $P_{\mathrm{v}}(k)\mathbb{C}^2$ over point $k \in \mathrm{BZ}$.

1.4 Band structures beyond electronic systems

As we have seen in the introduction (see section 1.3, page 15), any system with waves propagating in a periodic structure is described by Bloch theory, and therefore has a band structure, etc. This is the case e.g. for photonic crystals, cold atoms in photonic lattices, or mechanical metamaterials. In a classical context, the energy of eigenstates is replaced by the frequency of eigenmodes. In such systems (except perhaps fermionic cold atoms), a gapped system is not an "insulator", because (i) without electrical current to carry, the notion of an insulator is dubious, (ii) the Pauli principle does not apply, and (iii) room temperature is usually not a good approximation for zero temperature. This modification is crucial to many points of views: for example, it is usually no more possible to use the ground state to define topological properties (and as a consequence, we expect a part of the experimental signatures of a nontrivial topology to be lost). Yet, the *band structure* still has distinct topological properties, which lead to clearly observable consequences such as protected edge states. As we shall see, the issue is very similar, even for electrons in solids, when the system is subject to a time-periodic modulation. In the following, we will therefore focus on the topological properties of the band structure, not of the ground state, which we expect to be generalizable (i) to classical systems and (ii) to periodically driven systems.

2 Topological insulators

In this section, we review topological insulators. We start with the Haldane model, an example of Chern insulator, with properties similar to the quantum Hall effect. Then, we describe the SSH model of polyacetylene, an example of one-dimensional topological insulator protected by chiral symmetry, and the Bernevig-Hughes-Zhang model to illustrate Kane-Mele insulators protected by time-reversal invariance. Finally, we review the classification of unitary evolutions according to the ten Cartan-Altland-Zirnbauer symmetry classes, and the corresponding "periodic table" classifying topological insulators according to their CAZ symmetry class and the space dimension.

2.1 The Haldane model

2.1.1 Introduction

Less than one year after the experimental discovery of the quantum Hall effect by von Klitzing, Dorda and Pepper [KDP80] in 1980, Laughlin proposed his famous pumping argument [Lau81], which, in retrospect, highlights that the quantum Hall effect is the manifestation of an anomaly. In parallel, so as to say, anomalies were discovered in the context of high energy physics in the end of the '60s with the Adler-Bell-Jackiw axial/chiral anomaly [Adl69; BJ69] (in even dimensional spacetime), which was followed by the parity anomaly (in odd dimensional spacetime) by Niemi, Semenoff and Redlich [NS83; Red84a; Red84b]. On the one hand, the quantum Hall effect was explicitly linked to anomalies as soon as 1984 [Ish84; FSWS84; Jac84]. On the other hand, in the context of lattice gauge theory, Nielsen and Ninomiya [NN81a; NN81c; NN81b] proved in 1981 that under certain conditions, it is not possible to implement chiral fermions on a lattice (an analogue of Nielsen-Ninomiya theorem was later developed for two dimensional graphene by Hatsugai [Hat11]). They later illustrated this theorem on electrons in a crystal and linked it to an analogue of the ABJ anomaly in solid state physics [NN83]. This idea was extended to the parity anomaly by Semenoff [Sem84], who proposed a "condensed-matter simulation of a three-dimensional anomaly" (this is the title of his paper) in a graphite monolayer. Finally, four years later, Haldane [Hal88] extended Semenoff's model by adding local magnetic fluxes to the unit cell to Semenoff's model, organized so that the total magnetic flux in a unit cell vanishes (so the net magnetic flux through the system vanishes, the vector potential has the lattice periodicity, and Bloch theorem applies). Two striking consequences arise from this last step. First, the system exhibits a quantum Hall effect behavior without a magnetic field; this behavior, dubbed "anomalous quantum Hall effect" (and later *Chern insulator*) is manifested in the appearance of a quantized Hall conductance. Second, the phase diagram of the system exhibits insulating phases with different Hall conductances, namely 0 and ± 1 (in units of e^2/h). In the semi-metallic critical phases that lie at the transition lines between the different insulators, the breaking of time-reversal invariance allows a single Dirac cone (or chiral fermion) to exist at low energy. A last point worth to mention is that in 1988, the same year as Haldane's paper [Hal88] (but in the soon-to-be former USSR) Volovik [Vol88b; Vol88a] described an analogue of the quantum Hall effect without a magnetic field in two-dimensional films of ^{3}He-A, where time-reversal symmetry is broken and the nontrivial structure of the complex order parameter may induce a nontrivial topology.

In 1982 Thouless, Kohmoto, Nightingale and den Nijs (TKNN) [TKNN82] recognized the topological nature of the quantum Hall effect, which were soon recognized to be Chern invariants by Avron, Seiler and Simon [ASS83; Sim83]. But TKNN were (rightfully) concerned with the problem of electrons in a magnetic field, which they described with the Harper-Hofstadter model, a complicated situation where Bloch theorem does not generically apply (only when a magnetic unit cell can be defined). The Haldane model is the first example of a topological insulator realized in a periodic crystal, where Bloch theorem applies, a much simpler situation which is easier to study and to extend.

2.1.2 The tight-binding model

Spinless electrons on a sheet of graphene (so in space dimension $d = 2$) are described with a simple tight-binding Hamiltonian (see paragraph 1.1.3), to which is added a staggered potential (or mass term) M_x which breaks inversion symmetry [Sem84] and Aharanov–Bohm phases corresponding to complex hopping amplitudes which break time-reversal invariance [Hal88]. The Aharanov–Bohm phases may correspond to local magnetic fluxes, organized so that there is no net magnetic flux in an unit cell (so the system is not supposed to be under an external magnetic field, in contrast with the quantum Hall effect). In the tight-binding description, Aharanov–Bohm phases are taken into account through a Peierls substitution,

$$t_{xy} \to t_{xy} \exp\left(-\mathrm{i}\frac{e}{\hbar}\int_{\Gamma_{xy}} \vec{A}\cdot \mathrm{d}\,\vec{\ell}\right) \tag{3.72}$$

where t_{xy} is the hopping parameter from site y to site x (e.g. with a term $t_{xy}\,|x\rangle\langle y|$), Γ_{xy} the trajectory from site x to site y and $\vec{A}$ is a potential vector accounting for the presence of the magnetic flux. In our case, the substitution is simply

$$t' \to t'\mathrm{e}^{\pm \mathrm{i}\phi} \tag{3.73}$$

with a sign depending on the sublattice and of the direction of the hopping, in order to ensure that the total magnetic flux through a unit cell is zero. To be more precise, equation (3.39) is modified into

$$H = t\sum_{\langle x,y\rangle} |x\rangle\langle y| + t'\sum_{\langle x,y\rangle_2} \mathrm{e}^{\mathrm{i}\phi_{x,y}}\,|x\rangle\langle y| + \sum_{x\in\mathcal{C}} M_x\,|x\rangle\langle x| \tag{3.74}$$

with, as in the previous paragraph,

$$M_x = \begin{cases} +M & \text{when } x \in A \\ -M & \text{when } x \in B \end{cases} \tag{3.75}$$

and with

$$\phi_{x,y} = \begin{cases} \pm\phi & \text{when } x,y \in A \text{ and } x-y \in \Delta_2^{\pm} \\ \mp\phi & \text{when } x,y \in B \text{ and } x-y \in \Delta_2^{\pm} \end{cases} \tag{3.76}$$

where the second neighbors positions are

$$\Delta_2 = \Delta_2^+ \cup \Delta_2^- = (a_1, -a_2, a_2-a_1) \cup (a_2, -a_1, a_1-a_2)\,. \tag{3.77}$$

The definition of $\phi_{x,y}$ (done coherently so that $t_{ji} = \overline{t_{ij}}$) ensures that the phase accumulated through $A \to A$ hopping is opposite of the one gained through $B \to B$ hopping, in the following sense: the same oriented closed path $[x, x+a_2, x+a_1]$ will catch a flux $\mp 3\phi$ according to whether $x \in A/B$ (see figures 3.10, 3.11a and 3.11b). Namely, the path Γ_{A} in figure 3.11a catches a flux -3ϕ while the path Γ_{B} catches a flux $+3\phi$

The corresponding Bloch Hamiltonian is

$$H = h^* H^\sigma \qquad \text{i.e.} \qquad H(k) = h_\mu(k)\cdot\sigma_\mu \tag{3.78}$$

with

$$\begin{aligned} h_0(k) &= 2t' \cos\phi \sum_{\delta_2 \in \Delta_2^+} \cos(k \cdot \delta_2) \\ h_x(k) &= t\left[1 + \cos(k \cdot a_1) + \cos(k \cdot a_2)\right] \\ h_y(k) &= t\left[\sin(k \cdot a_1) + \sin(k \cdot a_2))\right] \\ h_z(k) &= M - 2t' \sin\phi \sum_{\delta_2 \in \Delta_2^+} \sin(k \cdot \delta_2). \end{aligned} \tag{3.79}$$

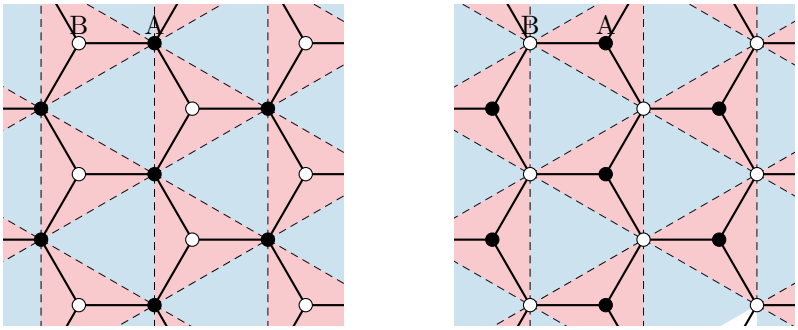

(a) Point view of A sublattice. **(b) Point of view of B sublattice.**

Figure 3.10: Staggered fluxes in the Haldane model. A simple picture of the local magnetic fluxes can be painted when we separate sublattices A and B. As the net flux through a unit cell vanishes, the first-nearest-neighbors are not affected by the Peierls substitution and we can focus on the second-nearest-neighbors hoppings. As they are diagonal in sublattice, we can separate the discussion. For example, figure (a) represents a possible flux distribution *from the point of view of sites in the sublattice A*. The red triangles contain a flux 3ϕ, and the blue ones a flux -3ϕ. Obviously, the total flux vanishes. The picture is similar from the point of view of B sites, in figure (b) (the color code is the same), but with different triangles. It is indeed possible to find a flux distribution that make both points of view simultaneously possible, see figure 3.11b. (All fluxes are oriented in the same way, towards the reader.)

In order to make the discussion a bit more general, we will consider all possible 2×2 Bloch Hamiltonians instead, a natural thing to do as we are interested in topological properties.

2.1.3 The two-by-two Hamiltonian again

As we have seen, a two-by-two Bloch Hamiltonian can always be written as $H(k) = h^* H^\sigma$ where $h : \mathrm{BZ} \to \mathbb{R}^4$. Here, $\mathbb{R}^4$ can be thought as a parameter space. In the following, we will consider a gapped system (in the sense of equation (3.60)). As we are mainly interested in the topological properties of this Hamiltonian, we are allowed to smoothly modify the function h as long as it does not close the band gap. The valence (and conduction) bundle will be affected by such modifications, but they will remain in the same equivalence class, i.e. their topological properties won't be

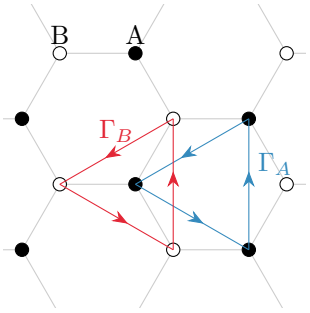

(a) Phases accumulated on a closed loop. The phase accumulated over a closed loop Γ_A connecting only A sites is the opposite of the phase accumulated over the same loop Γ_B translated so that it connects only B sites.

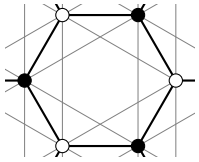

(b) Possible flux distribution. A possible choice of fluxes to ensure the phase distribution (3.76): put -6ϕ in the inner hexagon and $+\phi$ in each branch of the star (this ensures a vanishing total flux through the unit cell).

Figure 3.11: Flux distribution and phase accumulation in the Haldane model.

affected. We will therefore be able to reduce the parameter space $\mathbb{R}^4$ to a 2-sphere and use our knowledge of the bundles on the sphere generated by a "band flattened Hamiltonian" with eigenvalues ± 1.

First, suppose that $h_0 \equiv 0$. When this is the case, the system is gapped as long as $\vec{h}$ never vanishes (we shall see that indeed $\vec{h}$ never vanishes for the Haldane model, except on transition lines where the topological nature of the phase changes). The coefficient h_0 should be discarded or added back with some care, as it could change the nature (gapped or not) of the system, but topological properties will not be affected, because the eigenstates do not depend on h_0, or alternatively because the system remains locally gapped as long as $\vec{h}$ never vanishes. From now, we may use the same notation h for the map $\mathrm{BZ} \to \mathbb{R}^4$ including h_0 and the map $\mathrm{BZ} \to \mathbb{R}^3$ without h_0, as the context makes clear which of these is considered.

Second, notice that as long as $h_0 = 0$, the eigenvectors and projectors of section 2.3 only depend on the normalized vector

$$x = \frac{h}{\|h\|} = \begin{pmatrix} x_1 \\ x_2 \\ x_3 \end{pmatrix} = \begin{pmatrix} \sin\theta\cos\phi \\ \sin\theta\sin\phi \\ \cos\theta \end{pmatrix} \tag{3.80}$$

and in these spherical coordinates, the projectors read

$$P^\sigma_\pm(\theta,\phi) = \frac{1}{2}\begin{pmatrix} 1 \pm \cos\theta & \pm\sin\theta\, \mathrm{e}^{-\mathrm{i}\phi} \\ \pm\sin\theta\, \mathrm{e}^{+\mathrm{i}\phi} & 1 \mp \cos\theta \end{pmatrix}. \tag{3.81}$$

As a consequence, it is sufficient to have a map $n : \mathrm{BZ} \to S^2$ defined by

$$n = \vec{h}/\|\vec{h}\|. \tag{3.82}$$

See also figure 3.12. This procedure is sometimes called *band flattening*, as we can define a "band flattened Hamiltonian" $n \cdot \sigma$ with eigenvalues $E/|E| = \pm 1$ (so the energy bands are now *flat*, they do not depend on k).

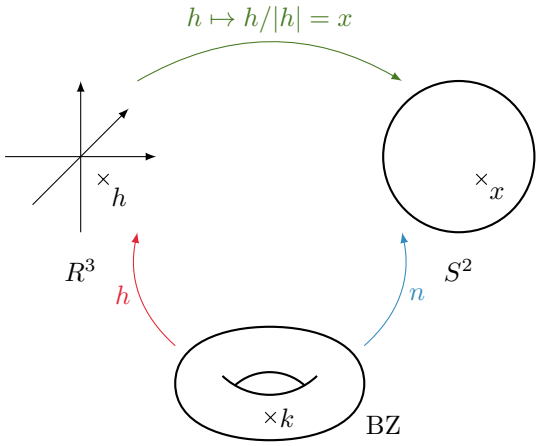

Figure 3.12: Mapping from the vector bundle on a sphere to the Bloch bundle. The map $p : h \mapsto x = h/|h|$ goes from $\mathbb{R}^3\backslash 0$ to the sphere S^2. A two-by-two Bloch Hamiltonian is described by a map $h : \mathrm{BZ} \to \mathbb{R}^3$. When the Bloch Hamiltonian is gapped, this application never vanishes and can be composed with p to get a map $n : \mathrm{BZ} \to S^2$ (which also defines a band flattened Bloch Hamiltonian), the topological properties of which are easy to visualize. To reduce the number of notations, I used the letter h both for a point of $\mathbb{R}^3\backslash 0$ and for the map $\mathrm{BZ} \to \mathbb{R}^3$.

The pullback of the bundle $E_\pm$ (defined in section 2.3) by n defines the valence bundle $E_\mathrm{v} = n^* E_-$ and the conduction bundle $E_\mathrm{c} = n^* E_+$, both of which are (possibly nontrivial) bundles on the Brillouin torus. As the conduction and valence subbundles combine to form the trivial total Bloch bundles, their topologies are opposite[7], so we can focus e.g. on the valence bundle, and let $P = n^* P^\sigma_-$ be the corresponding projector. As we have seen, this complex vector bundle may be nontrivial. As the Brillouin torus is a 2-manifold, the valence bundle is (stably) trivial as long as its first Chern number vanishes. This invariant is obtained by integrating over the Brillouin zone the pull-back by n of the curvature form F_{S^2} on the sphere,

$$C_1 = \frac{\mathrm{i}}{2\pi} \int_{\mathrm{BZ}} n^* F_{S^2} \tag{3.83}$$

For example, in terms of the projector $P = n^* P^\sigma_-$, the curvature is

$$n^* F_{S^2} = \mathrm{tr} P \mathrm{d}P \wedge \mathrm{d}P. \tag{3.84}$$

We can also pull back formula (2.71) for the curvature (with our $F_{S^2} = \mathrm{tr} K_-$). As n depends on the two components k_x and k_y of the quasi-momentum $k \in \mathrm{BZ}$,

$$\mathrm{d}n_j = \frac{\partial n_j}{\partial k_a} \mathrm{d}k^a \qquad \text{and} \qquad \mathrm{d}n_j \wedge \mathrm{d}n_k = \frac{\partial n_j}{\partial k_a} \frac{\partial n_k}{\partial k_b} \, \mathrm{d}k_a \wedge \mathrm{d}k_b \tag{3.85}$$

[7] To be more precise, the Bloch bundle is $E = E_\mathrm{v} \oplus E_\mathrm{c}$ (for valence and conduction), and we know that E is trivial, so $\mathrm{ch}(E)$ vanishes. From equation (2.38), we deduce $\mathrm{ch}(E_\mathrm{v}) = -\mathrm{ch}(E_\mathrm{c})$.

so we have

$$n^* F_{S^2} = \frac{-\mathrm{i}}{4}\,\epsilon^{ijk}\, n_i \frac{\partial n_j}{\partial k_a}\frac{\partial n_k}{\partial k_b}\,\mathrm{d}k_a \wedge \mathrm{d}k_b = \frac{-\mathrm{i}}{2}\,\vec{n}\cdot\left(\frac{\partial \vec{n}}{\partial k_x}\times\frac{\partial \vec{n}}{\partial k_y}\right)\,\mathrm{d}k_x \wedge \mathrm{d}k_y \quad (3.86)$$

where $\times$ is the 3-vector cross product. It is convenient to use a slight variation of the last formula to express the curvature directly in terms of h as

$$n^* F_{S^2} = \frac{-\mathrm{i}}{2}\,\frac{\vec{h}}{\|h\|^3}\cdot\left(\frac{\partial \vec{h}}{\partial k_x}\times\frac{\partial \vec{h}}{\partial k_y}\right)\,\mathrm{d}k_x \wedge \mathrm{d}k_y \quad (3.87)$$

Notice that we did not simply replace n with $h/\|h\|$: the norm was factored out of the differential operators, an observation which facilitates greatly the actual computations.

At the end, the first Chern number is

$$C_1 = \frac{1}{4\pi}\int_{\mathrm{BZ}} \frac{\vec{h}}{\|h\|^3}\cdot\left(\frac{\partial \vec{h}}{\partial k_x}\times\frac{\partial \vec{h}}{\partial k_y}\right)\,\mathrm{d}k_x \wedge \mathrm{d}k_y \quad (3.88)$$

(arrows on vectors are especially put in expressions where dot/cross products appear, to avoid any confusion). We recognize the degree (or index) of the map $h \equiv \vec{h} : \mathrm{BZ} \to \mathbb{R}^3$ (see [DFN85]). This identification provides an intuitive picture of the first Chern number, and will allow us to compute it easily. When k spreads over the Brillouin torus, $\vec{h}$ describes a closed surface $\Sigma \subset \mathbb{R}^3$ (which projects on a closed surface $\hat{\Sigma} \subset S^2$, described by $\vec{n}$). The degree of h (or n) is equivalently given by

- the integral formula (3.88), which may be interpreted as the (normalized) flux through the surface Σ of a magnetic monopole located at the origin (and giving rise to a field strength F_{S^2}),
- the number of times the surface Σ wraps around the origin (in particular, it is zero if the origin is outside the interior of Σ ; more precisely it is the homotopy class of Σ in the punctured space $\mathbb{R}^3 - 0$) ; equivalently, the system is trivial iff $\hat{\Sigma}$ does not completely cover S^2,
- the number of (algebraically counted) intersections of a ray coming from the origin with Σ. This last method was notably used by [SPFK12] to engineer two-dimensional Chern insulators with arbitrarily large Chern numbers.

We may now compute the Chern invariant explicitly, either numerically or analytically. A numerical computation is quite useful (and sometimes necessary) when the analytic expression of n (or P) and its derivatives are unknown or too complicated; in this case, it is possible to simply discretize the integral over the torus, but a more efficient method was proposed by Fukui, Hatsugai and Suzuki [FHS05]. For now however, let us focus on the analytical computation.

To determine the phase diagram of the Haldane model, let us first find the points in the parameter space where the local gap closes (i.e. where h vanishes) at some point(s) of the Brillouin torus. In graphene, which corresponds to $(M, \phi) = (0, 0)$ in the diagram, the two energy bands are degenerate at the Dirac points K et K'

(defined at equation (3.37)). At a generic point of the diagram, this degeneracy is lifted, and the system is an insulator ($h \neq 0$), except when

$$|M| = 3\sqrt{3}t' \sin\phi \tag{3.89}$$

where the gap closes (at least) at one of the Dirac points K and K'. The corresponding lines separate four possibly different insulating states. To know their nature, we must determine the first Chern number, which is also the number of intersections between a ray coming from the origin and the oriented closed surface Σ spanned by h. Alternatively, we can consider half of the number of intersections with a line instead of a ray. A good choice for this line is the Oz axis, as $D_z = h^{-1}(Oz \cap \Sigma)$ is simply the set of Dirac points K and K', so

$$C_1 = \frac{1}{2}\sum_{k\in D_z} \operatorname{sign}\left[\vec{h}(k)\cdot\vec{\nu}(k)\right] = \frac{1}{2}\sum_{k\in D_z} \operatorname{sign}\left[h_z(k)\right] \operatorname{sign}\left[\left(\frac{\partial\vec{h}}{\partial k_x}\times\frac{\partial\vec{h}}{\partial k_y}\right)_z\right] \tag{3.90}$$

where $\nu(k)$ is the normal vector to Σ at k (it is the cross product in the rhs). The masses are

$$h_z(K) = M + 3\sqrt{3}t'\sin\phi \qquad \text{and} \qquad h_z(K') = M - 3\sqrt{3}t'\sin\phi. \tag{3.91}$$

On the other hand, $\nu_z(k) = 3\sqrt{3}/2t^2 \sin(\sqrt{3}k_y)$ so the first Chern number turns out to be

$$C_1 = \frac{1}{2}\left[\operatorname{sign}\left(\frac{M}{t'} + 3\sqrt{3}\sin(\phi)\right) - \operatorname{sign}\left(\frac{M}{t'} - 3\sqrt{3}\sin(\phi)\right)\right]. \tag{3.92}$$

It is represented on the phase diagram of figure 3.13.

2.1.4 Edge states

A striking consequence of a nontrivial bulk topology is the appearance of *metallic edges* at the surface of a topological insulator, or, to be more precise, at the interface between two insulators with different topologies. Such edge states display peculiar properties: in the case of Chern insulators, they are *chiral*, or "one-way": they propagate in one direction only along the edge. Moreover, they are "topologically protected", in the sense that they are immune to defects or disorder in the interface, because there are no states available for backscattering.

Chiral edge states can be seen as domain walls between two phases, which arise from the interpolation between two different values of a parameter. Such a situation was first studied by Jackiw and Rebbi [JR76], who considered a fermionic field (corresponding here to the Bloch vector) coupled to a scalar field (here, the space-dependent mass term) with a soliton solution (here, the edge state). This soliton wave function carries a fractional charge $\pm e/2$, which is both interpreted as the topological charge of the soliton and as the electric charge of the fermionic mode. Su, Schrieffer and Heeger studied a soliton at the interface between two phases of polyacetylene [SSH79], which is now understood as an edge state (in a one-dimensional system with chiral symmetry, see section 2.2.3). This kind of domain wall states with a linear dispersion were also predicted at the interface between semiconductors with different

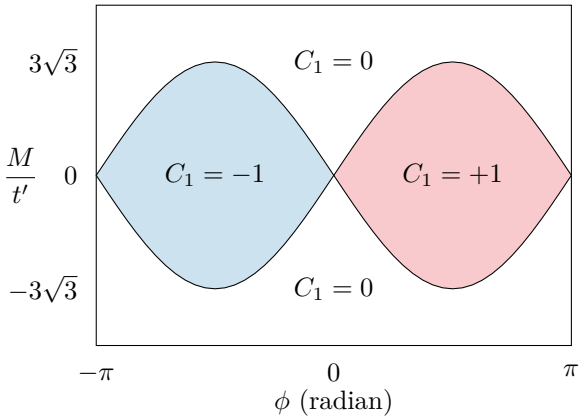

Figure 3.13: Phase diagram of the Haldane model. The Haldane Hamiltonian is gapped, except on the critical lines (in black), where the system is a semi-metal with only one Dirac cone, except at the bicritical points $(\phi, M/t_2) = (\pi\mathbb{Z}, 0)$. The point $(0, 0)$ corresponds to bare graphene. The insulating phase are characterized by their first Chern number C_1, which is color coded (white: 0; red: $+1$; blue: -1). The phase diagram is represented on the plane $(\phi, M/t_2)$, but the parameter manifold is in fact a cylinder $S^1 \times \mathbb{R}$ as ϕ is a phase.

dopings by Volkov and Pankratov [Vol85]. Another step in the understanding of such phenomena was taken by Callan and Harvey [CH85], who gave a cancellation relation (the so-called "anomaly inflow") between the anomalous behavior of a domain wall (the edge state) and the flow of a relevant charge from the higher-dimensional space in which it is embedded (the bulk). Kaplan [Kap92] realized that this allowed to construct chiral lattice fermions in $2n$ dimensions on the boundary of a $(2n + 1)$ lattice, as a way to circumvent the Nielsen–Ninomiya theorem.

Let us illustrate the appearance of such chiral topological edge states in the Haldane model. As the transition between different phases happen only when the gap closes, which are the Dirac points K and K', it is enough to focus on a low energy description around them. We linearize the Haldane Hamiltonian around K (or K') by writing $k = K + q$ to the massive Dirac Hamiltonian

$$H_{\mathrm{l}}(q) = \hbar v_{\mathrm{F}}\, q \cdot \sigma_{2\mathrm{d}} + m\, \sigma_z \tag{3.93}$$

with $q = (q_x, q_y)$ (up to a rotation) and $\sigma_{2\mathrm{d}} = (\sigma_x, \sigma_y)$, and $m = h_z(K)$ (in the following, we set $\hbar v_{\mathrm{F}} = 1$). The same holds at K', with a mass m'. In terms of the original parameters,

$$m = h_z(K) = M + 3\sqrt{3}t' \sin\phi \qquad \text{and} \qquad m' = h_z(K') = M - 3\sqrt{3}t' \sin\phi. \tag{3.94}$$

As $C_1 = (\mathrm{sign}(m) - \mathrm{sign}(m'))/2$, the masses m and m' of the Dirac points K and K' have the same sign in the trivial phase with $C_1 = 0$, and have opposite signs in the topological phase with $C_1 = \pm 1$. We can now consider an interface at $y = 0$ between a (nontrivial) Haldane insulator with a Chern number $C_1 = 1$ for $y < 0$ and

a (trivial) insulator with $C_1 = 0$ for $y > 0$. Necessarily, one of the masses changes sign at the interface: $m(y < 0) < 0$ and $m(y > 0) > 0$, whereas the other one has a constant sign $m' > 0$ (see figure 3.14). It is natural to set $m(0) = 0$, which implies that the gap closes at the interface. A more precise analysis shows that there are indeed surface states. As the mass m depends on the position, it is more convenient to express the single-particle Hamiltonian in space representation. By inverting the Fourier transform in (3.93) (which amounts to the replacement $q \to -\mathrm{i}\nabla$), we obtain the Hermitian Hamiltonian:

$$H_\mathrm{l} = -\mathrm{i}\nabla \cdot \sigma_\mathrm{2d} + m(y)\sigma_z = \begin{pmatrix} m(y) & -\mathrm{i}\partial_x - \partial_y \\ -\mathrm{i}\partial_x + \partial_y & -m(y) \end{pmatrix}. \tag{3.95}$$

In order to get separable PDE, let us rotate the basis with the unitary matrix:

$$U = \frac{1}{\sqrt{2}} \begin{pmatrix} 1 & 1 \\ 1 & -1 \end{pmatrix} \tag{3.96}$$

to obtain the Schrödinger equation:

$$U \cdot H_\mathrm{l} \cdot U^{-1} \begin{pmatrix} \alpha \\ \beta \end{pmatrix} = \begin{pmatrix} -\mathrm{i}\partial_x & \partial_y + m(y) \\ -\partial_y + m(y) & \mathrm{i}\partial_x \end{pmatrix} \begin{pmatrix} \alpha \\ \beta \end{pmatrix} = E \begin{pmatrix} \alpha \\ \beta \end{pmatrix}. \tag{3.97}$$

This matrix equation corresponds to two separable PDE

$$(-\mathrm{i}\partial_x - E)\,\alpha = S_1 = -(\partial_y + m(y))\,\beta \tag{3.98a}$$

$$(\mathrm{i}\partial_x - E)\,\beta = S_2 = -(-\partial_y + m(y))\,\alpha \tag{3.98b}$$

In order to obtain normalizable solutions, the corresponding separations constants S_1 and S_2 must be zero. We can then solve separately for α and β. For our choice of $m(y)$, there is only one normalizable solution, which reads in the original basis

$$\psi_{q_x}(x, y) \propto \mathrm{e}^{\mathrm{i}q_x x} \exp\left[-\int_0^y m(y')\,\mathrm{d}y'\right] \begin{pmatrix} 1 \\ 1 \end{pmatrix} \tag{3.99}$$

and has an energy $E(q_x) = E_\mathrm{F} + \hbar v_\mathrm{F} q_x$. This solution is localized transverse to the interface where m changes sign (see figure 3.14).

The edge state crosses the chemical potential at $q_x = 0$, with a positive group velocity v_F and thus corresponds to a *right moving* chiral edge state. One would get a *left moving* chiral edge state by reversing the Chern numbers, see table 3.1.

The precise understanding of the bulk-boundary correspondence is a difficult problem, which has led to a number of developments, both in physics and in mathematical physics. It is possible to make the naive description that we sketched a bit more precise through the use of Green functions, a method which was first used by Volovik [Vol88a] in ^{3}He-A, and which was extended to topological insulators of the Altland-Zirnbauer classification by Gurarie and Essin [Gur11; EG11], and by Rudner et al. [RLBL13] and Nathan et al. [NR15] to the case of topological periodically driven systems. It is also worth to mention the corresponding developments in mathematical physics. In the case of IQHE, the first rigorous result on the bulk-edge correspondence as obtained by Hatsugai [Hat93a; Hat93b], in the case of rational magnetic fluxes and

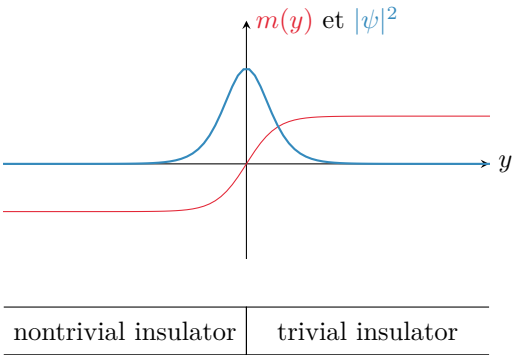

Figure 3.14: Description of a soliton at an interface. The mass $m(y)$ and the wavefunction amplitude $|\psi|^2$ are drawn along the coordinate y orthogonal to the interface $y = 0$ between a nontrivial Chern insulator and a trivial Chern insulator.

sign(m)	sign(m')	C_1	edge states
$+1$	$+1$	0	none
$+1$	-1	$+1$	left-moving
-1	$+1$	-1	right-moving
-1	-1	0	both $\simeq$ none

Table 3.1: Possible transitions in the Haldane model. We consider the possible combinations of (nonzero) masses in the Haldane model, the corresponding first Chern number, and the edge state at an interface with a trivial insulator where $(m, m') = (1, 1)$. Only situations with $C_1 \neq 0$ correspond to topological edge states. The interface with two counter-propagating edge states can be adiabatically connected to a trivial situation with no edge states, which can be mixed together and gapped by a perturbation. For example, an impurity may induce backscattering between the two counter-propagating edge states, spoiling quantized conductance in a sample connected with electrodes.

specific boundary conditions. An important step was taken by Kellendonk, Richter and Schulz-Baldes [SKR99; KRS02; KS04] who extended Hatsugai results to the case of arbitrary magnetic fluxes and boundary conditions with K-theoretic methods and defined an edge invariant characterizing the quantized current. This result was also demonstrated by Elbau and Graf [EG02]. A challenge is to extend such constructions to the case with symmetries. The case of two-dimensional Kane-Mele (fermionic time-reversal invariant) systems was studied by Graf and Porta [GP13b] and Avila, Schulz-Baldes and Villegas-Blas [ASV12], and the case of complex classes by Prodan and Schulz-Baldes [PS16]. Another look at the issue comes from Thiang, Mathai and collaborators [MT15b; MT15a; HMT16] who use T-duality to relate K-theoretic bulk invariants and edge invariants; the K-theoretic bulk-boundary correspondence is also studied by Bourne, Kellendonk and Rennie [BKR16]. This list is not nearly complete; a review of recent literature on the subject in mathematical physics is included in [BCR15].

2.1.5 The (anomalous) quantum Hall effect and Chern insulators, or class A

The Haldane model is the canonical example of **Chern insulator**, or *class A topological insulator*, a kind of topological insulators which require no symmetry at all, and can exist in all even space dimensions. Indeed, there are other models which exhibit this topology; for example, the spin up part of the BHZ model that we will study in section 2.3.4 is a Chern insulator. The Haldane model is limited to values $0, \pm 1$ of the first Chern number, but any integer value is allowed: it is possible to design tight-binding Hamiltonians (yet perhaps not realistic ones) with arbitrary first Chern number [SPFK12; DWD14]. Several experimental realizations of Chern insulators exist in various domains of physics: if was realized with cold atoms in an optical lattice [JMDL14], in lattices of gyroscopes connected by springs (implemented with magnets) [NKRV15], in gyromagnetic photonic crystals [WCJS09] and in thin films of ferromagnetic topological insulators [CZKZ15; CZFS13; BFKP15].

Chern insulators may exist in any even space dimension (weak versions, see section 2.4.3 page 105, may indeed exist in odd space dimensions). Namely, the topology of a spectral projector family P on a $d = 2n$-dimensional Brillouin torus is characterized by the n-th Chern invariant (2.56) (page 50)

$$C_n[P] \in \mathbb{Z}. \tag{3.100}$$

2.2 Chiral symmetric topological insulators, or class AIII

2.2.1 Chiral symmetry and chiral topological invariants

A Hamiltonian H is **chiral invariant** if

$$\Gamma H \Gamma^{-1} = -H \tag{3.101}$$

where Γ is a unitary **chiral operator** Γ squaring to the identity $\Gamma^2 = \mathrm{Id}$ (in general, the chiral operator may square to a phase $\Gamma^2 = \mathrm{e}^{\mathrm{i}\phi}\,\mathrm{Id}$, which can be eliminated through a redefinition). In other words, the chiral operator Γ anticommutes with the Hamiltonian, $\{H, \Gamma\} = 0$. When the Hamiltonian is translation invariant, the chiral operator is assumed to commute with the space translations, and a Bloch Hamiltonian is chiral invariant if

$$\Gamma H(k) \Gamma^{-1} = -H(k). \tag{3.102}$$

The chiral operator acts only on internal and sublattice degrees of freedom, or equivalently whose Bloch representation is a constant matrix (not depending on k). In such a system, the energy spectrum is symmetric with respect to zero (i.e. by $E \to -E$), so a reference for the energies $E = 0$ is naturally provided by chiral symmetry (see paragraph 2.4.4 page 106). Due to this symmetry, the Hamiltonian can have a gap around zero energy only if the size of the Bloch matrix $H(k)$ is even, so we will suppose that it is the case and denote this size by $2M$. In this situation, there is a basis called a **chiral basis** where $\Gamma \cong \mathrm{diag}(1, \dots, 1, -1, \dots, -1)$. Moreover, when H has no zero mode, then $\mathrm{tr}\Gamma = 0$[8], so in the chiral basis, the matrix representing operator

[8] Suppose that H has no zero mode. Let $(\psi_1, \dots, \psi_M)$ be the eigenvectors of H with positive energy; in the basis $(\psi_1, \Gamma\psi_1, \psi_2, \Gamma\psi_2, \dots, \psi_M, \Gamma\psi_M)$ the chiral operator Γ is represented by the block-diagonal matrix $\mathrm{diag}(\sigma_x, \dots, \sigma_x)$ (where σ_i are Pauli matrices), which is traceless.

Γ has the form

$$\Gamma \cong \begin{pmatrix} \mathrm{Id}_M & 0 \\ 0 & -\mathrm{Id}_M \end{pmatrix} \in U(2M). \tag{3.103}$$

Despite the existence of several such bases, we will choose one and refer to it as *the* chiral basis, as nothing actually depends on this choice.

The (Bloch) Hamiltonian is block-antidiagonal in the chiral basis,

$$H(k) \cong \begin{pmatrix} 0 & f(k) \\ f^\dagger(k) & 0 \end{pmatrix}. \tag{3.104}$$

More generally, consider an operator X such that

$$\{\Gamma, X\} = 0 \qquad \text{i.e.} \qquad \Gamma X \Gamma = -X \tag{3.105}$$

and let us write the block matrix of this operator in the chiral basis

$$X \cong \begin{pmatrix} a & b \\ c & d \end{pmatrix}. \tag{3.106}$$

By computing the block product,

$$\Gamma X \Gamma \cong \begin{pmatrix} a & -b \\ -c & d \end{pmatrix} \tag{3.107}$$

so that (3.105) leads to the condition

$$0 = \Gamma X \Gamma + X = \begin{pmatrix} 2a & 0 \\ 0 & 2d \end{pmatrix} \tag{3.108}$$

and therefore $a = 0$ and $d = 0$, so *an operator that anticommutes with the chirality operator is block-antidiagonal in the chiral basis.* In the same vein, *an operator that commutes with the chirality operator is block-diagonal in the chiral basis.*

2.2.2 Chiral topological invariants

When the Hamiltonian is gapped, it is possible to define its valence projector P and the corresponding unitary operator $Q = \mathrm{Id} - 2P$. In the chiral basis, Q is also block-antidiagonal, of the form

$$Q = \begin{pmatrix} 0 & q \\ q^\dagger & 0 \end{pmatrix}. \tag{3.109}$$

The blocks q and $q^\dagger$ are unitary matrices of size M. When the space dimension d is odd, $d = 2n+1$, it is possible to compute the winding number, or odd Chern number (see (2.59)), of the map $q : \mathrm{BZ} \to U(M)$ to define the **chiral invariant**

$$g[P] = W_n(q, \mathrm{BZ}) = \int_{\mathrm{BZ}} \widetilde{\mathrm{ch}}_n(q) \in \mathbb{Z}. \tag{3.110}$$

associated to the band described by the projector P.

Chiral symmetry is sometimes also called **sublattice symmetry**. In a tight-binding system with *bipartite hoppings*, the crystal is separated into two sets of sublattices A and B, with hopping terms only connecting A to B (or B to A). This structure naturally induces a chiral operator (see e.g. equation (3.111)). However, other internal degrees of freedom may also participate in this structure in a nontrivial way, so this denomination is slightly misleading.

Note that the chiral symmetry is not unambiguously defined (see also [NG15a]). For example, in the SSH model (see next section), we could take

$$\Gamma_1 = \sum_{x\in\tilde{\Gamma}} |x, A\rangle\langle x, A| - |x, B\rangle\langle x, B| \tag{3.111}$$

(where the $\tilde{\Gamma}$ on which the sum runs is the Bravais lattice) or choose

$$\Gamma_2 = -\Gamma_1. \tag{3.112}$$

The choice of the (ordered) fundamental domain should be done in a manner which guarantees that Γ is represented by the matrix $\Gamma = \mathrm{diag}(1, \dots, 1, -1, \dots, -1)$, in this case σ_3 (and not e.g. $-\sigma_3$; indeed, we could choose another matrix representation for the chiral operator, which would give an equivalent but different set of invariants). The chiral topological invariants are *not* independent of the definition of the chiral operator. Another point of view on this topic comes from the mathematical literature, where Thiang [Thi15b; Thi15a] (see also De Nittis and Gomi [NG15a]) show that the chiral invariant is only a relative object, which can be used to compare phases, but which has no absolute meaning [(9)].

The nontrivial topology of Chern insulators, in class A, can be interpreted as stemming from the nontriviality of the spectral vector bundles over the torus corresponding to the energy bands of the system. In the case of chiral topological insulators, in class AIII, a similar picture has been developed by De Nittis and Gomi [NG15a] who define *chiral vector bundles* (a generalization inspired from chiral topological insulators, which are a particular case of the construction). Prodan and Schulz-Baldes [PS16] studied classes A and AIII in the framework on noncommutative geometry and K-theory, providing definitions applicable in disordered systems; they also consider the case of approximate chiral systems and explore the consequences of this deviation from the ideal behavior.

Besides polyacetylene (and the SSH model to which the next section is devoted), examples of chiral systems include graphene (and artificial equivalents; see [PRSH13] and references therein) and isostatic mechanical lattices in the harmonic approximation [KL13; PCV15]. In the two-dimensional situations (e.g. in graphene) it is only possible to observe *weak* topological invariants, which are in fact one-dimensional topological invariants which remain defined thanks to translation invariance, see paragraph 2.4.3, page 105. In general, lower-dimensional or so-called weak topological invariants do not always lead to topologically protected edge modes. This is indeed the case in graphene, where armchair edges do not support edge states, in contrast

[(9)] The same is in fact true for the Chern invariants of class A, but the vacuum provides a canonical reference.

with zigzag and bearded edges which do. The same kind of behavior was observed in 2D mechanical systems.

2.2.3 The SSH model

We already encountered the SSH model developed by Su, Schrieffer and Heeger [SSH79] to describe polyacetylene in section 1.1.4 (page 67). Its Bloch Hamiltonian is

$$H(k) = \vec{h} \cdot \vec{\sigma} = (J_1 + J_2 \cos(k))\sigma_1 + J_2 \sin(k)\sigma_2 \tag{3.113}$$

where σ_i are the Pauli matrices in the basis of sublattices A and B. This Hamiltonian has chiral symmetry with the unitary chiral operator

$$\Gamma = \sigma_3. \tag{3.114}$$

One can indeed check that $\Gamma^2 = \mathrm{Id}$ and

$$\Gamma H(k) \Gamma^{-1} = -H(k). \tag{3.115}$$

The chiral invariant can be computed as follows. Define $n = \vec{h}/\|\vec{h}\|$ and consider the valence projector (pulled back from equation (2.68))

$$P = n^* P_-^\sigma = -n \cdot \sigma \tag{3.116}$$

to find that in this case

$$q(k) = -[n_x - \mathrm{i}n_y] = J_2 \left(\mathrm{e}^{-\mathrm{i}k} - \frac{J_1}{J_2} \right). \tag{3.117}$$

Its winding number

$$g = \frac{\mathrm{i}}{2\pi} \int_{\mathrm{BZ}} \mathrm{d}k \, q^{-1}(k) \partial_k q(k) \tag{3.118}$$

can be computed e.g. by the residue theorem, and we find that

$$g = \frac{\mathrm{i}}{2\pi} \int_{\mathrm{BZ}} \mathrm{tr} \left(q^{-1} \mathrm{d}q \right) = \begin{cases} 1 & \text{when } |J_1/J_2| < 1 \\ 0 & \text{when } |J_1/J_2| > 1 \end{cases}. \tag{3.119}$$

The two different phases of polyacetylene ((a) and (b) in figure 3.3) correspond respectively to $g = 0$ and $g = 1$, and the gap closes at the topological transition when $|J_1/J_2| = 1$.The main message of the work of Su, Schrieffer and Heeger work is that a soliton appears at the interface between the two varieties of *trans*-polyacetylene, which is associated with a fermionic excitation mode. In the framework of topological insulators, this fermionic mode can be understood as a topological edge state between two topologically distinct phases. However, the description of the motion of the exitation/soliton is not accounted for in the topological band theory, as it requires to take into account the coupling between electronic modes and phonon modes, which is not included in this description (the lattice is fixed). Again, more details on the physics of solitons in polymers may be found in the reviews [BCM92; HKSS88].

Finally, notice that the SSH Hamiltonian is also time-reversal invariant (see section 2.3.1) with a time-reversal operator $\Theta = \mathcal{K}$ (where $\mathcal{K}$ is complex conjugation), as we

have $\Theta H(k)\Theta^{-1} = H(-k)$. As a consequence, the system is in fact in class BDI. However, it is possible to add a time-reversal breaking perturbation which preserves chiral symmetry in the Bloch Hamiltonian, for example a term $J_3 \cos(k)\sigma_2$ without modifying the topology of the system (at least for a small enough J_3), which is therefore essentially due to chiral symmetry.

2.3 Kane-Mele topological insulators, or class AII

2.3.1 The time-reversal operation

Time-reversal amounts to the transformation in time $t \to -t$. As such, quantities like spatial position, energy, or electric field are even under time-reversal, whereas quantities like time, linear momentum, angular momentum, or magnetic field are odd under time-reversal operation. Within quantum mechanics, the time-reversal operation is described by an antiunitary **time-reversal operator** Θ (which is allowed by Wigner's theorem) [Le 12; Sak93; Kit87], i.e. (i) it is antilinear, i.e. $\Theta(\alpha x) = \overline{\alpha}\Theta(x)$ for $\alpha \in \mathbb{C}$ and (ii) it satisfies $\Theta^\dagger\,\Theta = \mathrm{Id}$, i.e. $\Theta^\dagger = \Theta^{-1}$. The simplest example of a time-reversal operator is the complex conjugation, which we denote by $\mathcal{K}$ (acting on the left), so $\mathcal{K}z = \overline{z}$. When spin degrees of freedom are included, time-reversal operation has to reverse the different spin expectation values: the corresponding standard representation of the time-reversal operator is [Sak93] $\Theta = \mathrm{e}^{-\mathrm{i}\pi S_y/\hbar}\,\mathcal{K}$, where S_y is the y component of the spin operator. The unitary part of the time-reversal operator is therefore a π rotation in the spin space. Therefore, and because the spin operator $\mathrm{e}^{-\mathrm{i}\pi S_y/\hbar}$ is real and unaffected by $\mathcal{K}$, in an integer spin system, the time-reversal operator is involutive, i.e. $\Theta^2 = \mathrm{Id}$. In contrast, for an half-integer spin system, this operation is anti-involutive: $\Theta^2 = -\mathrm{Id}$. The first situation ($\Theta^2 = \mathrm{Id}$) is usually called "bosonic" while the second one ($\Theta^2 = -\mathrm{Id}$) is usually called "fermionic". When there are no other special symmetry, $\Theta^2 = \mathrm{Id}$ corresponds to class AI and $\Theta^2 = -\mathrm{Id}$ to class AII. This denomination can be misleading as it is also possible to consider synthetic or effective time-reversal operators which are not related to the nature of the underlying particles. For example, a fermionic time-reversal $\Theta^2 = -\mathrm{Id}$ can even be implemented[10] in classical mechanical systems [SH15].

A first quantized single-particle Hamiltonian H is said to be **time-reversal invariant** if it commutes with the time-reversal operator,

$$\Theta H \Theta^{-1} = H. \tag{3.120}$$

Here, H does not depend on time. The more general situation of a time-dependent Hamiltonian will be considered in chapter 4.

In the context of Bloch theory, the time-reversal invariance is expressed in terms of the Bloch Hamiltonian as

$$\Theta H(k) \Theta^{-1} = H(-k). \tag{3.121}$$

[10] Note that strictly speaking, the system of Süsstrunk and Huber is not in class AII: the fermionic time-reversal is in fact the composition of a bosonic time-reversal with a unitary symmetry. The Hamiltonian should be block-diagonalized to remove this unitary symmetry before any mention of symmetry classes. However, it is convenient not to do it. A practical consequence of this difference is that a breaking of that additional unitary symmetry is sufficient to remove any topological protection.

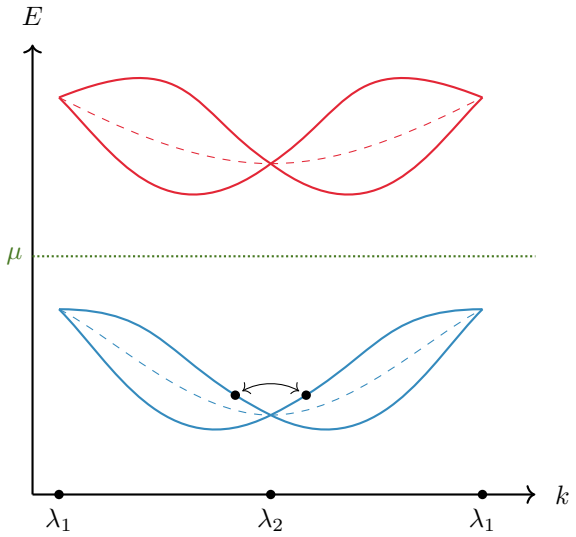

Figure 3.15: Typical spectrum of a time-reversal invariant system. Typical energy spectrum of a time-reversal invariant system (continuous lines) on a closed loop of the Brillouin torus. At the TRIM λ_i, there is always a degeneracy of the filled bands (resp. empty bands). A Kramers pair is drawn as two black circles. When inversion symmetry is present, the filled bands (resp. empty bands) are everywhere degenerate (dashed lines).

The time-reversal operator Θ relates the Bloch states at k and $-k$, or in other words it is an antiunitary map[(11)] which relates the fiber over k of the Bloch bundle to the fiber over $-k$. This is intuitively understood with a plane wave $\psi(k,x) = \mathrm{e}^{-\mathrm{i}kx}$. Here, time-reversal is simply complex conjugation, so $\Theta\psi(k,x) = \mathrm{e}^{-\mathrm{i}kx} = \psi(-k,x)$, so Θ indeed relates k to $-k$.

In the following, we will focus on a fermionic time-reversal $\Theta^2 = -\mathrm{Id}$. This property is essential for what follows. A system which is time-reversal invariant with this kind of time-reversal operator, but which is neither chiral nor particle-hole symmetric is said to be in class AII.

2.3.2 Kramers pairs

Time-reversal invariance implies the existence of so-called **Kramers pairs** of eigenstates: equation (3.121) implies that the image by time-reversal of any eigenstate of the Bloch Hamiltonian $H(k)$ at k is an eigenstate of the Bloch Hamiltonian $H(-k)$ at $-k$, with the same energy, as

$$H(k)\,|\psi(k)\rangle = E(k)\,|\psi(k)\rangle \qquad \text{implies} \qquad H(-k)\,|\Theta\psi(k)\rangle = E(k)\,|\Theta\psi(k)\rangle\,. \quad (3.122)$$

This is the Kramers theorem [Sak93; Kit87]. These two eigenstates, that a priori live in different fibers, are called **Kramers partners**. The property $\Theta^2 = -\mathrm{Id}$ implies

(11) We should in fact define an antiunitary automorphism $\hat{\Theta}$ of the Bloch bundle $\pi : E \to \mathrm{BZ}$ with $\pi \circ \hat{\Theta} = \vartheta \circ \pi$, where $\vartheta : \mathrm{BZ} \to \mathrm{BZ}$ is the involution defined by $\vartheta(k) = -k$.

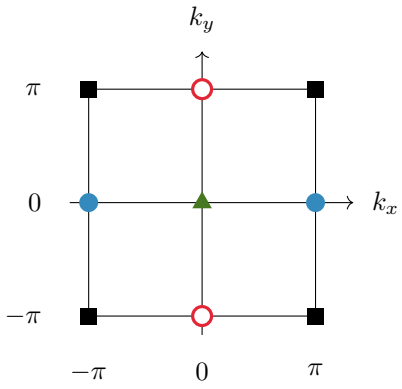

Figure 3.16: Time-reversal invariant momenta in 2D. The four time-reversal invariant momenta in dimension $d = 2$: $(0, 0)$, $(\pi, 0)$, $(0, \pi)$ et (π, π). The Brillouin torus T^2 is represented as a primitive cell, whose sides must be glued together; points equivalent up to a lattice vector have been drawn with the same symbol.

that the two Kramers partners are orthogonal. Note that the orthogonality of these Kramers partners in different fibers has only a meaning if we embed these fibers in the complete trivial bundle $T^2 \times \mathbb{C}^{2n}$ corresponding to the whole state space of the Bloch Hamiltonian.

Some points of the Brillouin torus appear of high interest: the **time-reversal invariant momenta** (TRIM) λ that are invariant under time-reversal [FKM07], i.e. which verify $\lambda = -\lambda + G$ where G is a reciprocal lattice vector. In other words, they are the fixed points of the map $\vartheta(k) = -k$ defined on the torus. Explicitly, they are the points $\lambda = G/2$, with G a reciprocal lattice vector (see figure 3.16 for the example of a two dimensional square lattice). In the following, we denote the set of TRIM in the Brillouin zone as Λ.

At time-reversal invariant points, the two partners of a Kramers pair live in the same fiber. As they are orthogonal and possess the same energy, the spectrum is necessarily always degenerate at TRIM (see figure 3.15). As we shall see in the following, the constraints imposed by the presence of Kramers partners around the valence Bloch bundle are at the origin of the topology of Kane–Mele insulators.

2.3.3 Topology of (fermionic) time-reversal invariant systems

A time-reversal invariant system with $\Theta^2 = -\mathrm{Id}$ is always topologically trivial from the point of view of Chern invariants. However, Kane and Mele discovered [KM05a; KM05b] that a more subtle kind of topology, protected by time-reversal invariance, may be present in two dimensions. Fu and Kane [FKM07], Roy [Roy09], Moore and Balents [MB07] realized that this particular topology can also arise in space dimension $d = 3$.

Let us consider a two- or three-dimensional band insulator, and let $k \mapsto (e_i(k))_{i=1}^{2m}$ be a global frame of the valence bundle, i.e. a collection of never-vanishing global

sections of the valence bundle that form a basis of its fiber over each point. This global frame exists since the corresponding first Chern number vanishes, owing to time-reversal invariance. As time-reversal connects opposite momenta k and $-k$, the natural way to define "matrix elements" of the time-reversal operator is the **sewing matrix** defined by Fu and Kane [FK06] as

$$w_{ij}(k) = \langle e_i(-k)|\Theta e_j(k)\rangle \tag{3.123}$$

so

$$\Theta e_i(k) = \sum_j w_{ji}(k) e_j(-k) \qquad \text{or} \qquad e_i(-k) = \sum_j \overline{w}_{ij}(k)\Theta e_j(k). \tag{3.124}$$

The sewing matrix is unitary

$$w^\dagger(k)w(k) = \mathrm{Id} \tag{3.125}$$

and has property

$$w(-k) = -w^T(k). \tag{3.126}$$

As a consequence, the sewing matrix is antisymmetric at time-reversal invariant momenta, so its pfaffian $\operatorname{Pf} w$ is defined at those points. For example, for a system with only two filled bands, the sewing matrix at a TRIM $\lambda \in \Lambda$ takes the simple form:

$$w(\lambda) = \begin{pmatrix} 0 & t(\lambda) \\ -t(\lambda) & 0 \end{pmatrix} \tag{3.127}$$

with $|t(\lambda)| = 1$, and its pfaffian is $\operatorname{Pf} w(\lambda) = t(\lambda)$.

The **Fu-Kane-Mele $\mathbb{Z}_2$ invariant** is then defined by

$$(-1)^\nu = \prod_{\lambda\in\Lambda} \frac{\operatorname{Pf} w(\lambda)}{\sqrt{\det w(\lambda)}}. \tag{3.128}$$

This expression in only meaningful provided that w is calculated from a continuous basis (which always exists thanks to time-reversal invariance). If so, the square root of $\det w(k)$ can be defined globally as $\det w(k)$ has no winding. The topological invariant seems to depend only on the behaviour of the sewing matrix w at the TRIM, but the requirement of a globally-defined square root means that the formula (3.128) is in fact not really localized on TRIM.

The case of $(-1)^\nu = 1$ corresponds to a trivial situation, whereas $(-1)^\nu = -1$ corresponds to a topologically nontrivial situation, where a global frame of Kramers pairs cannot be defined (see below). The most striking observable consequence of a nontrivial Kane-Mele topology is visible at an interface with a trivial system, where a Kramers pair of counter-propagating chiral states appear, which are called **helical edge states**. As Kramers partners are orthogonal, backscattering between them is prevented; hence, a Kramers pair of edge states is robust to weak disorder. The one-dimensional edge states of two-dimensional topological insulators lead to characteristic transport signatures in a multiterminal setup, and the two-dimensional surface states of three-dimensional topological insulators can be observed through ARPES measurements (see paragraph 1.2, page 11). From the point of view of mathematics,

the Fu-Kane-Mele invariant characterizes complex vector bundles (representing energy bands) endowed with a particular structure due to the time-reversal operation, which were called "Quaternionic vector bundles" [NG15b; NG16] (see also [FM13]). A nonvanishing Chern invariant is an obstruction to construct a global frame; similarly, it was rigorously shown by Fiorenza, Monaco and Panati [FMP16] and independently by De Nittis and Gomi [NG15b; NG16] that a nonvanishing Fu-Kane-Mele invariant is an obstruction to find a global time-reversal invariant frame, that is a set of Kramers pairs of global sections which form a basis of each fiber. This property was already conjectured by Fu and Kane [FK06]. Another form of the $\mathbb{Z}_2$ invariant that expresses this point of view is [FK06]

$$\nu = \frac{1}{2\pi}\left[\oint_{\partial \mathrm{EBZ}} A - \int_{\mathrm{EBZ}} F\right] \pmod 2 \tag{3.129}$$

where EBZ represents the *effective Brillouin zone*, defined as a fundamental domain for the action $\theta(k) = -k$ of time-reversal on the Brillouin torus (essentially half of the Brillouin torus), A is a special version of the Berry connection, constructed from Kramers pairs on two halves of the effective Brillouin zone, and $F = \mathrm{d}A$ is the corresponding curvature. In the trivial case, the Stokes theorem can be applied, and ν vanishes, but there is a topological obstruction to do so in the nontrivial case, when $\nu = 1$. The equivalence between this expression and the previous one was demonstrated in [FK06], and is reviewed in [Bernevig, § 10.5]. Moore and Balents [MB07] have discussed the obstruction point of view using homotopy theory arguments; they interpreted the Kane-Mele invariant as a "Chern parity" and generalized it to three dimensions. A new light was shed on their construction by my co-advisor Krzysztof Gawędzki [Gaw15], as a follow-up of our work on the Floquet equivalent of Kane-Mele insulator.

The actual computation of the Kane-Mele invariant in a system is not straightforward (except when there is inversion symmetry, see next paragraph). Formula (3.128) requires a smooth frame of the valence bundle (so the square root is well-defined), and an analytical expression is usually required. This is particularly problematic to work with ab-initio simulations of actual materials. A numerical method was proposed by Fukui and Hatsugai [FH07] (see also [XYFW10]) as a discretization of the obstruction formula (3.129) in a lattice Brillouin zone. Another method, mainly due to Soluyanov and Vanderbilt [SV11], consists in following the evolution of the charge centers of Wannier functions (the authors released the code under an open-source license under the name Z2Pack). On the material science side, a lot of activity has happened in the ten last years to find new compounds candidates to be topological insulators (or superconductors and semi-metals), that was recently reviewed by Bansil, Lin and Das [BLD16].

When the Hamiltonian has an additional inversion (also called parity) symmetry

$$PH(k)P^{-1} = H(-k) \tag{3.130}$$

with a unitary inversion operator P with $P^2 = \mathrm{Id}$ commuting with the time-reversal operator Θ, the Kane-Mele invariant takes a particularly simple form [FKM07] as the product of the parity eigenvalues of half of the filled bands at all TRIM. The

energy eigenstates at a TRIM λ form Kramers pairs $\psi_i^{\pm}$ (with an arbitrary choice of $\pm$). Besides, at the TRIM, $H(\lambda)$ and P commute, so the energy eigenstates $\psi_i^{\pm}(\lambda)$ also have a well-defined parity eigenvalues, which are the same for two Kramers partners $\xi_i^+(\lambda) = \xi_i^-(\lambda) = \pm 1$. The Fu-Kane-Mele invariant can then be expressed as [FKM07]

$$(-1)^\nu = \prod_{\lambda\in\Lambda}\prod_i \xi_i^+(\lambda). \tag{3.131}$$

This expression allows to identify candidate materials for topological insulators from their band structure, as the materials where a band inversion occurs at one TRIM, meaning that the nature of the highest valence band and the lowest conduction band are exchanged near this point.

2.3.4 The Bernevig-Hughes-Zhang model

The first model for a class AIII topological insulator was developed by Kane and Mele, who considered a graphene sheet with spin-orbit coupling [KM05a]. Unfortunately, spin-orbit coupling is too small in graphene for the effect to be measurable. The first experimental evidences of the quantum spin Hall effect were observed in HgTe-CdTe quantum wells, a quasi-two-dimensional system, following the prediction of Bernevig, Hughes and Zhang [BHZ06], who proposed a tight-binding model (now called the BHZ Hamiltonian) regularizing the $k \cdot p$ description of the quantum well. Here, we present a slightly modified version of the BHZ model; like the original regularized model, it has inversion symmetry, and we can use the framework developed by Fu and Kane [FKM07] to characterize its topological properties.

In HgTe quantum wells, the bands near Fermi level are a s-type band with $J = 1/2$ and a p-type band with $J = 3/2$. Spin-orbit coupling respectively split such states into $m_J = \pm 1/2$ and $m_J = \pm 1/2, \pm 3/2$ states. The relevant degrees of freedom participating in the band crossing and kept in the BHZ model are the s-type states with $m_J = \pm 1/2$ and the two p-type states with $m_J = \pm 3/2$. To simplify the notations, we will denote the two s (resp. p) orbitals by $s\uparrow$ and $s\downarrow$ (resp. $p\uparrow$ and $p\downarrow$), which amounts to work in the basis

$$(\mathrm{s},\mathrm{p}) \otimes (\uparrow,\downarrow) = (\mathrm{s}\uparrow, \mathrm{s}\downarrow, \mathrm{p}\uparrow, \mathrm{p}\downarrow). \tag{3.132}$$

In this basis, the time-reversal and inversion (parity) operators read

$$\Theta = (\mathrm{Id} \otimes \mathrm{i}\, s_y)\, \mathcal{K} \qquad \text{and} \qquad P = \sigma_z \otimes \mathrm{Id}. \tag{3.133}$$

The most general time-reversal invariant and parity invariant Hamiltonian can be written as a linear combination of the following matrices:

$$\Gamma_1 = \sigma_z \otimes \mathrm{Id}\ ;\ \Gamma_2 = \sigma_y \otimes \mathrm{Id}\ ;\ \Gamma_3 = \sigma_x \otimes s_x\ ;\ \Gamma_4 = \sigma_x \otimes s_y\ ;\ \Gamma_5 = \sigma_x \otimes s_z \tag{3.134}$$

where s_i are spin Pauli matrices and σ_i are orbital Pauli matrices. Such an Hamiltonian

$$H(k) = d_0(k)\mathrm{Id} + \sum_j d_j(k)\Gamma_j. \tag{3.135}$$

is everywhere degenerate, due to the combination of inversion and time-reversal symmetries, and its spectrum reads

$$E_{\pm}(k) = d_0(k) \pm \sqrt{\sum_{i=1}^{5} d_i^2(k)}. \tag{3.136}$$

In the following, we will set $d_0(k) = 0$ as this coefficient plays no role in the topological properties (yet it can cause an indirect gap closing). Time-reversal and inversion symmetries require the function d_1 to be even, and the functions $d_2, \dots, d_5$ to be odd. For this class of Bloch Hamiltonians, the presence of inversion symmetry allows to use the simplified expression of the Fu-Kane-Mele invariant. As the inversion operator is $P = \Gamma_1$, the parity eigenvalues at TRIM are $d_1(\lambda)$, and the Fu-Kane-Mele invariant reads

$$(-1)^{\nu} = \prod_{\lambda \in \Lambda} \operatorname{sign} d_1(\lambda). \tag{3.137}$$

The BHZ model [BHZ06] corresponds to non-vanishing coefficients

$$\begin{aligned} d_1(k) &= (M - J - 4B) + 2B(\cos k_x + \cos k_y) + J \cos k_x \cos k_y \\ d_2(k) &= A \sin k_y \\ d_5(k) &= A \sin k_x \end{aligned} \tag{3.138}$$

The Fu-Kane-Mele invariant can be computed from the parity eigenvalues at the four TRIM

$$\begin{aligned} d_1(0,0) &= (M - J - 4B) + 4B + J \\ d_1(0,\pi) &= (M - J - 4B) - J \\ d_1(\pi,0) &= (M - J - 4B) - J \\ d_1(\pi,\pi) &= (M - J - 4B) - 4B + J. \end{aligned} \tag{3.139}$$

and we find

$$(-1)^{\nu} = \operatorname{sign}(M) \operatorname{sign}(M - 8B). \tag{3.140}$$

Hence this model realizes a nontrivial Kane-Mele topological insulator when $M/8B < 1$ for $M > 0$ and when $M/8B > 1$ when $M < 0$ (and a trivial insulator elsewhere, except at the transition lines). In this model, there is no spin-flip term, so spin along the quantization axis is conserved. Yet, spin-flip terms can be added to the Hamiltonian without spoiling its topology, as long as time-reversal invariance is preserved and the gap does not close (similarly, inversion symmetry can also be broken). If time-reversal invariance is broken, however, the Kane-Mele topological invariant is no longer defined and the system may even be deformed into a trivial Kane-Mele insulator without closing the gap [ETN13].

2.3.5 Edge states

At the boundary between a Kane–Mele topological insulator and a trivial insulator, Kramers pairs of counter-propagating gapless edge states (called helical edge states) appear. The origin of these edge states can be understood in a similar fashion as for Chern insulators through Jackiw–Rebbi solitons (see section 2.1.4, 84).

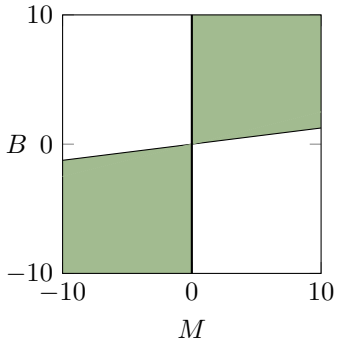

Figure 3.17: Phase diagram of the BHZ model. We represent a part of the phase diagram of the BHZ model. Colors represent the Fu-Kane-Mele invariant, where white represents KM = 0 (trivial phase), whereas green (■) represents KM = 1 (nontrivial phase).

Let us consider the BHZ model (3.135) (with coefficients (3.138)). In the trivial phase, the parity eigenvalues $-d_1$ at all TRIM have a uniform sign, say a positive one, whereas in the nontrivial phase, there is one TRIM where this sign is negative, say $\lambda_0 = (0, 0)$, while it is positive at the three others (obviously we can switch "positive" and "negative" and/or choose another singled out TRIM). To continuously describe an interface from a trivial to a Kane-Mele topological phase without breaking time-reversal symmetry requires a change of sign of d_1 at the TRIM λ_0: this corresponds to a gap closing and the appearance of a surface state. Let us consider an interface at $y = 0$ between a trivial insulator for $y > 0$ where d_1 is positive at all TRIM, and a nontrivial Kane-Mele topological insulator for $y < 0$ where only $d_1(\lambda_0)$ is negative. We focus on the low-energy behavior around the point λ_0, while a smooth evolution of the bands is expected elsewhere on the Brillouin torus. Let us define a mass $m(y)$ smoothly interpolating between the asymptotic "bulk" values $m(y \in \text{bulk}) = d_1[\lambda_0](y)$, so with $m(y > 0) > 0$ and $m(y < 0) < 0$. The low-energy spectrum of this interface can by described by a linearized Hamiltonian around the TRIM λ_0 which reads, up to a rotation of the local coordinates on the Brillouin zone (q_x, q_y):

$$H_{\text{l}}(q) = q_x \Gamma_5 - q_y \Gamma_2 + m(y)\, \Gamma_1. \tag{3.141}$$

In this expression, we used the oddness of the functions $d_{i\geq 2}$ around λ_0, following from time-reversal invariance, and with local coordinates chosen so that $d_5(q) = q_x$ and $d_2(q) = -q_y$ to simplify the computations. To describe edge states, it is useful to block-diagonalize the Hamiltonian in the "orbital tensor spin" basis $(\text{s}\uparrow, \text{p}\uparrow, \text{s}\downarrow, \text{p}\downarrow)$ in which it reads in real space representation (through the substitution $q \to -\text{i}\nabla$):

$$H_{\text{l}} = \begin{pmatrix} H_\uparrow & 0 \\ 0 & H_\downarrow \end{pmatrix}, \tag{3.142}$$

with

$$H_\uparrow = \begin{pmatrix} -\text{i}\partial_x & m(y) + \partial_y \\ m(y) - \partial_y & \text{i}\partial_x \end{pmatrix} \qquad \text{and} \qquad H_\downarrow = \begin{pmatrix} +\text{i}\partial_x & m(y) + \partial_y \\ m(y) - \partial_y & \text{i}\partial_x \end{pmatrix}. \tag{3.143}$$

Exactly as in section 2.1.4, we observe that the Schrödinger equation

$$\begin{pmatrix} H_\uparrow & 0 \\ 0 & H_\downarrow \end{pmatrix} \psi(x,y) = E\psi(x,y) \tag{3.144}$$

has solutions (remember that we work in the "orbital tensor spin" basis)

$$\begin{aligned} \psi_{q_x,\uparrow}(x,y) &\propto \mathrm{e}^{-\mathrm{i}q_x x} \exp\left[-\int_0^y m(y')\,\mathrm{d}y'\right] \begin{pmatrix} 0 \\ 1 \\ 0 \\ 0 \end{pmatrix}, \\ \psi_{q_x,\downarrow}(x,y) &\propto \mathrm{e}^{+\mathrm{i}q_x x} \exp\left[-\int_0^y m(y')\,\mathrm{d}y'\right] \begin{pmatrix} 0 \\ 0 \\ 0 \\ 1 \end{pmatrix}, \end{aligned} \tag{3.145}$$

These states constitute a Kramers pair of edge states. The first one is a spin-up right-moving state, while the second one is a spin-down left-moving state. A schematic representation of such a pair of edge states is represented in figure 3.18. This demonstrates, at least physically, the existence of helical edge states at the interface between a trivial and a topological insulating phase in the BHZ model. References on more precise and formal considerations on the bulk-edge correspondence are found at the end of section 2.1.4, page 84

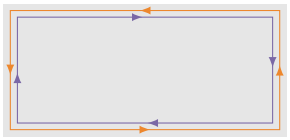

Figure 3.18: Edge states of a Kane-Mele insulator. In a Kane-Mele insulator (also called QSHE state), there are on each interface two counter-propagating helical edge states which form a Kramers pair. As a consequence, backscattering from an edge state to its counter-propagating partner is not allowed.

2.4 Classification of topological insulators

As we have seen, there are different kinds of topological insulators, depending on the symmetries of the system and its space dimension. A classification of the possible topological phases was achieved by Schnyder, Ryu, Furusaki and Ludwig [SRFL08; SRFL09; RSFL10] and Kitaev [Kit09], according to particular non-spatial symmetries: time-reversal, charge-conjugation and chiral symmetry. Those symmetries are, to some extent, more robust than e.g. an inversion symmetry, because they stem from the structure of the system, that is, the nature of the constituents of the low-energy description of the phase. For example, a system without magnetic field nor rotation is always time-reversal invariant (if we except weak interaction, which is not relevant in a solid state setting). At low energy, a superconductor has charge-conjugation symmetry to a very good approximation, and a tight-binding system with bipartite hoppings has a chiral symmetry, as long as the symmetry breaking intra-sublattice

hopping terms can actually be neglected. Moreover, as we shall see, such particular symmetries are what is left when all usual unitary symmetries are removed (through a block-diagonalization). Instead of classifying e.g. Hamiltonians, it is convenient to focus on unitary evolutions, even when the Hamiltonian do not depend on time [Zir10]; in this way, Floquet systems are naturally included in the standard classification scheme. The classification of unitary evolutions according to whether they posses or not such kind of symmetries leads to ten classes, called Cartan-Altland-Zirnbauer classes. For each of those classes and for each space dimension, a different kind of topological insulator is possible, corresponding to the different kinds of evolutions generated by gapped Bloch Hamiltonians. The description of all those possibilities is summarized in the "periodic table of topological insulators" of Kitaev and Schnyder, Ryu, Furusaki, Ludwig. The current section aims at giving a brief overview of this classification. For more details, the reader is directed towards the original articles [SRFL08; SRFL09; RSFL10] and [Kit09], and also to the reviews [CTSR15] and [Lud15]. The classification of unitary evolutions is explained in a particularly clear way in the article of Freed and Moore [FM13]. On the classification of topological insulators, let me also mention the articles from Thiang and Mathai [Thi15a; MT15b] and Kellendonk [Kel15].

2.4.1 The ten-fold way: symmetries and the classification of unitary evolutions

We aim at classifying unitary time evolutions of quantum systems (though it should be possible to adapt the method to any system governed by linear differential equations), which are described by an evolution operator $U(t,t')$. Starting from a state ψ_0 at t', the evolution operator $U(t,t')$ is a endomorphism of the Hilbert space which maps an initial state $\psi(t')$ at some time t' to the state $\psi(t) = U(t,t')\psi(t')$ of the system at another time t. To simplify, I will for now fix the origin of times at $t_0 = 0$ and only consider $U(t) = U(t, t_0 = 0)$. A unitary evolution is generated by an infinitesimal generator $H(t)$, the Hamiltonian of the system, through the equation

$$\mathrm{i}\partial_t U(t) = H(t)U(t) \tag{3.146}$$

with an initial value $U(0) = \mathrm{Id}$, and where $\hbar$ has been set to 1 for simplicity. When the Hamiltonian does not depend on time, this equation yields the simple form

$$U(t) = \mathrm{e}^{-\mathrm{i}tH}. \tag{3.147}$$

We aim at classifying unitary evolutions according to their symmetries, which form a group G (so we can combine them). Wigner theorem states that any of such symmetry $g \in G$ can be represented as a unitary *or* an antiunitary operator acting on the Hilbert space. Such a representation should be written $\rho(g)$, but we will shorten it as g to simplify. To track down if the representation is unitary or antiunitary, we define a map $\phi : G \to \mathbb{Z}_2$ with

$$\phi(g) = \begin{cases} +1 & \text{if } g \text{ is unitary} \\ -1 & \text{if } g \text{ is antiunitary.} \end{cases} \tag{3.148}$$

We say that g is a **symmetry** of U when

$$gU(t)g^{-1} = U(\tau(g)t) \tag{3.149}$$

where

$$\tau(g) = \begin{cases} +1 & \text{if } g \text{ preserves the orientation of time} \\ -1 & \text{if } g \text{ reverses the orientation of time} \end{cases} \tag{3.150}$$

is another map $\tau : G \to \mathbb{Z}_2$. At the level of the Hamiltonian, g is a symmetry of the evolution generated by H when

$$gH(t)g^{-1} = \phi(g)\tau(g)H(\tau(g)t) \tag{3.151}$$

and we write

$$\chi(g) = \phi(g)\tau(g). \tag{3.152}$$

For a time-independent Hamiltonian, χ tracks down if H commutes $(+1)$ or anticommutes (-1) with g. By definition, we have $\phi \cdot \tau \cdot \chi = 1$.

As a consequence, there are four types of symmetries according to whether ϕ and τ are ± 1, which correspond to

- $(\phi, \tau) = (1, 1)$ (so $\chi = 1$) are the usual **unitary symmetries**,
- $(\phi, \tau) = (1, -1)$ (so $\chi = -1$) are called **chiral symmetries**,
- $(\phi, \tau) = (-1, 1)$ (so $\chi = -1$) are called **charge-conjugation symmetries**,
- $(\phi, \tau) = (-1, -1)$ (so $\chi = 1$) are called **time-reversal symmetries**.

Another name for charge-conjugation symmetries is **particle-hole symmetries**, and chiral symmetries are sometimes also called **sublattice symmetries**. We write $G_{\phi,\tau}$ the corresponding subsets of G.

Usual unitary symmetries are easy to deal with, and enable to block-diagonalize the Hamiltonian (or in other words to split the Hilbert space into irreducible representation spaces). The ten-fold classification aims at classifying the possible evolutions when all usual unitary symmetries have already been taken into account and "removed" by working in irreducible representation spaces, where usual unitary symmetries are scalar matrices (scalar multiples of Id).

As we shall see, a consequence of this restriction is that there is only one possible time-reversal, charge-conjugation, and chiral operators at a time. An antiunitary operator A can be written as $A = U\mathcal{K}$, where U is unitary, so two antiunitary operators $A_1 = U_1\mathcal{K}$ and $A_2 = U_2\mathcal{K}$ are related by the unitary $V = U_2U_1^{-1}$ through $A_2 = VA_1$. So on the one hand, if $A_1, A_2 \in G_{-1,-1}$ (resp. $G_{-1,1}$) are two time-reversal (resp. charge-conjugation) operators, then $V \in G_{1,1}$. On the other hand, all unitaries symmetries (and in particular V) on an irreducible representation space are scalar (and hence phases). Similarly, two chiral symmetries $U_1, U_2 \in G_{1,-1}$ are related by the unitary symmetry $V = U_2U_1^{-1} \in G_{1,1}$, so they are scalar multiples one of each other. Hence, up to a phase, there is only one time-reversal operator Θ, one charge-conjugation operator C, and one chiral operator Γ. Moreover, when the square of an antiunitary operator A is a scalar matrix, then $A^2 = \pm\mathrm{Id}$, so we have either $\Theta^2 = \pm\mathrm{Id}$ and similarly, either $C^2 = \pm\mathrm{Id}$. By contrast, $\Gamma^2 = \mathrm{e}^{\mathrm{i}\phi}\mathrm{Id}$ is an arbitrary phase, which is not constrained, but usually chosen so that $\Gamma^2 = \mathrm{Id}$. Finally, the product ΘC is an element of $G_{1,-1}$ i.e. a chiral symmetry, so we have $\Theta C = \Gamma$, possibly up to a phase.

Evolutions are then classified according to the presence or not of those discrete symmetries. A given (class of) evolution may have no such symmetries at all, or only time-reversal symmetry, and so on. We are led to consider the ten possible cases, which are called **Cartan-Altland-Zirnbauer classes** and are enumerated in table 3.2.

	label	s	symmetries	Θ^2	C^2
complex CAZ classes	A	0	Id		
	AIII	1	Id, Γ		
real CAZ classes	AI	0	Id, Θ	$+1$	
	BDI	1	$\mathrm{Id}, \Theta, C, \Gamma$	$+1$	$+1$
	D	2	Id, C		$+1$
	DIII	3	$\mathrm{Id}, \Theta, C, \Gamma$	-1	$+1$
	AII	4	Id, Θ	-1	
	CII	5	$\mathrm{Id}, \Theta, C, \Gamma$	-1	-1
	C	6	Id, C		-1
	CI	7	$\mathrm{Id}, \Theta, C, \Gamma$	$+1$	-1

Table 3.2: Cartan-Altland-Zirnbauer classes. The Cartan-Altland-Zirnbauer classes correspond to the different possibilities to arrange the three kinds of special symmetries that are time-reversal Θ, charge-conjugation C and chiral symmetry Γ. We give the possible combinations of operators, which are always defined up to a phase, and for their squares. CAZ classes are labeled with a nomenclature borrowed from Cartan's classification of symmetric spaces. The parameter s gives the K-group which classifies the corresponding topological insulators: for complex classes, it is $\mathrm{K}^{-s}(\mathrm{BZ})$ whereas for real classes it is $\mathrm{KR}^{-s}(\mathrm{BZ})$.

2.4.2 The periodic table of topological insulators

On the level of Bloch evolution operators (see section 1.1.5), g is a symmetry of U when

$$gU(t,k)g^{-1} = U(\tau(g)t, \phi(g)k). \tag{3.153}$$

A plane wave (or the phase factor of Bloch waves) $\mathrm{e}^{-\mathrm{i}k\cdot x}$ is mapped to $\mathrm{e}^{-\mathrm{i}(-k)\cdot x}$ by complex conjugation (and therefore by any antiunitary operator), hence the action on k.

The classification of topological insulators has been developed for gapped static Hamiltonians, for which the evolution operator is $U(t,k) = \exp(-\mathrm{i}tH(k))$, and the spectrum of H is gapped around zero energy. Hence, the Bloch bundle (see section 1.1, page 57) is composed of two well-defined spectral subbundles, the valence bundle and the conduction bundle. This separation can be taken into account as a $\mathbb{Z}_2$ graduation of the Bloch bundle by the operator $Q(k) = \mathrm{Id} - 2P(k)$. In class A, when there are no symmetry at all, we have seen in section 2.2.3 (page 46) that such graded Bloch bundles are classified (up to stable homotopy) by the group $K^0(\mathrm{BZ})$. The case of class AIII (with only chiral symmetry) is also straightforward: we need to classify the unitary maps $q : \mathrm{BZ} \to U(N)$ that appear in equation (3.109), page 89. As there

are no other constraint on q, such maps, and therefore the graded Bloch bundles in class AIII are classified by $K^1(\mathrm{BZ})$, as we have seen in section 2.2.3. The classes A and AIII are therefore called **complex classes**, as the corresponding topological insulators (i.e. graded Bloch bundles) are classified by complex K-theory. Antiunitary operators (time-reversal and charge-conjugation) correspond to $\phi = -1$ and therefore relate k and $-k$: there is a non-trivial involution of the Brillouin torus $\kappa : \mathrm{BZ} \to \mathrm{BZ}$ defined by $\kappa(k) = -k$ (with momenta $k \in \mathrm{BZ}$ only defined modulo reciprocal lattice vectors), which lifts to antilinear maps on the Bloch bundle from the fiber over k to the fiber over $\kappa(k)$ implementing time-reversal or charge-conjugation. Complex vector bundles with such a structure were studied by Atiyah [Ati66], who called them Real vector bundles. They are classified by KR-theory, a particular variety of K-theory. The eight other classes are therefore called **real classes**. Schnyder, Ryu, Furusaki and Ludwig [SRFL08; SRFL09; RSFL10] and Kitaev [Kit09] showed that topological insulator (graded Bloch bundles with the corresponding antiunitary maps) are classified by the KR-group $\mathrm{KR}^{-s}(\mathrm{BZ})$, where BZ is the d-dimensional Brillouin torus, and where the correspondence between the value of s and the Real class is given by table 3.2. It is convenient to use *reduced K-groups* $\widetilde{\mathrm{K}}^{-s}(\mathrm{BZ})$ and $\widetilde{\mathrm{KR}}^{-s}(\mathrm{BZ})$ instead of $\mathrm{K}^{-s}(\mathrm{BZ})$ and $\mathrm{KR}^{-s}(\mathrm{BZ})$ to factor out the dimension of the bundles, which is irrelevant in the classification of topological phases. Finally, replacing the Brillouin zone BZ_d by a sphere S^d gives the principal, or so-called "strong" topological invariants (see paragraph 2.4.3 below). The result of this classification is the celebrated **periodic table of topological insulators and superconductors** reproduced in table 3.3.

As we are concerned with topological properties, we do not really classify particular Hamiltonians, but rather classes of Hamiltonians, and it may happen that some Hamiltonians in a given class have more symmetries than required, or in other words, accidental symmetries. For example, a Hamiltonian $H(\lambda)$ depending on some parameter λ which is usually in class A (with no symmetry) may accidentally fall in class AII (with time-reversal invariance squaring to $-\mathrm{Id}$) for specific values of λ. For instance, it is the case for the Haldane model with $\phi = 0$, see section 2.1 and figure 3.13. In this situation, we still wish to consider that the system is in class A. Indeed, the presence of a point where the system is time-reversal invariant inside of a region of the phase diagram (but not at a region boundary where the gap closes!) guarantees that the corresponding phase is topologically trivial.

This overview was focused on the bulk K-theoretic classification of topological insulator, which is mainly due to Kitaev [Kit09], but it is worth to mention several other approaches. On the same K-theoretic line, see also the articles of Freed and Moore [FM13] who use twisted K-theory, of Thiang and Mathai [Thi15a; MT15b], and of Bourne, Carey and Rennie [BCR15] which includes a review of several approaches in mathematical physics. Another approach to bulk invariants is to use homotopy theory directly, which enables to capture the non-stable range [KG15]. Historically, the first approach to the classification is due to Schnyder, Ryu, Furusaki and Ludwig [SRFL08; SRFL09; RSFL10], and is based on the (lack of) Anderson localization of the low-energy edge states located at the boundary of a topological insulator. Another more recent point of view based on anomalies, which connects the bulk and edge approaches, has emerged from the study of the response functions of topological

phases [RML12].

As we have already mentioned, the principle of this classification is general enough to apply to physical systems beyond static electronic Hamiltonians. The physical meaning and realization of the symmetry depend on the particular type of physical system, as well as the implementable topological phases, but the big picture seems to stay the same. The classification of topological phases was studied by De Nittis and Lein [NL14] in photonic crystals, and by Süsstrunk and Huber in mechanical metamaterials [SH16]. The ten-fold classification was also recently extended to Floquet systems by Roy and Harper [RH16].

It is possible to enrich the spectrum of possible phases (and also to constrain it) when additional unitary symmetries like spatial crystalline symmetries are considered. This possibility was first discovered by Fu [Fu11] who called *topological crystalline insulators* the corresponding phases. In principle, the ten-fold classification should be paired with the classification of crystallographic point groups to obtain a full classification, a task which is in progress. A review is included in [CTSR15], and relevant papers published more recently include [WL16; SSG15; DL16]. Such phases are however usually less robust because the crystal symmetries are more easily broken, e.g. by disorder, and the bulk-boundary correspondence is only applicable for boundaries which are invariant under the relevant symmetry, at least on average.

2.4.3 Strong and weak invariants

The periodic table of topological insulators 3.3 only mentions "strong invariants". Let us first illustrate the idea of strong and weak invariants on an example, the Haldane model. As the first Chern invariant which characterizes the topology of the Haldane model is only defined for a two-dimensional torus: the first Chern invariant is a *strong topological invariant* in $d = 2$. However, it is possible to stack layers of identical sheets of Haldane models to build a three-dimensional system, which will still be characterized by a first Chern number. But this system is not "fully three-dimensional", as (i) it already exists in a lower dimension, and (ii) it requires some kind of translational invariance in the stacking direction for the invariant to be relevant. As a consequence, this first Chern number is said to be a *weak topological invariant* in this case. In fact, the Brillouin torus is a 3-torus, which contains three independent 2-tori, each of which corresponds to one first Chern number: there are three independent weak topological invariants in $d = 3$. The most common example of weak invariants is found in class AII, where three-dimensional time-reversal invariant topological insulators are characterized by one strong $\mathbb{Z}_2$ index as well as three weak $\mathbb{Z}_2$ indexes.

Mathematically, the origin of weak topological invariants is that the torus is not a sphere. We recall the reader that that the Brillouin zone BZ is a d-torus, where d is the space dimension, $\mathrm{BZ} \simeq T^d$. When weak invariants vanish, the Bloch Hamiltonian may be viewed as defined not on a d-torus, but on a d-sphere (as we did without caution in section 2.1). More precisely, we recall that topological invariants are elements of the K-group $\widetilde{\mathrm{K}}^{-s}(T^d)$ (for complex classes) or $\widetilde{\mathrm{K}}^{-s}(T^d)$ (for real classes), where d is

the space dimension and s labels the CAZ class. Kitaev [Kit09] showed that

$$\widetilde{\mathrm{KR}}^{-s}(T^d) \cong \bigoplus_{j=0}^{d} \binom{j}{d} \widetilde{\mathrm{KR}}^{-s}(S^j). \tag{3.154}$$

Similarly for complex classes,

$$\widetilde{\mathrm{K}}^{-s}(T^d) \cong \bigoplus_{j=0}^{d} \binom{j}{d} \widetilde{\mathrm{K}}^{-s}(S^j). \tag{3.155}$$

The part $\widetilde{\mathrm{KR}}^{-s}(S^d)$ (or $\widetilde{\mathrm{K}}^{-s}(S^d)$) of this direct sum corresponds to **strong topological invariants**, and the reminder corresponds to **weak topological invariants**, which already exist in lower space dimensions.

For example, let us consider chiral systems (in class AII): in $d = 1$, there is only one strong invariant, associated to the whole one-dimensional Brillouin torus; in $d = 2$, there is no strong invariant, but there are two weak invariants associated to two independent loops on the Brillouin torus (e.g. along k_x and k_y); in $d = 3$, there are three weak invariants (associated e.g. to loops along k_x, k_y and k_z) and one strong invariant associated to the whole three-dimensional Brillouin torus. Similarly, in class A, there is only a strong invariant in $d = 2$ (the first Chern number), but in $d = 3$ there are three weak invariants (the first Chern numbers associated to three independent subtori of the three-dimensional Brillouin torus, which can e.g. be viewed as three planes k_xOk_y, k_yOk_z and k_yOk_z with periodic boundary conditions).

2.4.4 Chiral and charge-conjugation symmetries and the origin of energies

Chiral and charge-conjugation operators *anticommute* with the Hamiltonian when the corresponding symmetries are present,

$$\Gamma H \Gamma^{-1} = -H \qquad \text{and/or} \qquad CHC^{-1} = -H. \tag{3.156}$$

As a consequence, they distinguish the "origin of energies" $E = 0$. In contrast, time-reversal or a usual unitary symmetry, collectively written g, would not induce such a choice as

$$gHg^{-1} = H \qquad \text{implies} \qquad g(H + E_0\mathrm{Id})g^{-1} = H + E_0\mathrm{Id} \tag{3.157}$$

for any (real) E_0. As a consequence, the classes with chiral and/or charge-conjugation (BDI, D, DIII, CII, C, CI) are only relevant when the gap separating the valence and conduction bundles is at energy $E = 0$.

Indeed, the actual value of the origin of energies has not to be zero, and one may choose to define e.g. chiral symmetry as

$$\{\Gamma, H - E_0\mathrm{Id}\} = 0. \tag{3.158}$$

The key point is that for a chiral and/or charge-conjugation symmetric Hamiltonian, there is only one value of E_0 for which this relation is valid. It is indeed convenient to redefine the Hamiltonian such that $E_0 = 0$ in the symmetry relation.

In a solid state setting, this is not a crucial remark, as we are generally interested in the low-energy excitations on top of the ground state, and the Fermi level appears as a natural reference of energies for anticommuting symmetries (e.g. charge-conjugation is defined with respect to E_F in superconductors). However, there are situations where the band structure exhibits several gaps, each of which may host edge states that can be probed experimentally (see the article [SLIY15] for an experimental example in photonic crystals). In this situation, some care has to be taken to avoid mistakes. It will be convenient to borrow from the language of *gap invariants* that will be developed in chapter 4; all we need to know is that we may replace the band invariants like the Chern number with bulk gap invariants which directly give the number of edge states that would appear in a finite system. For example, in a two-dimensional system, chiral symmetry prohibits a nonvanishing Chern-like invariant for the gap around $E = E_0$. However, this constraint does not apply for other gaps in the band structure, which may therefore host chiral edge states. Conversely, in a one-dimensional system, only the gap around $E = E_0$ may be nontrivial due to the $\mathbb{Z}$ topology in class AIII.

This subtlety is fully taken into account in the standard interpretation of the periodic table, which characterizes graded Bloch bundles (with only one valence band and one conduction band). Here the origin of energy is by definition set to zero. However, this interpretation is not very practical in the context of classical topological phases (neither in the context of periodically driven systems), where the whole band structure can be probed. As a consequence, the precise setup of the periodic table is often overlooked.

		symmetries			space dimension							
		Θ	C	Γ	1	2	3	4	5	6	7	8
complex	A	0	0	0	0	$\mathbb{Z}$	0	$\mathbb{Z}$	0	$\mathbb{Z}$	0	$\mathbb{Z}$
AZ classes	AIII	0	0	1	$\mathbb{Z}$	0	$\mathbb{Z}$	0	$\mathbb{Z}$	0	$\mathbb{Z}$	0
	AI	+	0	0	0	0	0	$2\mathbb{Z}$	0	$\mathbb{Z}_2$	$\mathbb{Z}_2$	$\mathbb{Z}$
	BDI	+	+	1	$\mathbb{Z}$	0	0	0	$2\mathbb{Z}$	0	$\mathbb{Z}_2$	$\mathbb{Z}_2$
	D	0	+	0	$\mathbb{Z}_2$	$\mathbb{Z}$	0	0	0	$2\mathbb{Z}$	0	$\mathbb{Z}_2$
real	DIII	−	+	1	$\mathbb{Z}_2$	$\mathbb{Z}_2$	$\mathbb{Z}$	0	0	0	$2\mathbb{Z}$	0
AZ classes	AII	−	0	0	0	$\mathbb{Z}_2$	$\mathbb{Z}_2$	$\mathbb{Z}$	0	0	0	$2\mathbb{Z}$
	CII	−	−	1	$2\mathbb{Z}$	0	$\mathbb{Z}_2$	$\mathbb{Z}_2$	$\mathbb{Z}$	0	0	0
	C	0	−	0	0	$2\mathbb{Z}$	0	$\mathbb{Z}_2$	$\mathbb{Z}_2$	$\mathbb{Z}$	0	0
	CI	+	−	1	0	0	$2\mathbb{Z}$	0	$\mathbb{Z}_2$	$\mathbb{Z}_2$	$\mathbb{Z}$	0

Table 3.3: Periodic table of topological insulators and superconductors. According to the Cartan-Altland-Zirnbauer class of the Hamiltonian $(\mathrm{A}, \mathrm{AIII}, \dots, \mathrm{CI})$ and the dimension $d = 1, \dots, 8$, a class of systems may exhibit different kinds of topological phases. In the columns "symmetries", Θ is the time-reversal, C the charge-conjugation and Γ the chiral symmetry; 0 indicates the absence of a symmetry, $\pm$ indicate the presence of an antiunitary symmetry and the sign of its square $\pm\mathrm{Id}$, and a 1 in the column of the unitary chiral symmetry indicates its presence. In the right part of the table, a "0" indicates that there is only one kind of topological insulator in this CAZ class and dimension, the trivial one. A "$\mathbb{Z}$" indicates that there is a countable infinity of different topological phases, which may be labeled by an integer. A "$2\mathbb{Z}$" indicates that an additional symmetry constrains the $\mathbb{Z}$-valued invariant to be even (see the remark 3.24 of [BCR15] and the theorem 5 of [NS14] for details). Finally, a "$\mathbb{Z}_2$" indicates that there are only two kinds of phases, the trivial one and a nontrivial one. Due to a phenomenon called *Bott periodicity* in K-theory, dimensions d and $d+8$ are equivalent for this classification, which is why only dimensions 1 to 8 are present. Bott periodicity is also at the origin of the repetitive diagonal structure of the periodic table. The periodic table only mentions *strong* invariants. It only deals with a system with one conduction band and one valence band with a gap at zero energy, a crucial point when chiral or charge-conjugation symmetries are present.

Chapter 4

Periodically driven systems and their topology

1 Introduction

The current chapter is devoted to the study of the topology of periodically driven systems, where the Hamiltonian depends on time in a periodic fashion: $H(t+T) = H(t)$. In general, a time-dependent Hamiltonian is an effective description of a system exchanging energy with an environment. When the Hamiltonian is time-periodic, the exchanges of energy are quantized multiples of the $h/T = \hbar\omega$. Indeed, a full description should include a quantum description of both the system and the environment, which should then be described by a partial density matrix. Such a full description is still lacking despite progress in several directions, see e.g. [GD15] who use a quantized electromagnetic field instead of classical light, [BBKR13; BD15] and [VRM14b; VRM14a; VRM15] who attempt to extend topological phase to open systems and at finite temperature; we do not know to what extent are topological Floquet systems robust to the coupling to a possibly dissipative environment. However, experimental input (mostly outside of solid state physics) show that a classical, effective description is enough to capture the essential properties of Floquet topological phases. Indeed, deviations from this description should be expected, and a necessary step will be to understand the conditions in which the real dynamic is accurately reproduced by an effective description.

Several routes led to the study of the topology of systems subjected to a time-periodic driving.

- In solid state physics, the study of the interplay between photoinduced properties (like the photovoltaic effect) and the (quantum) (spin) Hall effects [YMN07] led to several propositions to induce topological phases with light [OA09; IT10; LRG11]. Floquet theory is a natural framework to describe the interaction between matter and the electromagnetic field. In particular, several studies focused on illuminated graphene [CPRT11; DGP13; GDP14].
- In cold atoms physics, both the coupling of atoms with light and periodically shaken optical lattices are standard tools to control the effective tight-binding Hamiltonian [LSAD07], both of which are described in the framework of Floquet theory.
- Periodically-driven systems such as kicked rotors and quantum walks were already viewed as toy models allowing to study various problems such as Anderson local-

ization; they are therefore potential candidates susceptible to host the geometrical phase structures of topological systems [KRBD10; Asb12].
– The simplest out-of-equilibrium situations are quenches (see e.g. [DSV11; FGDY14; KSSV14; CCB15] for applications to topological systems) and periodic driving. As such, they are natural situations to study with the aim of probing and/or inducing topological properties in out-of-equilibrium systems. Floquet theory provides a well-grounded framework which enables rich theoretical investigations; in contrast, the toolbox applicable to an arbitrary time evolution is much less extensive.

In a first section below, I review the framework of Floquet theory, with a focus on the specificities necessary to define topological invariants. As I will be interested in defining such invariants in presence of symmetries (time-reversal, charge-conjugation and chiral symmetry), I focus on their consequences on the main objects in Floquet theory, the effective Hamiltonian and the periodized evolution operator. Finally, the topological properties are discussed in three situations: in class A and AIII in any dimensions, and in class AII in dimensions two and three. The case of class A (without symmetries) was first studied by Rudner, Lindner, Berg and Levin [RLBL13], who developed most of the framework that is used in this thesis. I carried out the (straightforward) extension of their work to any (even) dimension. The case of class AIII (with chiral symmetry only), on the other hand, was first studied by Asbóth, Tarasinski, and Delplace [ATD14] in one dimension with different methods. I reinterpreted their work in the general framework initially developed for class A invariants, and extended it to any (odd) dimension. Additional antiunitary symmetries impose constraints on the two topological invariants characterizing complex CAZ classes A and AIII, which I explicit and discuss in details. Finally, the case of class AII (with fermionic time-reversal only) was studied for the first time in our article [CDFG15b] and is discussed in section 3.4, page 152.

2 Description of periodically driven systems

2.1 Time-dependent Hamiltonians and unitary evolutions

The evolution of a linear system is described by a family of linear maps called **evolution operators** acting on its Hilbert state space $\mathcal{H}$. An initial state ψ_0 at time t_0 is mapped by the evolution operator $U(t, t_0)$ to the state $\psi(t) = U(t, t_0)\psi_0$ which describes the state of the system at time t, from an initial state ψ_0 at time t_0. Evolution operators should respect the composition rule

$$U(t, t_1)U(t_1, t_0) = U(t, t_0) \tag{4.1}$$

and the constraint $U(t, t) = \mathrm{Id}$ for all t. Such an evolution is generated by a Hamiltonian $H(t)$ through the differential equation

$$\mathrm{i}\hbar\partial_t U(t, t_0) = H(t)U(t, t_0) \tag{4.2}$$

with initial condition $U(t, t) = \mathrm{Id}$. In the following, we will frequently set $\hbar = 1$ to lighten the notations.

It will often be convenient to set the origin of time such as $t_0 = 0$ to focus on the simplified evolution operator

$$U(t) = U(t, t_0 = 0) \tag{4.3}$$

with $U(0) = \mathrm{Id}$. This simplification should be done with some care as the choice of the origin of time may hide subtleties, especially when symmetries are present.

Unless stated otherwise, we will assume in the following that $U(t, t_0)$ are unitary operators (and that $H(t)$ is Hermitian). In quantum mechanics, the conservation of probability restricts the evolution operators to be unitary (this corresponds to restricting the Hamiltonian to be Hermitian). The propagation of electromagnetic waves is cast in the same framework by replacing the Hamiltonian with the Maxwell operator (see paragraph 1.3.1 of the introduction, page 16); in this context, the evolution operator is still a unitary operator, due to the conservation of the electromagnetic field energy. Similarly, mechanical systems can be described in a Hamiltonian framework (as exemplified in the paragraph 1.3.2 of the introduction, page 19, and explained in a more general way by Süsstrunk and Huber in [SH16]); here, the conservation of mechanical energy (especially the lack of dissipative forces) ensures the unitarity of the evolution. However, the effective description of a dissipative system and/or of a system where energy is injected may require a non-unitary description. In this case, we may still be able to define topological properties (see paragraph 3.2.2, page 129), but the possible appearance of unstable or damped modes may hinder experimental relevance. Even when the Hamiltonian does not depend on time, peculiar behavior may happen in cases where non-diagonalizable Hamiltonians are present in the phase diagram [Lee16]. In classical systems, regimes where the evolution is non-linear are easily accessible, which do not fall in this framework; we expect that the study of the topology of such nonlinear systems will require either perturbation theory or different tools, like field theory [VUG14].

2.1.1 Computation of the evolution operator

When the Hamiltonian does not depend on time, the evolution operator is simply the exponential of its generator

$$U(t) = \exp\left(-\frac{\mathrm{i}}{\hbar}\, tH\right). \tag{4.4}$$

When the Hamiltonian does depend on time, things are more complicated: the evolution operator is the time-ordered exponential

$$U(t) = T\exp\left(-\frac{\mathrm{i}}{\hbar}\int_0^t H(s)\mathrm{d}s\right) \tag{4.5}$$

which is in general impossible to compute analytically. Alternatively, the evolution operator can be expressed as the infinite series

$$U(t) = \lim_{\delta t/t\to 0}\prod_{n=1}^{[t/\delta t]}\exp\left(-\frac{\mathrm{i}}{\hbar}\, n\delta t\, H(n\delta t)\right) \tag{4.6}$$

which highlights the fact that the full time evolution is simply a sequence of infinitesimal evolution with constant Hamiltonians. This formula allows for a simple numerical evaluation of the evolution operator by discretizing the infinite product with a small but finite δt. An example of implementation of this method (not optimized at all) can be found as a supplementary material of my article [Fru16].

2.2 Floquet theory

2.2.1 Setup and general idea

The principle of the theory of space-periodic and time-periodic systems are both encompassed in the mathematical framework of differential equations with periodic coefficients (see [Kuc93]), which was discovered several times, at least by George Hill in 1877 [Hil86], Gaston Floquet in 1883 [Flo83], Alexander Lyapunov in 1896 [Lya96; Lya99] and Felix Bloch in 1928 [Blo29]. In physics, it is customary to use the name "Bloch theory" when space-periodic system are considered, and the name "Floquet theory" when time-periodic systems are considered. We follow this practice. Time-periodic Hamiltonians were first studied by Shirley [Shi65], Zel'dovich [Zel67] and Sambe [Sam73], who developed the framework of Floquet theory that I will present in the following paragraphs. Since then, several extensions and refinements of Floquet theory were carried out (e.g. with multiple frequencies), which are reviewed by Chu [CT04].Other modern reviews include the very pedagogical tutorial [Hol15] as well as the more complete reviews [BDP15; GD14].

Let us consider a time-periodic Hamiltonian which satisfies for all times t,

$$H(t+T) = H(t) \tag{4.7}$$

where T is the **driving period**. We also define the **driving frequency** $f = 1/T$ and the **driving angular frequency** $\omega = 2\pi/T$. Equivalently, we may consider a time-periodic unitary evolution with for all t and t',

$$U(t+T, t'+T) = U(t, t'). \tag{4.8}$$

The direct implication is due to the unicity of the solution of the Cauchy initial value problem, while the reverse can be shown from $H = \mathrm{i}U^{-1}\dot{U}$.

In this case, **Floquet theory** allows to separate long- and short-time scales, defined with respect to the driving period T. Indeed, the stroboscopic behavior of the system happens to be described by powers of the Floquet operator, as

$$U(nT) = [U(T)]^n \tag{4.9}$$

for an integer $n \in \mathbb{Z}$, and more generally[(1)]

$$U(t+nT) = U(t)[U(T)]^n. \tag{4.10}$$

As a consequence, we expect the **Floquet operator** $U(T)$ to describe the essential features of the evolution of the system on long-time scales. In particular, the "stroboscopic evolution" observed at each period is fully described by $U(T)$, through equation

[(1)] This equality is e.g. proven by induction from the fact that $H(t+T) = H(t)$ and $U(t+T, t'+T) = U(t, t')$ are equivalent, combined with the group structure of evolution operators.

(4.9), and it is convenient to consider $U(T)$ as the exponential of an Hermitian *effective Hamiltonian* as (this definition will be made precise in the following)

$$U(T) \approx \mathrm{e}^{-\mathrm{i}TH^{\mathrm{eff}}}. \tag{4.11}$$

which can be understood as a time-independent "averaged Hamiltonian" which would generate the same *stroboscopic* evolution as the time-periodic $H(t)$. Indeed, the effective Hamiltonian only contains informations on the long-time scales. The full evolution over one driving period $U(t \in [0, T])$, which is sufficient to reconstruct the whole time-evolution, contains informations on the short-time scale evolution. The main idea of Floquet theory is to separate the two contributions by decomposing the evolution operator as

$$U(t) \approx V(t)\mathrm{e}^{-\mathrm{i}tH^{\mathrm{eff}}} \tag{4.12}$$

where H^{eff} is the Hermitian *effective Hamiltonian* containing the long-time scales features while $V(t) = V(t+T)$ is a *periodized evolution operator* essentially containing the short-time scale informations.

In the next sections, we will be concerned with Bloch Hamiltonians depending on a quasi-momentum $k \in \mathrm{BZ}$ (see section 1.1, page 57). As nearly everything in the Floquet description of time-periodic Hamiltonians gracefully translates to Bloch Hamiltonians without subtleties by simply adding the parameter k as an argument for U, H^{eff} or V, we will not always mention it, and the reader may consider that in the following paragraphs, the index α in fact also contains k. There is, however, one subtlety. As we shall see in the next paragraph, the effective Hamiltonian is defined as a logarithm of the Floquet operator. Defining a smooth effective Hamiltonian $k \mapsto H^{\mathrm{eff}}(k)$ is only possible when (i) the spectrum Floquet operator is gapped and (ii) the branch cut of the complex logarithm is chosen in a gap: hence, operators $U(T, k)$ must share a *common* gap.

2.2.2 The effective Hamiltonian and the periodized evolution operator

The Floquet operator $U(T)$ is unitary, and can therefore be diagonalized on its eigenstates ϕ_α defined by

$$U(T)\left|\phi_\alpha\right\rangle = \lambda_\alpha \left|\phi_\alpha\right\rangle \tag{4.13}$$

as

$$U(T) = \sum_\alpha \lambda_\alpha \left|\phi_\alpha\right\rangle\!\left\langle\phi_\alpha\right| . \tag{4.14}$$

The eigenvalues $\lambda_\alpha \in U(1)$ are called **Floquet eigenvalues**.

As it was first recognized by Rudner, Lindner, Berg and Levin [RLBL13], the choice of the branch cut of the logarithm used in the definition of the effective Hamiltonian is crucial to define topological properties. When the spectrum of $U(T)$ is gapped, it is possible to find a **cut** $\varepsilon \in \mathbb{R}$ for the logarithm so that $\mathrm{e}^{-\mathrm{i}\varepsilon} \notin \sigma(U(T))$ lies in a gap of the spectrum $\sigma(U(T))$ of the Floquet operator (see figure 4.1) and it is possible to define the **effective Hamiltonian** containing the long-time scales features

$$H_\varepsilon^{\mathrm{eff}} = \frac{\mathrm{i}}{T} \log_{-\varepsilon} U(T) \tag{4.15}$$

through the spectral decomposition (4.14) as

$$H_\varepsilon^{\text{eff}} = \frac{\mathrm{i}}{T} \sum_\alpha \log_{-\varepsilon}(\lambda_\alpha) \left|\phi_\alpha\right\rangle\!\left\langle\phi_\alpha\right| . \tag{4.16}$$

where $\log_\varphi$ is the complex logarithm with cut along an axis with angle φ, defined as

$$\log_{-\varepsilon}(\mathrm{e}^{\mathrm{i}\varphi}) = \mathrm{i}\varphi \qquad \text{for} \qquad -\varepsilon - 2\pi < \varphi < -\varepsilon. \tag{4.17}$$

The Floquet operator $U(T)$ and the effective Hamiltonian H_η^{eff} share the same eigenstates (due to equation (4.16)), and

$$H_\eta^{\text{eff}} \left|\phi_\alpha\right\rangle = \epsilon_{\eta,\alpha} \left|\phi_\alpha\right\rangle \tag{4.18}$$

where we temporarily used the letter η for the logarithm cut to prevent notation clashes, and where

$$\epsilon_{\eta,\alpha} = \frac{\mathrm{i}}{T} \sum_\alpha \log_{-\eta}(\lambda_\alpha) \tag{4.19}$$

are called the **quasi-energies** of the system. They are related to the Floquet eigenvalues by

$$\lambda_\alpha = \exp\left[-\mathrm{i}T\epsilon_{\eta,\alpha}\right] . \tag{4.20}$$

As usual in the literature of Floquet topological phases, the Floquet eigenvalues λ_α will be referred to as "quasi-energies" when the meaning is clear. Consequently, the spectrum $\sigma(U(T)) = \{\lambda_\alpha\}_i$ of $U(T)$ is called the **quasi-energy spectrum**. In a translation invariant system, the quasi-momentum k is part of the abstract index α, and the quasi-energy spectrum is composed of quasi-energy bands, like in figure 4.1. It is also convenient to define a **dimensionless quasi-energy** $\varepsilon = T\epsilon$ which lies e.g. from 0 to 2π instead of 0 to ω, which are also referred to as "quasi-energies". Finally, it is also customary to omit the cut index and consider ϵ_α (resp. ε_α) as only defined modulo integer multiples of the driving angular frequency $\omega = 2\pi/T$ (resp. of 2π).

The **periodized evolution operator** containing the short-time scale informations is then defined as

$$V_\varepsilon(t) = U(t)\mathrm{e}^{\mathrm{i}tH_\varepsilon^{\text{eff}}} \tag{4.21}$$

so that for all t,

$$V_\varepsilon(t+T) = V_\varepsilon(t). \tag{4.22}$$

The end result of this section is the announced decomposition of the evolution operator as

$$U(t) = V_\varepsilon(t)\mathrm{e}^{-\mathrm{i}tH_\varepsilon^{\text{eff}}}. \tag{4.23}$$

2.2.3 Floquet modes and the expansion of the evolution operator

By defining time-periodic *Floquet modes* and their Fourier harmonics, called *Floquet sidebands*, it is possible to expand the evolution operator over an overcomplete system of *constant* vectors, so that all the time evolution is made explicit. Beyond technical usefulness in several situations, this decomposition allows for a physical interpretation

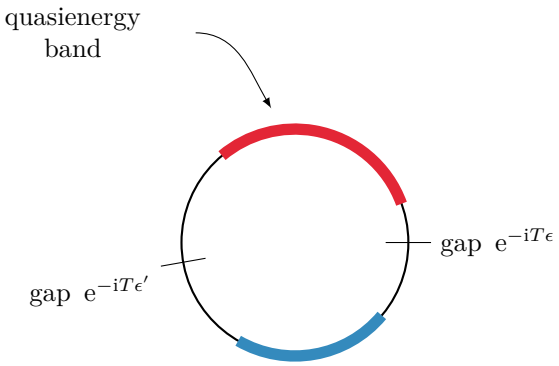

Figure 4.1: A quasi-energy spectrum. The spectrum of the unitary evolution operator after one period $U(T)$ is called the quasi-energy spectrum, and it lies on the unit circle $U(1)$. As in static systems, the quasi-energy spectrum of a crystal is composed of bands (there are two bands in this example, in blue and in red) separated by gaps.

of processes in terms of absorption and emission of quanta of the driving field (photons, phonons, etc.).

The time-periodic **Floquet modes** are defined as

$$|u_{\varepsilon,\alpha}(t)\rangle \equiv V_\varepsilon(t)\,|\phi_\alpha\rangle = |u_{\varepsilon,\alpha}(t+T)\rangle \tag{4.24}$$

by applying the periodized evolution operator on the basis of eigenstates of $U(T)$, so we essentially consider their time-evolution and factor out the long-time phase factor contained in the effective Hamiltonian. The evolution operator is first expanded as

$$U(t,t') = U(t,0)\,\mathrm{Id}\,U^{-1}(t',0) = \sum_\alpha U(t)\,|\phi_\alpha\rangle\langle\phi_\alpha|\,U^{-1}(t'). \tag{4.25}$$

From the decomposition (4.23), one has

$$U(t)\,|\phi_\alpha\rangle = V_\varepsilon(t)\mathrm{e}^{-\mathrm{i}tH^{\mathrm{eff}}_\varepsilon}\,|\phi_\alpha\rangle = \mathrm{e}^{-\mathrm{i}t\epsilon_{\varepsilon,\alpha}}V_\varepsilon(t)\,|\phi_\alpha\rangle\,. = \mathrm{e}^{-\mathrm{i}t\epsilon_{\varepsilon,\alpha}}\,|u_{\varepsilon,\alpha}(t)\rangle\,. \tag{4.26}$$

Combining both, we obtain an expression in terms of the Floquet modes,

$$U(t,t') = \sum_\alpha \mathrm{e}^{-\mathrm{i}(t-t')\epsilon_{\varepsilon,\alpha}}\,|u_{\varepsilon,\alpha}(t)\rangle\langle u_{\varepsilon,\alpha}(t')| \tag{4.27}$$

In this expression, the time-periodic Floquet modes contain the short-time scales information, whereas the exponentials of quasi-energies describe the long-time dynamics.

The Floquet modes are time-periodic and can therefore be expanded in Fourier series as

$$|u_{\varepsilon,\alpha}(t)\rangle = \sum_{p\in\mathbb{Z}} \mathrm{e}^{-\mathrm{i}p\omega t}\,|u^{(p)}_{\varepsilon,\alpha}\rangle \qquad \text{where} \qquad |u^{(p)}_{\varepsilon,\alpha}\rangle = \frac{1}{T}\int_0^T \mathrm{d}t\;\mathrm{e}^{ip\omega t}\,|u_{\varepsilon,\alpha}(t)\rangle\,. \tag{4.28}$$

Here, the p-th harmonics $u^{(p)}_{\varepsilon,\alpha}$ are called **Floquet sidebands**. Alternatively, the periodized evolution operator can also be expanded in Fourier series as

$$V_\varepsilon(t) = \sum_{p\in\mathbb{Z}} \mathrm{e}^{-\mathrm{i}p\omega t} V^{(p)}_\varepsilon. \tag{4.29}$$

and the sidebands read

$$|u^{(p)}_{\varepsilon,\alpha}\rangle = V^{(p)}_\varepsilon |\phi_\alpha\rangle . \tag{4.30}$$

The vectors $|u^{(p)}_{\varepsilon,\alpha}\rangle$ are not mutually orthogonal. Instead, the orthogonality of eigenstates of the Floquet operator

$$\langle \phi_\alpha \mid \phi_\beta\rangle = \delta_{\alpha,\beta} \tag{4.31}$$

implies for $q \in \mathbb{Z}$ the relation

$$\sum_{p\in\mathbb{Z}} \langle u^{(p)}_{\varepsilon,\alpha} \mid u^{(p+q)}_{\varepsilon,\beta}\rangle = \delta_{\alpha,\beta}\delta_{q,0}. \tag{4.32}$$

Finally, the evolution operator is expanded on the linearly dependent family of sidebands as

$$U(t,t') = \sum_\alpha \sum_{p,p'\in\mathbb{Z}} \mathrm{e}^{-\mathrm{i}(t-t')\epsilon_{\varepsilon,\alpha}} \mathrm{e}^{-\mathrm{i}\omega(pt-p't')} |u^{(p)}_{\varepsilon,\alpha}\rangle\langle u^{(p')}_{\varepsilon,\alpha}| . \tag{4.33}$$

The key point is that the time dependence is fully contained is the phase factors, as the sidebands $|u^{(p)}_{\varepsilon,\alpha}\rangle$ do not depend on time.

2.2.4 The effective Hamiltonian and the Schrödinger equation

Floquet theory can also be interpreted as providing a time-dependent unitary rotation of the time-dependent **Floquet Hamiltonian**

$$H_{\mathrm{F}}(t) = H(t) - \mathrm{i}\partial_t \tag{4.34}$$

into the time-independent effective Hamiltonian, as detailed below. Indeed, the evolution operator is solution of the differential equation

$$H_{\mathrm{F}}(t)U(t) = (H(t) - \mathrm{i}\partial_t)U(t) = 0 \tag{4.35}$$

with an initial condition $U(t) = \mathrm{Id}$. Along with equation (4.21), this yields

$$H_{\mathrm{F}}(t)V_\varepsilon(t) = (H(t) - \mathrm{i}\partial_t)V_\varepsilon(t) = V_\varepsilon(t)H^{\mathrm{eff}}_\varepsilon \tag{4.36}$$

or in other words

$$V^{-1}_\varepsilon(t)H_{\mathrm{F}}(t)V_\varepsilon(t) = V^{-1}_\varepsilon(t)(H(t) - \mathrm{i}\partial_t)V_\varepsilon(t) = H^{\mathrm{eff}}_\varepsilon. \tag{4.37}$$

As a consequence, the quasi-energies $\epsilon_{\varepsilon,\alpha}$ are eigenvalues of the Floquet Hamiltonian $H_{\mathrm{F}}(t)$; the corresponding eigenstates are the Floquet modes defined in equation (4.24), as the last equation applied to eigenstates $|\phi_\alpha\rangle$ of $U(T)$ yields

$$H_{\mathrm{F}}(t)\,|u_{\varepsilon,\alpha}(t)\rangle = \epsilon_{\varepsilon,\alpha}\,|u_{\varepsilon,\alpha}(t)\rangle . \tag{4.38}$$

2.2.5 Floquet theory in Sambe space

An approach developed by Sambe [Sam73] (which was already present in essence in Shirley's paper [Shi65]) consists in using the preceding observation to fully map the time-dependent and time-periodic Hamiltonian to a time-independent Hamiltonian acting on a larger "composite space" called the *Sambe space*. In contrast with the effective Hamiltonian which only contains the long-time (or stroboscopic) dynamics, the *Sambe Hamiltonian* takes into account the full dynamics and should allow to fully solve the time-dependent problem. In practice, an approximation scheme is necessary to reduce infinite matrices to finite ones. The Sambe space approach is particularly useful to numerically compute the quasi-energy spectrum of a system and the corresponding Floquet states.

As we have seen in the last paragraph, the Floquet modes are eigenstates of the Floquet Hamiltonian,

$$(H(t) - \mathrm{i}\hbar\partial_t)\,|u_{\varepsilon,\alpha}(t)\rangle = \epsilon_{\varepsilon,\alpha}\,|u_{\varepsilon,\alpha}(t)\rangle\,. \tag{4.39}$$

For better clarity, we exceptionally include the $\hbar$'s in this paragraph. Both the LHS and the RHS of this equation are time-periodic. After a Fourier decomposition and a rearrangement of the terms, it is equivalent to the set of equations

$$\sum_{q\in\mathbb{Z}} \Big(H^{(p-q)} - \delta_{p,q}\, p\hbar\omega\,\mathrm{Id}\Big)\,|u^{(q)}_{\varepsilon,\alpha}\rangle = \epsilon_{\varepsilon,\alpha}\,|u^{(p)}_{\varepsilon,\alpha}\rangle \tag{4.40}$$

for all $p \in \mathbb{Z}$, where $H^{(p)}$ are the harmonics of the time-periodic Hamiltonian, decomposed as

$$H(t) = \sum_{p\in\mathbb{Z}} \mathrm{e}^{-\mathrm{i}p\omega t} H^{(p)} \tag{4.41}$$

and where the Floquet sidebands $u^{(p)}_{\varepsilon,\alpha}$ were defined in equation (4.28). In matrix form, this set of equations reads

$$\mathcal{H}_{\mathrm{S}}\,|\mathcal{U}_{\varepsilon,\alpha}\rangle = \epsilon_{\varepsilon,\alpha}\,|\mathcal{U}_{\varepsilon,\alpha}\rangle \tag{4.42}$$

The infinite matrix $\mathcal{H}_{\mathrm{S}}$ is called the **Sambe Hamiltonian**, and is defined as

$$\mathcal{H}_{\mathrm{S}} = \mathcal{H}_{\mathrm{S,H}} - \mathcal{H}_{\mathrm{S},\Omega} \tag{4.43}$$

where

$$\mathcal{H}_{\mathrm{S,H}} = \begin{pmatrix} & & \vdots & & & \\ & H^{(1)} & H^{(0)} & H^{(-1)} & H^{(-2)} & H^{(-3)} & \\ \cdots & H^{(2)} & H^{(1)} & H^{(0)} & H^{(-1)} & H^{(-2)} & \cdots \\ & H^{(3)} & H^{(2)} & H^{(1)} & H^{(0)} & H^{(-1)} & \\ & & \vdots & & & & \end{pmatrix} \tag{4.44}$$

and

$$\mathcal{H}_{\mathrm{S},\Omega} = \begin{pmatrix} \ddots & & & & & \\ & (p-1)\,\hbar\omega & & & & \\ & & p\,\hbar\omega & & & \\ & & & (p+1)\,\hbar\omega & & \\ & & & & \ddots & \end{pmatrix}. \tag{4.45}$$

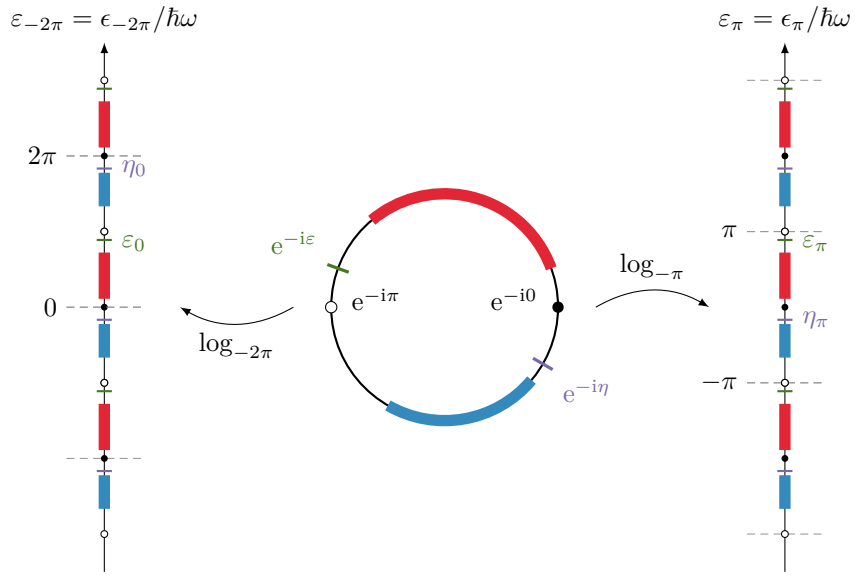

Figure 4.2: Quasi-energy spectrum on the circle and on the line. The quasi-energy spectrum on the circle (i.e. the spectrum of the Floquet operator $\sigma(U(T)) \subset U(1)$) can be unfolded on the real line through the logarithm. The effective Hamiltonian $H_\eta^{\mathrm{eff}} = (\mathrm{i}/T)\log_{-\eta} U(T)$ has eigenvalues on a single domain of length 2π depending on the cut, e.g. $]-\pi, \pi[$ if $\eta = -\pi$. On the other hand, the spectrum of the Floquet Hamiltonian consists of an infinite number of copies of the unfolded quasi-energy spectrum, shifted by integer multiples of 2π.

It acts on a composite space, the **Sambe space**, where the Floquet sideband modes were gathered into the infinite tuple

$$|\mathcal{U}_{\varepsilon,\alpha}\rangle = \begin{pmatrix} \vdots \\ u_{\varepsilon,\alpha}^{(p-1)} \\ u_{\varepsilon,\alpha}^{(p)} \\ u_{\varepsilon,\alpha}^{(p+1)} \\ \vdots \end{pmatrix}. \tag{4.46}$$

The Floquet Hamiltonian has an infinity of redundant solutions: if $u_{\varepsilon,\alpha}(t)$ is a solution with eigenvalue $\epsilon_{\varepsilon,\alpha}$, so that

$$H_{\mathrm{F}}(t) u_{\varepsilon,\alpha}(t) = \epsilon_{\varepsilon,\alpha} u_{\varepsilon,\alpha}(t) \tag{4.47}$$

then the gauge transformation

$$u_{\varepsilon,\alpha}(t) \to \mathrm{e}^{\mathrm{i}\Delta p\, \hbar\omega t} u_{\varepsilon,\alpha}(t) \tag{4.48}$$

provides a new eigenstate with eigenvalue $\epsilon_{\varepsilon,\alpha} + \Delta p\, \hbar\omega$. In the composite Sambe state (4.46), this substitution corresponds to

$$u_{\varepsilon,\alpha}^{(p)} \to u_{\varepsilon,\alpha}^{(p+\Delta p)}. \tag{4.49}$$

As a consequence, if we shift the sidebands of an eigenstate of the Sambe Hamiltonian with eigenvalue $\epsilon_{\varepsilon,\alpha}$ (replacing $u^{(p)}_{\varepsilon,\alpha}$ with $u^{(p+\Delta p)}_{\varepsilon,\alpha}$ for all p), the resulting state is still an eigenstate of the same Sambe Hamiltonian, but with eigenvalue $\epsilon_{\varepsilon,\alpha} + \Delta p\,\hbar\omega$. This shift can be applied to the Sambe Hamiltonian instead, as the operator $\mathcal{H}_{\mathrm{S}} + \Delta p\,\hbar\omega\mathrm{Id}$ is the Sambe Hamiltonian that would be obtained with a shift of Δp sidebands. As

$$\mathrm{e}^{-\mathrm{i}\Delta p\hbar\omega t}\,\mathcal{H}_{\mathrm{S}}\,\mathrm{e}^{\mathrm{i}\Delta p\hbar\omega t} = (\mathcal{H}_{\mathrm{S}} + \Delta p\,\hbar\omega\mathrm{Id}) + \Delta p\,\hbar\omega\mathrm{Id})\,|\mathcal{U}_{\varepsilon,\alpha}\rangle \tag{4.50}$$

the Sambe Hamiltonian also has an infinity of redundant solutions.

2.2.6 The origin of times

In all the discussion on Floquet theory, I have fixed an origin of times $t_0 = 0$ in order to reduce the evolution operator family $U(t_1, t_0)$ to a single-parameter family $U(t) = U(t, t_0 = 0)$. At first sight, this choice seems to be purely arbitrary, and nothing should depend on it. However,

- from the technical point of view, in presence of antiunitary symmetries, topological invariants are naturally expressed when the origin of time is chosen as an invariant point of the action $t \to -t$ of the symmetry; this point will be discussed in the next paragraph 2.4.2;
- from the physical point of view, initial conditions may be crucial, in particular when it is taken into account that the time-periodic modulation is turned on at some initial time $t_{\mathrm{i}} \neq t_0$ [GD14] (when e.g. $H(t) \propto \sin(t - t_0)$). Despite this potential susceptibility to initial conditions, we do not expect that the initial time should have an incidence on the the topological properties of the system, an hypothesis supported by numerical experimentations.

In the general case, recall that the evolution operator is defined by the differential equation

$$\mathrm{i}\hbar\partial_t U(t, t_0) = H(t)U(t, t_0) \tag{4.51}$$

with initial condition $U(t, t) = \mathrm{Id}$. Hence, an origin of times was previously implicitly fixed in the Hamiltonian $H(t)$ when $t_0 = 0$ (this is obvious with an example, e.g. $H(t) = H_0 + \sin(t)H_1$). A shift in the time t_0 in the evolution operators corresponds to a shift of this implicit origin of times. Crucially, the evolution operators with different "origin times" are related by a unitary transformation

$$U(t_1 + T, t_1) = U(t_1, t_0)\,U(t_0 + T, t_0)\,U^{-1}(t_1, t_0) \tag{4.52}$$

so they have the same spectrum. As a consequence, a family of effective Hamiltonians with the same cut can be defined (again by spectral theory) as

$$H^{\mathrm{eff}}_{\varepsilon,t0} = \frac{\mathrm{i}}{T}\log_{-\varepsilon} U(t_0 + T, t_0) \tag{4.53}$$

as well as periodized evolution operators

$$V_\varepsilon(t, t_0) = U(t, t_0)\mathrm{e}^{\mathrm{i}(t-t_0)H^{\mathrm{eff}}_{\varepsilon,t_0}}. \tag{4.54}$$

They are time-periodic, with $V(t + T, t_0) = V(t, t_0) = V(t, t_0 + T)$ and indeed $V(t_0, t_0) = \mathrm{Id}$.

Following Rahav, Gilary and Fishman [RGF03], Goldman and Dalibard [GD14] have proposed to use a canonical effective Hamiltonian $H^{\text{eff}}_{\text{can}}$ generating all the origin-time dependent effective Hamiltonians H^{eff}_{t0} through the gauge transformations

$$H^{\text{eff}}_{t0} = \mathrm{e}^{\mathrm{i}K(t_0)}\, H^{\text{eff}}_{\text{can}}\, \mathrm{e}^{-\mathrm{i}K(t_0)}. \tag{4.55}$$

This canonical effective Hamiltonian shares the same spectrum as any of the H^{eff}_{t0}, and seems to be more convenient for perturbative expansions (see [GGN15] and [BDP15, § 3]). However, it does not seem straightforward to extend the definition of this object to fully take into account the branch cuts of the logarithm, which prevents for the time being to use it to define Floquet topological invariants.

2.3 Symmetries of time-dependent and time-periodic evolutions

The role of symmetries – in this section, we will use the term *symmetry* to design time-reversal, charge-conjugation and chiral symmetry only – in Floquet phases was first studied by Kitagawa, Rudner, Berg and Demler, both in quantum walks [KRBD10] and in generic evolutions [KBRD10]. Several refinements were made, both in papers devoted to the study of a given symmetry class [JKAA11; ATD14; CDFG15b; Fru16] and in works towards a full classification [NR15; RH16]. Crucially, studies on chiral symmetric [ATD14] and time-reversal invariant [CDFG15b] systems showed that the full time-evolution is constrained by symmetries, and not only the Floquet operator $U(T)$ and/or the effective Hamiltonian H^{eff}. In other words, situations where only the effective Hamiltonian is e.g. time-reversal invariant *do not* correspond to a time-reversal invariant time-evolution[(2)]. In retrospect, this assertion is natural in view of the classification of time evolutions of section 2.4.1 (page 101), where we have seen that the general form of a symmetry of the Bloch evolution is

$$gU(t,k)g^{-1} = U(\tau(g)t, \phi(g)k) \tag{4.56}$$

where $\tau(g)$ tracks whether g reverses time, and $\phi(g)$ whether g is unitary or antiunitary. For example, an evolution is time-reversal invariant when

$$\Theta U(t,k)\Theta^{-1} = U(-t,-k). \tag{4.57}$$

This property of U implies, but is not equivalent to the time-reversal constraint on the effective Hamiltonian

$$\Theta H^{\text{eff}}(k)\Theta^{-1} = H^{\text{eff}}(-k), \tag{4.58}$$

as an evolution satisfying (4.58) can break time-reversal invariance.

[(2)] However, such a situation may be interesting in itself. For example, an evolution which is not time-reversal invariant but with a time-reversal invariant evolution effective Hamiltonian (i.e. satisfying (4.58)) may only be topological in an anomalous way, with the same gap invariant in all gaps. More generally, there may be various constraints on the evolution, but they are not necessarily symmetries.

2.4 Symmetries

Explicitly, an evolution is **time-reversal invariant** when

$$\Theta U(t,k)\Theta^{-1} = U(-t,-k) \tag{4.59a}$$

where Θ is antiunitary. It is **charge-conjugation invariant** when

$$CU(t,k)C^{-1} = U(t,-k) \tag{4.59b}$$

where again C is antiunitary. Finally, it is **chiral invariant** (or chiral) when

$$\Gamma U(t,k)\Gamma^{-1} = U(-t,k) \tag{4.59c}$$

where Γ is unitary. In terms of the time-dependent Hamiltonians, those constraints are equivalent to

$$\Theta H(t,k)\Theta^{-1} = H(-t,-k) \tag{4.60a}$$
$$CH(t,k)C^{-1} = -H(t,-k) \tag{4.60b}$$
$$\Gamma H(t,k)\Gamma^{-1} = -H(-t,k). \tag{4.60c}$$

The effective Hamiltonian and the periodized evolution operator inherit the preceding constraints as follows. For the effective Hamiltonian, they are respectively

$$\Theta H_\varepsilon^{\mathrm{eff}}(k)\Theta^{-1} = H_\varepsilon^{\mathrm{eff}}(-k) \tag{4.61a}$$
$$CH_\varepsilon^{\mathrm{eff}}(k)C^{-1} = -H_{-\varepsilon}^{\mathrm{eff}}(-k) + \frac{2\pi}{T}\mathrm{Id} \tag{4.61b}$$
$$\Gamma H_\varepsilon^{\mathrm{eff}}(k)\Gamma^{-1} = -H_{-\varepsilon}^{\mathrm{eff}}(k) + \frac{2\pi}{T}\mathrm{Id} \tag{4.61c}$$

and for the periodized evolution operator,

$$\Theta V_\varepsilon(t,k)\Theta^{-1} = V_\varepsilon(-t,-k) \tag{4.62a}$$
$$CV_\varepsilon(t,k)C^{-1} = V_{-\varepsilon}(t,-k)\mathrm{e}^{-2\pi\mathrm{i}t/T} \tag{4.62b}$$
$$\Gamma V_\varepsilon(t,k)\Gamma^{-1} = V_{-\varepsilon}(-t,k)\mathrm{e}^{2\pi\mathrm{i}t/T} \tag{4.62c}$$

Time periodicity may be used to replace $-t$ with $T-t$ in this set of equations. The preceding properties are obtained by spectral decomposition of the Floquet operator $U(T,k)$, and using the logarithm identity

$$\log_{-\varepsilon}(\mathrm{e}^{-\mathrm{i}\phi}) = -\log_\varepsilon(\mathrm{e}^{\mathrm{i}\phi}) - 2\pi\mathrm{i}. \tag{4.63}$$

I derived them for time-reversal in [CDFG15a] and for chiral symmetry in [Fru16]. The case of charge-conjugation is very similar.

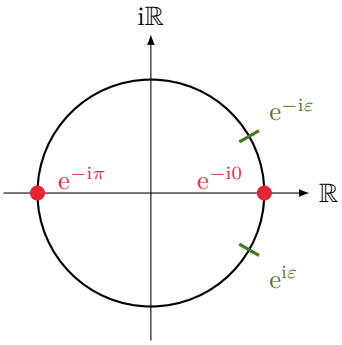

Figure 4.3: Real gaps of the quasi-energy spectrum. The gaps at quasi-energies $\lambda = \pm 1$, corresponding to arguments $\varepsilon = 0$ or π are particular gaps, invariant by the reflection by the real axis (going from $e^{i\varepsilon}$ to $e^{-i\varepsilon}$) characteristic of chiral symmetry and charge-conjugation.

2.4.1 Special gaps for charge-conjugation and chiral symmetry

When describing the constraints due to charge-conjugation and chiral symmetry, in equations (4.62), we observe that only for two special values of the cut ε, namely $\varepsilon = 0$ and $\varepsilon = \pi$ does the constraint act on a single periodized evolution operator, i.e. with the same cut. It is indeed obvious for $\varepsilon = 0$, for which equations (4.62) become

$$CV_0(t,k)C^{-1} = V_0(t,-k)e^{-2\pi it/T} \tag{4.64a}$$
$$\Gamma V_0(t,k)\Gamma^{-1} = V_0(-t,k)e^{2\pi it/T} \tag{4.64b}$$

For $\varepsilon = \pi$, we need another logarithm identity

$$\log_{-(\varepsilon-2\pi)}(e^{i\phi}) = \log_{-\varepsilon}(e^{i\phi}) + 2\pi i. \tag{4.65}$$

Hence,

$$V_{-\varepsilon}(t,k) = V_{2\pi-\varepsilon}(t,k)e^{2\pi it/T} \tag{4.66}$$

and equations (4.62) become

$$CV_\pi(t,k)C^{-1} = V_\pi(t,-k) \tag{4.67a}$$
$$\Gamma V_\pi(t,k)\Gamma^{-1} = V_\pi(-t,k). \tag{4.67b}$$

As a consequence, we will see that it is only possible to (technically) define topological invariants protected by such symmetries for the **real gaps** $\varepsilon = 0$ and $\varepsilon = \pi$ (dubbed this way as $e^{-i0} = 1$ and $e^{-i\pi} = -1$ are the only real Floquet eigenvalues on the circle, see figure 4.3). Moreover, we do not expect these symmetries to impose the vanishing of other existing topological invariants (without symmetries or protected by time-reversal invariance) in gaps different than the real gaps. Yet, both charge-conjugation and chiral symmetries can relate the existing invariants in gaps $+\varepsilon$ and $-\varepsilon$ (for $\varepsilon \neq 0, \pi$), as we shall see with the example of chiral symmetry.

2.4.2 Symmetries and their invariant points

We mentioned in paragraph 2.2.6 that the origin of times may have physical consequences (though expectedly not on topological properties) when the turning on and off of the time-periodic perturbation is taken into account. On the technical level, correctly choosing the origin of times is crucial to define and to compute topological invariants. For concreteness, let me focus on time-reversal invariance, and consider two time-independent Hermitian operators H_0 and H_1, respectively even and odd with respect to time reversal, that is satisfying

$$\Theta H_0 \Theta^{-1} = H_0 \qquad \text{and} \qquad \Theta H_1 \Theta^{-1} = -H_1. \tag{4.68}$$

Then, consider the two Hamiltonians

$$H(t) = H_0 + H_1 \sin(\omega t) \qquad \text{and} \qquad H'(t) = H_0 + H_1 \cos(\omega t). \tag{4.69}$$

Both Hamiltonians represent the same physical situation, and differ only in the choice of the origin of times (modulo a driving period T). Indeed, the first Hamiltonian is time-reversal invariant,

$$\Theta H(t) \Theta^{-1} = H(-t) \qquad \text{whereas} \qquad \Theta H'(t) \Theta^{-1} \neq H'(-t). \tag{4.70}$$

The second Hamiltonian seems not to be time-reversal invariant, but it obviously is with another choice for the reversal point

$$\Theta H'(t_\mathrm{r} + t) \Theta^{-1} = H'(t_\mathrm{r} - t) \tag{4.71}$$

with $\omega t_\mathrm{r} = -\pi/2$ i.e. $t_\mathrm{r} = T/4$.

More generally, time-reversal invariant or chiral symmetry act with respect to a *reversal point* t_r, which is left invariant, and time-reversal or chiral invariant Hamiltonian verify

$$\Theta H(t_\mathrm{r} + t, k) \Theta^{-1} = H(t_\mathrm{r} - t, -k) \qquad \text{and/or} \qquad \Gamma H(t_\mathrm{r} + t, k) \Gamma^{-1} = H(t_\mathrm{r} - t, k). \tag{4.72}$$

Indeed, when the Hamiltonian is time-periodic with period T, this choice of reversal point is relative to a particular period of time, as any $t_\mathrm{r} + nT/2$ with integer $n \in \mathbb{Z}$ is a reversal point if t_r is. In this situation, we should consider the evolution operator family $U(t) = U(t_\mathrm{r} + t, t_\mathrm{r})$ to define effective Hamiltonian and periodized evolution operators. In doing so, we ensure that the periodized evolution operator is constrained in a way which enables to define topological properties in the most straightforward way.

The map $t_0 \mapsto V_\varepsilon(t, t_0)$ provide a homotopy between the periodized evolution operators at different initial times t_0. In classes where only time-local symmetries (unitary symmetries and charge-conjugation), the constraints enabling to define topological invariants can be respected along this homotopy, and as a consequence, the topological invariants do not depend on the starting point. In contrast, with symmetries non local in time, the origin of times t_0 must be a reversal point for the topological invariants to be defined, and the preceding argument cannot be applied. Indeed, the invariants

computed with $t_0 = t_\mathrm{r}$ and with $t_0 = t_\mathrm{r} + T$ where t_r is a reversal point are necessarily equal, but this is not necessarily the case of $t_0 = t_\mathrm{r}$ and $t_0 = t_\mathrm{r} + T/2$.

Another open question is the following: an evolution may be time-reversal and chiral invariant with different reversal points, and it is not clear how to define topological invariants is such a situation.

3 Topology of periodically driven crystals

In the following section, we aim at defining topological invariants for wave-supporting spatially-periodic systems submitted to a time-periodic excitation or modulation (Floquet topological phases). Kitagawa el al. [KBRD10; KBFR12] first observed that usual invariants are not sufficient, because of the periodicity of quasi-energy. For example in figure 4.4, both (a) and (c) have bands with vanishing Chern invariants, despite the existence of topologically protected chiral edge states in (c). The first complete characterization of the bulk topology of a Floquet system was done in class A in two space dimensions by Rudner, Lindner, Berg, and Levin [RLBL13]. The framework they laid down can be extended to include Floquet topological phases with symmetries, as I will discuss in this part. It is also noticeable that this framework (and its extension with symmetries) also describes certain kinds of directed scattering networks [CC88; HC96] which appear e.g. in optical [HPWP15] and acoustic [FKA15] systems, that are also described by unitary "evolution operators", as first pointed out by Chong and collaborators [LC13; PC14; GGSY16].

Besides the definition of *bulk invariants*, I should mention that several routes were considered to study Floquet topological phases and their interplay with symmetries:

- A bulk K-theoretic classification was recently developed by Roy and Harper [RH16]. Essentially, they find that Floquet topological phases are classified by the K-group $\widetilde{\mathrm{K}}^{-s+1}(S^1 \times \mathrm{BZ}_d)$ for complex classes and $\widetilde{\widetilde{\mathrm{KR}}}^{-s+1}(S^1 \times \mathrm{BZ}_d)$ for real classes, where s (understood mod. 2 for complex classes and mod. 8 for real classes) labels the CAZ class and BZ_d is the d-dimensional Brillouin torus. They observe that the K-theoretical isomorphisms $\widetilde{\mathrm{K}}^{-s+1}(S^1 \times \mathrm{BZ}_d) \simeq \widetilde{\mathrm{K}}^{-s}(\mathrm{BZ}_d)$ and $\widetilde{\widetilde{\mathrm{KR}}}^{-s+1}(S^1 \times \mathrm{BZ}_d) \simeq \widetilde{\widetilde{\mathrm{KR}}}^{-s}(\mathrm{BZ}_d)$ relate the Floquet classification and the equilibrium classification (in fact, the isomorphisms are formulated in terms of relative K-groups, and the preceding equalities should be thought as symbolical). Clément Tauber and I observed this relation as the manifestation of the Bott isomorphism for complex classes, see Clément's thesis [Tau15] and reference [Fru16].
- Another kind of topological invariants focusing on the edge was developed for equilibrium systems by Akhmerov, Beenakker, Fulga and Hassler, [ADHW11; FHAB11; FHA12]. This method was recently extended for several classes to Floquet phases by Fulga and Maksymenko [FM16] and Tarasinski, Asbóth and Dahlhaus [TAD14]. Here, the edge states are detected through their effect on the reflection part of the scattering matrix, in the spirit of the Levinson theorem.
- A point of view on topological phases due to Chen, Gu, Liu and Wen [CGLW13; GW14; CGLW12] aims at classifying symmetry-protected topological (SPT) many-

body localized (MBL) phases through group cohomology. Recently, von Keyserlingk and Sondhi [KS16b; KS16a] (whose work was summarized and generalized by Else and Nayak [EN16]) and independently Potter, Morimoto and Vishwanath [PMV16] generalized this point of view to Floquet systems. The spirit of this method is slightly different as *states* instead of evolutions are classified here.

The results of the bulk K-theoretic classification are in nice agreement with the known bulk invariants: in fact, the bulk invariants are implementable ways to actually *compute* the invariants predicted by K-theory, as in the equilibrium case. On the other hand, scattering edge invariants do agree with the bulk invariants, but the equivalence between them, though physically intuitive, is not completely clear and requires additional work. Indeed, the identity of both classes of invariants is the core of the bulk-edge correspondence, which is a difficult subject. I want to stress that this equivalence is not fully understood yet, despite several advances on the subject [RLBL13; NR15; TD15; RH16].

Finally, note that in this section, the driving (and therefore the Hamiltonian) will always be supposed time-periodic unless specified otherwise.

3.1 Band invariants and gap invariants

In addition to being able to create an artificial gauge field i.e. a relative phase pattern inducing the usual equilibrium-like topological phases, a periodic modulation can also lead to specific situations unreachable at equilibrium. This phenomenon is essentially due in the one hand to the the existence of a "new gap" at quasienergy $\mathrm{e}^{-\mathrm{i}\pi} = -1$, which can potentially host topological edge states, and in the other hand (obviously) to the time-dependence of the Hamiltonian. Even though the physical picture is quite similar to the equilibrium case, the usual invariants (like the Chern invariants, the chiral invariants or the Kane-Mele invariants) are not sufficient to fully characterize the bulk topology of periodically driven phases [KBRD10]. Indeed, such invariants characterize the topology of a band (and as such they are called **band invariants**), and it appears that the bulk topology of a (linear) evolution is not fully captured by the topology of the quasienergy bands of the Floquet operator $U(T)$. Instead, new **gap invariants** computed from the full time-evolution (over one period) have to be defined [RLBL13], which are able to completely capture its bulk topological properties. A particularly noticeable behavior of periodically-driven phases is the existence of topological phases where all *band* invariants vanish, despite a nontrivial bulk topology; such phases were called **anomalous topological phases** (see figure 4.4). Notably, different realizations of such anomalous phases were experimentally observed in photonic systems [HPWP15; GGSY16; MSVA16; MZNS16]. Interestingly, anomalous phases and more generally phases were all gap invariants are non-vanishing cannot be implemented as a static lattice Hamiltonian, because the spectrum of the Floquet operator $U(T)$ of the system with edges has no gap.

The main picture is the following: we expect that for each CAZ class and each space dimension d there is a set of gap invariants $I_{\mathrm{gap}}(\mathrm{CAZ}, d, \varepsilon, U)$ associated to Bloch-Floquet time evolution $U : [0,T] \times \mathrm{BZ}_d \to U(N)$ respecting the symmetry constraints corresponding to the CAZ class, for each quasi-energy $\mathrm{e}^{-\mathrm{i}\varepsilon} \notin \sigma(U(T))$ in a quasi-energy gap of the Floquet operator $U(T)$. Such invariants are expected to be

related to the standard band invariants associated to symmetry-equivariant projectors $P : [0, T] \times \mathrm{BZ}_d \to M_N(\mathbb{C})$ on (quasi-energy) bands $I_{\mathrm{band}}(\mathrm{CAZ}, d, P)$ by

$$I_{\mathrm{gap}}(\mathrm{CAZ}, d, \varepsilon', U) - I_{\mathrm{gap}}(\mathrm{CAZ}, d, \varepsilon, U) = I_{\mathrm{band}}(\mathrm{CAZ}, d, P_{\varepsilon,\varepsilon'}) \tag{4.73}$$

where $P_{\varepsilon,\varepsilon'}$ is the spectral projector corresponding to the quasi-energy band between ε and ε' (in the right order, see figure 4.5 and the following paragraphs).

This general structure was first discovered by Rudner et al. [RLBL13], and we shall see in the following paragraphs that it stands in several cases. Along with the classifications of references [NR15] and [RH16], those examples provides strong evidences that this structure should hold in the general case. The simplest invariants characterize "complex" CAZ classes A and AIII: such invariants are simply winding numbers of a unitary map on a compact manifold. As we shall see in paragraphs 3.2.7, page 139 and 3.3.6, page 148, additional symmetries put constraints on the two topological invariants characterizing complex CAZ classes. Such constraints on the periodized evolution operator can either force the invariants to vanish or let them essentially unconstrained. The vanishing of class A and AIII invariants can either make room for a finer $\mathbb{Z}_2$ invariant or signal that all phases are trivial in the corresponding pair (CAZ class, dimension). On the contrary, when the invariants of complex classes do not vanish, they characterize the topological phases in the corresponding (CAZ class, dimension) pair, essentially as if the antiunitary symmetries were not present: it is possible to compute the relevant invariant irrespective of antiunitary symmetries. The process of forgetting antiunitary symmetries maps the real CAZ classes to the two complex classes by AI,D,AII,C $\to$ A and BDI,DIII,CI,CII $\to$ AIII [CTSR15], as illustrated by the colors in table 4.1, page 161.

The bulk invariants are expected to predict the existence of topologically protected states with particular properties (e.g. chiral or helical edge states) at the interface between two topologically distinct Floquet systems with the same driving frequency, and when the symmetries are not broken at the interface. Namely,

$$I_{\mathrm{gap}}(\mathrm{CAZ}, d, \varepsilon, U_1) - I_{\mathrm{gap}}(\mathrm{CAZ}, d, \varepsilon, U_2) \tag{4.74}$$

should give the number of edge states at quasi-energy ε at the interface between a phase whose bulk is described by U_1 and a phase whose bulk is characterized by U_2 (see figure 4.4), counted algebraically (e.g. with chirality). When the invariant is a torsion invariant, say $\mathbb{Z}_p$-valued, the corresponding number should also be interpreted as modulo p quantity.

3.2 Class A: without any symmetry

3.2.1 Definition of the invariant

The simplest case happens when all symmetries are broken in the symmetry class, that is when there are no constraint on the Hamiltonian.

When the dimension d of the space (and therefore of the Brillouin torus BZ) is even, $d = 2n$, then V_ε is a map from the odd-dimensional manifold $M = S^1 \times \mathrm{BZ}$ to the unitary group $U(N)$, where S^1 represents a period of time, e.g. $[0, T]$, so we can

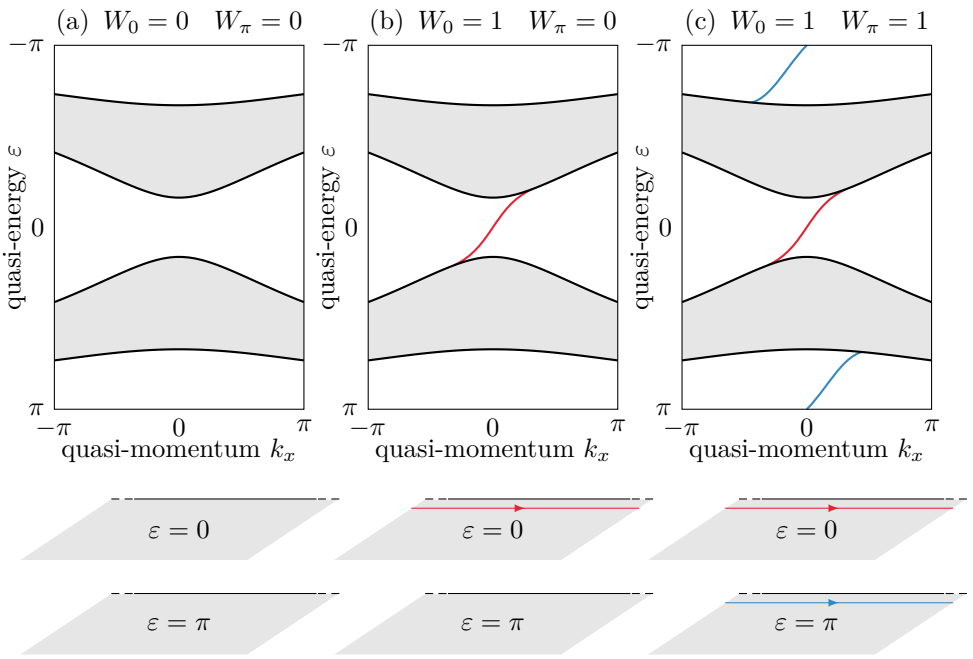

Figure 4.4: Topologically distinct situations. We illustrate several possible and topologically distinct situations in the example of a 2D class A driven system (similar to Chern insulators). In all situations, the quasi-energy spectra are gapped, with two gaps in $\varepsilon = 0$ and $\varepsilon = \pi$. In (a), the system is entirely trivial, and there is no topologically protected edge state. In (b), the gap $\varepsilon = 0$ is nontrivial, whereas the gap $\varepsilon = \pi$ is trivial; more precisely, there are bulk gap invariants $W_0 = 1$ and $W_\pi = 0$. The main physical manifestation of the non-vanishing W_0 is the existence of a chiral edge state in the corresponding bulk gap on a system with an interface with vacuum. Similarly, in (c) both gaps are nontrivial, and there is a chiral edge state in each gap. As $W_0 = W_\pi$, this phase is anomalous: all the bulk band invariants (here the first Chern invariants of the bands) vanish.

define a $\mathbb{Z}$-valued invariant, extending the definition of [RLBL13] to all even space dimensions by

$$W_\varepsilon[U] = W_n(V_\varepsilon, S^1 \times \mathrm{BZ}) = \deg(V_\varepsilon) \in \mathbb{Z} \tag{4.75}$$

where the degree (or winding, or odd Chern invariant) of a map V from a $(2n+1)$-dimensional closed manifold M to the unitary group $U(N)$ is defined in equation (2.59), page 50. Essentially, it counts the number of times the map V winds around nontrivial $(2n+1)$-cycles in $U(N)$.

We can write explicitly

$$W_\varepsilon[U] = \int_M \widetilde{\mathrm{ch}}_n(V_\varepsilon) \tag{4.76}$$

where the odd Chern character (see section 2.2.4 and equation (2.59) page 50) is

$$\widetilde{\mathrm{ch}}_n(V) = (-1)^n \frac{n!}{(2n+1)!} \left(\frac{\mathrm{i}}{2\pi}\right)^{n+1} \mathrm{tr}\left[(V^{-1}\mathrm{d}V)^{2n+1}\right] \tag{4.77}$$

In terms of the derivatives of V,

$$\mathrm{tr}\left[(V^{-1}\mathrm{d}V)^{2n+1}\right] = \epsilon^{i_1 i_2 \cdots i_{2n+1}} \mathrm{tr}\left[(V^{-1}\partial_{i_1}V)\cdots(V^{-1}\partial_{i_{2n+1}}V)\right] \mathrm{d}x_1 \ldots \mathrm{d}x_{2n+1},$$

where ϵ is the Levi-Civita symbol. In our case, $M = \mathrm{BZ} \times S^1$ and we may use the first $2n$ variables to describe the Brillouin zone, $x_1 = k_1$ to $x_{2n} = k_{2n} = k_d$ and the last one for the time, $x_{2n+1} = t$. As an example, in $d = 2$ (so $n = 1$), the invariant is expressed as

$$W_\varepsilon[U] = \frac{1}{24\pi^2} \int_{\mathrm{BZ}\times S^1} \mathrm{d}k_x \mathrm{d}k_y \mathrm{d}t \;\; \mathrm{tr}\left(3[V_\varepsilon^{-1}\partial_{k_x}V_\varepsilon, V_\varepsilon^{-1}\partial_{k_y}V_\varepsilon]V_\varepsilon^{-1}\partial_t V_\varepsilon\right). \tag{4.78}$$

Note that due to the logarithm identity

$$\log_{\varepsilon+2\pi}(\mathrm{e}^{\mathrm{i}\phi}) = \log_\varepsilon(\mathrm{e}^{\mathrm{i}\phi}) + 2\pi\mathrm{i} \tag{4.79}$$

we have

$$V_{\varepsilon+2\pi}(t,k) = V_\varepsilon(t,k)\mathrm{e}^{2\pi\mathrm{i}t/T} \tag{4.80}$$

from which we obtain

$$W_{\varepsilon+2\pi}[U] = W_\varepsilon[U] \tag{4.81}$$

as expected.

Physically, $W_\varepsilon[U]$ gives the number of chiral edge states (counted algebraically with chirality) in the quasienergy gap ε (see figure 4.4). An argument for this bulk-boundary correspondence was given by Rudner et al. [RLBL13] in two space dimensions, and should be straightforwardly generalized to all even space dimensions. In class A the vacuum provides a unambiguous reference where $W = 0$ in all gaps. The W invariants can therefore be directly interpreted as the number of edge states at the interface with vacuum. As mentioned in the introduction, there are now several experimental confirmations of this theoretical description [HPWP15; GGSY16; MSVA16; MZNS16].

3.2.2 Towards topological invariants in attenuated and amplified evolutions

As we mentioned in section 2.2.4 (page 48), the winding numbers are still defined when the operators are not unitary but still invertible. I suggest that this property can be used to define topological invariants in situations where attenuation (and/or amplification) is present, which is indeed the case in experimental situations. To produce a periodized evolution operator, we still require that $U(t,k)$ is (a) invertible, so that a winding may be defined, and (b) diagonalizable, at least at time T, so that spectral decomposition can be used to define the effective Hamiltonian. Several different routes may be taken here. The spectrum of the Floquet operator $U(T,k)$ now lies on the punctured complex plane $\mathbb{C}\backslash 0$, which can be retracted to $U(1)$ (through $\rho \mathrm{e}^{i\theta} \to \mathrm{e}^{i\theta}$). If the retracted spectrum has a gap, an effective Hamiltonian can be defined by spectral decomposition, and an invertible periodized evolution operator V_ε can therefore be defined, as well as its degree. In fact, the periodized evolution operator can be decomposed in polar form as

$$V_\varepsilon(T,k) = V_{\varepsilon,U}(t,k) V_{\varepsilon,H}(t,k) \tag{4.82}$$

where $V_{\varepsilon,U}$ is unitary and $V_{\varepsilon,H}$ is hermitian positive-definite. The winding of V_ε is then simply the winding of the unitary map $V_{\varepsilon,U}$. Another route consists in using the polar decomposition of the evolution operator $U(t,k)$ to deform it into a unitary map, and use the usual framework from there. Both methods are similar and should agree, but this is not completely obvious as polar decomposition do not necessarily commute with the periodization.

At least in some cases, such an extension should be relevant in systems with an attenuation. A clue in this direction is that in the simplest case of a constant attenuation proportional to the identity (which commutes with everything), the invariant characterizing the evolution without attenuation is recovered.

Yet, unusual behaviors were predicted in the presence of singular matrices when the Hamiltonian is not Hermitian [Lee16; RLL16]: here, the topology is fundamentally dependent on the existence of dissipative non-Hermitian components, and even if (extensions of) the usual band gap-based invariants are still relevant, they will indeed not characterize this different type of topology. Besides, parametric instabilities were studied in mechanical [SOPC16] and optomechanical [PBSM15] versions of (Floquet) topological phases with amplification, as well as in generic bosonic systems [EBPB15]. Whether an extension of the winding number invariants (4.76) is still relevant in presence of such behaviors is an open question.

3.2.3 Relation with band invariants

The topology of time-independent systems in class A is characterized by the Chern invariants of their bands (see section 2.1, 78). For example, the valence band of the Haldane model may have a first Chern invariant $C_1 = 0, \pm 1$. Similarly, quasi-energy bands can also have non-vanishing Chern invariants, which have a clear physical meaning: in a finite system, the Chern invariant of a band gives the *change* in the number of topological edge states that appear in the bulk gaps above and below the band. As a consequence, the Chern invariants must be related to (and expressed in terms of) the winding gap invariants. In the following, we extend this correspondence,

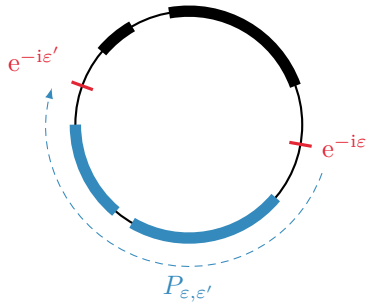

Figure 4.5: Projectors on quasi-energy bands. For two quasi-energies (or cuts) ε and ε' with $-2\pi < \varepsilon, \varepsilon' < 0$, $P_{\varepsilon,\varepsilon'}(k)$ is the spectral projector on eigenstates with eigenvalues $e^{-i\eta}$ in the arc joining $e^{-i\varepsilon}$ and $e^{-i\varepsilon'}$ clockwise on the circle $U(1)$. Cuts are represented in red, the range of the spectral projector as a dashed blue line, and the bands that are captured in the range of this spectral projector for an example quasi-energy spectrum are colored in blue. The remaining bands (not in the range of the projector) are represented in black.

discovered by Rudner et al. [RLBL13] in $d = 2$, to the general case of an even dimensional space.

Let ε and ε' be two quasi-energies and $P_{\varepsilon,\varepsilon'}(k)$ the spectral projector on states with quasi-energy between ε and ε'. More precisely, for $-2\pi < \varepsilon, \varepsilon' < 0$, $P_{\varepsilon,\varepsilon'}(k)$ is the spectral projector on eigenstates with eigenvalues $e^{-i\eta}$ in the arc joining $e^{-i\varepsilon}$ and $e^{-i\varepsilon'}$ clockwise on the circle $U(1)$, see figure 4.5. The difference between the gap invariants W is related to a Chern invariant (see equation (2.56) page 50 and section 2.1 page 78) as

$$W_{\varepsilon'}[U] - W_{\varepsilon}[U] = -C_n(P_{\varepsilon,\varepsilon'}). \tag{4.83}$$

which characterizes the vector bundle $\mathcal{E}_{\varepsilon,\varepsilon'}$ over BZ with fiber $P_{\varepsilon,\varepsilon'}(k)\mathbb{C}$ over $k \in \mathrm{BZ}$, corresponding to the quasi-energy band between ε and ε'.

This equality can be proven as follows: as the degree is additive, namely $\deg(u \cdot v) = \deg(u) + \deg(v)$ (provided all quantities are well-defined), we have

$$W_{\varepsilon'}[U] - W_{\varepsilon}[U] = \deg(V_{\varepsilon'}) - \deg(V_{\varepsilon}) = \deg([V_{\varepsilon}]^{-1}V_{\varepsilon'}). \tag{4.84}$$

Moreover, the difference between effective Hamiltonians at different gaps is equal to the spectral projector on the quasi-energy band between these gaps,

$$H^{\mathrm{eff}}_{\varepsilon'} - H^{\mathrm{eff}}_{\varepsilon} = (2\pi/T)P_{\varepsilon,\varepsilon'} \tag{4.85}$$

so

$$[V_{\varepsilon}(t,k)]^{-1}V_{\varepsilon'}(t,k) = e^{2\pi i t/T\, P_{\varepsilon,\varepsilon'}(k)} \tag{4.86}$$

and the winding of this last unitary map can be shown to be (up to a minus sign) the Chern invariant of projector family $P_{\varepsilon,\varepsilon'}$ (this is detailed in the appendix of the reference [Fru16]).

3.2.4 Interlude: the time-independent half-BHZ model

Let us introduce an equilibrium model, the restriction to spins up of the Bernevig-Hugues-Zhang model (see section 2.3.4, page 97) which will be referred to as the **half-BHZ model**. Like the Haldane model (see section 2.1, page 78), realizes an anomalous quantum Hall equilibrium phase, but on a square lattice with two orbitals per site, denoted s and p for simplicity. The tight-binding Hamiltonian with nearest and next-to-nearest neighbors hoppings can therefore be written as a two-by-two matrix on the (s, p) basis as

$$\begin{aligned} H_{\text{h-BHZ}} = \sum_{x,y} \Bigg[& \left[(M - J - 4B)\,\sigma_z - \mu\sigma_0 \right] |x,y\rangle \langle x,y| \\ & + \left[\frac{A}{2\mathrm{i}}\sigma_x + B\sigma_z \right] |x,y\rangle \langle x+1,y| + \left[\frac{A}{2\mathrm{i}}\sigma_y + B\sigma_z \right] |x,y\rangle \langle x,y+1| \\ & + \frac{J}{4}\sigma_z \left(|x,y\rangle \langle x+1,y+1| + |x,y\rangle \langle x+1,y-1| \right) \Bigg] + \text{h.c.} \end{aligned} \tag{4.87}$$

where $\sigma_{x,y,z}$ are the Pauli matrices and σ_0 the identity matrix and (x, y) labels sites of the square lattice.

This corresponds to the Bloch Hamiltonian

$$H(k) = h_i(k)\sigma_i \tag{4.88}$$

with coefficients

$$\begin{aligned} h_x(k) &= A \sin k_x \\ h_y(k) &= A \sin k_y \\ h_z(k) &= (M - J - 4B) + 2B(\cos k_x + \cos k_y) + J \cos k_x \cos k_y. \end{aligned} \tag{4.89}$$

We show an example of energy spectrum of this Hamiltonian on figure 4.6.

The first Chern invariant can be computed (see section 2.1, page 78) as

$$C_1 = \frac{1}{2}\left[\text{sign}(M) + \text{sign}(M - 8B) - 2 \cdot \text{sign}(M - 2J - 4B) \right]. \tag{4.90}$$

corresponding to phase diagram partially represented in figure 4.7.

3.2.5 Example: The harmonically driven half-BHZ model

Let us now consider a periodically driven system, which illustrates the effect of a periodic drive on the topology. Following [RLBL13], we submit the half-BHZ model (4.87) to a periodic on-site perturbation

$$\Delta H(t) = \sum_{x,y} F \left[\sin(\omega t)\sigma_x + \cos(\omega t)\sigma_y \right] |x,y\rangle \langle x,y| . \tag{4.91}$$

corresponding to a Bloch Hamiltonian

$$\Delta H(t,k) = F \left[\sin(\omega t)\sigma_x + \cos(\omega t)\sigma_y \right]. \tag{4.92}$$

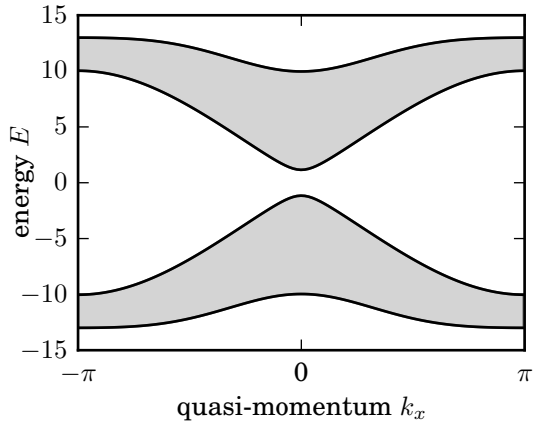

Figure 4.6: Energy spectrum of the half-BHZ Hamiltonian. The energy spectrum of a strip of material (infinite in the x direction, but finite in the y direction) of the half-BHZ Hamiltonian (4.87) with parameters $A = 4$, $B = 1.5$, $J = 1.5$ and $M = -1$ is represented. For this set of parameters, the bandwidth is BW $\simeq 26$.

Depending on the strength F and the angular frequency ω, this perturbation can drive the system either towards a topologically nontrivial out-of-equilibrium state or in a topologically trivial out-of-equilibrium state. This is exemplified in figure 4.10, where the quasi-energy spectrum of a finite strip is numerically computed in three situations. As expected, the bulk gap invariant $W_\epsilon[U]$ (also numerically computed, but this time from the bulk Hamiltonian, see next paragraph) gives the number of edge states counted algebraically with chirality at an interface with the vacuum. For example, with the parameters of figure 4.6 for the unperturbed Hamiltonian and $\omega = 20$ and $F = 8$, we find $W_0[U] = 1$ and $W_\pi[U] = 0$, and indeed one chiral edge state (per interface, i.e. one in red and one in blue) is found in figure 4.10(b) in the gap $\varepsilon = 0$. For $\omega = 6.5$ and $F = 5.0$, we find $W_0[U] = 0$ and $W_\pi[U] = -2$, which corresponds to what is observed in figure 4.10(c): there are two edge states (again, per interface) in the gap $\varepsilon = \pi$; moreover, for a given interface (e.g. for red states, located at the top interface) edge states in 4.10(b) and 4.10(c) have opposite chirality.

Various out-of-equilibrium topological phases can be obtained depending on the amplitude F and the angular frequency ω of the time-periodic perturbation, and a phase diagram may be numerically obtained by direct computation of the invariant for varying driving parameters, see figure 4.8, or for fixed driving parameters with different parameters of the unperturbed Hamiltonian, see figure 4.9. Two important points can be learned from those phase diagrams.

– When the driving frequency ω is too small with respect to the undriven system bandwidth E_{bw}, i.e. when $\hbar\omega \ll E_{\text{bw}}$, then the quasi-energy gaps Δ_ε typically vanish. This is the case for low driving frequency ($\omega \lesssim 5$) in figure 4.9 and for high values of the hopping amplitude $B \gtrsim 5$ in figure 4.9. Hence, a driving frequency *at least* of the order of the bandwidth of the undriven systems seems to be necessary to open a sizable gap. A possible explanation of this behavior is that at low driving

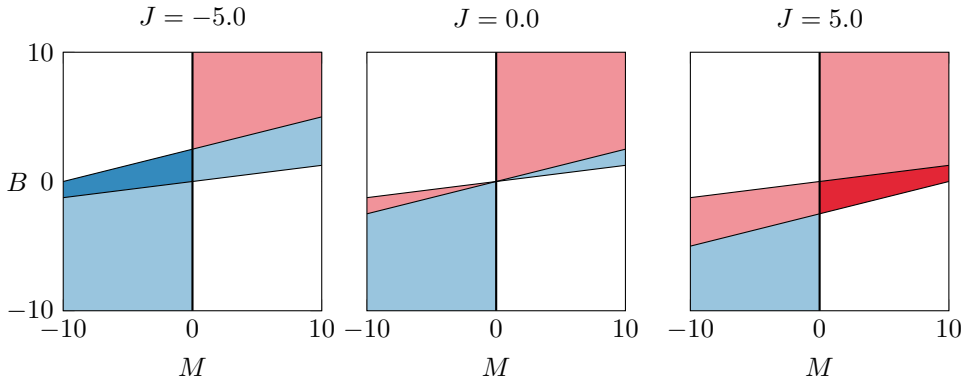

Figure 4.7: Phase diagram of the half-BHZ model. We represent a part of the phase diagram of the half-BHZ model for different values of the second-nearest-neighbors coupling J. Colors represent first Chern invariant, where white represents $C_1 = 0$, light red (■) represents $C_1 = +1$, red (■) represents $C_1 = +2$, light blue (■) represents $C_1 = -1$, blue (■) represents $C_1 = -2$.

frequency, a lot of closely spaced topological phase transitions are found in the (F, ω) plane, which seem to prevent any significant (and physically relevant) gap opening. The analysis of even simpler models (see paragraph 3.2.6, page 137) gives some evidences that topological transitions tend to be equally spaced in *driving period* (e.g. on the (F, T) plane), which correspond to transition lines becoming closer and closer as the driving frequency decreases.

– Except at low driving frequency (see previous point), topological phases appear to be extended phases (not critical phases reduced to a line, or a very narrow region), both in the driving parameter space and in the parameter space of the unperturbed Hamiltonian. As a consequence, we can expect such topological phases to be robust against small perturbations. A small (spatial or temporal) variation of the material parameters and/or the driving parameters should not spoil the existence of the phase (and of the corresponding edge states on a finite sample), as long as the variation is confined to only one region of the phase diagram. The effect of a lack of uniformity of the drive (amplitude, frequency, phase) was rarely studied. In class A, numerical simulations seem to show that a disorder in the driving phase does not affect the topological properties [FKA15].

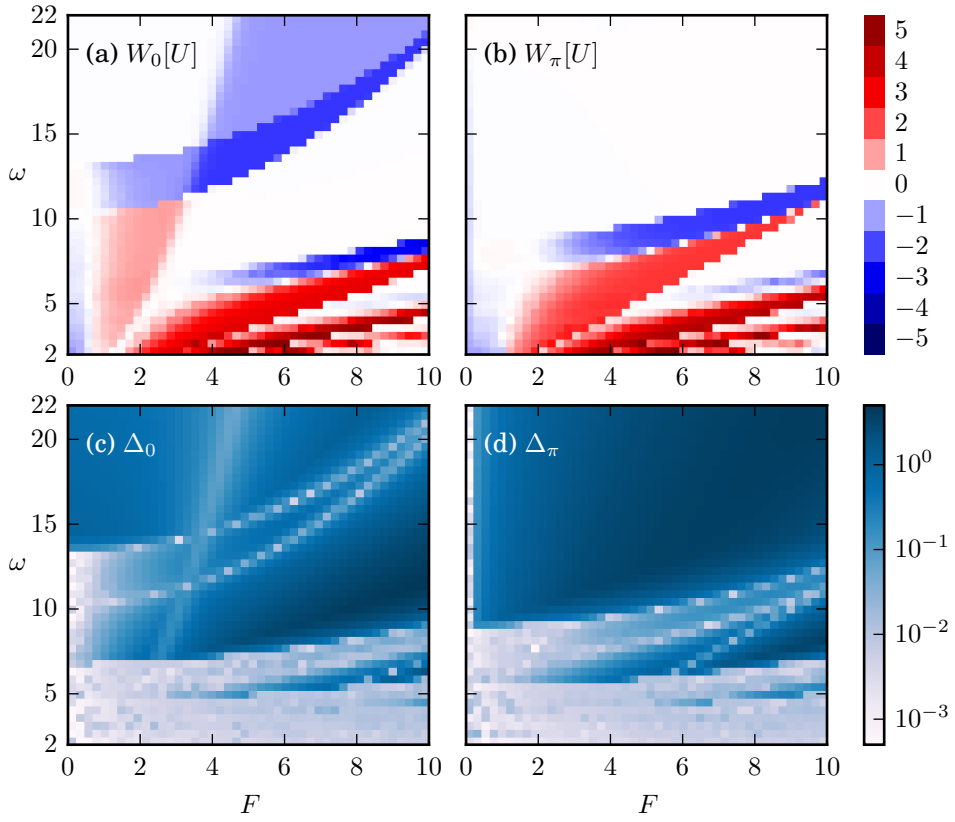

Figure 4.8: Topological phase diagram of the harmonically driven half-BHZ model. Numerically computed values of (a,b) the index $W_\varepsilon[U]$ and (c,d) the amplitude Δ_ε of the corresponding quasi-energy gaps are plotted against the amplitude F and the angular frequency ω of the drive, for (a,c) $\varepsilon = 0$ and (b,d) $\varepsilon = \pi$. The color bar in (a,b) only displays quantized values for better clarity, but the numerical estimations of $W_\varepsilon[U]$ are not rounded. In (c,d), quasi-energies are normalized in a range of $2\pi \sim 10^1$ and the gap Δ_ε is in logarithmic scale. Blue regions corresponds to large gaps, whereas white regions corresponds to small or vanishing gaps. Due to the finite numerical precision, the estimation of the gap does not strictly vanish at topological transitions. We observe that (i) the amplitude of a gap ε always vanishes at a topological transition which changes $W_\varepsilon[U]$, (ii) at low angular frequency, in the bottom region, both gaps are really small, perhaps due to the numerous topological transitions. The bottom part of the phase diagrams (a,b) are not guaranteed to be meaningful, because (i) the quasi-energy gaps are really small and (ii) the numerical estimations of the invariants are not well-quantized (a better estimation would require a finer discretization both in time and momentum). In contrast, the top part should be meaningful, at least far from transition zones. This data corresponds to a unperturbed half-BHZ Hamiltonian (4.87) with parameters $A = 4$, $B = 1.5$, $J = 1.5$ and $M = -1$ submitted to the perturbation (4.92). The evolution operator was computed in discretized time and momentum, with steps $\delta t = 0.005$ and $\delta k = 0.05$, see paragraph 2.1.1 page 111.

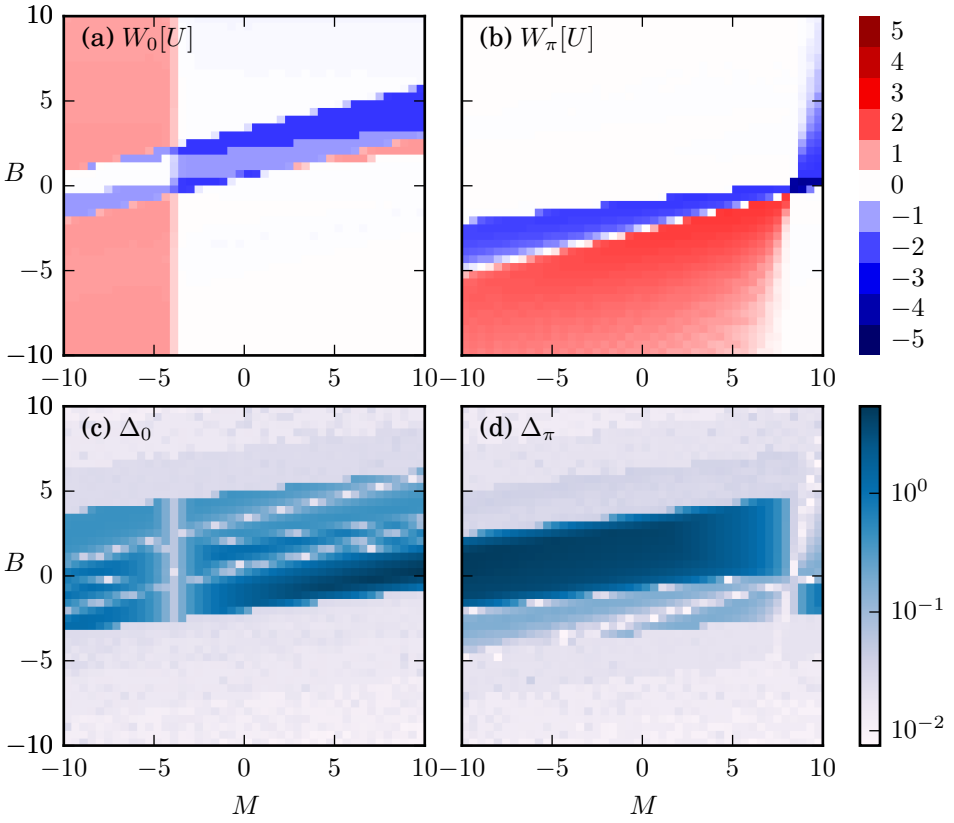

Figure 4.9: Topological phase diagram at fixed driving of the HDHBHZ model. The numerically computed values of (a,b) the index $W_\varepsilon[U]$ and (c,d) the amplitude of the corresponding quasi-energy gaps are plotted against the undriven Hamiltonian parameters (M, B) for fixed driving parameters $\omega = 20$ and $F = 8$, for the two gaps $\varepsilon = 0$ and $\varepsilon = \pi$. Again, the only meaningful parts of the diagrams (a,b) are which where the gap is not too small. Notice that the gap vanishes for large hopping parameter B: this is similar to what happens in figure 4.8 for small driving angular frequency ω: gaps typically close when the bandwidth of the undriven system (essentially proportional to B) is small compared to the driving frequency $\hbar\omega$. See figure 4.8 for details the model, the computation and the visual representation.

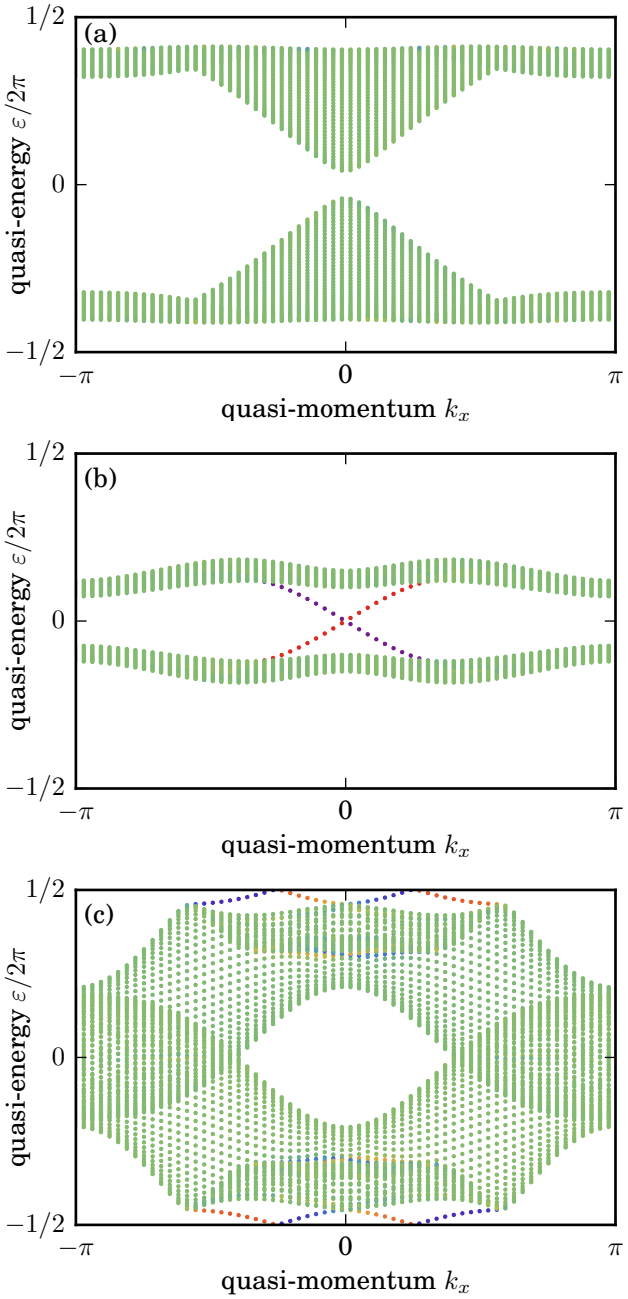

Figure 4.10: Quasi-energy spectra of the harmonically-driven half-BHZ model. The quasi-energy spectra of a strip (infinite in the x dimension, but finite in the y dimension) of a harmonically-driven half-BHZ model are plotted for various driving parameters: (a) $\omega = 20$ and $F = 2$, (b) $\omega = 20$ and $F = 8$ and (c) $\omega = 6.5$ and $F = 5.0$. The parameters of the unperturbed system are the same as in figure 4.6. Colors are computed from the mean position of the states corresponding to each point: a green color (■) indicates a state with average position in the center of the strip; a orange/red color (■) indicates a state located at the top edge of the strip, whereas a blue/violet color (■) indicates a state located at the bottom of the strip.

3.2.6 Example: The periodically kicked half-BHZ model

In the previous paragraph, we considered an example of harmonically driven system. In an attempt to understand the common features in the topological phase diagram of Floquet systems, we introduce another system, the periodically kicked half-BHZ model, which is simple enough to allow an analytical understanding of Floquet phase transitions. Perturbative analysis of Floquet topological transitions were studied by Rudner, Lindner, Berg and Levin [RLBL13] and by Kundu, Fertig and Seradjeh [KFS14], but with other methods and other objectives. Here, (i) we observe that Floquet topological transitions between gapped phases happen through a semi-metallic phase where a Dirac cone closes, an observation in agreement with [KFS14] and (ii) we try to explain (or at least get an intuition of) the general low-driving frequency behavior of Floquet topological systems.

Starting again from the unperturbed half-BHZ model (4.87), we submit it to the time-periodic perturbation

$$\Delta H(t,k) = \gamma\sigma_z \sum_{n\in\mathbb{Z}} \delta(t-nT) \tag{4.93}$$

which introduces a dephasing γ between orbitals s and p at every period. Indeed, for a small $\epsilon > 0$ (not the quasi-energy!),

$$U(T-\epsilon) = \mathrm{e}^{-\mathrm{i}TH_0} \qquad \text{and} \qquad U(T+\epsilon) = \mathrm{e}^{-\mathrm{i}\gamma\sigma_z}\,\mathrm{e}^{-\mathrm{i}TH_0}. \tag{4.94}$$

The advantage of this model is that it allows an analytic perturbation expansion near the "Dirac points" of the system, where $H_0 \propto \sigma_z$ commute with $\gamma\sigma_z$.

The first Chern invariant of the conduction band of the undriven system is computed as

$$C_1 = \frac{1}{2}\left(m^{(0,0)} + m^{(\pi,\pi)} - m^{(0,\pi)} - m^{(\pi,0)}\right) \tag{4.95}$$

where K is an edge of the first Brillouin zone, and where we defined

$$m^K = h_z(K). \tag{4.96}$$

Topological phase transitions (of driven or undriven systems) only occur when a gap closes, and they typically do occur when it is the case, due to band inversions. In this extremely simplified model, gap closings occur at the potential crossing (Dirac) points of the unperturbed model which form the set $D = \{(0,0),(\pi,\pi),(\pi,0),(0,\pi)\}$. We expect that the transition lines should be understood from what happens at these points alone.

Let us determine the effective Hamiltonian (in the sense of Floquet theory) at Dirac points $K \in D$. Near such points, the low-energy Hamiltonian is a Dirac Hamiltonian

$$H_0^K(q) = H_0(K+q) = m^K\sigma_z + \mathcal{O}(q) \tag{4.97}$$

so up to terms linear or of higher order in q,

$$\mathrm{e}^{-\mathrm{i}H_0^K(0)T}\mathrm{e}^{-\mathrm{i}\gamma\sigma_z} = \mathrm{e}^{-\mathrm{i}(m^KT+\gamma)\sigma_z}. \tag{4.98}$$

Hence, the (Floquet) effective Hamiltonian near $K \in D$ is a Dirac Hamiltonian with an *effective mass*

$$m_{\text{eff}}^K = m^K T + \gamma \mod 2\pi \tag{4.99}$$

Indeed, $\mathrm{e}^{-\mathrm{i}(m+2\pi)\sigma_z} = \mathrm{e}^{-\mathrm{i}m\sigma_z}$ so this effective mass is only defined modulo 2π. Hence, its sign is not well-defined and we do not expect to be able to directly compute any topological *invariant* directly from the effective masses. In contrast, we expect (topological) transition lines of the driven model where the quasienergy gap $\varepsilon = 0$ closes to be

$$\exists K \in D \quad m_{\text{eff}}^K = 0 \mod 2\pi \tag{4.100}$$

Moreover, we expect that crossing the transition line corresponding to $K = (0,0)$ should have the same effect that with the line corresponding to $K = (\pi,\pi)$ (reducing the topological invariant by one), whereas crossing the two degenerate lines $K = (0,\pi)$ and $K = (\pi,0)$ should *increase* the topological invariant by two (one for each point), essentially due to the relative signs in equation (4.95).

As the quantity exchanged between the driving field and the system is energy, it is more relevant to use the driving angular frequency $\omega = 2\pi/T$ (or in fact $\hbar\omega$) than the driving period T. Hence, we define the sets of transition lines at point K and quasi-energy $\varepsilon = 0$ in the (γ,ω) plane by

$$\mathcal{C}_K^0 = \left\{ (\gamma,\omega) \middle| \frac{2\pi m^K}{\omega} + \gamma \in 2\pi\mathbb{Z} \right\}. \tag{4.101}$$

Indeed, the same story can be played for the gap $\varepsilon = \pi$, and similarly we define

$$\mathcal{C}_K^\pi = \left\{ (\gamma,\omega) \middle| \frac{2\pi m^K}{\omega} + \gamma \in 2\pi\mathbb{Z} + \pi \right\}. \tag{4.102}$$

The corresponding curves are plotted in color over the numerically determined topological phase diagram of the system in figure 4.12. There is a very good agreement between the analytically predicted and numerically observed transition lines, and the prediction concerning the different transitions lines are also in agreement with the numerics.

It is possible to *estimate* the quasi-energy gap Δ_0 from the effective masses as

$$\Delta_0^{\text{est.}} = \min_{K\in D} \min_{n\in\mathbb{Z}} \left| m_{\text{eff}}^K - 2\pi n \right|. \tag{4.103}$$

This estimation assumes that the gap is minimal at one of the points $K \in D$. Similarly, we estimate the gap Δ_π by

$$\Delta_\pi^{\text{est.}} = \min_{K\in D} \min_{n\in\mathbb{Z}} \left| m_{\text{eff}}^K - (2\pi n + \pi) \right|. \tag{4.104}$$

Even though the estimation does not reproduce all features (compare figures 4.12(c,d) and 4.11(c,d)), we observe that in many cases, the behavior near Dirac points controls both the gap and the topological properties of the Floquet system. There is in particular a noticeable discrepancy between the numerically computed gap and its estimation from the effective masses near $\gamma = 0$ and $\gamma = \pi$, which both correspond

to scalar perturbations (multiplication by ±Id). The case of $\gamma = 0$ is not surprising, as it corresponds to a vanishing perturbation. The second situation is less obvious. Far from those particular values, the qualitative agreement is remarkable (but not surprising, as the model is very simple).

The most important take-away of this analysis is the following: from equation (4.99), it is clear that transition lines at fixed γ are regularly spaced on the T parameter line. Hence, transitions line become closer and closer when $\omega = 2\pi/T$ decreases: this is clearly visible in figure 4.11. This behavior seems to be a general property of (topological) Floquet systems. Two striking consequences of this observations are (i) that the gap is forced to be small by the close vicinity of phase transitions in the parameter space and (ii) that a small perturbation in the driving angular frequency or in the driving amplitude (as transition lines are not horizontal) will induce a topological transition, thus spoiling any kind of topological protection.

3.2.7 Constraints on W's due to symmetries

The invariant W was defined in any even space dimension for topological phases in class A, where no symmetry is present. In the following, we study the constraints due to symmetries (time-reversal, charge-conjugation and chiral symmetry) on this invariant: depending on the space dimension, such constraints can be trivially satisfied, or can force the W invariants to vanish. In the first situation, W characterizes the topological phases in the corresponding symmetry class, essentially as if the additional symmetries were not present: it is possible to *forget* them in order to compute the relevant invariant. For example, this is the case of class D (with bosonic charge conjugation) in $d = 2$. In the second situation where the symmetries force the W invariants to vanish, either all phases are trivial in the symmetry class or a finer invariant protected by the additional symmetries exists. For example, still in space dimension $d = 2$, both bosonic and fermionic time-reversals (classes AI and AII) cause the vanishing of W invariants, but only the fermionic version (class AII) allows a finer Kane-Mele-like invariant to be defined. The aim of the current paragraph is to find out when W invariants vanish, and when they are still defined. Without surprise, we recover (a part of) the standard pattern of the periodic table 3.3, page 108.

We first need to recall several properties of the odd Chern character (defined in section 2.2.4, page 48). Remember that the odd Chern character $\widetilde{\mathrm{ch}}_n(V)$ associated to a unitary map $V : M \to U(N)$, where M is a $(2n+1)$-dimensional manifold, is a $(2n+1)$-th differential form. As the odd Chern character is real or imaginary, depending on the parity of n,

$$\widetilde{\mathrm{ch}}_n(\overline{V}) = (-1)^{n+1}\widetilde{\mathrm{ch}}_n(V). \tag{4.105}$$

Second, if U_0 is a *constant* unitary matrix of the right size, then

$$\widetilde{\mathrm{ch}}_n(U_0 V U_0^{-1}) = \widetilde{\mathrm{ch}}_n(V). \tag{4.106}$$

In fact we even have

$$\widetilde{\mathrm{ch}}_n(U_0 V) = \widetilde{\mathrm{ch}}_n(V) = \widetilde{\mathrm{ch}}_n(V U_0^{-1}). \tag{4.107}$$

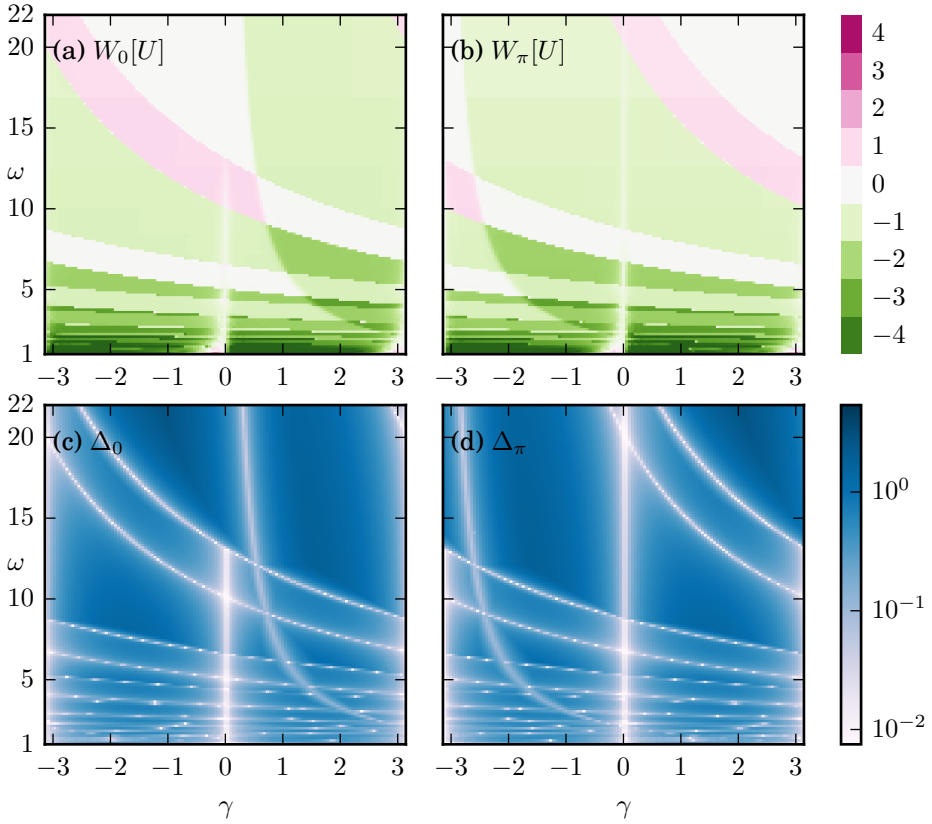

Figure 4.11: Topological phase diagram of the kicked HBHZ model. Numerically computed values (a,b) of the index $W_\varepsilon[U]$ and (c,d) of the amplitude of the corresponding quasi-energy gaps against the driving parameters (ω, γ), for the two gaps $\varepsilon = 0$ and $\varepsilon = \pi$. As expected, this diagram is 2π-periodic in γ. Near $\gamma = 0$ and $\gamma = \pm\pi$ (only for $\hbar\omega$ smaller than half an unperturbed system bandwidth for the gap $\varepsilon = 0$), the gap closes, and the numerical computation of the topological invariants fail to converge. Similarly, the values of the topological invariants are not to be fully trusted at low frequency, due to the numerous and close transitions, and because the color index was capped for clarity (numerical values go down to -8). The evolution operator was computed in discretized time and momentum, with steps $\delta t = 0.025$ and $\delta k = 0.025$, see paragraph 2.1.1 page 111. The topological invariants $W_\varepsilon[U]$ are numerically computed by direct integration from the numerically computed periodized evolution operator.

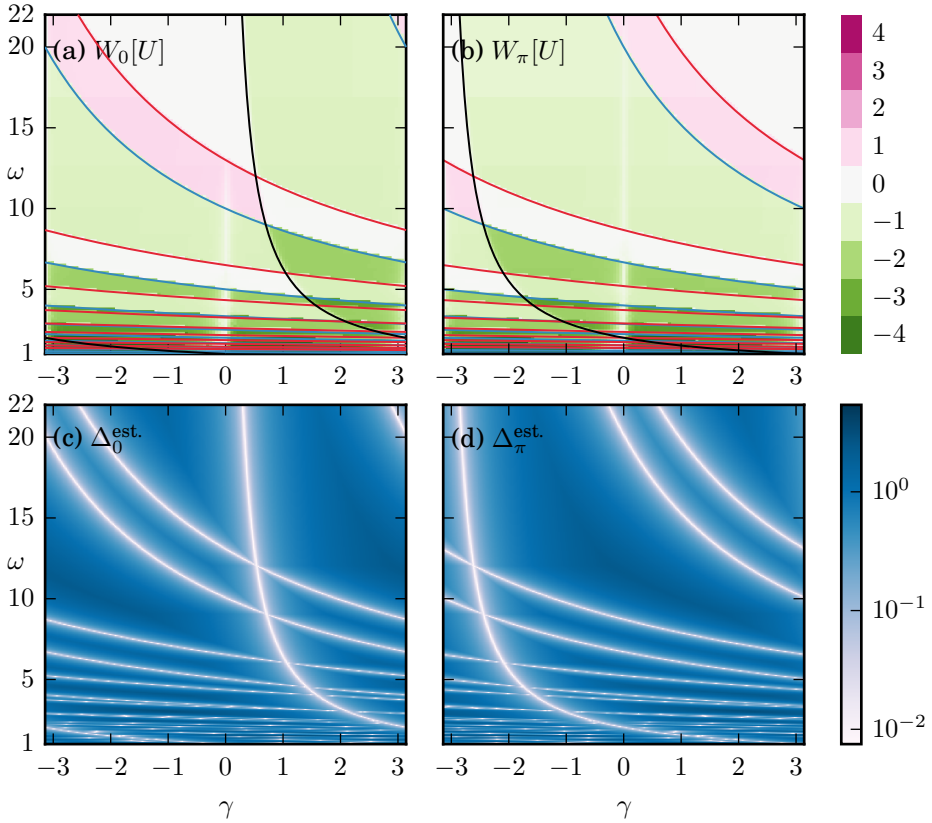

Figure 4.12: Analytical estimation of the transition lines and gaps of the kicked HBHZ model. In (a) and (b), the analytically computed transition lines are plotted in colors (black (—) for $K = (0, 0)$, red (—) for $K = (\pi, \pi)$ and blue (—) for the "double" line corresponding to $K = (0, \pi)$ and $K = (\pi, 0)$), on top of the numerical values of figure 4.11(a,b). In (c,d), the amplitudes of the gaps Δ_0 and Δ_π estimated from the effective masses at potential transition points are plotted, and should be compared with figure 4.11(c,d): there is a qualitative difference only near $\gamma = 0$ and $\gamma = \pm\pi$. Interestingly, for the gap $\varepsilon = 0$, the discrepancy near $\gamma = 0$ only occurs for $\hbar\omega$ smaller than half an unperturbed system bandwidth (approx. 13).

Indeed, such properties translate into the winding numbers, so

$$W_n(\overline{V}, M) = (-1)^{n+1} W_n(V, M) \tag{4.108}$$

and

$$W_n(U_0 V U_0^{-1}, M) = W_n(V, M). \tag{4.109}$$

Indeed, if ϕ is a map which depends only on time (or more generally on less than $2n+1$ variables) and $n > 0$, then

$$W_n(\phi V, M) = W_n(V, M). \tag{4.110}$$

Also, let us recall that if D is a diffeomorphism on the manifold M, then

$$W_n(V \circ D, M) = \begin{cases} +W_n(V, M) & \text{if } D \text{ preserves orientation} \\ -W_n(V, M) & \text{if } D \text{ reverses orientation.} \end{cases} \tag{4.111}$$

To use the preceding properties to deduce constraints on the W invariant, it is convenient to express the constraints on the periodized evolution operators in terms of unitary operators and complex conjugation. Let U_Θ a unitary matrix so that $\Theta = U_\Theta \mathcal{K}$ (so $\Theta^{-1} = \mathcal{K} U_\Theta^{-1} = \overline{U_\Theta}^{-1} \mathcal{K}$). Similarly, let U_C a unitary matrix so that $C = U_C \mathcal{K}$ (so $C^{-1} = \mathcal{K} U_C^{-1} = \overline{U_C}^{-1} \mathcal{K}$). In terms of such operators, symmetry constraints (4.62) read

$$U_\Theta \overline{V_\varepsilon} U_\Theta^{-1} = V_\varepsilon \circ \vartheta \tag{4.112a}$$

$$U_C \overline{V_\varepsilon} U_C^{-1} = \phi \times V_{-\varepsilon} \circ \kappa \tag{4.112b}$$

$$\Gamma V_\varepsilon \Gamma^{-1} = \phi^{-1} \times V_{-\varepsilon} \circ \tau \tag{4.112c}$$

where $\phi(t,k) = \mathrm{e}^{-2\pi \mathrm{i} t/T}$ and where ϑ, κ and τ are diffeomorphisms on $S^1 \times \mathrm{BZ}$ defined by

$$\vartheta(t,k) = (-t,-k) \tag{4.113a}$$

$$\kappa(t,k) = (t,-k) \tag{4.113b}$$

$$\tau(t,k) = (-t,k) \tag{4.113c}$$

As BZ is even-dimensional when W's are defined, ϑ reverses orientation, while κ preserves orientation; τ is indeed orientation-reversing.

Due to this set of properties, we get, when the corresponding symmetries are present,

$$(-1)^{n+1} W_n(V_\varepsilon) \equiv W_n(\Theta V_\varepsilon \Theta^{-1}) = -W_n(V_\varepsilon) \tag{4.114a}$$

$$(-1)^{n+1} W_n(V_\varepsilon) \equiv W_n(C V_\varepsilon C^{-1}) = W_n(V_{-\varepsilon}) \tag{4.114b}$$

$$W_n(V_\varepsilon) \equiv W_n(\Gamma V_\varepsilon \Gamma^{-1}) = -W_n(V_{-\varepsilon}) \tag{4.114c}$$

As a consequence, as $d = 2n$,

- in dimensions $d = 2$ and $d = 6$, time-reversal invariance implies the vanishing of W's in all gaps;
- in dimensions $d = 4$ and $d = 8$ with time-reversal invariance, W's do not vanish and provide the $\mathbb{Z}$ (or $2\mathbb{Z}$) invariants for classes AI and AII;
- in dimensions $d = 4$ and $d = 8$, charge-conjugation invariance implies the vanishing of W's *in real gaps*;
- in dimensions $d = 2$ and $d = 6$ with charge-conjugation invariance, W's do not vanish and provide the $\mathbb{Z}$ (or $2\mathbb{Z}$) invariants for classes C and D *in real gaps*;
- in all dimensions with charge-conjugation invariance, but in other gaps (neither 0 nor π), the W's invariants of class A still apply; however, the invariants in gap ε and $-\varepsilon$ are related by charge-conjugation, and are opposite or equal depending on the dimension;
- in all (even) dimensions, chiral symmetry implies the vanishing of W's *in real gaps*; in others gaps, the W's invariants of class A still apply and the invariants in gap ε and $-\varepsilon$ are opposite due to chiral symmetry.

The same statements hold with the usual $d \to d + 8$ periodicity. For example, the case of $d = 8$ should also hold for $d = 0$.

Hence, we recover half of the $\mathbb{Z}$ (or $2\mathbb{Z}$) invariants present in the periodic table 3.3 (page 108) and predict the vanishing of the W invariants in a certain number of its cells. As we shall see, the other half of $\mathbb{Z}$ or $2\mathbb{Z}$ invariants are provided by the chiral invariant defined in the next section 3.3.

3.3 Class AIII: with chiral symmetry

3.3.1 Overview

When the space dimension d is odd, $d = 2n + 1$, there is a $\mathbb{Z}$-valued bulk gap invariant

$$G_\varepsilon[U] \in \mathbb{Z} \tag{4.115}$$

defined *only* for the real gaps $\varepsilon = 0$ or π associated to a chiral symmetric evolutions U such that

$$\Gamma U(t, k)\Gamma^{-1} = U(-t, k). \tag{4.116}$$

This invariant is related to the usual chiral band invariant $g[P] \in \mathbb{Z}$ associated to a projector (respecting chiral symmetry!) by

$$G_\varepsilon[U] - G_{\varepsilon'}[U] = g[P_{\varepsilon'\varepsilon}] \tag{4.117}$$

where $P_{\varepsilon,\varepsilon'}(k)$ is the spectral projector on states with quasi-energy between ε and ε'. For the definition of the chiral band invariant, see paragraph 2.2.2 of chapter 3, page 89.

As in class A, we expect that topologically protected edge states should appear at the boundary of a finite system in the bulk gap(s) endowed with nontrivial invariants, and that the number of edge states counted with chirality should match the corresponding gap invariant. Such expectations are backed (i) by analogies with the static case, and (ii) by numerical simulations in one and three dimensions. First steps

towards a bulk-boundary correspondence in the one-dimensional case were provided by Asbóth and collaborators in [AO13; ATD14].

Note that subtleties may arise due to the fact that in contrast with the situation of class A, here the vacuum does not provide an *unambiguous* reference for a trivial system, e.g. because of the choice of the chiral operator (see the discussion in paragraph 2.2.2 of chapter 3, page 89 as well as the references therein). We are faced with the fact that the invariants G are **relative invariants**, which have no physical significance alone (only differences of G's, e.g. at an interface or at a phase transition, are physically meaningful). Strictly speaking, a bulk-boundary correspondence should be formulated *only* in terms of differences of G's at an interface, which requires a consistent choice of chiral operator in both systems, but a full analysis of this problem is outside of the scope of this thesis.

3.3.2 The chiral invariant

The general constraint on the periodized evolution operators of equation (4.62) due to chiral symmetry (see paragraph 2.3, page 120), namely

$$\Gamma V_\varepsilon(t,k)\Gamma^{-1} = V_{-\varepsilon}(-t,k)\mathrm{e}^{2\pi \mathrm{i}t/T} \tag{4.118}$$

is not very convenient to define a topological invariant specific to chiral systems, because (i) it relates different periodized operators with cuts in opposite quasi-energy gaps (in a chiral symmetric system, the quasi-energy spectrum is symmetric with respect to the real axis) and (ii) it relates operators at opposite times. Let us first address the issue of opposite times: the periodicity of V implies that $V_\varepsilon(-t,k) = V_\varepsilon(T-t,k)$ so at half-period (in $t = T/2$),

$$\Gamma V_\varepsilon(T/2,k)\Gamma = -V_{-\varepsilon}(T/2,k). \tag{4.119}$$

We therefore expect that the periodized evolution operators at half-period can characterize the topology of chiral systems. However, note that we work with the *periodized* evolution operators which contain information on the whole dynamics, due to the multiplication with the exponential of the effective Hamiltonian.

As we have already mentioned in paragraph 2.4.1 page 122, chiral symmetry relates states at opposite quasi-energies. As a consequence, chiral symmetric topological invariants can only be defined for the *real* (or *chiral*) gaps $\mathrm{e}^{-i\varepsilon} = \pm 1$ corresponding to arguments $\varepsilon = 0$ or π (if they exist), and in this case, we have seen that the constraints reduce to

$$\begin{aligned} \Gamma V_0(t,k)\Gamma^{-1} &= V_0(-t,k)\mathrm{e}^{2\pi \mathrm{i}t/T} \\ \Gamma V_\pi(t,k)\Gamma^{-1} &= V_\pi(-t,k). \end{aligned} \tag{4.120}$$

Note that one could relate operators describing the same gap ε (not necessarily 0 or π) through chiral symmetry, but generically the phase $\mathrm{e}^{2\pi \mathrm{i}t/T}$ would need to be replaced by a discontinuous operator accounting for the phase jumps of the logarithm. The corresponding map would therefore not be suitable to define a topological invariant. At half-period, those constraints yield

$$\begin{aligned} \Gamma V_0(T/2,k)\Gamma &= -V_0(T/2,k) \\ \Gamma V_\pi(T/2,k)\Gamma &= +V_\pi(T/2,k). \end{aligned} \tag{4.121}$$

Hence, in the chiral basis where $\Gamma \cong \mathrm{diag}(1,\dots,1,-1,\dots,-1)$, see paragraph 2.2.2 page 89, the periodized evolution operators at half-period are, depending on the gap, block-diagonal or block-antidiagonal,

$$V_0(T/2) \cong \begin{pmatrix} 0 & V_0^+ \\ V_0^- & 0 \end{pmatrix} \qquad \text{and} \qquad V_\pi(T/2) \cong \begin{pmatrix} V_\pi^+ & 0 \\ 0 & V_\pi^- \end{pmatrix} \tag{4.122}$$

where $V_0^\pm : \mathrm{BZ} \to U(M)$ are unitary maps and the variable k was omitted for clarity. Note that the inverse matrices are

$$[V_0(T/2)]^{-1} \cong \begin{pmatrix} 0 & [V_0^-]^{-1} \\ [V_0^+]^{-1} & 0 \end{pmatrix} \quad \text{and} \quad [V_\pi(T/2)]^{-1} \cong \begin{pmatrix} [V_\pi^+]^{-1} & 0 \\ 0 & [V_\pi^-]^{-1} \end{pmatrix}.$$

When the space and therefore the Brillouin torus are odd-dimensional (let $d = 2n+1$ be this odd dimension), the winding of the periodized evolution operator at fixed time, $w(t) = \deg(k \mapsto V_\varepsilon(t,k))$, is well-defined, but vanishes. This degree is homotopy invariant and V is smooth, so $w(t)$ does not actually depend on time; as $V_\varepsilon(t=0,k) = \mathrm{Id}$ for any k, $w(0) = 0$ and so $w(t) = 0$ for any time t. In particular, this is the case for $t = T/2$, which we shall use in the following.

We can use chiral symmetry to circumvent the vanishing of this winding number: as it will turn out, the two unitary submatrices that we identified in the previous section cancel each other in $w(T/2)$. However, we can use the block-(anti)diagonal structure of $V_\varepsilon(T/2)$ (equation (4.122)) to define two unitary windings $\deg(V_\varepsilon^\pm)$ from the periodized evolution operator. Computing $w(T/2)$ from the block-(anti)diagonal form of $V_\varepsilon(T/2)$, we see that

$$0 = w(T/2) = \deg(V_\varepsilon^+) + \deg(V_\varepsilon^-), \tag{4.123}$$

so there is actually only one independent invariant, which we denote by

$$G_\varepsilon[U] = \deg(V_\varepsilon^+). \tag{4.124}$$

This is the general topological index for a chiral symmetric Floquet system in odd space dimension. Let us emphasize again that this invariant is only defined for gaps $\varepsilon = 0$ or π.

The map $k \mapsto V_\varepsilon^+(k)$ does not depend on time (it is defined from the periodized evolution operator V_ε at half period), so the degree in (4.124) is computed as an integral over the Brillouin torus only. For example, in $d = 1$

$$G_\varepsilon[U] = \frac{\mathrm{i}}{2\pi} \int_{\mathrm{BZ}} \mathrm{tr}\left((V_\varepsilon^+)^{-1} \partial_k V_\varepsilon^+\right) \mathrm{d}k \tag{4.125}$$

and in $d = 3$,

$$\begin{aligned} G_\varepsilon[U] = & \frac{1}{24\pi^2} \int_{\mathrm{BZ}} \mathrm{d}k_x \mathrm{d}k_y \mathrm{d}k_z \\ & \mathrm{tr}\left(3[(V_\varepsilon^+)^{-1}\partial_{k_x} V_\varepsilon^+, (V_\varepsilon^+)^{-1}\partial_{k_y} V_\varepsilon^+](V_\varepsilon^+)^{-1}\partial_{k_z} V_\varepsilon^+\right). \end{aligned} \tag{4.126}$$

Let me stress again that as V_ε is computed both from the evolution operator U and the effective Hamiltonian $H_\varepsilon^{\mathrm{eff}}$, the invariant G_ε still depends on the whole evolution (and not only of the state of the system at half period).

3.3.3 Relation with band invariants

We now seek to relate the *gap invariant* $G_\varepsilon[U]$ to the *band invariant* used to characterize equilibrium systems computed for a quasi-energy band and described in paragraph 2.2.2, page 89. In analogy with the case without symmetry, we expect this band invariant to be equal to the difference between the gap invariants in the two gaps surrounding the band; as we will show, this is indeed the case, and

$$G_\varepsilon[U] - G_{\varepsilon'}[U] = g[P_{\varepsilon'\varepsilon}] \tag{4.127}$$

where $P_{\varepsilon,\varepsilon'}(k)$ is the spectral projector on states with quasi-energy between ε and ε'. As there are only two possible values for ε or ε', it is sufficient to show that

$$G_0[U] - G_\pi[U] = g[P_{0\pi}]. \tag{4.128}$$

Using the identity

$$[V_\pi(t,k)]^{-1} V_0(t,k) = \mathrm{e}^{2\pi \mathrm{i} t/T\, P_{\pi,0}(k)} \tag{4.129}$$

we have

$$[V_\pi(T/2,k)]^{-1} V_0(T/2,k) = \mathrm{e}^{\mathrm{i}\pi P_{\pi,0}(k)} = Q_{\pi,0}(k). \tag{4.130}$$

We can compute the block product

$$[V_\pi(T/2,k)]^{-1} V_0(T/2,k) = \begin{pmatrix} 0 & [V_\pi^+(k)]^{-1} V_0^+(k) \\ [V_\pi^-(k)]^{-1} V_0^-(k) & 0 \end{pmatrix} \tag{4.131}$$

Besides, from equations (4.130) and (4.121) we infer that $Q_{\pi,0}$ is block-antidiagonal in the chiral basis, namely

$$Q_{\pi,0}(k) \cong \begin{pmatrix} 0 & q_{\pi,0}^+(k) \\ q_{\pi,0}^-(k) & 0 \end{pmatrix} \in U(2M) \tag{4.132}$$

and therefore,

$$[V_\pi^+(k)]^{-1} V_0^+(k) = q_{\pi,0}^+(k). \tag{4.133}$$

As the degree is additive, we end up with

$$\deg(V_0^+) - \deg(V_\pi^+) = \deg(q_{\pi,0}^+) \tag{4.134}$$

which is the identity (4.127) that we wanted to show.

3.3.4 Example: the driven SSH model in one dimension

A simple example of Floquet system with chiral symmetry is the *driven SSH model* [GP13a; ATD14; LAT15]. We start from the Su-Schrieffer-Heeger model described in paragraph 2.2.3, page 91 and periodically modulate in time the tight-binding coefficients J_1 and J_2, which corresponds to a Bloch Hamiltonian

$$H(t,k) = (J_1(t) + J_2(t)\cos(k))\sigma_1 + J_2(t)\sin(k)\sigma_2 \tag{4.135}$$

where σ_i are the Pauli matrices in the basis of sublattices A and B. We choose $J_1(t) = J_1 + A\cos(\omega t)$ and $J_2(t) = J_2$. Chiral symmetry is represented by the operator $\Gamma = \sigma_3$, which anticommutes with the Hamiltonian whilst reversing time,

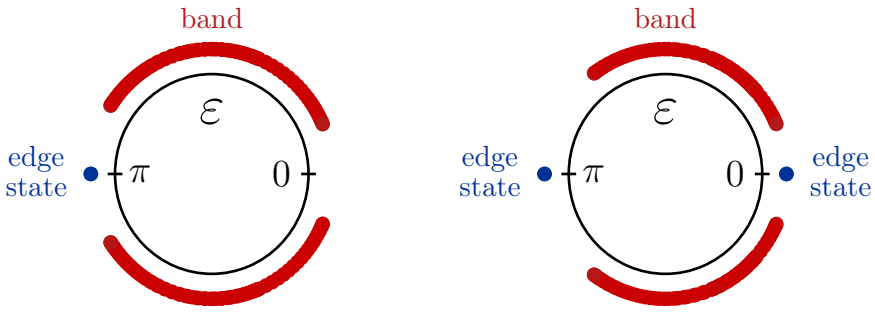

(a) nontrivial **(b)** anomalous

Figure 4.13: Quasi-energy spectrum of the driven SSH model in a finite system. Quasi-energy spectrum of a finite system (with edges) of the driven SSH model (a) for $J_1 = 3/2$, $J_2 = 1$, $A = 6$ and $T = 2.35$ and (b) for $J_1 = 1$, $J_2 = 3/2$, $A = 6$ and $T = 2.35$. The undriven system with $A = 0$ is trivial. In contrast, the driven phases presented here are both topologically nontrivial and exhibit nonvanishing chiral invariants, with (a) $G_\pi[U] = 1$ and $G_0[U] = 0$ and (b) $G_0[U] = G_\pi[U] = 1$. As a consequence, edge states appear in the quasi-energy spectra of the finite systems (in blue, as opposed to the bulk bands which are in red), (a) only in gap π and (b) both in gap 0 and in gap π. The second case (b) is an "anomalous" situations where the system is topologically non trivial despite vanishing chiral band invariants. The quasi-energy spectra are obtained by diagonalization in the Sambe space truncated to 19 sidebands for a system of length 80. The invariants were computed from the bulk Hamiltonian by direct integration.

$\Gamma H(t,k)\Gamma = -H(-t,k)$. Note that for this choice of modulation, we still have (bosonic) time-reversal symmetry with $\Theta = \mathcal{K}$, as $\Theta H(t,k)\Theta^{-1} = H(-t,-k)$, so this particular Hamiltonian is in fact in class BDI. However, in space dimension $d = 1$, time-reversal symmetry does not prevent the chiral invariant to be nonzero, and time-reversal breaking terms will not change its value (except, obviously, if they close a gap). This illustrates that the chiral gap invariant that we defined in the previous paragraph enables to compute all the $\mathbb{Z}$ or $2\mathbb{Z}$ invariants in chiral classes (i.e. classes BDI,DIII,CI,CII $\to$ AIII), a property that will be discussed in the paragraph 3.3.6, page 148.

As we have seen in paragraph 2.2.3, page 91, the undriven system with $A = 0$ is a band insulator when $|J_2/J_1| \neq 1$, and it is topologically nontrivial when $|J_2/J_1| > 1$. At the edge of a finite nontrivial system appear topologically protected zero modes (with an energy inside the bulk gap) exponentially located close to the boundary. In contrast, the edge of a trivial system does not generically host zero modes.

Turning on the driving from a trivial point of the equilibrium phase diagram, say $J_1 = 3/2$ and $J_2 = 1$, one can bring the system to an out-of equilibrium phase where edge modes appear inside the bulk gap, as in the equilibrium case, as illustrated in figure 4.13 (a), where $G_0[U] = 0$ and $G_\pi[U] = 1$. In figure 4.13 (b), the bulk invariants

$G_0[U] = G_\pi[U] = 1$ correspond to a finite system with one edge mode in each chiral gap ($\varepsilon = 0$ and π), an example of an anomalous topological phase where all band invariants vanish despite a nontrivial topology.

3.3.5 Example: a chiral driven system in three dimensions

To illustrate the 3D chiral invariant, I considered a three-dimensional driven tight-binding system with chiral symmetry, obtained by a periodic modulation of the parameters of a minimal tight-binding model for chiral topological insulators adapted from [WDMS15]. Let us considered electrons with spin 1/2 on a crystal with two sublattices (or orbitals) A and B, with Bloch Hamiltonian

$$H(t,k) = \begin{pmatrix} 0 & \mathrm{i}h_0\mathrm{Id} + h_i(t,k)\sigma_i \\ [\mathrm{i}h_0\mathrm{Id} + h_i(t,k)\sigma_i]^\dagger & 0 \end{pmatrix} \tag{4.136}$$

in basis $(A\uparrow, A\downarrow, B\uparrow, B\downarrow)$, and where

$$\begin{aligned} h_0 &= m(t) + \cos k_x + \cos k_y + \cos k_z, \\ h_1 &= \delta + \sin k_x, \\ h_2 &= \sin k_y, \\ h_3 &= \sin k_z. \end{aligned} \tag{4.137}$$

Chiral symmetry is represented by the matrix $\Gamma = \sigma_3 \otimes s_0$ (where s_μ and σ_μ are Pauli matrices, with σ_μ acting on sublattice degrees of freedom and s_μ acting on spin degrees of freedom). This Hamiltonian is chiral, $\Gamma H(t,k)\Gamma = -H(-t,k)$, provided that $m(t) = m(-t)$, so we take $m(t) = m_0 + m_1\cos(\omega t)$. In the following, we fix $\delta = 1/2$. The undriven system with $m_1 = 0$ is a chiral topological insulator in class AIII, and has a nontrivial chiral (band) invariant $g \neq 0$ for $|m_0| < 1$ (where $g = -2$) and for $1 < |m_0| < 2$ (where $g = 1$) [WDMS15]. We set $m_0 = 1.75$ so $g = 1$ in the undriven system. We expect the periodic driving to induce topological phase transitions; indeed, for a driving of angular frequency $\omega = 5$ and amplitude $m_1 = 1$, the numerical computation of the invariants (4.124) gives $G_0 = 1$ and $G_\pi = -2$, a situation only possible in driven systems, as there are surface states both in the gaps at quasi-energy $\varepsilon = 0$ and at quasi-energy $\varepsilon = \pi$.

The numerical computation of the quasi-energy spectrum of a finite system reveals the appearance of Dirac cones in the quasi-energy spectrum (that is, of isolated points on the Brillouin zone where a quasi-energy gap closes with linear dispersion) at the surface of the system. As expected from the bulk-boundary correspondence principle, we found that at each (bottom and top) interface, the bulk gap ε hosts G_ε Dirac cones. This is illustrated in figures 4.14 and 4.15.

3.3.6 Constraints on the chiral invariant due to other symmetries

In paragraph 3.2.7, page 139, we have shown that additional symmetries can either force the W invariants to vanish or left them unconstrained, depending on the CAZ class and the space dimension. In the second case, by forgetting about such symmetries and computing the invariant, we obtain topological invariants characterizing the corresponding (CAZ class, dimension) pair. The same game can be played for

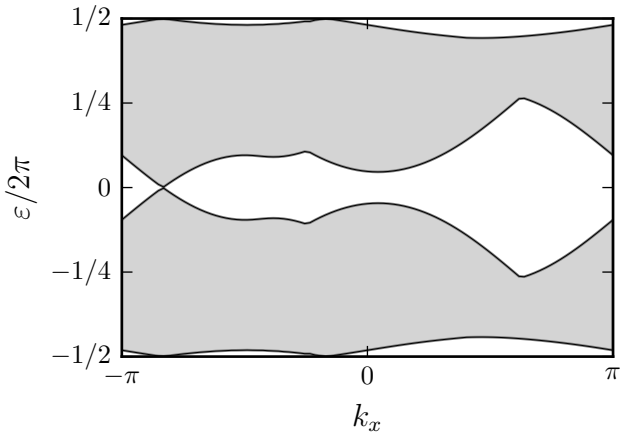

Figure 4.14: Quasi-energy spectrum of a 3D driven chiral system in a finite system. Projection along k_x of the quasi-energy spectrum of a finite system (with edges) of the 3D driven chiral model for $\delta = 1/2$, $m_0 = 1.75$, $m_1 = 1$, and $\omega = 5$. Bands are in gray, and both bulk and surface states are represented. The driven system is topological, with $G_0[U] = 1$ and $G_\pi[U] = -2$. As a consequence, surface states with linear dispersion (Dirac cones) appear in the quasi-energy spectrum of the finite system. In agreement with the bulk topological invariants, for each (bottom and top) surface boundary of the system, there are one Dirac cone in bulk gap 0 and two Dirac cones in bulk gap π. The quasi-energy spectrum is obtained by diagonalization in the Sambe space truncated to 7 sidebands for a system of length 15. The invariants were computed from the bulk Hamiltonian by direct integration (e.g. we obtain here $G_0 = 0.99$ and $G_\pi = -1.97$ which are rounded to the values given in the main text).

the chiral invariant: for example, in space dimension $d = 1$, systems in class BDI are characterized by the chiral invariant of class AIII. Again, we recover a part of the periodic table 3.3, page 108. Along with the results of paragraph 3.2.7, all $\mathbb{Z}$ or $2\mathbb{Z}$ invariants are found, in agreement with the K-theoretic analysis of [RH16].

When chiral symmetry and another (non unitarily implemented) symmetry is present, then all three symmetries are necessarily present, as the third is the product of the two other ones, possibly up to a phase. In this paragraph, we are therefore concerned with the situation where time-reversal, charge-conjugation and chiral symmetry are present. To simplify the reasoning, we will assume that all unitary symmetries were considered and that we work in an irreducible representation space, as in the section 2.4.1 on the ten-fold way, page 101. In such a case, we can always choose to adjust the phases[(3)] of the three operators such that

$$\Gamma = \sqrt{\pm}\Theta C = \sqrt{\pm} C\Theta \qquad \text{and} \qquad \Gamma^2 = \mathrm{Id} \tag{4.138}$$

[(3)] Starting from a time-reversal and a charge-conjugation operators Θ_0 and C_0, we do not necessarily have $\Theta_0 C_0 = C_0 \Theta_0$. However, they are related by a unitary operator, which is, in an irreducible representation space, a scalar matrix (i.e. a phase), so $C_0\Theta_0 = \mathrm{e}^{\mathrm{i}\phi}\Theta_0 C_0$. Let e.g. $C = \mathrm{e}^{-\mathrm{i}\phi/2} C_0$ and $\Theta = \Theta_0$, then $C\Theta = \Theta C$. As C and C_0 are unitary, their square do not change; $C^2 = C_0^2 = \pm\mathrm{Id}$. Finally, recall that $\Theta^2 C^2 = \pm\mathrm{Id}$ and define $\Gamma = \sqrt{\Theta^2 C^2}\Theta C$ so that $\Gamma = \pm\Theta C = \pm C\Theta$ and $\Gamma^2 = \mathrm{Id}$.

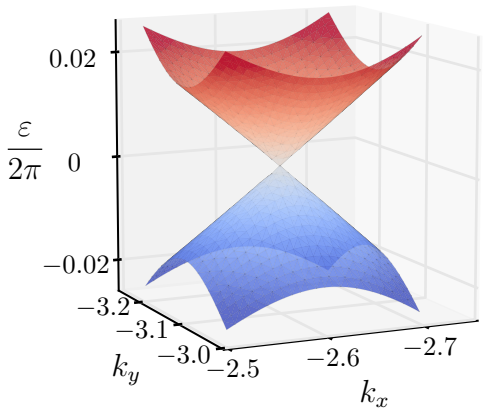

Figure 4.15: Zoom on a Dirac cone in the surface quasi-energy spectrum of a 3D driven chiral system. Three dimensional view of the Dirac cone in bulk gap 0 of the quasi-energy spectrum of figure 4.14. The dispersion is clearly linear in the neighborhood of the Dirac cone (located approximately at $k_x = -2.62$ and $k_y = -\pi$). The cone then merges in the bulk bands (shown in figure 4.14).

where the $\sqrt{\pm}$ depends on whether $\Theta^2 = \pm C^2$. As a consequence,

$$\Gamma\Theta\Gamma^{-1} = \pm\Theta \qquad \text{and} \qquad \Gamma C\Gamma^{-1} = \pm C \tag{4.139}$$

so they are either block-diagonal or block-antidiagonal in the chiral basis (see paragraph 2.2.1, page 88) according to whether time-reversal and charge-conjugation square to the same or not. Indeed, in both cases the constraints due to charge-conjugation and time-reversal will turn out to be redundant, as we already have taken into account their composition through chiral symmetry.

In the chiral basis, we have seen at equation (4.122) that the evolution operator at half-period is either block-diagonal or block-antidiagonal. We introduce the refined notations

$$V_0(T/2) \cong \begin{pmatrix} 0 & V_0^{+-} \\ V_0^{-+} & 0 \end{pmatrix} \qquad \text{and} \qquad V_\pi(T/2) \cong \begin{pmatrix} V_\pi^{++} & 0 \\ 0 & V_\pi^{--} \end{pmatrix}. \tag{4.140}$$

We will need to use the relations (see equation (4.123))

$$W_n[V_0^{+-}] + W_n[V_0^{-+}] = 0 \qquad \text{and} \qquad W_n[V_\pi^{++}] + W_n[V_\pi^{--}] = 0 \tag{4.141}$$

where n is such that $d = 2n + 1$.

Classes BDI and CII. When $\Theta^2 = C^2$, both operators are block-diagonal in the chiral basis,

$$\Theta \cong \begin{pmatrix} \Theta^{++} & 0 \\ 0 & \Theta^{--} \end{pmatrix} \qquad \text{and} \qquad C \cong \begin{pmatrix} C^{++} & 0 \\ 0 & C^{--} \end{pmatrix} \tag{4.142}$$

where $\Theta^{\pm\pm}$ and $C^{\pm\pm}$ are antiunitary matrices, with $(\Theta^{++})^2 = \pm\mathrm{Id}$ and $(\Theta^{--})^2 = \pm\mathrm{Id}$ according to whether $\Theta^2 = \pm\mathrm{Id}$ (the same goes mutatis mutandis for charge conjugation). Hence, constraints on the periodized evolution operator at half-period read, for time-reversal

$$\begin{aligned} \Theta^{++}\, V_0^{+-} (\Theta^{--})^{-1} &= V_0^{+-} \circ \tilde\kappa \\ \Theta^{--}\, V_0^{-+} (\Theta^{++})^{-1} &= V_0^{-+} \circ \tilde\kappa \\ \Theta^{++}\, V_\pi^{++} (\Theta^{++})^{-1} &= V_\pi^{++} \circ \tilde\kappa \\ \Theta^{--}\, V_\pi^{--} (\Theta^{--})^{-1} &= V_\pi^{-} \circ \tilde\kappa \end{aligned} \tag{4.143}$$

where

$$\tilde\kappa(k) = -k \tag{4.144}$$

is the restriction to BZ of the diffeomorphism κ on $S^1 \times \mathrm{BZ}$. The chiral invariant is only defined for an odd space dimension $d = 2n+1$ with integer n. As a consequence, the Brillouin torus is odd-dimensional and $\tilde\kappa$ reverses the orientation.

Similar constraints arise for charge conjugation,

$$\begin{aligned} C^{++}\, V_0^{+-} (C^{--})^{-1} &= -V_0^{+-} \circ \tilde\kappa \\ C^{--}\, V_0^{-+} (C^{++})^{-1} &= -V_0^{-+} \circ \tilde\kappa \\ C^{++}\, V_\pi^{++} (C^{++})^{-1} &= V_\pi^{++} \circ \tilde\kappa \\ C^{--}\, V_\pi^{--} (C^{--})^{-1} &= V_\pi^{-} \circ \tilde\kappa. \end{aligned} \tag{4.145}$$

Such constraints yield

$$\begin{aligned} W_n[\overline{V_0^{\pm\mp}}, \mathrm{BZ}] &= W_n[V_0^{\pm\mp} \circ \tilde\kappa, \mathrm{BZ}] \\ W_n[\overline{V_\pi^{\pm\pm}}, \mathrm{BZ}] &= W_n[V_\pi^{\pm\pm} \circ \tilde\kappa, \mathrm{BZ}] \end{aligned} \tag{4.146}$$

so

$$\begin{aligned} W_n[V_0^{\pm\mp}, \mathrm{BZ}] &= (-1)^n W_n[V_0^{\pm\mp}, \mathrm{BZ}] \\ W_n[V_\pi^{\pm\pm}, \mathrm{BZ}] &= (-1)^n W_n[V_\pi^{\pm\pm}, \mathrm{BZ}]. \end{aligned} \tag{4.147}$$

Hence, in the case $\Theta^2 = C^2$, the chiral invariant $G_\varepsilon[U] = W_n[V_\varepsilon^+]$ (with $V_0^+ = V_0^{+-}$ and $V_\pi^+ = V_\pi^{++}$) vanishes for odd n, and is not constrained for even n.

Classes DIII and CI. When $\Theta^2 = -C^2$, both operators are block-antidiagonal in the chiral basis,

$$\Theta \cong \begin{pmatrix} 0 & \Theta^{+-} \\ \Theta^{-+} & 0 \end{pmatrix} \qquad \text{and} \qquad C \cong \begin{pmatrix} 0 & C^{+-} \\ C^{-+} & 0 \end{pmatrix} \tag{4.148}$$

where $\Theta^{\pm\mp}$ and $C^{\pm\mp}$ are again antiunitary matrices, but this time with $\Theta^{+-}\Theta^{-+} = \pm\mathrm{Id}$ and $\Theta^{-+}\Theta^{+-} = \pm\mathrm{Id}$ according to whether $\Theta^2 = \pm\mathrm{Id}$ (and again, the story is identical for charge conjugation). Constraints on the periodized evolution operator at half-period now read, for time-reversal

$$\begin{aligned}
\Theta^{+-}\, V_0^{-+}(\Theta^{-+})^{-1} &= V_0^{+-} \circ \tilde{\kappa} \\
\Theta^{-+}\, V_0^{+-}(\Theta^{+-})^{-1} &= V_0^{-+} \circ \tilde{\kappa} \\
\Theta^{+-}\, V_\pi^{--}(\Theta^{+-})^{-1} &= V_\pi^{++} \circ \tilde{\kappa} \\
\Theta^{-+}\, V_\pi^{++}(\Theta^{-+})^{-1} &= V_\pi^{--} \circ \tilde{\kappa}
\end{aligned} \tag{4.149}$$

and for charge conjugation

$$\begin{aligned}
C^{+-}\, V_0^{-+}(C^{-+})^{-1} &= -V_0^{+-} \circ \tilde{\kappa} \\
C^{-+}\, V_0^{+-}(C^{+-})^{-1} &= -V_0^{-+} \circ \tilde{\kappa} \\
C^{+-}\, V_\pi^{--}(C^{+-})^{-1} &= V_\pi^{++} \circ \tilde{\kappa} \\
C^{-+}\, V_\pi^{++}(C^{-+})^{-1} &= V_\pi^{--} \circ \tilde{\kappa}
\end{aligned} \tag{4.150}$$

Such constraints yield

$$\begin{aligned}
W_n[\overline{V_0^{\pm\mp}}, \mathrm{BZ}] &= W_n[V_0^{\mp\pm} \circ \tilde{\kappa}, \mathrm{BZ}] \\
W_n[\overline{V_\pi^{\pm\pm}}, \mathrm{BZ}] &= W_n[V_\pi^{\mp\mp} \circ \tilde{\kappa}, \mathrm{BZ}]
\end{aligned} \tag{4.151}$$

which along with equation (4.141) finally give

$$\begin{aligned}
W_n[V_0^{\pm\mp}, \mathrm{BZ}] &= (-1)^{n+1} W_n[V_0^{\pm\mp}, \mathrm{BZ}] \\
W_n[V_\pi^{\pm\pm}, \mathrm{BZ}] &= (-1)^{n+1} W_n[V_\pi^{\pm\pm}, \mathrm{BZ}].
\end{aligned} \tag{4.152}$$

Hence, when $\Theta^2 = -C^2$, the chiral invariant $G_\varepsilon[U] = W_n[V_\varepsilon^+]$ vanishes for even n, and is not constrained for odd n.

To sum up, in the classes where all symmetries are present,

- when $\Theta^2 = C^2$ (classes BDI and CII) it vanishes for odd n, i.e. for dimensions $d = 3, 7, 11, \ldots$ and it is not constrained for even n, i.e. for dimensions $d = 1, 5, 9, \ldots$;
- when $\Theta^2 = -C^2$ (classes DIII and CI), it vanishes for even n, i.e. for dimensions $d = 1, 5, 9, \ldots$ and it is not constrained for odd n, i.e. for dimensions $d = 3, 7, 11, \ldots$.

In the cases where the chiral invariant is not vanishing, it characterizes the topological phases in the corresponding CAZ class. For example, in $d = 1$ the (driven) SSH model of paragraph 3.3.4, page 146 is strictly speaking in class BDI, but is characterized by the chiral invariant defined for systems with chiral symmetry alone (class AIII).

3.4 Class AII: with fermionic time-reversal

3.4.1 Overview

In space dimensions $d = 2$ and $d = 3$, it is possible to define a new $\mathbb{Z}_2$-valued bulk gap invariant

$$\mathrm{K}_\varepsilon[U] \in \mathbb{Z}_2 \tag{4.153}$$

associated to time-reversal invariant evolutions U such that

$$\Theta U(t,k)\Theta^{-1} = U(-t,-k). \tag{4.154}$$

This invariant is related to the Kane-Mele band invariant $\mathrm{KM}[P] \in \mathbb{Z}_2$ associated to a (time-reversal invariant) projector by

$$\mathrm{K}_\varepsilon[U] - \mathrm{K}_{\varepsilon'}[U] = \mathrm{KM}[P_{\varepsilon'\varepsilon}] \tag{4.155}$$

where $P_{\varepsilon,\varepsilon'}(k)$ is the spectral projector on states with quasi-energy between ε and ε'.

In agreement with the bulk-boundary correspondence principle, we expect that topologically protected edge states should appear at the boundary of a finite system in the bulk gap(s) endowed with nontrivial invariants. In a nontrivial bulk gap, a Kramers pair of counter-propagating chiral edge states (i.e. a pair of helical edge states) should appear, like in a Kane-Mele insulator. Again, such expectations are backed (i) by analogies with the static case, and (ii) by numerical simulations in the two-dimensional case.

3.4.2 Definition of the invariant in two dimensions

As we have seen in section 3.2.7, page 139, in two dimensions the W invariant (and the first Chern invariant) vanish due to time-reversal invariance (TRI). In the case of a fermionic TRI (fTRI), this vanishing can be interpreted as due to Kramers partners giving opposite contribution. Indeed, in a system with fTRI Kramers pairs $(\psi_j, \Theta\psi_j)$ of eigenstates respectively of $U(T,k)$ and $U^{-1}(T,-k)$ evolve in time in opposite direction (see also figure 4.16):

$$\Theta U(t,k)\psi_j(k) = U(-t,-k)\Theta\psi_j(k). \tag{4.156}$$

To define topological properties, it is more convenient to phrase this property in terms of the periodized evolution operator:

$$\Theta V_\varepsilon(t,k)\psi_j(k) = V_\varepsilon(-t,-k)\Theta\psi_j(k) = V_\varepsilon(T-t,-k)\Theta\psi_j(k). \tag{4.157}$$

As announced, this property implies the vanishing of $W_\varepsilon[U]$, and of all Chern invariants of the quasi-energy bands. To circumvent this cancellation, we proposed to isolate the contribution of only one member of each Kramers pair, in a spirit similar to the construction by Moore and Balents in static systems [MB07]. Moore and Balents used an "effective Brillouin zone", defined as a fundamental domain of the action $\tilde{\vartheta}$ defined by $\tilde{\vartheta}(k) = -k$ (essentially one half of the Brillouin zone, with only one representative for each $(k,-k)$ couple). In time-dependent systems, Kramers pairs are not "local in time", and we instead have to consider the action of ϑ defined as $\vartheta(t,k) = (-t,-k)$. To keep only one member of each Kramers pair, we simply restrict the time-evolution of V_ε to half a period, i.e. from times $t = 0$ to $t = T/2$. The second key observation is that time $t = T/2$ is a symmetry point of time-reversal (as $T - T/2 = T/2$), so time-reversal acts locally in time at $T/2$. Hence, Kramers pairs are "local in time" at $t = T/2$. The topological invariant turns out to arise from the comparison of Kramers partners at $t = 0$ and $t = T/2$: to do so, we observe

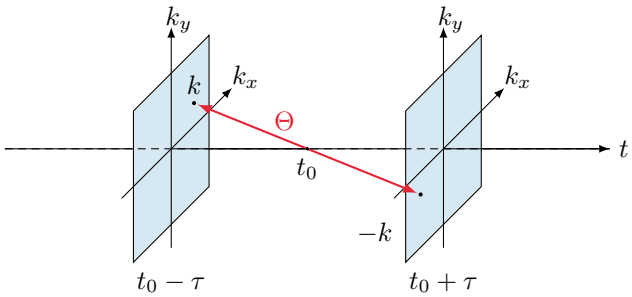

Figure 4.16: Action of time-reversal. Time-reversal relates states at point $(t_0 + \tau, k)$ to states at point $(t_0 - \tau, -k)$.

that it is possible to deform the map $k \mapsto V_\epsilon(T/2, k)$ to the identity through a contraction of the Kramers pairs present at $t = T/2$. In this contracted map, Kramers pairs are preserved at all times. The concatenation of this contraction with the half of the original periodized evolution operator results in a periodic map containing the information on the topological winding of Kramers pairs during the first half-period, see figure 4.17.

More concretely, we consider a smooth map $\widehat{V}_\epsilon$ from $[0, T] \times \mathrm{BZ}$ to $U(N)$ such that

$$\widehat{V}_\epsilon(t, k) = V_\epsilon(t, k) \qquad \text{for } 0 \leq t \leq T/2 \tag{4.158a}$$

and

$$\Theta \widehat{V}_\epsilon(t, k) \Theta^{-1} = \widehat{V}_\epsilon(t, -k) \quad \text{for } T/2 \leq t \leq T \tag{4.158b}$$

with $\widehat{V}_\epsilon(T, k) = \mathrm{Id} = \widehat{V}_\epsilon(0, k)$. The second part of this virtual evolution from $t = T/2$ to $t = T$ is not unique, and the homotopy class of the map $\widehat{V}_\epsilon$ depends on the choice of this contraction. However, the time-reversal invariance condition (4.158b) ensures that a change in the contraction $\widehat{V}_\epsilon(T/2 \leq t \leq T, k)$ can only change the winding of $\widehat{V}_\epsilon$ by an even integer, so the quantity

$$K_\epsilon[U] = \deg(\widehat{V}_\epsilon) \mod 2 \tag{4.159}$$

is well-defined. This $\mathbb{Z}_2$-valued topological invariant is the generalization for periodically driven systems of the Kane-Mele invariant. In a semi-infinite system, $K_\epsilon[U]$ is expected to give the parity of the number of Kramers pairs of counter-propagating chiral edge states that lie in the corresponding bulk quasienergy gap, a property which is evidenced by numerical simulations.

Finally, there is a direct relation between the K index and the Kane-Mele invariant of quasi-energy bands, namely

$$\mathrm{K}_\varepsilon[U] - \mathrm{K}_{\varepsilon'}[U] = \mathrm{KM}[P_{\varepsilon'\varepsilon}] \tag{4.160}$$

where $P_{\varepsilon,\varepsilon'}(k)$ is the (time-reversal invariant) spectral projector on states with quasi-energy between ε and ε'. This relation is the exact analogue of ones obtained for the W invariants of class A and the G invariants of class AIII.

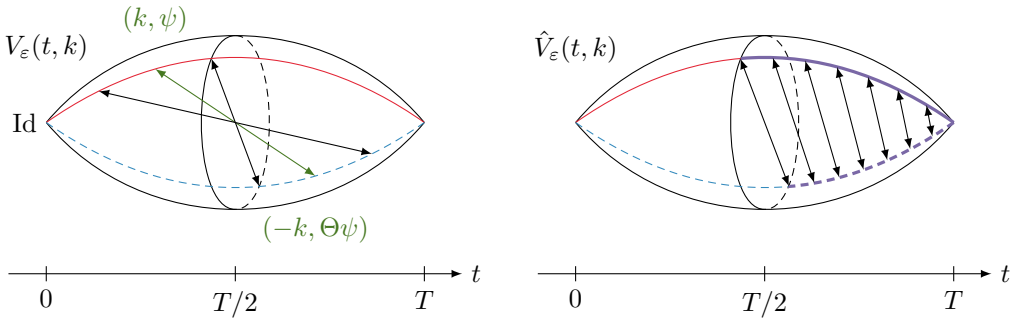

Figure 4.17: Sketch of the periodized evolution over one period. (a) Periodized evolution $V(t,k)$. Time-reversal relates pairs $(\psi,\Theta\psi)$ of states at (t,k) and $(-t,-k)$, as shown by black arrows. (b) Contracted half-evolution $\hat{V}(t,k)$. The second half of the initial evolution was discarded and replaced by a contraction respecting an equal-time constraint depicted as black arrows.

The detailed construction of $K_\epsilon[U]$, the proof of the existence of contractions (4.158b), of the independence of $K_\epsilon[U]$ upon their choice (in $\mathbb{Z}_2$), and of the link with Kane-Mele invariants are discussed in the reference [CDFG15a].

3.4.3 A simplification when spin is conserved

The expression of the K invariant (4.160) greatly simplifies when the projection S_z of spin along a fixed axis is conserved. In this situation, there is an additional unitary symmetry (corresponding to spin rotation around the quantization axis) commuting with the Hamiltonian[(4)] Hence, the evolution operator U can be block-diagonalized in the $(\uparrow,\downarrow)$ basis, as well as V_ϵ. The two blocks are related by time-reversal and the K index can be related to the W index of the spin blocks by

$$K_\epsilon\left[\begin{pmatrix} U_\uparrow & 0 \\ 0 & U_\downarrow \end{pmatrix}\right] = \frac{W_\epsilon[U_\uparrow] - W_\epsilon[U_\downarrow]}{2} \mod 2\,, \tag{4.161}$$

where $W_\epsilon[U_\uparrow] = W_\epsilon[\Theta U_\downarrow \Theta^{-1}] = -W_\epsilon[U_\downarrow]$. This expression is reminiscent of the "spin Chern number" [SWSH06]. Indeed, when considering the difference between indices at two quasienergy gaps, the usual spin Chern number is recovered.

3.4.4 Example: a toy time-dependent lattice model

To illustrate the index K, we consider a periodic evolution largely inspired by the model developed by Rudner et al. [RLBL13]. We define a piecewise constant in time

(4) We could infer from this property that the CAZ classification cannot be applied directly in this situation, and that each block should be considered separately. However, we know independently that the K index remains well-defined even in the absence of S_z conservation (as long as TRI is preserved), so we can consider that H is indeed in class AII, and that the additional unitary symmetry is only "accidental".

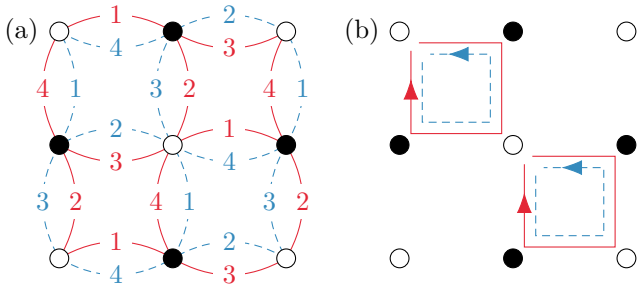

Figure 4.18: Time-dependent lattice model. Representation of the time evolution. (a) The only nonvanishing hopping amplitudes between sites are represented for the time steps $n = 1, \ldots, 4$ as a link labeled with n. This is done for spin up (red solid lines) and spin down (blue dashed lines). (b) The time sequence of U_n is summarized around plaquettes, which mimics closed orbits. Full and empty circles represent the two sublattices.

(Bloch) Hamiltonian

$$H(t,k) = \begin{cases} H_1(k) & \text{for } 0 \leq t/T < 1/N \\ \cdots & \\ H_n(k) & \text{for } (n-1)/N \leq t/T < n/N \\ \cdots & \\ H_N(k) & \text{for } (N-1)/N \leq t/T < 1. \end{cases} \tag{4.162}$$

where N is the number of time steps, which is extended by periodicity to all times through $H(t+T) = H(t)$ for all t. Hence, the corresponding Floquet operator is

$$U(T) = S_N S_{N-1} \cdots S_1 \tag{4.163}$$

where

$$S_n = \exp\left(-\mathrm{i}\frac{T}{N} H_n\right). \tag{4.164}$$

It is convenient to write the step Hamiltonians in terms of spin blocks as

$$H_n(k) = \begin{pmatrix} H_n^{\uparrow\uparrow}(k) & H_n^{\downarrow\uparrow}(k) \\ H_n^{\uparrow\downarrow}(k) & H_n^{\downarrow\downarrow}(k) \end{pmatrix} \tag{4.165}$$

with $n = 1, \ldots, N$. The time-reversal invariance of the evolution translates here into

$$H^{\downarrow\downarrow}(t,k) = \overline{H}^{\uparrow\uparrow}(-t,-k) \tag{4.166}$$

which means that $H^{\downarrow\downarrow}$ is the time-reversed copy of $H^{\uparrow\uparrow}$, and

$$H^{\uparrow\downarrow}(t,k) = -\overline{H}^{\downarrow\uparrow}(-t,-k) \tag{4.167}$$

for off-diagonal components. These TRI constraints translate for the step Hamiltonians into

$$H_n^{\downarrow\downarrow}(k) = \overline{H}_{N-n+1}^{\uparrow\uparrow}(-k) \tag{4.168}$$

and

$$H_n^{\uparrow\downarrow}(k) = -\overline{H}_{N-n+1}^{\downarrow\uparrow}(-k) \tag{4.169}$$

Here, we will first consider the case of $N = 4$ steps and of a spin-conserving dynamics, where off-diagonal blocks vanish. An easy way to obtain a TRI evolution is to specify the time-evolution of spins up, and to deduce the evolution of spins down by time-reversed invariance. To specify the dynamics of spins up, we use a time-dependent lattice model which mimics chiral classical "cyclotron" orbits on a square lattice [RLBL13]. We distinguish two sublattices A and B on the square lattice (see figure 4.18) and define the corresponding step Hamiltonian for spins ↑ as

$$H_1^{\uparrow\uparrow} = J\,T_{+x}^{\mathrm{A}\to\mathrm{B}} + \text{h.c.} + \Delta\sigma_z \tag{4.170a}$$
$$H_2^{\uparrow\uparrow} = J\,T_{-y}^{\mathrm{B}\to\mathrm{A}} + \text{h.c.} + \Delta\sigma_z \tag{4.170b}$$
$$H_3^{\uparrow\uparrow} = J\,T_{-x}^{\mathrm{A}\to\mathrm{B}} + \text{h.c.} + \Delta\sigma_z \tag{4.170c}$$
$$H_4^{\uparrow\uparrow} = J\,T_{+y}^{\mathrm{B}\to\mathrm{A}} + \text{h.c.} + \Delta\sigma_z \tag{4.170d}$$
$$H_5^{\uparrow\uparrow} = 0. \tag{4.170e}$$

where e.g. $T_{+x}^{\mathrm{A}\to\mathrm{B}}$ is the translation operator by one horizontal lattice spacing from sublattice A to B, see figure 4.18, and $\Delta\sigma_z$ is a staggered potential on the A/B sublattice. Hamiltonians $H_\alpha^{\downarrow\downarrow}$ for spin ↓ states are deduced by the TRI constraints, and correspond to orbits cycling in opposite direction.

Time-reversal preserving spin-flip terms may be added to the dynamics by setting nonzero off-diagonal blocks $H_\alpha^{\downarrow\uparrow}$ obtained from $H_\alpha^{\uparrow\uparrow}$ by replacing J by J', and by setting $H^{\uparrow\downarrow}(t,k) = -\overline{H}^{\downarrow\uparrow}(-t,-k)$, as imposed by the TRI constraint (4.167).

On the one hand, the quasienergy spectrum of the Floquet operator in a strip geometry (periodic in the x direction, but finite in the y direction) is shown on figure 4.19 for various parameters. On the other hand, the K invariants are computed from formula (4.161) in a situation without spin-flip, and the spin-flip terms are turned on while making sure that the gap do not close (a direct computation of the K invariant should be possible but was not done, see paragraph 3.4.5). The number of Kramers pairs of helical edge states on each interface is indeed accurately predicted by the invariant. Indeed, breaking time-reversal invariance spoils the existence of protected edge states, as illustrated on figure 4.20 (where in (d), a term $H_5^{\uparrow\downarrow}(k) = +\overline{H}_1^{\downarrow\uparrow}(-k)$ was added).

3.4.5 To be done: numerical computation of the K invariant in the general case

In principle, it should be possible to numerically evaluate the K invariant in the general case, simply by discretizing the degree integral of $\hat{V}_\varepsilon$ (in this paragraph, the index ε will be dropped to shorten notations). However, for this method to be practically applicable, the contraction $\hat{V}_\varepsilon(T/2 \le t \le T)$ must be constructed explicitly. This is at least possible when $V_\varepsilon(T/2)$ is gapped at quasi-energy $\eta = -\pi$. In general, the logarithm (similar to an effective Hamiltonian)

$$G_{\varepsilon,\eta}(k) = \frac{\mathrm{i}}{T/2}\log_{-\eta} V_\varepsilon(T/2,k) \tag{4.171}$$

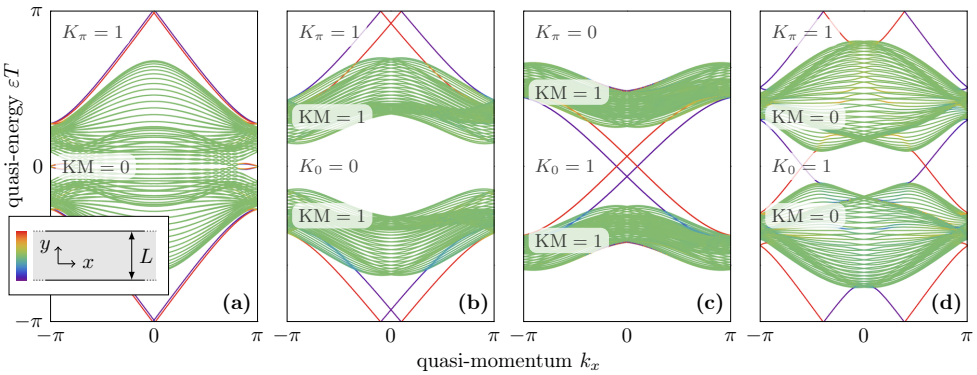

Figure 4.19: Quasienergy spectra of the TRI periodic evolution for a strip geometry. The spectra reveal helical edge states in gap $\epsilon = 0$ and/or π. The parity of the number of pairs of edge states in a bulk gap localized on each boundary is given by the corresponding value K_ϵ. Colors correspond to the density of states along y: red and purple states are localized at opposite edges (see inset). The parameters are (a) $J = 3\pi$, $J' = \pi$, $\Delta = 0$, (b) $J = 3\pi/2$, $J' = 1/2$, $\Delta = \pi/2$, (c) $J = -5\pi$, $J' = 1/2$, $\Delta = 9\pi/2$, (d) $J = 15\pi/2$, $J' = \pi$, $\Delta = 2\pi$. For clarity, in the case (a), a small boundary mass term was added to distinguish edge states.

where $\mathrm{e}^{-\mathrm{i}\eta}$ is in a spectral gap of $V_\varepsilon(T/2)$ satisfies

$$\Theta G_{\varepsilon,\eta}(k)\Theta^{-1} = -G_{\varepsilon,-\eta-2\pi}(-k) \tag{4.172}$$

where we used the logarithm identity $\overline{\log_\alpha(z)} = \log_{2\pi-\alpha}(\overline{z})$, so for $\eta = -\pi$

$$\Theta G_{\varepsilon,-\pi}(k)\Theta^{-1} = -G_{\varepsilon,-\pi}(-k) \tag{4.173}$$

and it provides a contraction

$$\hat{V}_\varepsilon(T/2 \le t \le T) = \mathrm{e}^{\mathrm{i}(t-T)G_{\varepsilon,-\pi}(k)} \tag{4.174}$$

with $\hat{V}_\varepsilon(T/2) = V(T/2)$, $\hat{V}_\varepsilon(T) = \mathrm{Id}$, and for $T/2 \le t \le T$,

$$\Theta \hat{V}_\varepsilon(t,k)\Theta^{-1} = \hat{V}_\varepsilon(t,-k). \tag{4.175}$$

Numerical explorations show that $V_\varepsilon(T/2)$ is gapped in interesting situations, but this method still has to be implemented, which was not done for lack of time, and due to difficulties with the numerics.

3.4.6 The K invariant in three dimensions

As a follow-up of our work on the two-dimensional time-reversal invariant Floquet systems, my co-advisor Krzysztof Gawędzki extended the construction of the K index to a more general context, which in particular includes three-dimensional Floquet systems [Gaw15]. The main idea is that in space dimension $d = 3$ (with fermionic time-reversal invariance), the map on the Brillouin 3-torus defined by

$$\check{V}_\varepsilon(k) = V_\varepsilon(T/2,k) \tag{4.176}$$

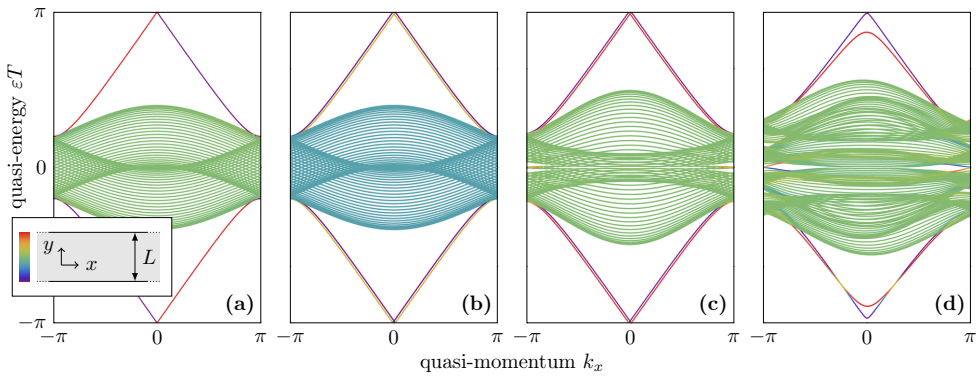

Figure 4.20: Effect on TR preserving and breaking spin-flip terms. Quasi-energy spectra for a strip geometry (inset) for $J = 3\pi$ and $\Delta = 0$. We consider (a) spin $\uparrow$ only, (b) spin $\uparrow$ and spin $\downarrow$ with no coupling ($J' = 0$), (c) spin $\uparrow$ and spin $\downarrow$ with $J' = 1/2$, (d) spin $\uparrow$ and spin $\downarrow$ with $J' = 1/2$ and time-reversal breaking term.

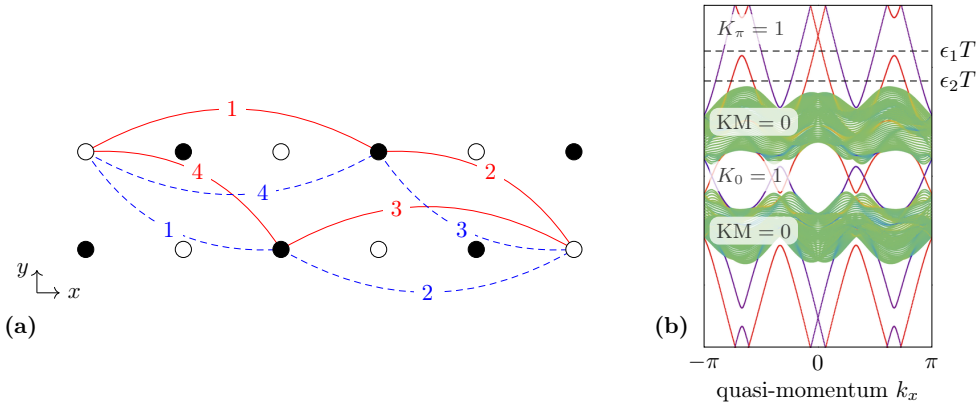

Figure 4.21: Illustration of the $\mathbb{Z}_2$ nature of the invariant. (a) Extended lattice model with hopping terms J_2, spin up (red solid lines) and spin down (blue dashed lines). (b) Quasi-energy spectrum of the extended lattice model for a ribbon geometry with $J_2 = 5\pi/2$, $J = 0$, $\Delta = \pi$ and $J' = 1$. The number of edge states in a gap is not the same at quasi-energies ϵ_1 and ϵ_2, but the parity is fixed and given by the K index.

is very similar to the map $V_\varepsilon^{2d}(t,k)$ defined on $S^1 \times \mathrm{BZ}_2 \simeq T^3$ in space dimension $d = 2$, as

$$\Theta \check{V}_\varepsilon(k)\Theta^{-1} = \check{V}_\varepsilon(-k) \tag{4.177}$$

with $k \in \mathrm{BZ}_3 \simeq T^3$. A construction similar to the one in [CDFG15a], but taking account the possible winding numbers in the k_x, k_y and k_z directions enables to associate a $\mathbb{Z}_2$-valued index $\mathcal{K}$ to any Θ-equivariant map $V : T^3 \to U(N)$, i.e. which satisfies

$$\Theta V \Theta^{-1} = V \circ \rho \tag{4.178}$$

where $\rho(x) = -x$ for $x \in T^3$. This construction depends on a choice of the fundamental domain for ρ, and the independence of the index on this choice is a nontrivial fact, which was proven by Krzysztof using the framework of equivariant bundle gerbes [Gaw15]. In this context, the two-dimensional index (4.160) can be defined as

$$\mathrm{K}_\varepsilon^{2d} = \mathcal{K}(V_\varepsilon^{2d}) \tag{4.179}$$

where $x = (t,k)$ and $k \in \mathrm{BZ}_2$. This alternative definition indeed matches the previous one. Furthermore, equipped with this index, the topological invariant characterized a fermionic-time-reversal invariant evolution in space dimension $d = 3$ can be defined as

$$\mathrm{K}_\varepsilon^{3d} = \mathcal{K}(\check{V}_\varepsilon) \tag{4.180}$$

where this time $x = k$ for $k \in \mathrm{BZ}_3$. This invariant is the generalization for time-periodic evolutions of the strong Kane-Mele invariant [FKM07], and like the two-dimensional version, it is related to the strong Kane-Mele invariant of quasi-energy bands by

$$\mathrm{K}_\varepsilon^{3d}[U] - \mathrm{K}_{\varepsilon'}^{3d}[U] = \mathrm{KM}^{3d}[P_{\varepsilon\varepsilon'}] \tag{4.181}$$

where $P_{\varepsilon,\varepsilon'}(k)$ is the spectral projector on states with quasi-energy between ε and ε'.

The existence of a generalization to Floquet systems of the three-dimensional strong Kane-Mele invariant is in agreement with the results of Nathan and Rudner [NR15] and with the K-theoretic results of Roy and Harper [RH16].

4 Conclusion and perspectives

4.1 Bulk invariants

As we have seen in this chapter, bulk topological invariants for time-periodic evolutions of crystals can be defined from the periodized evolution operators $V_\varepsilon(t,k)$ in a large number of cases (in color in table 4.1). Defining similar bulk invariants to take into account the missing $\mathbb{Z}_2$ classes of this table is the most obvious follow-up. This would confirm the results of Nathan and Rudner [NR15] and Roy and Harper [RH16] according to which the equilibrium classification is essentially exported to Floquet systems, but with gap invariants. However, with the time-dependency of Floquet systems new possibilities may arise which cannot be cast in this classification: for example, the reversal points of time-reversal and chiral symmetry may not coincide.

Continuing on the topic of bulk invariants, a natural question is whether "topological crystalline insulators" [Fu11; CTSR15] have a Floquet generalization. On the one hand, defining a mirror W invariant should be quite easy. On the other hand, band invariants for TCI generically do not have a summation property, and for example the mirror Chern number does not [CYR13] (in contrast, the Chern number of a composite band is the sum of the Chern numbers of the independent bands composing it); this compromises the existence of a simple relation like equation (4.73) between band invariants and gap invariants. This loss will certainly increase the complexity of a theory of topological Floquet-crystalline phases, but not prevent it.

		symmetries			space dimension							
		Θ	C	Γ	1	2	3	4	5	6	7	8
complex	A	0	0	0	0	$\mathbb{Z}$	0	$\mathbb{Z}$	0	$\mathbb{Z}$	0	$\mathbb{Z}$
AZ classes	AIII	0	0	1	$\mathbb{Z}$	0	$\mathbb{Z}$	0	$\mathbb{Z}$	0	$\mathbb{Z}$	0
	AI	+	0	0	0	0	0	$2\mathbb{Z}$	0	$\mathbb{Z}_2$	$\mathbb{Z}_2$	$\mathbb{Z}$
	BDI	+	+	1	$\mathbb{Z}$	0	0	0	$2\mathbb{Z}$	0	$\mathbb{Z}_2$	$\mathbb{Z}_2$
	D	0	+	0	$\mathbb{Z}_2^{a}$	$\mathbb{Z}$	0	0	0	$2\mathbb{Z}$	0	$\mathbb{Z}_2$
real	DIII	−	+	1	$\mathbb{Z}_2$	$\mathbb{Z}_2^{b}$	$\mathbb{Z}$	0	0	0	$2\mathbb{Z}$	0
AZ classes	AII	−	0	0	0	$\mathbb{Z}_2$	$\mathbb{Z}_2$	$\mathbb{Z}$	0	0	0	$2\mathbb{Z}$
	CII	−	−	1	$2\mathbb{Z}$	0	$\mathbb{Z}_2^{b}$	$\mathbb{Z}_2$	$\mathbb{Z}$	0	0	0
	C	0	−	0	0	$2\mathbb{Z}$	0	$\mathbb{Z}_2$	$\mathbb{Z}_2$	$\mathbb{Z}$	0	0
	CI	+	−	1	0	0	$2\mathbb{Z}$	0	$\mathbb{Z}_2$	$\mathbb{Z}_2$	$\mathbb{Z}$	0

Table 4.1: Periodic table of (Floquet) topological phases. The periodic table 3.3 (page 108) is reproduced. Here, the labels 0, $\mathbb{Z}$, etc. indicate the *gap invariants* available in the corresponding CAZ class and space dimension. Colored cells indicates the invariants already identified in the periodized evolution operator framework (this obviously also includes the always trivial phases 0). Cells in red correspond to phases characterized by the W invariant, and it is also the case of orange cells, where a non-vanishing W is compatible with additional symmetries. Similarly, cells in blue correspond to phases characterized by the chiral G invariant, and it is also the case of purple cells, where a non-vanishing G is compatible with additional symmetries. Finally, the green cells correspond to the fermionic-TRI invariants in $d = 2, 3$. The remaining cells where the definition of the invariant remains to be done are all $\mathbb{Z}_2$ invariants. Some of them, labeled by an exponent (a) are already known in another formulation from Jiang et al. [JKAA11]. Others, labeled by an exponent (b) are expected to be closely related to known invariants in the upper or lower CAZ class.

4.2 Observables vs. invariants

An open question is what physical quantities are related to gap and bulk invariants. We expect the following:

– As discussed previously, gap invariants are expected to give the number of edge modes. Hence, they should be related to *scattering experiments* which essentially probe the existence (and robustness) of an edge state e.g. at a fixed energy. This

is what happens when energy is injected on the edge. In particular, we expect in analogy with equilibrium systems that conductances should be related to gap invariants. A more precise discussion of this relation is found in the context of electronic solid-state physics in the next chapter. Indeed, strong experimental evidences of the relation between nontrivial bulk invariants and the existence of protected edge states were found in various contexts, even in the anomalous case [HPWP15; GGSY16; MSVA16; MZNS16].

– On the other hand, topological insulators were predicted to give rise to peculiar electromagnetic responses functions (or more generally, responses functions to a gauge field coupled to the TI) [QHZ08; EMV09; QLZZ09]; for example, three-dimensional Kane-Mele insulators are predicted to have a magnetoelectric response, due to a topological theta-term in the effective field theory for the electromagnetic gauge field in presence of the topological insulator. In particular, this peculiar magnetoelectric response leads to quantized Faraday rotation, which was recently observed experimentally [DSPA16] in strained HgTe. Indeed, we expect similar effects in a Floquet system. However, it is not clear to the author whether such a response function is a property of the fundamental state or a property of the full spectrum (including empty states). In the first case, I expect that band invariants should be related to the response functions, and for example an anomalous system would not display a signature of its bulk topology through response functions. In the second case, it is possible that the gap invariants are relevant quantities to study the response functions. Answering this question is particularly interesting as an ongoing effort is based on topological response functions to characterize topological phases in terms of anomalies, a very general point of view allowing generalizations beyond the translationally-invariant interaction-less case [RML12; WW13; Lud15; Wit16]. An extension of this point of view to Floquet systems would be highly relevant.
– A related topic to both of those points is the generalization to Floquet systems of the Green function approach to (bulk) topological invariants [Vol88a; Gur11; EG11], which (i) appear as prefactors of the topological terms of the effective action and (ii) are an important tool to formalize the bulk-edge correspondence, which is still not fully understood. In particular, it should be possible to relate analytically scattering (edge) invariants [FM16; TAD14] and bulk invariants, at least in simple situations.

4.3 Some other perspectives

Another crucial question relevant to understand the experimental manifestations of Floquet topological phases is what are the effects of imperfections and disorder? In particular, imperfections/disorder in the modulation of the drive are always present in experiments. In contrast, the effect of variations of the amplitude, frequency and phase of the driving field are not understood theoretically. Physically, we expect an effective broadening of the quasi-energy bands, and a corresponding reduction of the quasi-energy gap, but as long as the parameters are "sufficiently" peaked in a single region of the topological phase diagram, we expect topological properties to resist disorder. Beyond such qualitative arguments, a full study is required and still lacking. A disorder in frequency corresponding to a *quasi*-monochromatic source

would be particularly interesting to understand. Alas, even the Floquet operator is not clearly defined in such a situation (see however [VPM16] and reference therein). To define invariants, non-commutative geometry may be of some help (the odd and even Chern invariants both have equivalents formulations in the NCG framework, see e.g. [PS16]), but their precise formulation is far from straightforward. An easier preliminary task consists of using numerical simulations to refine and validate our physical intuitions. Time-resolved simulations are particularly well-suited to study disorder in the modulation, and my work transport (see the next chapter, page 165) is a first step in this direction.

In experiments, in addition to imperfections and disorder in the lattice system, there are potentially more harmful dissipative processes. We do not expect a single answer to the question of whether topology does survive to dissipative processes or not. In particular, there is a sharp contrast between classical systems, where damping (or amplification) can be taken into account in a "single-particle" description, and quantum systems (solids and cold atoms) where a full description requires (i) a many-body approach and (ii) to take into account the quantum nature of the driving field and the dissipative reservoirs.

In quantum systems, the generalization of (even undriven) topological insulators to interacting systems is a vast and topical subject that I will not develop here. On the other hand, a crucial topic specific to driven systems is the domain of validity of the effective Floquet description. In an illuminated sheet of graphene, for example, the full description of the system should at least include a quantum electromagnetic field and a quantum phonon bath (in addition to electronic reservoirs in transport setups). It is not clear to what extent topological properties survive in this context (and how to define them). There are a few studies on the subject, with Floquet systems connected to a phonon bath [DOM14] and with a quantized electromagnetic field [GD15]. Indeed, the effect of dissipation is also relevant for equilibrium systems, but is more pressing here as energy is injected by the driving field. Taking into account the quantum nature of the driving field may be less crucial (though interesting), as classical light should be well-described by the Floquet approach.

In classical wave systems, like mechanical structures or photonic crystals, a periodic driving is a natural route to induce topological properties. In such systems, non-linearities are nearly always present to some extent, and the question of the interplay between non-linear behavior and topology becomes of fundamental importance. In the non-linear regime, topological classical wave systems depart from their quantum counterparts, and promise both new physical phenomena and technological applications. For example, the effect of topological states on solitons was explored in optical [LC16] and mechanical [CUV14; VUG14] systems; similarly, non-linear dynamics can be affected by a underlying topological state [GTB16]. A very promising phenomenon is the self-induced topological transitions (e.g. at large enough amplitude) which were proposed in non-linear optical systems [LPRS13; HKA16].

On the fundamental side, the Laughlin argument [Lau81] relates the quantized Hall conductivity of a 2D system to the quantized adiabatic charge transport through a quasi-one dimensional Thouless pump [Tho83], a perspective related to the previously mentioned anomalies point of view. Extending this argument to periodically-driven

systems leads to considering topological "Floquet adiabatic pumps", the study of which requires an adiabatic Floquet theory, i.e. (t, t') Floquet theory [BH89; PM93]. There are several studies on the geometric phases in such systems which may serve as a ground for such as study, see [Vie09] and the reference therein. Notably, the article of Viennot [Vie09] relates geometric phases to gerbe holonomies stemming from "the appearance of changes in the Floquet blocks at the transitions between two local charts of the parameter manifold", a behavior reminiscent of Nathan and Rudner's [NR15] interpretation of anomalous phases as arising from singularities on the edges of the phase Floquet/Brillouin zones at intermediate times (it is unclear to the author of these lines whether such behaviors are actually related or not).

Chapter 5

Transport properties of (topological) Floquet states

1 Overview

Transport measurement are a tool of choice to study the properties of electrons in condensed matter. Indeed, robust quantized conductances are the hallmark of two-dimensional topological phases, from the IQHE to Kane-Mele insulators (see the paragraphs 1.1 and 1.2 of the Introduction, on pages 4 and 11). A natural question is whether the topological properties of Floquet states manifest themselves on transport properties in a solid state setting (on the topic of the realizability of Floquet states in electronic condensed matter, see the paragraph 1.4.1 of the Introduction, page 25). As the system is periodically driven, averaging over (at least) one driving period will certainly be required to obtain stationary transport properties. Up to this technical difference, we expect in analogy with equilibrium systems (i) a signature of the presence of edge states, for example as a quantized average conductance, and (ii) a signature of their chiral (or helical, etc.) character, which should manifest itself in multiterminal setups.

In this chapter, I will present the results of time-resolved numerical simulations of electronic transport in two-dimensional Floquet systems, with a focus on topological states. This work should be understood as a proof-of-concept and as a first step towards a more systematic study: there is no disorder, and the driven interface transparency is not fully understood yet. The time-resolved simulations are based on the tkwant code developed by the group of Xavier Waintal, based on their algorithmic work on the subject [GWSH14]. This code enables us to compute (time-averaged) differential conductances of a Floquet system for both a two-terminal and a three-terminal geometry. The multi-terminal differential conductances indeed probe the chiral nature of the topological state, and we observe that in the case at hand, the conductances seem to be quantized. Hence, DC transport appears as an accurate probe of Floquet topological states. This requires that this DC transport is described by the effective unitary Floquet description. The validity of this description implies that the dissipation occurs mostly inside the leads, i.e. that the system is small enough for the travel times through it to be small compared with times scales of other source of dissipation (phonons, photons, etc). In that situation, the differential conductance of the system depends on the intermediate time evolution of the driven system and

can be accurately described starting from the unitary dynamics of the driven system and its associated topological properties. This should be the case for small enough samples in which transport remains ballistic on the length scale of the sample, even in the presence of dissipation or weak interactions.

2 Electronic transport in a periodically driven system

2.1 Generalized Landauer-Büttiker formalism

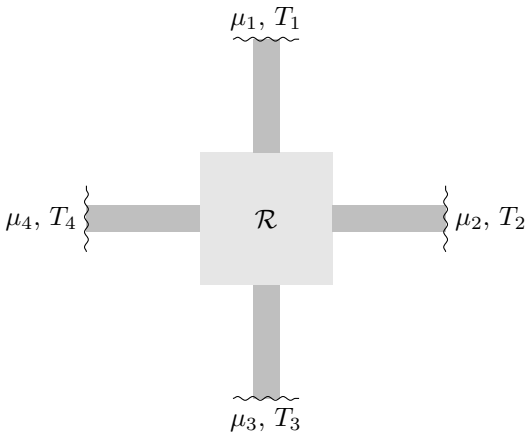

Figure 5.1: Mesoscopic transport setup. A central scattering region $\mathcal{R}$ (light gray) is connected to electronic reservoirs at fixed temperatures T_ℓ and chemical potentials μ_ℓ through ideal quasi-one-dimensional leads (dark gray).

The standard setup for mesoscopic transport is composed of a central *scattering region* $\mathcal{R}$, which constitutes the system of interest, connected through several semi-infinite metallic **leads** to **electronic reservoirs** at equilibrium, with fixed chemical potential and temperature, see figure 5.1. The leads are assumed to be quasi-one dimensional systems, with several **channels** corresponding to the transverse modes of the semi-infinite lead. In the longitudinal direction, the wave functions in the lead are plane waves $\mathrm{e}^{-\mathrm{i}qx}$, where q is the longitudinal momentum. Hence, the modes of the lead separate into incoming and outgoing modes distinguished by, respectively, $\vec{q} \cdot \vec{n} < 0$ and $\vec{q} \cdot \vec{n} < 0$, where $\vec{n}$ is the normal to the interface defined as going out of the scattering region. The main idea is that by measuring the currents flowing from one lead to another, scattering properties of the system can be probed, which depends on the available states on the system. More specifically, the *differential conductances* are relevant quantities, related to the transmission coefficients from one lead to another through the Landauer-Büttiker formalism [Lan57; Lan70; BILP85; Büt86; Büt88b] (a review is found in the beginning of [Bee97]). In particular, such quantities allow to probe the existence and nature of edge states, and thus to probe the topological nature of a state of matter, as demonstrated for the quantum Hall effect by Büttiker [Büt88a].

Here, the system $\mathcal{R}$ is periodically driven in time, so quantities of interest like the current or the differential conductances are expected to depend on time. After a transient regime, we expect the scattering amplitudes to acquire the periodicity in time of the driven central region. In such a steady state, we expect that the rolling average over a driving period T should not depend on time, and in the following we will consider this kind of suitably averaged quantities. The study of out-of-equilibrium transport, and in particular of time-dependent transport is naturally described in the Keldysh framework. However, for a system without interactions between electrons, the steady-state can be studied with the simpler Floquet scattering formalism [JWM94; KLH05; MB02; AM06; SKRG08]. Note that even without interactions between electrons, transient regimes are not described in this framework.

In this section, I focus on the results required to discuss the results of the numerical simulation. Details on the formalism, including a derivation of the generalized Landauer and Fisher-Lee formulas, are included in the appendix B, page 187.

The rolling average over a period T of the current leaving each lead

$$\mathcal{I}_\ell(t) = \frac{1}{T}\int_t^{t+T} \mathrm{d}t' \ \langle \hat{J}_\ell(t')\rangle \tag{5.1}$$

where $\langle \hat{J}_\ell(t')\rangle$ is the expectation value of the current leaving lead ℓ at time t' can be expressed in a *scattering form*. This average current satisfies a relation [MB02; KLH05; SKRG08]:

$$\mathcal{I}_\ell(t) = \frac{e}{h}\int \mathrm{d}E \ \sum_{\ell'\neq\ell} \left[T_{\ell\ell'}(t,E) f_{\ell'}(E) - T_{\ell'\ell}(t,E) f_\ell(E)\right], \tag{5.2}$$

where $f_\ell(E)$ is the Fermi-Dirac distribution of the lead ℓ at equilibrium at the chemical potential μ_ℓ, and $T_{\ell'\ell}(E)$ are the time-averaged transmission coefficients from lead ℓ to lead ℓ' with an injection energy E. We define the differential conductance $G_{\ell\ell'}(t,E)$ as the sensitivity of the current leaving the lead ℓ to variations of the electrochemical potential $\mu_{\ell'}$ of the lead[(1)] ℓ', namely by

$$G_{\ell\ell'}(t,E) \equiv -e\left.\frac{\mathrm{d}\mathcal{I}_\ell}{\mathrm{d}\mu_{\ell'}}\right|_{\mu_{\ell'}=\mu_{\mathrm{sys}}+E}. \tag{5.3}$$

where μ_{sys} is the chemical potential of the scattering region. This definition is not symmetrized in the various chemical potentials μ_ℓ. Implicitly, it assumes the possibility to independently control the electrochemical potential of all leads and of the scattering region. In the long time stationary regime on which we focus where $t\to\infty$, the average conductances $G_{\ell\ell'}(t,E)$ are expected to reach a stationary value, which we denote by

$$G^\infty_{\ell\ell'}(E) = \lim_{t\to\infty} G_{\ell\ell'}(t,E). \tag{5.4}$$

The existence of such a limit is not an obvious facts. It is in fact tightly related to the existence of a stationary Floquet phase described by an effective unitary evolution,

(1) See [GWSH14] for a discussion on the distinction between chemical and electrical potential drops at the interface between the system and an electrode. Such subtleties are quietly neglected in the following.

which is questionable in a solid state setting (see the paragraph 1.4.1 of the Introduction, page 25). Recent theoretical studies have shown that well-designed reservoirs could even stabilize the filling of the quasi-energy band in such a phase [SBLR15]. We expect the time scale associated to the transient regime to be mainly controlled by dissipative processes, but a full modelization taking into account the driving field, the various dissipative processes and the coupling to the leads would be required to fully understand those issues. Here, we will assume that the stationary state described by $G^{\infty}_{\ell\ell'}$ can actually be reached, and focus on its properties.

We obtain from Eq. (5.2) the zero temperature time-averaged differential conductances

$$G^{\infty}_{\ell\ell'}(E) = \frac{e^2}{h} T_{\ell\ell'}(E) \qquad \text{for } \ell \neq \ell' \tag{5.5a}$$

$$G^{\infty}_{\ell\ell}(E) = -\frac{e^2}{h} \sum_{\ell' \neq \ell} T_{\ell'\ell}(E) \tag{5.5b}$$

which satisfy the rule

$$\sum_{\ell} G_{\ell,\ell'}(E) = 0 \tag{5.6}$$

for any ℓ'. Formula (5.5) is the generalization to Floquet systems of the standard **Landauer-Büttiker formula** for the differential conductance of multiterminal equilibrium systems.

2.2 Generalized Fisher-Lee relation

The average transmission coefficients $T_{\ell\ell'}(E)$ can be related to the Floquet-Green functions of the system, in a way analogous to the case of undriven conductors [FL81].

On the one hand, the **retarded Green function** $G(t,t')$ is defined as the solution of the Schrödinger equation

$$\left(\mathrm{i}\hbar\frac{\mathrm{d}}{\mathrm{d}t} - H^{\mathrm{sys}}(t) + \Sigma\right) G(t,t') = \delta(t-t') \tag{5.7}$$

describing the scattering region, where a non-Hermitian self-energy term Σ takes into account the coupling to the leads (see appendix A for details). It is related to the corresponding evolution operator by

$$G(t,t') = \frac{1}{\mathrm{i}\hbar}\mathcal{H}(t-t')U(t,t') \tag{5.8}$$

where $\mathcal{H}$ is the Heaviside step function. The **mixed time-energy representation** of the retarded Green function is defined by

$$G(t,E) = \frac{1}{\mathrm{i}\hbar}\int d\tau\ e^{\mathrm{i}E\tau/\hbar}\, G(t,t-\tau), \tag{5.9}$$

which can be decomposed into *harmonics* called the *Floquet-Green functions*

$$G^{(p)}(E) = \frac{1}{T}\int_0^T \mathrm{d}t\ \mathrm{e}^{\mathrm{i}p\omega t}\, G(t,E). \tag{5.10}$$

Floquet theory enables to express the Green-Floquet functions of the scattering region as

$$G^{(p)}(E) = \sum_{r,\alpha} \frac{|u_\alpha^{(p+r)}\rangle \langle \tilde{u}_\alpha^{(r)}|}{E - [\varepsilon_\alpha + r\hbar\omega - \mathrm{i}\hbar\gamma_\alpha]}. \tag{5.11}$$

where $\langle \tilde{u}_\alpha^{(p)}|$ and $|u_\alpha^{(p)}\rangle$ are respectively the left and right Floquet sideband modes and $\varepsilon_\alpha - \mathrm{i}\hbar\gamma_\alpha$ is the complex quasi-energy associated to the Floquet mode $|\psi_\alpha\rangle$ (see appendix A page 186 for details). A perturbation theory at low coupling with the leads enables to replace, at first order, the Floquet sideband modes and quasi-energies by their equivalent for the uncoupled problem, and to express the inverse lifetime γ_α.

On the other hand, the transmission coefficients can also be decomposed into *harmonics* as

$$T_{\ell'\ell}(E) = \sum_{p\in\mathbb{Z}} T_{\ell'\ell}^{(p)}(E), \tag{5.12}$$

where each $T_{\ell'\ell}^{(p)}(E)$ is the transmission coefficient for an electron injected in lead ℓ at the energy $E = \mu_\ell$ and leaving the system in lead ℓ' at the energy $E + p\hbar\omega$, *i.e.* after having exchanged p quanta with the driving perturbation (see figure 5.2). They are related to the Floquet-Green functions by the **generalized Fisher-Lee relation** [KLH05; SKRG08; AM06]

$$T_{\ell'\ell}^{(p)}(E) = \mathrm{Tr}\left[G^{\dagger(p)}(E)\hat{\Gamma}_{\ell'}(E + p\hbar\omega)G^{(p)}(E)\hat{\Gamma}_\ell(E)\right] \tag{5.13}$$

where $\hat{\Gamma}_\ell(E)$ is the coupling operator at energy E between the system and the electrode ℓ. This is the generalization to Floquet systems of the Fisher-Lee relation in undriven systems [FL81].

In a low-coupling regime where the damping rates γ_α are sufficiently small (see paragraph 4.3, page 180), the preceding analysis implies that the transmission coefficient $T_{\ell'\ell}(E)$) and thus the differential conductance $G_{\ell'\ell}(E)$ vanish when the injection energy E corresponds to a quasi-energy gap (that is to say, $E \neq \epsilon_\alpha + n\hbar\omega$ for all states α and sidebands n). This property allows one to probe the existence of gaps in the quasi-energy spectrum of the Floquet operator [KOBF11]. Moreover, we expect the differential conductance to be essentially proportional to the density of quasi-energy states.

3 Numerical simulations of DC transport

3.1 Methods

In practice, both a two-terminal geometry and a three-terminal geometry are considered. The time-dependent tight-binding model presented in the section 3.2.5 of chapter 4 (page 131) is implemented on a finite lattice, to which leads are attached. The leads are modeled by a simple tight-binding Hamiltonian on a square lattice with nearest neighbors hoppings with amplitude $J_0 = 8$ (so the bandwidth is $8J_0$,

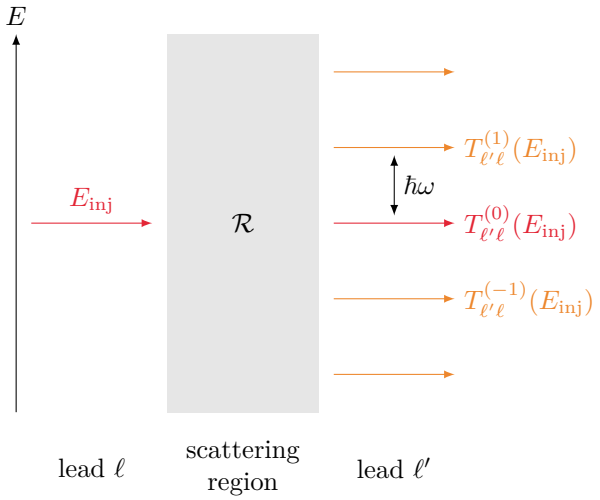

Figure 5.2: Sideband picture of Floquet scattering. A flow of electrons is injected in the scattering region from the lead ℓ at a well-defined, fixed energy E_{inj}. They travel in the scattering region, where they may absorb or emit quanta $\hbar\omega$ of the driving field ("photons"). Finally, they leave the scattering region in the outgoing modes of leads ℓ', at energies $E_{\mathrm{inj}} + p\hbar\omega$ where $|p|$ is the number of absorbed ($p > 0$) or emitted ($p < 0$) photons. The sideband transmission coefficient $T_{\ell'\ell}(E)$ gives the corresponding amplitude.

but the density of states is obviously not constant on the whole bandwidth). An onsite potential is added to the lead Hamiltonian to reduce mismatches between the incoming (and outgoing) states of the leads and the scattering states of the central region. The time-dependent numerical calculations are performed using a numerical method developed in the group of Xavier Waintal and described in [GWSH14]. This method is mainly based on the resolution of a Schrödinger equation with an additional term taking into account the coupling to the leads. Although the technique is based on wavefunctions, it is mathematically equivalent to more standard, but less efficient Green function approaches, and enables new kinds of time-resolved simulations [WW16a; WW16b]. The group of Xavier Waintal and in particular Joseph Weston developed an implementation of this method called tkwant, which is based on the kwant package [GWAW14]. I refer the reader to the article [GWSH14] and to the PhD thesis of Joseph for more details.

3.2 Two-terminal differential conductances: probing the quasi-energy band structure

First, the (averaged) differential conductance $G_{\mathrm{RL}}(t)$ is computed in a two-terminal setup through a sample of width $W = 60$ and length $L = 30$ sites. After a transient regime, the (rolling-averaged) differential conductance $\bar{G}(t)$ converges to a finite value (see figures 5.3 and 5.4). This transient regime can be understood as the time of flight of the state injected at the left lead to the right lead after the driving perturbation

has been turned on and the Floquet states developed inside the system. When the chemical potential of the incoming lead lies in a topological quasi-energy gap of the scattering region, transport occurs through a chiral state localized near the edge of the sample. We can easily evaluate the travel length L. On the other hand, the expected (quasi-)group velocity is extracted from the slope of the quasi-energy dispersion relation from Fig. 5.5 through

$$v_{\mathrm{g}} = \frac{1}{\hbar}\frac{\mathrm{d}\varepsilon}{\mathrm{d}k}, \tag{5.14}$$

and we obtain

$$v_{\mathrm{g}} \approx (0.15 \pm 0.01)\, a\omega \tag{5.15}$$

where a is the lattice spacing and ω the driving frequency. This correlates perfectly with the time Δt between the switching on of the driving field and the first increase from zero of the conductance: from the curve on figures 5.3 and 5.4 we find

$$\frac{L}{\Delta t} \approx (0.14 \pm 0.01)\, a\omega \tag{5.16}$$

in excellent agreement with (5.15). From the theoretical point of view, the relation between the quasi-group velocity and the duration of the transient regime is not obvious. On the one hand, v_{g} is the most simple dimensionally relevant quantity at hand. As there are no other ingredients in the numerical simulation, it is natural that it appears. On the other hand, we expect that other time-scales related to the coupling between the driving field and the system and between the dissipating baths and the system (which are not taken into account in this effective description) should control the duration of the transient regimes.

After this transient regime, the differential conductance $G_{\mathrm{RL}}(t)$ reaches a long time stationary limit G^{∞}_{RL}, as shown in the inset of figures 5.3 and 5.4. As expected, this asymptotic differential conductance is sensitive to the quasi-energy spectrum of the driven system. As shown on the left plot of figures 5.3 and 5.4, G^{∞}_{RL} reaches high values in a spectral band, but vanishes when the chemical potential $\mu_{\mathrm{L}} - \mu_{\mathrm{sys}}$ lies in a trivial spectral gap of the Floquet operator. The value of the differential conductance is correlated with the density of quasi-energy states. When the bulk quasi-energy gap is topological, the presence of the associated chiral states at the edge of the system shown in figure 5.5 leads to an almost perfectly quantized two terminal conductance as shown in the right plot of figures 5.3 and 5.4.

The correlation between the differential conductance as a function of the chemical potential $\mu_{\mathrm{L}} - \mu_{\mathrm{sys}} = E$ and the quasi-energy spectrum of the system is better visualized when plotting long time limit of the conductances $G^{\infty}_{\ell\ell'}$ as a function of E. In the numerical simulation, the chemical potential of the scattering region is taken as a reference, and we set $\mu_{\mathrm{sys}} = 0$. The numerical results are plotted in figure 5.5 for both a trivial and a topological gapped Floquet system, along with the quasi-energy band structures of the unconnected driven systems on a semi-infinite strip. The differential conductance vanishes only inside a trivial gap, except at the edge of the gap where finite size effects occurs due to imperfect transparencies of the contact with the leads, as shown on a magnified view around the gap $\epsilon = 0$ in figure 5.6. This demonstrates both that the quasi-energy spectrum of the finite system connected to infinite leads

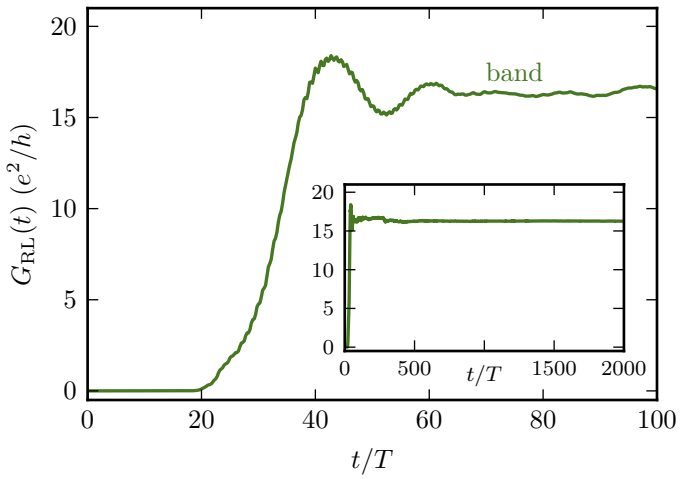

Figure 5.3: Transient behavior of two-terminal conductances in a band. We plot the two-terminal differential conductances as a function of time, in the transient regime, for the topologically trivial situation (a) of figure 5.5. Here, the incoming chemical potential is set in a quasi-energy band ($\mu_{\mathrm{L}}/\hbar\omega = -0.14$, green arrow in figure 5.5(b)). Longer simulations shown in inset were carried out to ensure convergence (not fully reached at $t/T = 100$). The asymptotic value is denoted by G^{∞}_{RL}.

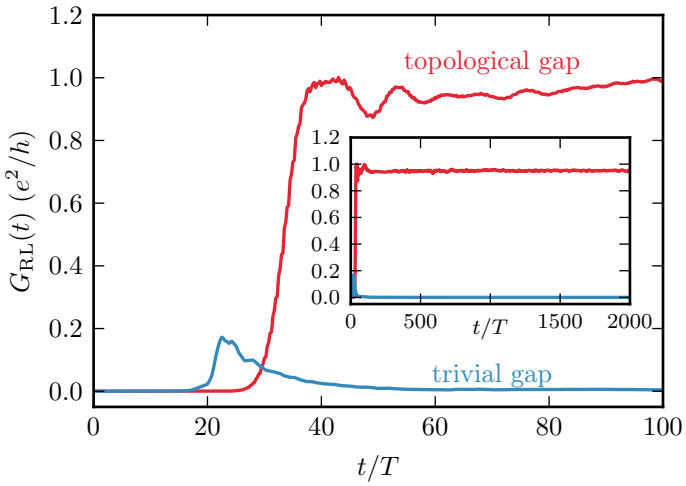

Figure 5.4: Transient behavior of two-terminal conductances in gaps. We plot the two-terminal differential conductances as a function of time, in the transient regime, for the topologically trivial situation (a) of figure 5.5 (in blue) and for the topologically non-trivial situation (b) of figure 5.5 (in red). Here, the incoming chemical potential is set in the quasi-energy gap $\varepsilon = 0$ ($\mu_{\mathrm{L}}/\hbar\omega = 0.02$, red and blue arrows in figure 5.5). Longer simulations shown in inset were carried out to ensure convergence (not reached at $t/T = 100$). The asymptotic value are denoted by G^{∞}_{RL}.

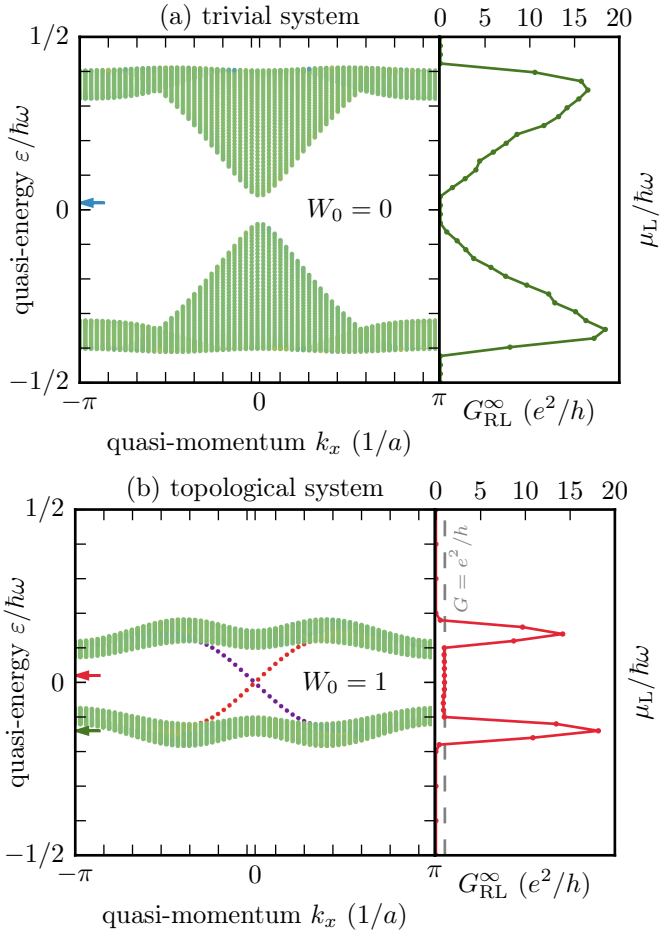

Figure 5.5: Comparison of quasi-energy spectra and two-terminal differential conductances. We plot (i) the quasi-energy spectrum of the driven half-BHZ model in an infinitely long ribbon, as a function of the quasi-momentum k_x in the direction of the ribbon and (ii) the asymptotic two-terminal differential conductances $G^{\infty}_{\mathrm{RL}}(E)$ for a finite system connected to infinite leads as a function of the chemical potential of the left lead, in two situations (a) and (b). In the trivial case (a), we find that the differential conductance vanishes in both gaps. In the topological case (b), states localized on the sides of the ribbon appear inside the topological gap $\epsilon = 0$, and in this gap the differential conductance G^{∞}_{RL} is quantized, with $G = 1e^2/h$. In both cases, the undriven Hamiltonian has parameters $M = -1.0$, $J = 1.5$, $A = 4.0$, $B = 1.5$ and the driving angular frequency is $\omega = 20$. The driving amplitude is (a) $F = 2$ and (b) $F = 8$; such parameters correspond to bulk Floquet topological invariants (a) $W_0 = 0 = W_\pi$ and (b) $W_0 = 1$ and $W_\pi = 0$. The quasi-energy spectra are obtained for strip of width $W = 60$ sites by diagonalization in Sambe space with 5 sidebands. Colors are computed from the mean position of the states: a green color (■) indicates a (delocalized) state with average position in the center of the ribbon; a orange/red color (■) indicates a state located at the top edge of the ribbon, whereas a blue/violet color (■) indicates a state located at the bottom of the ribbon. Conductances are computed for a finite sample of size $W \times L = 60 \times 30$ sites. Colored arrows indicate the chemical potential of the incoming lead used in the computations of figures 5.3 and 5.4.

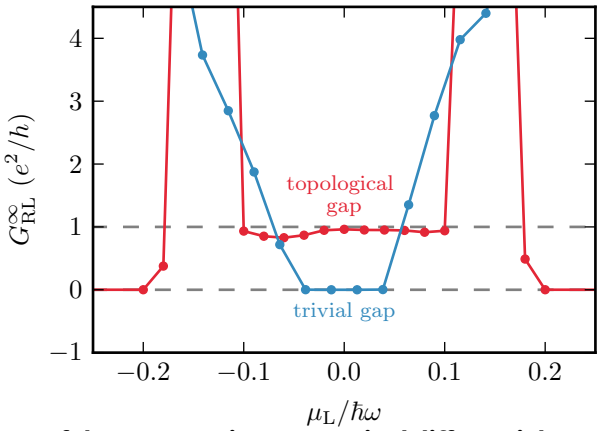

Figure 5.6: Zoom of the asymptotic two-terminal differential conductances. Zoom of figure 5.5: asymptotic two-terminal differential conductance G^{∞}_{RL} in units of e^2/h with respect to the chemical potential of the left lead (black dots and lines) around the quasi-energy gap $\epsilon = 0$ for a trivial (blue) and topological gap (red). The reference energy $\mu_{\mathrm{L}} = 0$ corresponds to an unbiased lead whose chemical potential identifies with the one of the driven system $\mu_{\mathrm{sys}} = 0$. The differential conductance vanishes in the quasi-energy gaps for a trivial spectral gap, but reaches an approximately constant and quantized value $G = e^2/h$ within the topological gap with one chiral edge mode.

is sufficiently close to the spectrum of the isolated infinite strip, and that the differential conductance is an accurate probe of this spectrum for the open system. In the topological case the asymptotic differential conductance remains constant and equal to the number $n = 1$ of edge states (in units of e^2/h) inside the topological gap as shown in figure 5.6. There are small deviations from $G^{\infty}_{\mathrm{RL}} = 1\,e^2/h \equiv G_0$ visible in figure 5.6. More precisely, we find numerically that

$$0.83 \leq G^{\infty}_{\mathrm{RL}}/G_0 \leq 0.96. \tag{5.17}$$

This deviation to exact quantization is attributed to an imperfect transparency of the interface, in a general sense, as discussed in section 4, page 177.

3.3 Multiterminal geometry

A crucial characteristic of the topological edge states associated with a nontrivial W bulk invariant is their chiral nature. To test the chirality of the topological edge states, we have computed differential conductances in a three-terminal geometry shown in figure 5.8, where the width of the contact with the electrodes is $W = 30$ sites, and the total length (between L and R contacts) is 50 sites. This corresponds to all three arms having a length of 10 sites. In this geometry, we monitor the two differential conductances

$$G_{R,T}(E) = -e\,\frac{\mathrm{d}\mathcal{I}_R}{\mathrm{d}\mu_T}\bigg|_{\mu_T=\mu_{\mathrm{sys}}+E} \qquad \text{and} \qquad G_{L,T}(E) = -e\,\frac{\mathrm{d}\mathcal{I}_L}{\mathrm{d}\mu_T}\bigg|_{\mu_T=\mu_{\mathrm{sys}}+E} \tag{5.18}$$

where $\mathcal{I}_{R,L}$ are the average currents leaving the R, L contacts. The chemical potential of the system is still set to $\mu_{\text{sys}} = 0$ (as if imposed e.g. by a backgate).

Again, we first consider the case of a topological gap $\epsilon = 0$ (case (b) of figure 5.5), and we set the chemical potential of the top lead μ_T inside this gap. The time evolution of the differential conductances are shown in figure 5.7: after a transient regime, the differential conductances converge to asymptotic values $G^{\infty}_{\text{LT}} = 0.0002 \pm 0.0001\, e^2/h$ and $G^{\infty}_{\text{RT}} = 0.94 \pm 0.01\, e^2/h$. The value of G^{∞}_{LT} is in agreement with the two terminal results, while the vanishing of G^{∞}_{RT} is in perfect agreement with the chiral nature of the edge state moving clockwise for the chosen parameters.

In contrast, probing the bulk modes by setting the chemical potential inside a bulk Floquet band leads to the behavior displayed in figure 5.8. After a longer transient regime due to slower group velocities, both conductances converge towards large finite values, confirming the absence of chirality for these bulk states.

The spatial structure of Floquet states is shown in insets of figures 5.7 and 5.8, which represent a color map of the local density of states $|\psi(t, x)|^2$ in the (near-) stationary regime. We observe that the topological edge states are indeed localized at the edge, while the bulk states are delocalized in the whole sample. The chiral nature of the states injected in the top lead is clearly apparent and confirms the transport results.

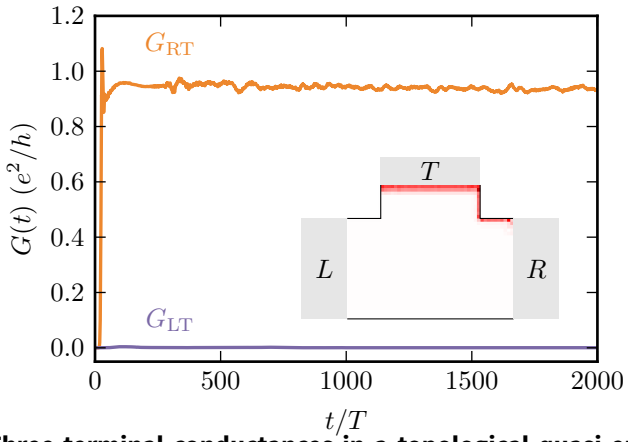

Figure 5.7: Three-terminal conductances in a topological quasi-energy gap. The three-terminal differential conductances G_{LT} (violet) and G_{RT} (orange) are plotted as functions of time for a chemical potential of the top lead in a topological bulk gap ($\mu_{\mathrm{L}}/\hbar\omega = 0.02$). After an initial transient regime, the nonlocal conductances reach asymptotic values $G^{\infty}_{\mathrm{LT}} = 0.0002 \pm 0.0001\, e^2/h$ and $G^{\infty}_{\mathrm{RT}} = 0.94 \pm 0.01\, e^2/h$. The simultaneous vanishing of G^{∞}_{LT} and the quantization of G^{∞}_{RT} to the two-terminal value demonstrates the chiral nature of topological edge states. This is corroborated by the local density of states $|\psi(t,x)|^2$ in the stationary regime (at $t/T = 1000$) shown in inset, which is entirely localized around the $T \to R$ edge, demonstrating furthermore the high transparency of the R contact for this edge mode. Simulations are done with a width of the contacts $W = 30$ sites and a total length of 50 sites.

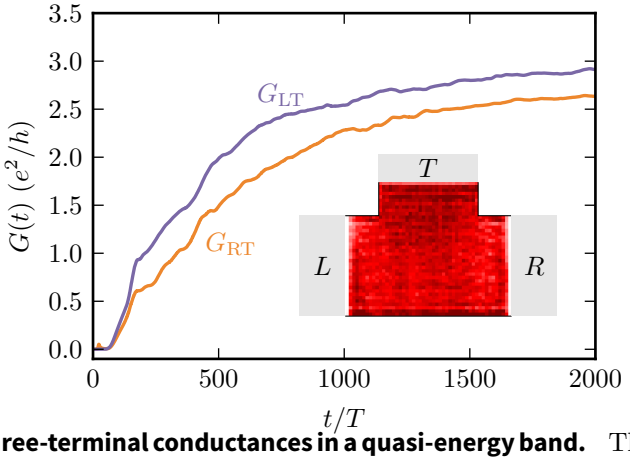

Figure 5.8: Three-terminal conductances in a quasi-energy band. The three-terminal differential conductance G_{LT} (violet) and G_{RT} (orange) are plotted as functions of time for a chemical potential of the top lead in a quasi-energy band ($\mu_{\mathrm{L}}/\hbar\omega = -0.14$). A longer transient regime is observed, in agreement with smaller group velocities than for the edge states, and large asymptotic values for both G_{LT} and G_{RT} are reached, confirming the non-chiral nature of the corresponding Floquet states. The local density of states $|\psi(t,x)|^2$ shown in inset for at $t/T = 1800$ demonstrates the delocalized nature of the Floquet states.

4 Discussion and perspectives

The aim of the current section is three-fold. First, a literature review puts the work presented in this chapter in perspective. In particular, a key point of our study is the use of time-resolved simulations, and in view of the literature, I discuss the advantages of such a method and the perspectives it offers. The deviations (5.17) to exact quantization in presence of topological edge states were initially attributed to the finite dispersion relation of the leads, which does not fully satisfy the wide band approximation and leads to imperfect transparencies of the contacts due to a mismatch between spatial wave functions. However, they may also appear as a more general kind of imperfect transparency, and as a signature of the "photon-inhibited transport" [FP15] requiring a *Floquet sum rule* [KS13; FP15; FP16] on the incoming sidebands to recover quantized conductances. This behavior should depend on the strength on the coupling between the leads and the scattering region, and I present a work in progress towards its understanding.

4.1 Literature review

Several studies on the transport in topological Floquet systems exist, which I will now review.

In condensed matter, the study of Floquet topological systems comes in great part from the study of photoinduced electric properties, starting with Yao, MacDonald and Niu [YMN07] and Oka and Aoki [OA09], who already study transport properties of an illuminated sheet of graphene, in particular to show the existence of a photoinduced DC Hall current.

Kitagawa, Oka, Brataas, Fu and Demler [KOBF11] aim at generalizing the usual approach to transport to Floquet systems. Building on the Floquet scattering formalism (see later), they express (i) a Floquet-Landauer formula and (ii) a Floquet-Fisher-Lee relation relating (a) the average current and conductances to the suitably define transmission coefficients, and (b) the transmission coefficients to the Floquet-Green function of the system of interest. In particular, they show that a gapped effective Hamiltonian should lead to vanishing conductances. Turning to the example of graphene under an off-resonant circularly polarized light of weak intensity, Kitagawa et al. also show, in a high-frequency perturbative expansion close to the Dirac points, that a topological Floquet system displays nearly quantized Hall conductance.

Gu, Fertig, Arovas and Auerbach [GFAA11] consider a ribbon of illuminated graphene connected to symmetrically biased two leads at equilibrium. Through numerical simulations of two-terminal conductance for various ribbon length L, they demonstrate a ballistic behaviour (for large L, the conductance G saturates to a constant value essentially quantized to e^2/h) in presence of topological edge states. On a ribbon with periodic boundary conditions (i.e. a cylinder), where edge states are removed in the direction of transport, they observe for short ribbons a superdiffusive evanescent bulk transport (where $G \sim 1/L^b$ with $b < 1$ instead of $b = 1$) in the quasi-energy gap.

Kundu and Seradjeh [KS13] study a different system: they consider transport in the Floquet generalization [JKAA11] of a one-dimensional Kitaev chain [Kit01], supporting unpaired "Floquet-Majorana fermions" at its ends. Kundu et al. consider a two-terminal setup with symmetric biases $\pm V$ and compute analytically and numerically (with disorder) the corresponding differential conductance $G(V) = \mathrm{d}I/\mathrm{d}V$. They find (i) that $G(0)$ and/or $G(\hbar\omega/2)$ are not quantized in the presence of a Floquet-Majorana mode at the corresponding quasi-energy, but (ii) that the expected quantization is recovered after the application of a "Floquet sum rule" consisting in summing the differential conductances $G(V + n\hbar\omega)$ over all harmonics $n \in \mathbb{Z}$. Notably, this work includes a study of the low-frequency regime.

Foa Torres, Perez-Piskunow, Balseiro and Usaj [TPBU14] consider illuminated graphene, like Gu et al. [GFAA11] and Kitagawa et al. [KOBF11]. The major differences are that Foa Torres et al. [TPBU14] consider (i) a multiterminal setup and (ii) only illuminate a central spot, away of which they smoothly turn off the driving before reaching the leads. Through numerical simulations based on Kwant code [GWAW14], they find that driving-induced topological edge states are not always accompanied by the expected quantized conductances. This discrepancy is attributed to a mismatch between the states in the illuminated spot and the states outside of this spot.

Kundu, Fertig and Seradjeh [KFS14] consider the *bulk* transport in a cylinder of illuminated graphene, at the transition between topologically distinct topological Floquet phases. Through numerical simulations, they observe that in certain cases, the bulk conductivity may be significantly reduced from the expected value of e^2/h due to mismatches between the wave functions of the lead and the wave functions in the illuminated sample. In other cases, the usual value is observed. Notably, they observe that in the situations when there is a mismatch, a small amount of disorder near the leads enhances the bulk conductivity with respect to the clean situations, as it allows a mixing between the mismatched states.

Farrell and Pereg-Barnea [FP16; FP15] use both analytical and numerical computation to show that in Floquet analogues of a two-dimensional QSHE, conductances expected to be quantized to $2e^2/h$ can be significantly smaller, and that a Floquet sum rule similar to the one first proposed by Kundu et al. [KS13], where the differential conductance is summed over the *incoming* sidebands, is necessary to recover the usual conductance quantization. This sum rule is necessary because states coming from the reservoirs do not fully access the Floquet sidebands: only a proportion $\langle u^{(p)} \mid u^{(p)} \rangle$ of the electric flux absorb the right number of photons to populate the sideband p. Through numerical computations, they show that this result still holds in disordered systems. Even if it is not the main focus of their papers, their conclusions also apply to transport Chern insulators, like illuminated graphene.

The global picture emerging from this corpus is that at least in certain situations, instead of a quantized transmission coefficient $T_{\ell,\ell'}(E)$ for energies E in a topological gap, like in equilibrium system, Floquet transmission coefficients are not directly quantized. Instead, a Floquet sum rule [KS13; FP15; FP16] has to be applied, and

the quantity

$$\tilde{T}_{\ell,\ell'}(E) = \sum_{m\in\mathbb{Z}} T_{\ell,\ell'}(E + m\hbar\omega) = \sum_{m,n\in\mathbb{Z}} T^{(n)}_{\ell,\ell'}(E + m\hbar\omega) \tag{5.19}$$

is quantized. When this sum rule is not applied, various kinds of deviations from quantization may be observed, which is consistent with the results of Foa Torres et al. [TPBU14] and Kundu et al. [KFS14]. With a high-frequency off-resonant light of weak amplitude, the conductance is essentially contained in the component $T_{\ell,\ell'}(E)$ corresponding to the incoming sideband $m = 0$, because the scalar products $\langle u^{(0)}_\alpha \mid u^{(0)}_\alpha \rangle$ are very close to the unity, so essentially only one component contributes to the sum (5.19). This corresponds to the situation studied by Kitagawa et al. [KOBF11].

4.2 Why using time-resolved simulations for Floquet transport?

The standard method used in the literature to study transport in periodically driven systems is to fully exploit the time periodicity and Floquet theory to numerically compute e.g. current or differential conductances through the Floquet-Landauer formalism. Obvious advantages of this method is that (i) it is computationally efficient compared to a time-resolved simulation and (ii) it directly includes the time-periodicity, which should help connecting the observable and analytically accessible quantities. However, a time-resolved numerical simulation, despite its numerical cost, also offers several advantages. The first obvious advantage is that transient regimes may be accessed. In our simulations, they are not directly experimentally relevant because transient regimes are not universal. Yet, features like the velocity of a wave packet should be experimentally accessible. The full modelization of the system including such processes is challenging but should be possible.

The robustness to imperfections and disorder is the hallmark of topological states. We therefore expect that e.g. an obstacle at the edge or a small fluctuation of the driving field should not modify the edge states, nor the edge state transport, at least if they do not break the symmetry(ies) protecting the topology. Transport signatures constitute an appropriate platform for the study of disordered Floquet systems, especially with a "disordered" driving field (in amplitude, frequency and/or phase), a situation which explicitly requires time-resolved numerics. In such situations, the definition of bulk invariants – and even of the quasi-energy spectrum – is not straightforward. On the other hand, it is conceptually easy to observe the effect of various kinds of disorder on the transport signatures. However, it may be technically challenging, especially if a large number of disorder realizations are required. Indeed, the effect of disorder on Floquet topological phases is not fully understood. In particular, the effect of an imperfect driving field is only known from experimental observations. The aforementioned transport studies indeed observe that a static disorder do not significantly affect the edge state transport, even though a few peculiar behaviors are observed in the bulk transport. Beyond such observations, there are studies on the control of conductance statistics by an a driving field by Kitagawa et al. [KOD12] and Gopar et al. [GM10], on so-called Floquet-Anderson topological phases by Titum et al. [TLRR15; TBRR16], and on disordered discrete-time quantum walks by

Rakovszky et al. [RA15], Edge et al. [EA15], Gannot [Gan15] and Verga [Ver16]. In particular, Edge et al. and Titum et al. observe transitions which seem to be in the quantum Hall effect universality class, and Rakovszky et al. and Gannot et al explore the interplay with symmetries. Finally, Fleury et al. [FKA15] observe the (lack of) effect of disorder in the phase of the driving field. Another approach is the scattering characterization of Floquet states developed by Fulga et al. [FM16] and Tarasinski et al. [TAD14], which also allows them to study disordered Floquet systems.

Finally, the transport through a system submitted to a time-periodic drive is well-understood in the context of nanostructures like tunnel junctions [KLH05; PA04; TG63], where the driving induces photon-assisted tunneling. Here, the setup is not exactly the same: in contrast with tunnel junctions, the system is not separated from the leads by insulating barriers[(2)]. Hence, the behavior of the interface between the time-dependent scattering region and the time-independent may differ from the known behavior of tunnel junctions. The time-resolved numerical simulations do not require particular assumptions on the interface, and may serve as a way to explore the different regimes through a controlled tight-binding description.

4.3 Floquet sum rule and quantized conductances at strong and weak coupling limits

Starting from the main results of Floquet scattering formalism, namely the Floquet-Landauer and the Floquet-Fisher-Lee formulas, we may hope to understand whether deviations to quantized conductance are to be expected, and if so, what are the physical parameters controlling such deviations. Unfortunately, the Fisher-Lee formula is not straightforwardly applied analytically. In order to obtain a simplified picture containing only the relevant ingredients, I will use several simplifying hypotheses which are not fully justified. The reader is hence advised to proceed with caution with the contents of the current section, which are exploratory.

4.3.1 The case of a static system

As the simplifications that I need are not fully controlled, it is useful to first consider a static system where the physics is well understood. The static system is described by its eigenstates $|\psi_\alpha\rangle$ associated to eigen-energies E_α, and damping rates γ_α. The transmission coefficient(s) of equation (5.113) of appendix B (page 198) is replaced by a single transmission coefficient depending on the injection energy E, expressed as

$$T_{\ell\ell'}(E) = \mathrm{Tr}\left[\sum_\alpha \frac{|\psi_\alpha\rangle\langle\psi_\alpha|}{E-[E_\alpha+\mathrm{i}\hbar\gamma_\alpha]}\Gamma^\ell(E)\sum_\alpha \frac{|\psi_\alpha\rangle\langle\psi_\alpha|}{E-[E_\alpha-\mathrm{i}\hbar\gamma_\alpha]}\Gamma^{\ell'}(E)\right]. \qquad (5.20)$$

For concreteness, focus on the case of Chern insulator with a chiral edge state at zero energy. As long as damping rates are small enough, only the chiral edge state ψ

[(2)] In terms of the quantities introduced in the analysis of appendix B where we follow [KLH05], the coupling Γ to the leads may be of the same order of magnitude (or even greater) than the tight-binding hopping amplitude t inside the scattering region, in contrast with the case of nanostructures where $\Gamma \ll t$, with e.g. typical values of $\Gamma/t = 0.1$ [KLH05].

contributes at $E = 0$, so

$$T_{\ell\ell'}(0) = \frac{1}{\gamma^2}\mathrm{Tr}\left[|\psi\rangle\langle\psi|\,\Gamma^{\ell}(0)\,|\psi\rangle\langle\psi|\,\Gamma^{\ell'}(0)\right]. \tag{5.21}$$

As the trace in this equation is a trace on the interfaces, or equivalently the transverse Hilbert space, we focus on the transverse part of both the coupling coefficients and the eigenstates. First, the state $|\psi\rangle$ is replaced by its transverse component $|\hat{\psi}\rangle$. Second, the coupling operator $\Gamma^{\ell}(0)$ are be replaced by transverse identity operators $\gamma^{\ell}(0)\mathrm{Id}$; this assumes that the interface are transparent enough so the transverse modes of the leads can accurately reconstruct (and host) any transverse mode of the scattering region. Of course, this simplified approach does not account for the chirality of the edge mode (so e.g. in a multiterminal setup, a non-zero quantized $T_{\ell,\ell'}(0) = 1$ should correspond to a vanishing $T_{\ell',\ell}(0) = 0$). The transmission coefficient becomes

$$T_{\ell\ell'}(0) \simeq \frac{\gamma^{\ell}(0)\gamma^{\ell'}(0)}{\gamma^2}\mathrm{Tr}\left[|\hat{\psi}\rangle\langle\hat{\psi}|\,|\hat{\psi}\rangle\langle\hat{\psi}|\right] \simeq \mathrm{Tr}\left[|\hat{\psi}\rangle\langle\hat{\psi}|\,|\hat{\psi}\rangle\langle\hat{\psi}|\right] \tag{5.22}$$

where indeed

$$\mathrm{Tr}\left[|\hat{\psi}\rangle\langle\hat{\psi}|\,|\hat{\psi}\rangle\langle\hat{\psi}|\right] = 1 \tag{5.23}$$

In a situation where ℓ and ℓ' are connected in the right order by a chiral edge state, we indeed expect

$$T_{\ell\ell'}(0) = 1. \tag{5.24}$$

4.3.2 The case of a driven system

We now move on to the case of a driven system, where again we focus on the transverse part of the Floquet sideband modes, and assume a good contact in the wide band limit to replace the coupling operators by transverse identities, so up to a prefactor accounting for the chirality of edge states, the equation (5.113) of appendix B (page 198) becomes

$$T^{(p)}_{\ell\ell'}(E) \simeq \gamma^2 \sum_{\substack{s,\alpha\\ r,\beta}} \frac{\langle \hat{u}^{(p+s)}_{\alpha} \mid \hat{u}^{(p+r)}_{\beta}\rangle\,\langle \hat{u}^{(r)}_{\beta} \mid \hat{u}^{(s)}_{\alpha}\rangle}{\big[E - [\varepsilon_\alpha + s\hbar\omega + \mathrm{i}\hbar\gamma_\alpha]\big]\big[E - [\varepsilon_\beta + r\hbar\omega - \mathrm{i}\hbar\gamma_\beta]\big]}. \tag{5.25}$$

Due to the equation (4.32) (page 116) applied to the first scalar product, the full transmission coefficient summed over *outgoing* sidebands is

$$T_{\ell\ell'}(E) = \sum_{p\in\mathbb{Z}} T^{(p)}_{\ell\ell'}(E) \simeq \sum_{\substack{s,\alpha\\ r,\beta}} \frac{\gamma^2\ \delta_{\alpha,\beta}\delta_{r,s}\,\langle \hat{u}^{(r)}_{\beta} \mid \hat{u}^{(s)}_{\alpha}\rangle}{\big[E - [\varepsilon_\alpha + s\hbar\omega + \mathrm{i}\hbar\gamma_\alpha]\big]\big[E - [\varepsilon_\beta + r\hbar\omega - \mathrm{i}\hbar\gamma_\beta]\big]} \tag{5.26}$$

that is to say

$$T_{\ell\ell'}(E) \simeq \sum_{s,\alpha} \frac{\gamma^2}{\Big[\big(E - (\varepsilon_\alpha + s\hbar\omega)\big)^2 + (\hbar\gamma_\alpha)^2\Big]}\,\langle \hat{u}^{(s)}_{\alpha} \mid \hat{u}^{(s)}_{\alpha}\rangle \tag{5.27}$$

Consider as a "first Floquet zone" that quasi-energies are by convention taken in the range $-\hbar\omega/2 < \varepsilon_\alpha \leq \hbar\omega/2$. The incoming energy E is uniquely written as $E = \varepsilon + n\hbar\omega$ with $-\hbar\omega/2 < \varepsilon \leq \hbar\omega/2$ and $n \in \mathbb{Z}$.

In a regime where the damping rates are small enough such that $\gamma \ll \omega$, only the $n = s$ term contributes (else the Lorentzian peak will be vanishingly small), so

$$T_{\ell\ell'}(\varepsilon + n\hbar\omega) \simeq \sum_\alpha \frac{\gamma^2}{(\varepsilon - \varepsilon_\alpha)^2 + (\hbar\gamma_\alpha)^2} \langle \hat{u}_\alpha^{(n)} \mid \hat{u}_\alpha^{(n)} \rangle \,. \tag{5.28}$$

Here,

$$\langle \hat{u}_\alpha^{(n)} \mid \hat{u}_\alpha^{(n)} \rangle \neq 1 \tag{5.29}$$

in the general case. Instead, Floquet sideband modes satisfy the normalization relation (4.32) (page 116), which is at the origin of the Floquet sum rule introduced by Kundu et al. [KS13] and Farell et al. [FP16], where the transmission coefficients also have to be summed over *incoming* sidebands so that

$$\sum_{n\in\mathbb{Z}} \langle \hat{u}_\alpha^{(n)} \mid \hat{u}_\alpha^{(n)} \rangle = 1 \tag{5.30}$$

Again, the additional prefactors due to the coupling with the leads should balance each other to give a quantized conductance, and we expect

$$\sum_{n\in\mathbb{Z}} T_{\ell\ell'}(\varepsilon - n\hbar\omega) = 1 \tag{5.31}$$

when there is one chiral edge state connecting leads ℓ and ℓ' in the right order.

The condition $\gamma \ll \omega$ corresponds to a **weak coupling** between the scattering region and the leads, which may not be the case. Another interesting regime is a **very strong coupling** regime where $\gamma \gg (2N+1)\omega$ where $2N+1$ is the number of relevant sidebands (with nonvanishing weight). Namely, we assume that N is the smallest integer such that

$$\sum_{-N\leq n\leq N} \langle \hat{u}_\alpha^{(n)} \mid \hat{u}_\alpha^{(n)} \rangle \approx 1 \tag{5.32}$$

I will call the quantity $\Delta_\mathrm{F} = (2N+1)\hbar\omega$ the **Floquet bandwidth**. In this situation, the Lorentzian in equation (5.27) is approximately constant on a range $2N\hbar\omega$, and

$$T_{\ell\ell'}(\varepsilon) \simeq \sum_{-N\leq s\leq N,\alpha} \langle \hat{u}_\alpha^{(s)} \mid \hat{u}_\alpha^{(s)} \rangle \tag{5.33}$$

and equation (5.32) ensures that this last sum is in fact 1.

4.3.3 Summary

To conclude, we identified two particular regimes (see figure 5.9), depending on the strength on the coupling γ between the leads and the scattering region with respect to the driving frequency:

– at weak coupling $\gamma \ll \omega$, a sum rule on incoming energies E has to be applied to the transmission coefficients $T_{\ell\ell'}(E)$ to recover quantized conductance;
– at very strong coupling $\gamma \ggg \omega$, no sum rule is necessary, as the transmission coefficients $T_{\ell\ell'}(E)$ are directly quantized.

More precisely, the very strong coupling regime is only attained when coupling $\hbar\gamma$ is large with respect to the "Floquet bandwidth" Δ_{F} which captures the sidebands with nonvanishing weight. For intermediate couplings, there is a crossover where we expect that neither $T_{\ell\ell'}$ nor the quantity $\tilde{T}_{\ell\ell'}$ obtained by the Floquet sum rule should be quantized.

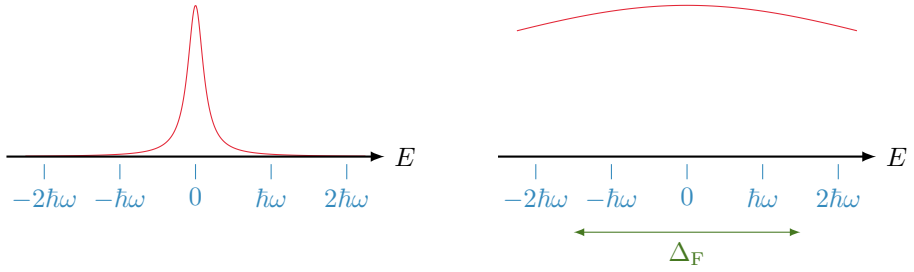

(a) low coupling regime (b) strong coupling regime

Figure 5.9: Strong an weak coupling regimes. In red, the Lorentzian prefactor $(E^2 + \gamma^2)^{-1}$ in the sum appearing in $T_{\ell\ell'}$ is plotted as a function of the argument E. At weak coupling, the Lorentzian is very peaked and selects only one sideband. On the other hand, at strong coupling, the Lorentzian is very large and all relevant sidebands contribute approximately with the same weight.

4.4 Back to numerical data

To elucidate the origin of the deviation (5.17) to exact quantization, we compute the sideband distribution of the topological edge state of figure 5.6. As it crosses $\varepsilon = 0$ at $k = 0$, we focus on the $k_x = 0$ component, where we find that, in a semi-infinite ribbon,

$$\langle u^{(0)} \mid u^{(0)} \rangle \simeq 0.78 \qquad \text{whereas} \qquad \langle u^{(\pm 1)} \mid u^{(\pm 1)} \rangle \simeq 0.11. \tag{5.34}$$

and nearly vanishing components on the other sidebands, see figure 5.10(a). Similar values are found for small but finite values of the longitudinal momentum k_x.

Preliminary results on a situation where two edge states appear in the gap $\varepsilon = \pi$ (for the same undriven Hamiltonian parameters, $\omega = 6.5$ and $F = 5.7$, see the phase diagram of model on the figure 4.8 at page 134) show a lack of quantization of the conductance, which approximately is $G^{\infty}_{\mathrm{RL}}/G_0 \simeq 0.6 \pm 0.1$ inside the topological gap, in contrast with an "expected" value counting the edge states of $G^{\infty}_{\mathrm{RL,cnt}}/G_0 = 2$. Again, we initially attributed this lack of quantization to a mismatch of wavefunctions, possibly related to the spatial structure of the edge modes (located at finite longitudinal momenta $\pm k^0_x$ instead of $k_x = 0$). The numerical computation of the sideband distribution reveals that the component $\langle u^{(0)} \mid u^{(0)} \rangle \simeq 0.11$ (at k^0_x) is very small, as seen

on figure 5.10(b), hinting that the lack of quantization may be attributed to a too weak coupling between the leads and the central region.

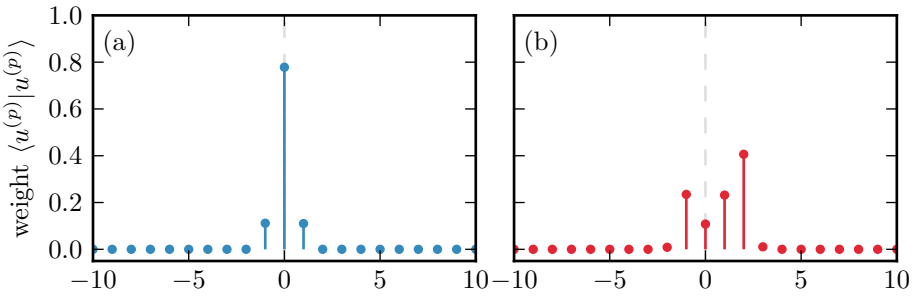

Figure 5.10: Sideband weights of the topological edge state. Sideband weights of the topological edge state(s) of the harmonically-driven half-BHZ model (a) for the parameters of figure 5.5 and (b) for the same undriven Hamiltonian parameters, $\omega = 6.5$ and $F = 5.7$. The weights $\langle u^{(p)}|u^{(p)}\rangle$ are computed on a semi-periodic ribbon of width 20 from a Sambe Hamiltonian truncated to 21 sidebands. The sideband weights sum to unity (as expected, but this property is imposed by the numerical computation here).

Interestingly, we do *not* observe that

$$G_{\mathrm{RL}}^{\infty}/G_0 = \langle u^{(0)} \mid u^{(0)}\rangle \times N_{\mathrm{s}} \tag{5.35}$$

where N_{s} is the number of topological edge states: the numerical values are higher in the two examples at hand. It is adventurous to generalize from such a small sample, but we can observe that in the two examples at hand, we do observe the empirical relation

$$G_{\mathrm{RL}}^{\infty}/G_0 \simeq \left[\langle u^{(0)} \mid u^{(0)}\rangle + \frac{1}{2}\langle u^{(-1)} \mid u^{(-1)}\rangle + \frac{1}{2}\langle u^{(1)} \mid u^{(1)}\rangle\right] \times N_{\mathrm{s}} \tag{5.36}$$

which is a hint that the coupling regime is probably intermediate.

Several steps are missing to fully understand the (lack of) quantization in presence of edge states. First, it is necessary to compute the transmission coefficients $T^{(p)}(E + q\hbar\omega)$ for different injection energies. An important difficulty for such a task is to produce leads with a large enough bandwidth, so that the wide-band approximation is valid. For static systems, this is possible, though not completely trivial and not systematic. In the case of Floquet transport, probing transport at different (incoming) sidebands requires an enormous bandwidth (essentially $N\hbar\omega$, where N is the number of sidebands to probe). Increasing the hopping terms helps to get a large bandwidth, but a too high hopping parameter J_0 also spoils the transparency, at least with a fixed lattice. Using a smaller lattice for the leads may help, but requires to carefully design the interface. Second, a numerical evaluation of the coupling strength γ is required to determine what coupling regime (weak, strong, or intermediate) is relevant in the simulations. Such a numerical evaluation should not pose particular difficulties. Tuning the coupling constant of the numerical simulation from weak to strong coupling

would allow to confirm the simplified picture developed in section 4.3 (at low coupling, a quantized conductance should be recovered after applying a sum rule; in contrast, in the strong coupling regime, the conductance should be directly quantized).

5 Conclusion and perspectives

The original motivations for this work were to set ground for time-resolved transport simulations of Floquet systems, which should allow to study such systems with defects and disorder, and in particular with imperfections in the driving. From the conceptual point of view, this is an easy task. However, a proper analysis of disordered systems requires averages on a large number of disordered configurations (e.g. to access level spacing or conductance statistics), and at the moment the numerical cost of time-resolved simulations is prohibitive. They may become possible in near future thanks to refined algorithms and/or smaller systems (if we manage to obtain good transparency even at small widths).

It appears that a preliminary task is to fully understand the interface between the driven scattering region and the static lead in the relevant context. All the framework of Floquet scattering has already been developed to study phenomena like photon-assisted tunneling [TG63; PA04; KLH05], but it is not clear whether the regime should be the same to probe topological edge states. In particular, it is not clear whether the "Floquet sum rule" should be valid in all regimes, or only for a tunnel interface i.e. for a low coupling between the system and the leads. Understanding the different coupling regimes and their consequences on transport signatures of topological Floquet states is a necessary first step. Another important question that we did not address is to what extent the driving field leaks in the leads. Experimentally, it is not reasonable to expect the driving field to switch from zero to a large finite amplitude on the length scale of one lattice spacing. We may either assume that only a part of the *sample* is submitted to the driving field (e.g. a laser spot): this is the route taken by Foa Torres, et al. [TPBU14]. This setup is questionable when the undriven system is an insulator: outside of the illuminated spot, we expect the system to be insulating, which should prevent the observation of any interesting feature if the undriven region is too large (note however that this setup would be similar to a tunnel junction). Another possibility is to consider a decreasing driving field inside the leads. This kind of setup is more controlled: it is reasonable to expect that the lead will remain conducting even under the driving field, and it is possible to ensure that it is the case. Here, the behavior of the lead and of the scattering region can be understood and controlled separately. In such a setup, the lead will also develop Floquet sidebands (similar to the Floquet/Volkov states in time-resolved ARPES measurements, see paragraph 1.4.1 of the Introduction, page 25), which complicates the analysis.

Despite such difficulties, transport measurements are a promising way to probe and understand topological Floquet states in electronic systems. Even if the experimental technology is not yet ready to realize and probe such electronic Floquet systems, transport simulations may be in the near future a good *numerical* tool to understand the robustness of Floquet states to various perturbations.

Appendix A – Floquet theory with a self-energy term

To describe transport properties, we need to consider a system connected to leads. An accurate description should take into account the (quantum) degrees of freedom of the reservoirs, and the system of interest should be treated as a subsystem described by a partial density operator. Despite several studies (see the general introduction, paragraph 1.4.1, page 25) in this direction, the description (and the fate) of topological properties of Floquet systems in such a situation is not known at the moment. However, from physical grounds and by analogy with experimental situations outside of the electronic solid state realm, we expect that an effective description of the coupling with the leads should, to an extent, leave topological properties unharmed. Hence, we will assume that the elimination of the degrees of freedom of the environment can be taken into account by adding a non-hermitian self-energy term in the Hamiltonian. It is the case in the wide-band limit (see paragraph B.2.3, page 196), where the coupling to the leads do not depend on energy, $\Gamma(E) \simeq \Gamma$, and gives rise to the anti-Hermitian term $\Sigma = \mathrm{i}\Gamma$. Such a self-energy broadens the Floquet levels by giving the corresponding Floquet eigenstates a finite lifetime. Indeed, the self-energy may also contain other sources of broadening, but we assume that the coupling to the leads is the dominant source of dissipation.

Hence, we are left with a time-dependent Schrödinger equation

$$\mathrm{i}\hbar\frac{\mathrm{d}}{\mathrm{d}t}\left|\psi(t)\right\rangle = \left(H(t) - \mathrm{i}\Sigma\right)\left|\psi(t)\right\rangle, \tag{5.37}$$

with a time-periodic Hamiltonian $H(t+T) = H(t)$ and an Hermitian self-energy term Σ. The corresponding evolution operator $U(t,t')$ is not unitary anymore, but we will assume that it is always invertible and diagonalisable. A few amendments have to be made to the usual Floquet theory in this case: as $U(T)$ is not necessarily unitary, the spectral theorem do not apply. However, we have assumed that it is diagonalizable, so there is a bi-orthonormal basis of left- and right-eigenstates $\langle\tilde{\phi}_\alpha|$ and $|\phi_\alpha\rangle$ such that

$$\begin{aligned} U(T)\left|\phi_\alpha\right\rangle &= \lambda_\alpha\left|\phi_\alpha\right\rangle \\ \langle\tilde{\phi}_\alpha|U(T) &= \langle\tilde{\phi}_\alpha|\,\lambda_\alpha \end{aligned} \tag{5.38}$$

and

$$\langle\tilde{\phi}_\alpha \mid \phi_\beta\rangle = \delta_{\alpha\beta} \qquad \text{and} \qquad \sum_\alpha \left|\phi_\alpha\right\rangle\langle\tilde{\phi}_\alpha| = \mathrm{Id}. \tag{5.39}$$

The corresponding eigenvalues are written as

$$\lambda_\alpha = \exp\left[-\mathrm{i}\left(\frac{\varepsilon_\alpha}{\hbar} - \mathrm{i}\gamma_\alpha\right)T\right]. \tag{5.40}$$

In this appendix, the eigenvalues λ_α are called the *Floquet eigenvalues*, the quantities ε_α are the *quasi-energies* and γ_α the *Floquet inverse lifetimes* or *damping rates*.

Essentially, all Floquet theory can be translated in this situation by replacing the bras $\langle\phi_\alpha|$ by the proper left-eigenstates $\langle\tilde{\phi}_\alpha|$. Indeed, they coincide when $\Sigma = 0$. In particular, there are left and right Floquet modes

$$\left|u_\alpha(t)\right\rangle = \exp\left[\mathrm{i}\left(\frac{\varepsilon_\alpha}{\hbar} - \mathrm{i}\gamma_\alpha\right)t\right]\left|\psi_\alpha(t)\right\rangle = \left|u_\alpha(t+T)\right\rangle, \tag{5.41}$$

and

$$\langle \tilde{u}_\alpha(t)| = \langle \tilde{\psi}_\alpha(t)| \exp\left[-\mathrm{i}\left(\frac{\varepsilon_\alpha}{\hbar} - \mathrm{i}\gamma_\alpha\right) t\right] = \langle \tilde{u}_\alpha(t+T)| \tag{5.42}$$

which are decomposed in Fourier series as left- and right-sideband modes $|u_\alpha^{(p)}\rangle$ and $\langle \tilde{u}_\alpha^{(p)}|$ (see the section 2.2 of chapter 4 for the detailed standard case, page 2.2).

The evolution operator can therefore be expanded as

$$U(t,t') = \sum_\alpha \exp\left[-\mathrm{i}\left(\frac{\varepsilon_\alpha}{\hbar} - \mathrm{i}\gamma_\alpha\right)(t-t')\right] |u_\alpha(t)\rangle \langle \tilde{u}_\alpha(t')| \,. \tag{5.43}$$

where the time-periodic part containing Floquet modes describes the short time-scale dynamics, whereas the exponentials containing quasi-energies ε_α and inverse lifetimes γ_α of Floquet modes describe the long time-scale dynamics. Indeed, this expression can be further expanded in terms of the Fourier modes of the Floquet modes (the Floquet sidebands) as

$$U(t,t') = \sum_\alpha \sum_{p,p'\in\mathbb{Z}} \exp\left[-\mathrm{i}\left(\frac{\varepsilon_\alpha}{\hbar} - \mathrm{i}\gamma_\alpha\right)(t-t') - \mathrm{i}\omega(pt - p't')\right] |u_\alpha^{(p)}\rangle \langle \tilde{u}_\alpha^{(p')}| \,. \tag{5.44}$$

Appendix B – Floquet scattering formalism: computation of the transmission coefficients

In the following section, we adapt the approach of Kohler, Lehmann and Hänggi [KLH05] to describe the scattering through a two-dimensional driven system connected to electronic reservoirs, such as the example depicted in the figure 5.1. We follow closely the approach of [KLH05], with notable differences only due to the geometry of the system.

B.1 Description of the setup

We consider a system composed of a central *scattering region* $\mathcal{R}$, which constitutes the system of interest, connected through several semi-infinite leads to electronic reservoirs at equilibrium, with fixed chemical potential and temperature (the temperature will be assumed to be zero in the following). The scattering region is described by a (periodic) time-dependent tight-binding Hamiltonian

$$H_{\mathrm{sys}} = \sum_{nn'\in\mathcal{R}} H_{nn'}(t) c_n^\dagger c_{n'} \qquad \text{with} \qquad H_{nn'}(t+T) = H_{nn'}(t). \tag{5.45}$$

Here, c_n is the annihilation operator of an electron in the localized state n, and the index n takes into account the position in the Bravais lattice as well as internal degrees of freedom (sublattice, spin, orbital, etc.)

A number N_{leads} of semi-infinite leads are connected to this system by ideal contacts. Wave functions in the semi-infinite lead are assumed to read

$$\psi_{\alpha q}(x,y) = \frac{1}{\sqrt{L}} \mathrm{e}^{-\mathrm{i}qx} \chi_\alpha(y) \tag{5.46}$$

where $x = 0$ corresponds to the interface with the system and where the **transverse modes** $|\chi\rangle$ are assumed to not depend on the longitudinal momentum q, and to form an orthonormal basis of the

$$\sum_{\alpha} |\chi_\alpha\rangle\langle\chi_\alpha| = \mathrm{Id}_{\mathrm{transverse}}. \tag{5.47}$$

Incoming and outgoing modes are distinguished by, respectively, $\vec{q} \cdot \vec{n} < 0$ and $\vec{q} \cdot \vec{n} < 0$, where $\vec{n}$ is the normal to the interface, defined as going out of the scattering region. Incoming and outgoing modes have a well-defined energy given by a dispersion relation of the form $E_{\ell\alpha q}$. The leads are described by the Hamiltonian

$$H_{\mathrm{leads}} = \sum_{\ell=1}^{N_{\mathrm{leads}}} \sum_{\alpha,q} E_{\ell\alpha q} c^\dagger_{\ell\alpha q} c_{\ell\alpha q}. \tag{5.48}$$

where α label the transverse modes of the semi-infinite lead and q the longitudinal momentum.

The annihilation operator of a state localized in a lead at position (x, y) is

$$c_\ell(x, y) = \sum_{\alpha,q} c_{\ell\alpha q} \chi^*_{\ell\alpha q}(y) \mathrm{e}^{\mathrm{i}qx}. \tag{5.49}$$

At the interface with the scattering region where $x = 0$, we consider

$$c_{\ell,n} = c_\ell(x = 0, y = y_{\ell,n}) = \sum_{\alpha,q} c_{\ell\alpha q} \chi^*_{\ell\alpha q}(y_{\ell,n}) \tag{5.50}$$

where $y_{\ell,n}$ is the transverse position of the site n at the interface with lead ℓ. It is more convenient to forget about internal degrees of freedom in the leads. Taking them into account can easily be achieved by separating each lead and reservoir into sub-leads and sub-reservoirs, each of which accounts for an internal degree of freedom. The contacts between the leads and the scattering region are then described by the Hamiltonian

$$H_{\mathrm{contacts}} = \sum_{\ell=1}^{N_{\mathrm{leads}}} \sum_{n \in \mathcal{I}_\ell} V_\ell c^\dagger_{\ell,n} c_n + \mathrm{h.c.} \tag{5.51}$$

where $\mathcal{I}_\ell$ is the set of all sites of the scattering region which are located at the interface with the lead ℓ. To simplify, we will assume that the hopping term V_ℓ does not depend on the site n. In terms of the transverse modes ladder operators, the contact Hamiltonian reads

$$H_{\mathrm{contacts}} = \sum_{\ell=1}^{N_{\mathrm{leads}}} \sum_{n \in \mathcal{I}_\ell} \sum_{\alpha,q} V_\ell \chi^*_{\ell\alpha}(y_{\ell,n}) c^\dagger_{\ell\alpha q} c_n + \mathrm{h.c.}. \tag{5.52}$$

Following Kohler et al. [KLH05] (and before them Jauho et al. [JWM94]), we assume that at an initial time t_0, far in the past, leads are at equilibrium at temperature T and chemical potential μ_ℓ. We may adopt the full Landauer-Büttiker setup and assume that the leads are at equilibrium with the reservoirs, in a grand-canonical

situation, or rather assume that they are large enough to act as their own reservoirs. In both cases, the leads are described at time t_0 by the density operator

$$\rho_0 \propto \mathrm{e}^{-\beta(H_{\text{leads}} - \sum_\ell \mu_\ell N_\ell)} \tag{5.53}$$

where $\beta = 1/kT$, where k is Boltzmann constant, and where the operator

$$N_\ell = \sum_{\alpha q} c^\dagger_{\ell\alpha q} c_{\ell\alpha q} \tag{5.54}$$

describes the number of electrons in the lead. The current operator going in (or out of) the lead will be computed as the change in N_ℓ, so a lead with a finite number of electrons is required and it is not possible to assume the leads to be strictly at equilibrium at all times. The average with respect to this density operator is defined as

$$\langle A \rangle_0 = \mathrm{tr}(\rho_0 A) \tag{5.55}$$

and is determined by

$$\langle c^\dagger_{\ell'\alpha q} c_{\ell\alpha q} \rangle_0 = f_\ell(E_{\ell\alpha q}) \delta_{\ell\ell'} \tag{5.56}$$

where again,

$$f_\ell(E) = \frac{1}{1 + \mathrm{e}^{\beta(E-\mu_\ell)}} \tag{5.57}$$

is the Fermi-Dirac distribution function of the reservoir ℓ.

B.2 Computation of the currents

In this paragraph, we seek to compute the operator describing the net current going out of the lead ℓ (and into the central region), defined as

$$I_\ell(t) = -\frac{\mathrm{i}(-e)}{\hbar} \left[H(t), N_\ell \right], \tag{5.58}$$

in terms of the transmission coefficients (which shall be defined later), and to express the transmission coefficients in terms of the Green function of the scattering region. This Green function, where the presence of the reservoirs is taken into account as a purely imaginary self-energy term, will be decomposed in Fourier harmonics, the *Green-Floquet functions*, which correspond to the sidebands of the periodically driven system, i.e. to the transport processes with a fixed number of absorptions/emissions of the driving field quanta. This descriptions allows to relate the transport processes and the spectrum of the Floquet operator $U(T)$ (or equivalently of the Sambe Hamiltonian, see section 2.2.5 of chapter 4, page 117).

The first step is to describe the dynamics of the system in a way which enables to trace out the reservoirs' degrees of freedom to end up with a set of Heisenberg equation of motion for the scattering region only, and which only depends on the initial equilibrium distribution functions of the leads. In a second time, the equations of motions are formally solved by Green functions, which enables to obtain a compact expression for the currents.

The Heisenberg equations of motion for the annihilation operators in the leads are

$$\frac{\mathrm{d}c_{\ell\alpha q}}{\mathrm{d}t} = \frac{\partial c_{\ell\alpha q}}{\partial t} + \frac{1}{\mathrm{i}\hbar}\left[c_{\ell\alpha q}, H(t)\right] = \frac{1}{\mathrm{i}\hbar}\left[c_{\ell\alpha q}, H_{\text{leads}} + H_{\text{contacts}}\right] \tag{5.59}$$

rewritten from (5.52) as

$$\frac{\mathrm{d}c_{\ell\alpha q}}{\mathrm{d}t} = \frac{1}{\mathrm{i}\hbar}\left(E_{\ell\alpha q}c_{\ell\alpha q} + \sum_{n\in\mathcal{I}_\ell} V_\ell \chi^*_{\ell\alpha}(n) c_n\right). \tag{5.60}$$

This equation is integrated as

$$c_{\ell\alpha q}(t) = c_{\ell\alpha q}(t_0)\mathrm{e}^{-\mathrm{i}E_{\ell\alpha q}(t-t_0)/\hbar} + \sum_{n\in\mathcal{I}_\ell} \frac{V_\ell \chi^*_{\ell\alpha}(n)}{\mathrm{i}\hbar} \int_0^{t-t_0} \mathrm{d}\tau\ \mathrm{e}^{-\mathrm{i}E_{\ell\alpha q}\tau/\hbar}\, c_n(t-\tau). \tag{5.61}$$

Similarly, the Heisenberg equations of motion for the annihilation operators in the scattering region are

$$\frac{\mathrm{d}c_n}{\mathrm{d}t} = \frac{1}{\mathrm{i}\hbar}\left[c_n, H_{\text{sys}} + H_{\text{contacts}}\right], \tag{5.62}$$

which can be rewritten as

$$\frac{\mathrm{d}c_n}{\mathrm{d}t} = \frac{1}{\mathrm{i}\hbar}\sum_{n'} H_{nn'}(t)c_{n'}(t) + \frac{1}{\mathrm{i}\hbar}\sum_{\ell=1}^{N_{\text{leads}}} [n\in\mathcal{I}_\ell]\sum_{\alpha q} V^*_\ell \chi_{\ell\alpha q}(y_{\ell,n})c_{\ell\alpha q}(t) \tag{5.63}$$

where $[P]$ is the Iverson bracket, defined for a proposition P as $[P] = 1$ when P is true and $[P] = 0$ when P is false.

Using the integrated expression 5.61 for the ladder operators in the leads, this yields

$$\begin{aligned}\frac{\mathrm{d}c_n}{\mathrm{d}t} =& \frac{1}{\mathrm{i}\hbar}\sum_{n'} H_{nn'}(t)c_{n'}(t) + \sum_{\ell=1}^{N_{\text{leads}}} [n\in\mathcal{I}_\ell]\,\xi^\ell_n(t) \\ &- \frac{1}{\hbar}\sum_{\ell=1}^{N_{\text{leads}}} [n\in\mathcal{I}_\ell] \sum_{n'\in\mathcal{I}_\ell}\int_0^\infty \mathrm{d}\tau \Gamma^\ell_{nn'}(\tau)c_{n'}(t-\tau)\end{aligned} \tag{5.64}$$

with

$$\Gamma_\ell(t) = \frac{|V_\ell|^2}{\hbar}\sum_{\alpha q} |\chi_\alpha\rangle\langle\chi_\alpha|\,\mathrm{e}^{-\mathrm{i}E_{\ell\alpha q}t/\hbar} \tag{5.65}$$

and

$$\xi^\ell_n(t) = \frac{V^*_\ell}{\mathrm{i}\hbar}\sum_{\alpha q}\chi_{\ell\alpha}(n)\mathrm{e}^{-\mathrm{i}E_{\ell\alpha q}(t-t_0)}c_{\ell\alpha q}(t_0). \tag{5.66}$$

The response function $\Gamma_\ell(t)$ of the lead is related by a Fourier transform to its spectral density

$$\Gamma_\ell(E) = 2\pi\sum_{\alpha q}|V_\ell|^2\,|\chi_\alpha\rangle\langle\chi_\alpha|\,\delta(E - E_{\ell\alpha q}). \tag{5.67}$$

The noise operator $\xi^\ell(t)$ in the equation of motion takes into account the coupling with the leads initially at equilibrium, and is fully determined by the average values (with respect to the initial density operator ρ_0)

$$\langle \xi_n^\ell(t) \rangle_0 = 0 \tag{5.68}$$

and

$$\begin{aligned} \langle [\xi_{n'}^{\ell'}(t')]^\dagger \xi_n^\ell(t) \rangle_0 &= \frac{1}{\hbar^2} \delta_{\ell\ell'} \sum_{q\alpha} |V_\ell|^2 \, \mathrm{e}^{-\mathrm{i}E_{\ell q\alpha}(t-t')/\hbar} \chi_{\ell\alpha}^*(n') \chi_{\ell\alpha}(n) f_\ell(E) \\ &= \delta_{\ell\ell'} \int \frac{\mathrm{d}E}{2\pi\hbar^2} \mathrm{e}^{-\mathrm{i}E(t-t')/\hbar} \Gamma_{nn'}^\ell(E) f_\ell(E). \end{aligned} \tag{5.69}$$

In other words, it is a delta-correlated Gaussian noise, similar to a Langevin fluctuating force, which is determined by the (equilibrium) statistics of the leads at time t_0. The other expectation values, if required, can be computed thanks to Wick theorem applied to the ladder operator at t_0. Through a Fourier transform of the noise operator

$$\xi_n^\ell(E) = \int \mathrm{d}t \, \mathrm{e}^{\mathrm{i}Et/\hbar} \, \xi_n^\ell(t) \qquad \text{i.e.} \qquad \xi_n^\ell(t) = \frac{1}{h} \int \mathrm{d}t \, \mathrm{e}^{-\mathrm{i}Et/\hbar} \, \xi_n^\ell(E) \tag{5.70}$$

this set of average values is simply expressed as

$$\langle \xi_n^\ell(E) \rangle_0 = 0 \quad \text{and} \quad \langle [\xi_{n'}^{\ell'}(E')]^\dagger \xi_n^\ell(E) \rangle_0 = 2\pi\delta_{\ell\ell'} \Gamma_{nn'}^\ell(E) f_\ell(E) \delta(E - E'). \tag{5.71}$$

The correlation function is related to the spectral distribution Γ^ℓ and to the equilibrium Fermi-Dirac distribution of the lead.

B.2.1 Floquet-Green functions

It is possible to formally solve the set of Heisenberg equations of motions for the annihilation operators in the scattering region through the retarded Green function of the system. In this approach, the coupling to the leads appears both *in* the equation of motion of the Green function through the response function and as a source of this equation through the noise operator[3]. First, the retarded Green function is solution of an integro-differential equation corresponding to the Heisenberg equations (5.64), which in the limit $t_0 \to \infty$ reads

$$\left(\mathrm{i}\hbar \frac{\mathrm{d}}{\mathrm{d}t} - H_{\mathrm{sys}}(t) \right) G(t, t') + \mathrm{i} \int_0^{t-t_0} \mathrm{d}\tau \, \Gamma(\tau) G(t - \tau, t') = \delta(t - t') \tag{5.72}$$

where we defined

$$\Gamma(t) = \sum_{\ell=1}^{N_{\mathrm{leads}}} \Gamma_\ell(t) \tag{5.73}$$

[3] Again, this is similar to what happens in a Langevin equation

$$m \frac{\mathrm{d}v}{\mathrm{d}t} = -m\gamma v + \xi(t) \qquad \text{or} \qquad m \frac{\mathrm{d}v}{\mathrm{d}t} + m\gamma v = \xi(t)$$

where the coupling to the fluid appears both in the viscous drag force $-m\gamma v$ and in the random Langevin force $\xi(t)$. In the electronic problem, the viscous damping is replaced by a self-energy term (contained in the response functions Γ^ℓ) and the Langevin force is replaced by the noise operators of the leads $\xi_\ell(E)$.

It is convenient to use the mixed time-energy representation defined by the Fourier transform

$$G(t,E) = \int \mathrm{d}\tau\ \mathrm{e}^{\mathrm{i}E\tau/\hbar} G(t, t-\tau). \tag{5.74}$$

The retarded Green function is related to the evolution operator $U(t,t')$ of the scattering region through

$$G(t,t') = \frac{1}{\mathrm{i}\hbar} U(t,t')\Theta(t-t'). \tag{5.75}$$

Due to the time-periodicity of the driving field, we have $U(t+T,t'+T) = U(t,t')$, so mixed time-energy Green functions are also time-periodic,

$$G(t+T,E) = G(t,E). \tag{5.76}$$

Hence, it is possible to Fourier transform them to define **Green-Floquet functions**

$$G^{(p)}(E) = \frac{1}{T}\int_0^T \mathrm{d}t\ \mathrm{e}^{\mathrm{i}p\omega t}\, G(t,E) \tag{5.77}$$

which describe the propagation of an electron with initial (injection) energy E absorbing (when $p>0$) or emitting (when $p<0$) $|p|$ photons[(4)].

Finally, the solutions to the Heisenberg equations of motion for annihilation operator of the scattering region read

$$c_n(t) = \mathrm{i}\hbar \sum_{\ell=1}^{N_{\mathrm{leads}}} \sum_{m\in\mathcal{I}_\ell} \int_0^\infty \mathrm{d}\tau\ G_{nm}(t,t-\tau)\, \xi_m^\ell(t-\tau) \tag{5.78}$$

where

$$G_{nm}(t,t-\tau) = \langle n \mid G(t,t-\tau) \mid m\rangle\,. \tag{5.79}$$

are the matrix elements of the Green function. Alternatively, in terms of the mixed time-energy Green function (with similarly defined matrix elements), they read

$$c_n(t) = \frac{\mathrm{i}}{2\pi} \sum_\ell \sum_{m\in\mathcal{I}_\ell} \int \mathrm{d}E\ \mathrm{e}^{-\mathrm{i}Et/\hbar}\, G_{nm}(t,E)\, \xi_m^\ell(E). \tag{5.80}$$

B.2.2 Current

The current going out of the lead ℓ into the scattering region is computed as the variation in time of the number of electrons in the lead

$$I_\ell(t) = \frac{-e}{\mathrm{i}\hbar}\,[H(t), N_\ell] = \frac{-e}{\mathrm{i}\hbar}\,[H_{\mathrm{contacts}}, N_\ell]\,, \tag{5.81}$$

that is

$$I_\ell(t) = \frac{-e}{\mathrm{i}\hbar} \sum_{n\in\mathcal{I}_\ell} \sum_q V_\ell c^\dagger_{\ell q\alpha}(t) c_n(t) + \mathrm{h.c.}. \tag{5.82}$$

(4) It is usual to call "photons" the quanta of the time-periodic driving field, even if it is not an electromagnetic field.

Using equations (5.61) and the definitions (5.65) and (5.66), the current operator is expressed as

$$I_\ell = -e\left(\sum_{n\in\mathcal{I}_\ell} c_n^\dagger(t)\xi_n^\ell(t) + \text{h.c.}\right) + \frac{e}{\hbar}\left(\sum_{m,n\in\mathcal{I}_\ell}\int_0^{t-t_0} \mathrm{d}\tau\; c_n^\dagger(t)\Gamma_{nm}^\ell(\tau)c_m(t-\tau) + \text{h.c.}\right) \tag{5.83}$$

The average current (with respect to the initial equilibrium distribution) $\langle I_\ell(t)\rangle_0$ can be expressed using the expressions (5.80) of the annihilation operators in the scattering region in terms of the Green functions as

$$\begin{aligned}\langle I_\ell(t)\rangle_0 = {}& \frac{\mathrm{i}e}{2\pi h}\sum_{\ell'=1}^{N_{\text{leads}}}\sum_{\substack{n\in\mathcal{I}_\ell\\ m\in\mathcal{I}_{\ell'}}}\int \mathrm{d}E\mathrm{d}E'\,\left[\mathrm{e}^{\mathrm{i}(E'-E)t}G_{nm}^*(t,E')\,\langle[\xi_m^{\ell'}(E')]^\dagger\xi_n^\ell(E)\rangle - \mathrm{e}^{-\mathrm{i}(E'-E)t}G_{nm}(t,E')\,\langle[\xi_n^{\ell'}(E')]^\dagger\xi_m^\ell(E)\rangle\,\right]\\ &+\frac{e}{2\pi h}\Big[\sum_{\ell',\ell''=1}^{N_{\text{leads}}}\sum_{\substack{n,m\in\mathcal{I}_\ell\\ n'\in\mathcal{I}_{\ell'}\\ m''\in\mathcal{I}_{\ell''}}}\int_0^{t-t_0}\mathrm{d}\tau\int\mathrm{d}E'\mathrm{d}E''\;\mathrm{e}^{\mathrm{i}E't/\hbar}\mathrm{e}^{-\mathrm{i}E''(t-\tau)/\hbar}G_{nn'}^*(t,E')\Gamma_\ell(\tau)G_{mm''}(t-\tau,E'')\,\langle[\xi_{n'}^{\ell'}(E')]^\dagger\xi_{m''}^{\ell''}(E'')\rangle + \text{c.c.}\Big]\end{aligned} \tag{5.84}$$

which becomes after replacing the average values (5.71) with their expressions and reindexing,

$$\begin{aligned}\langle I_\ell(t)\rangle_0 = {}& \frac{\mathrm{i}e}{h}\sum_{n,m\in\mathcal{I}_\ell}\int\mathrm{d}E\;\left(G_{nm}^*(t,E) - G_{mn}(t,E)\right)\Gamma_{nm}^\ell(E)f_\ell(E)\\ &+\frac{e}{h}\left(\sum_{\ell'=1}^{N_{\text{leads}}}\sum_{\substack{n,m\in\mathcal{I}_\ell\\ n',m'\in\mathcal{I}_{\ell'}}}\int\mathrm{d}E\;\int_0^{t-t_0}\mathrm{d}\tau\;\mathrm{e}^{\mathrm{i}E\tau/\hbar}G_{nn'}^*(t,E)\Gamma_{nm}^\ell(\tau)G_{mm'}(t-\tau,E)\Gamma_{m'n'}^{\ell'}(E)f_{\ell'}(E) + \text{c.c.}\right).\end{aligned} \tag{5.85}$$

A crucial technical point of the method of Kohler et al. [KLH05] enables to express the current in the standard scattering form by replacing the backscattering terms in its expression. Using the matrix elements between $\langle m|$ and $|n\rangle$ of the relation (38) of reference [KLH05] (the demonstration of this relation is exactly the same in our case), with $E = E'$ and after inserting closure

relations of $\mathrm{Id}_{\mathrm{transverse}}$ on each side of $\Gamma(\tau)$, we obtain the relation

$$G^*_{nm}(t,E) - G_{mn}(t,E) = \mathrm{i}\hbar \frac{\mathrm{d}}{\mathrm{d}t}\left(\sum_{r\in\mathcal{R}} G^*_{rm}(t,E)G_{rn}(t,E)\right) + 2\mathrm{i}\,\mathrm{Re}\left[\int_0^{t-t_0} \mathrm{d}\tau\ \mathrm{e}^{\mathrm{i}E\tau/\hbar} \sum_{\ell=1}^{N_{\mathrm{leads}}} \sum_{n_\ell, m_\ell \in \mathcal{I}_\ell} G^*_{m_\ell m}(t,E)\Gamma^\ell_{m_\ell n_\ell}(\tau) G_{n_\ell n}(t-\tau,E)\right] \tag{5.86}$$

This identity allows to replace backscattering terms in the current, and we obtain

$$\begin{aligned}
\langle I_\ell(t)\rangle_0 = {} & \frac{-e}{2\pi} \sum_{n,m\in\mathcal{I}_\ell} \int \mathrm{d}E\ \frac{\mathrm{d}}{\mathrm{d}t}\left(\sum_{r\in\mathcal{R}} G^*_{rm}(t,E)G_{rn}(t,E)\right)\Gamma^\ell_{nm}(E) f_\ell(E) \\
& - \frac{2e}{h}\,\mathrm{Re}\left[\int \mathrm{d}E\ \int_0^{t-t_0} \mathrm{d}\tau\ \mathrm{e}^{\mathrm{i}E\tau/\hbar} \sum_{\ell'=1}^{N_{\mathrm{leads}}} \sum_{\substack{n,m\in\mathcal{I}_\ell \\ n',m'\in\mathcal{I}_{\ell'}}} G^*_{m'm}(t,E)\Gamma^{\ell'}_{m'n'}(\tau) G_{n'n}(t-\tau,E)\Gamma^\ell_{nm}(E) f_\ell(E)\right] \\
& + \frac{2e}{h}\,\mathrm{Re}\left[\int \mathrm{d}E\ \int_0^{t-t_0} \mathrm{d}\tau\ \mathrm{e}^{\mathrm{i}E\tau/\hbar} \sum_{\ell'=1}^{N_{\mathrm{leads}}} \sum_{\substack{m,n\in\mathcal{I}_\ell \\ m',n'\in\mathcal{I}_{\ell'}}} G^*_{mm'}(t,E)\Gamma^\ell_{mn}(\tau) G_{nn'}(t-\tau,E)\Gamma^{\ell'}_{n'm'}(E) f_{\ell'}(E)\right]
\end{aligned} \tag{5.87}$$

which can be cast into the **scattering form**

$$\langle I_\ell(t)\rangle_0 = \frac{e}{h}\int \mathrm{d}E\ \left[\sum_{\ell'\neq\ell} T_{\ell\ell'}(E,t) f_{\ell'}(E) - \sum_{\ell'\neq\ell} T_{\ell'\ell}(E,t) f_\ell(E)\right] - \frac{\mathrm{d}q_\ell}{\mathrm{d}t} \tag{5.88}$$

where the **transmission coefficients** are

$$T_{\ell\ell'}(E,t) = 2\,\mathrm{Re}\left[\int_0^{t-t_0} \mathrm{d}\tau\ \mathrm{e}^{\mathrm{i}E\tau/\hbar} \sum_{\substack{m,n\in\mathcal{I}_\ell \\ m',n'\in\mathcal{I}_{\ell'}}} G^*_{mm'}(t,E)\Gamma^\ell_{mn}(\tau) G_{nn'}(t-\tau,E)\Gamma^{\ell'}_{n'm'}(E)\right] \tag{5.89}$$

and where

$$q_\ell(t) = \frac{e}{2\pi} \sum_{n,m\in\mathcal{I}_\ell} \int \mathrm{d}E \ \sum_{r\in\mathcal{R}} G^*_{rm}(t,E) G_{r,n}(t,E) \Gamma^\ell_{nm}(E) f_\ell(E) \tag{5.90}$$

can be interpreted as a transient oscillating charge which do not contribute to the average value over one time period.

For example, when there are only two terminals, say one on the right (R) and one on the left (L), we have

$$I_\mathrm{R} = \frac{e}{h} \int \mathrm{d}E \ [T_\mathrm{RL}(E,t) f_\mathrm{L}(E) - T_\mathrm{LR}(E,t) f_\mathrm{R}(E)] - \frac{\mathrm{d}q_\mathrm{R}}{\mathrm{d}t}. \tag{5.91}$$

As the mixed time-energy Green function is time-periodic, see equation (5.76), the oscillating charge $q_\ell(t)$ is also time-periodic so the contribution of its derivative to the current disappears in the average over one driving period. Using rolling time-averaged quantities over a driving period is relevant in particular when the driving period T is significantly smaller than the response time of the detector τ_d. Therefore, we consider the time-averaged current

$$\mathcal{I}_\ell = \overline{\langle I_\ell \rangle_0}^T = \frac{1}{T} \int_{t_1}^{t_1+T} \mathrm{d}t \ \langle I_\ell(t) \rangle_0 \,. \tag{5.92}$$

In the steady state, the average current do not depend on the initial time t_1, and we will assume that it is the case in the following. As the Fermi-Dirac distribution functions of the leads do not depend on time, only the transmission coefficients depend on time, and

$$\overline{\langle I_\ell(t) \rangle_0}^T = \frac{e}{h} \int \mathrm{d}E \ \left[\sum_{\ell'\neq\ell} \overline{T_{\ell\ell'}(E)}^T f_{\ell'}(E) - \sum_{\ell'\neq\ell} \overline{T_{\ell'\ell}(E)}^T f_\ell(E) \right], \tag{5.93}$$

where we defined **averaged transmission coefficients**

$$\overline{T_{\ell\ell'}(E)}^T = \frac{1}{T} \int_{t_1}^{t_1+T} \mathrm{d}t \ T_{\ell\ell'}(E,t). \tag{5.94}$$

The averaged transmission coefficients are expressed in terms of the Green-Floquet functions (5.77) as

$$\overline{T_{\ell\ell'}(E)}^T = \sum_{p\in\mathbb{Z}} T^{(p)}_{\ell\ell'}(E), \tag{5.95}$$

with sideband transmission coefficients

$$T^{(p)}_{\ell\ell'}(E) = \sum_{\substack{m,n\in\mathcal{I}_\ell \\ m',n'\in\mathcal{I}_{\ell'}}} (G^{(p)}_{mm'}(E))^* \Gamma^\ell_{mn}(E+p\hbar\omega) G^{(p)}_{nn'}(E) \Gamma^{\ell'}_{n'm'}(E) \tag{5.96}$$

which can be expressed as a trace on the interfaces as

$$T^{(p)}_{\ell\ell'}(E) = \mathrm{Tr}\left[[G^{(p)}(E)]^\dagger \Gamma^\ell(E+p\hbar\omega) G^{(p)}(E) \Gamma^{\ell'}(E) \right]. \tag{5.97}$$

In terms of these coefficients, the average current reads

$$\mathcal{I}_\ell = \frac{e}{h} \sum_{p\in\mathbb{Z}} \int \mathrm{d}E \left[\sum_{\ell'\neq\ell} T^{(p)}_{\ell\ell'}(E) f_{\ell'}(E) - \sum_{\ell'\neq\ell} T^{(p)}_{\ell'\ell}(E) f_\ell(E) \right] \tag{5.98}$$

B.2.3 Coupling operator in the wide-band limit

In the **wide-band limit**, the energy bands of the leads are assumed to have a significantly larger bandwidth than the scattering region, and a nearly constant density of states, so that the response functions $\Gamma_\ell(E)$ do not depend on the energy E (on the considered energy range),

$$\Gamma_\ell(E) \approx \Gamma_\ell \tag{5.99}$$

so the coupling operator reads

$$\Gamma = \sum_\ell \sum_\beta \tilde{\Gamma}_\ell \left|\chi_{\ell\beta}\right\rangle\left\langle\chi_{\ell\beta}\right| . \tag{5.100}$$

In the time representation, this means that the response of the leads is instantaneous, i.e. that the integral kernels

$$\Gamma^\ell(t) \approx \Gamma^\ell \delta(t) \tag{5.101}$$

are memory-free. This limit is very useful technically, but is not always relevant, neither in solid state experiments nor in our numerical simulations (where the leads are described by a tight-binding Hamiltonian). This may lead to deviations from the theoretical predictions.

B.3 Relating conductances and the quasi-energy spectrum

Floquet theory enables to compute the evolution operator, and therefore the retarded Green function. This allows to relate transmission coefficients (obtained from the Green function) to the quasi-energy spectrum of the scattering region.

B.3.1 General case

The evolution of the scattering region is described by equation (5.72) which is solved by the retarded Green function. In the wide-band limit (see paragraph B.2.3), equation (5.72) becomes a differential equation (not integro-differential). In terms of the mixed time-energy Green function (5.74), it reads

$$\left[\mathrm{i}\hbar\frac{\mathrm{d}}{\mathrm{d}t} - (H_{\mathrm{sys}} - \Sigma)\right] G(t,E) = 1 \tag{5.102}$$

where

$$\Sigma = \mathrm{i}\Gamma \tag{5.103}$$

us a non-Hermitian **self-energy term** (Γ is Hermitian) which takes into account the dissipative processes due to the coupling to the leads. To relate Floquet theory to the Green function $G(E,t)$, it is useful to come back to the Schrödinger equation

$$\mathrm{i}\hbar\frac{\mathrm{d}}{\mathrm{d}t}\left|\psi\right\rangle = (H_{\mathrm{sys}} - \Sigma)\left|\psi\right\rangle \tag{5.104}$$

solved by the retarded Green function. The corresponding non-Hermitian evolution is described by the generalized Floquet theory of section A, page 186 and the evolution operator can be expanded in terms of the harmonics of the Floquet modes using equation (5.44). As the Green function is related to the evolution operator by

$$G(t,t') = \frac{1}{\mathrm{i}\hbar}\mathcal{H}(t-t')U(t,t') \tag{5.105}$$

where $\mathcal{H}$ is the Heaviside step function, the Green-Floquet function reads

$$G^{(p)}(E) = \sum_{r,\alpha} \frac{|u_\alpha^{(p+r)}\rangle \langle \tilde{u}_\alpha^{(r)}|}{E - [\varepsilon_\alpha + r\hbar\omega - \mathrm{i}\hbar\gamma_\alpha]}. \tag{5.106}$$

B.3.2 Low-coupling limit

In a low-coupling limit where the self-energy term can be treated as a perturbation, the behavior of the scattering region coupled to the leads can be related to the behavior of an uncoupled scattering region, which is understood. In practice, we will use first order perturbation theory to solve equation (5.37). At zeroth order,

$$\left(H_{\mathrm{sys}} - \mathrm{i}\hbar\frac{\mathrm{d}}{\mathrm{d}t}\,|\psi\rangle\right)|u_\alpha^{[0]}(t)\rangle = \varepsilon_\alpha^{[0]}\,|u_\alpha^{[0]}(t)\rangle \tag{5.107}$$

where the exponent in square brackets indicates the order in perturbation theory (not to be confused with the index in parentheses, which indicates the Floquet harmonic). As the unperturbed evolution is unitary, $|u_\alpha^{[0]}(t)\rangle = |\tilde{u}_\alpha^{[0]}(t)\rangle$. To first order, complex quasi-energies become

$$\underline{\varepsilon}_\alpha^{[1]} = \varepsilon_\alpha^{[1]} - \mathrm{i}\hbar\gamma_\alpha^{[1]} \tag{5.108}$$

where

$$\varepsilon_\alpha^{[1]} = \varepsilon_\alpha^{[0]} \tag{5.109}$$

and

$$\gamma_\alpha^{[1]} = \frac{1}{\hbar}\int_0^T \frac{\mathrm{d}t}{T}\ \langle u_\alpha^{[0]}(t) \mid \Gamma \mid u_\alpha^{[0]}(t)\rangle = \frac{1}{\hbar}\sum_{\ell=1}^{N_{\mathrm{leads}}}\sum_\beta\sum_{p\in\mathbb{Z}}\tilde{\Gamma}_\ell\left|\langle\chi_{\ell\beta} \mid u_\alpha^{[0],(p)}\rangle\right|^2. \tag{5.110}$$

In the wide-band limit, the coupling operator reads

$$\Gamma = \sum_\ell\sum_\beta \tilde{\Gamma}_\ell\,|\chi_{\ell\beta}\rangle\langle\chi_{\ell\beta}|\,. \tag{5.111}$$

There is no correction to eigenstates at first order, so

$$|u_\alpha^{[1]}(t)\rangle = |\tilde{u}_\alpha^{[1]}(t)\rangle = |u_\alpha^{[0]}(t)\rangle\,. \tag{5.112}$$

In the following, we use first order quantities and omit the corresponding index to simplify notations.

From equations (5.97) and (5.106), the harmonic p of the averaged transmission coefficient is computed as

$$T^{(p)}_{\ell\ell'}(E) = \mathrm{Tr}\left[\sum_{\substack{s,\alpha\\ r,\beta}} \frac{|u^{(s)}_\alpha\rangle\langle u^{(p+s)}_\alpha|}{E-[\varepsilon_\alpha + s\hbar\omega + \mathrm{i}\hbar\gamma_\alpha]}\Gamma^\ell(E+p\hbar\omega)\frac{|u^{(p+r)}_\beta\rangle\langle u^{(r)}_\beta|}{E-[\varepsilon_\beta + r\hbar\omega - \mathrm{i}\hbar\gamma_\beta]}\Gamma^{\ell'}(E)\right]. \tag{5.113}$$

B.4 Effect of an electric potential drop

Numerically, it may be convenient to use an electric potential drop ΔV_ℓ between the lead ℓ and the scattering region instead of setting chemical potentials as on-site potentials. Here again, the reader is referred to [GWSH14] for a discussion on the distinction between chemical and electrical potential drops at the interface between the scattering region and the lead. Such an electric potential drop is taken into account by modifying the contact Hamiltonian into

$$H_{\mathrm{contacts}} = \sum_{\ell=1}^{N_{\mathrm{leads}}}\sum_{n\in\mathcal{I}_\ell}\sum_q V_\ell \mathrm{e}^{\mathrm{i}\Delta V_\ell t} c^\dagger_{\ell,y=y_\ell(n)} c_n + \mathrm{h.c.} \tag{5.114}$$

The same computation leads to transmission coefficients

$$T^{(p)}_{\ell\ell'}(E,\Delta V_\ell,\Delta V_{\ell'}) = T^{(p)}_{\ell\ell'}(E+\Delta V_{\ell'}). \tag{5.115}$$

In other words, in the wide band limit, the transmission coefficient $T^{(p)}_{\ell\ell'}$ are effectively considered at an injection energy $E+\Delta V_{\ell'}$ instead of E: in particular, varying the injection energy or the potential drop at the incoming lead should give the same result.

Chapter 6

Résumé en français

1 Introduction générale

L'étude des phénomènes physiques met généralement en jeu des observables locales, ou les corrélations entre des quantités locales. Dans certaines situations, des quantités "globales" qui ne dépendent pas des détails locaux de la description sont nécessaires. Dans le cadre de la physique du solide, les outils topologiques ont été utilisés pour la première fois pour caractériser les défauts d'une phase ordonnée [Mer79] : une telle phase ordonnée de la matière est caractérisée par un paramètre d'ordre, et les défauts topologiques apparaissent comme des configurations particulières du champ de paramètre d'ordre qui présentent des singularités. Par exemple, un film à deux dimensions d'hélium IV superfluide est décrit par un champ de paramètre d'ordre complexe $\psi(x) = \psi_0(x)\,\mathrm{e}^{\mathrm{i}\theta(x)}$ qui caractérise la brisure de symétrie $U(1)$. À deux dimensions, un exemple de défaut associé à un paramètre d'ordre $U(1)$ est un vortex, où le paramètre d'ordre ψ s'annule. La circulation autour du défaut est un entier appelé la charge topologique du vortex, qui mesure combien de fois la phase $\theta(x)$ s'enroule le long d'une boucle entourant le vortex. Cette charge topologique ne dépend pas des détails de la configuration du champ de paramètre d'ordre : elle est laissée invariante par des modification lisses du paramètre d'ordre à l'intérieur de la région entourée par la boucle : c'est la raison pour laquelle on dit qu'il s'agit d'une quantité topologique.

La topologie s'occupe de propriétés globales, qui sont invariantes sous l'action de certaines transformations, comme les déformations lisses. Ces propriétés globales peuvent distinguer des objets qui se ressemblent localement, ou au contraire rassembler des objets qui semblent différents à première vue. L'exemple archétypal d'une telle propriété globale est le nombre de trous (ou *genre* g) d'une surface bidimensionnelle (voir les figures 6.1 et 6.2). Par exemple, une sphère n'a aucun trou, alors qu'un tore a un trou: il n'est ainsi pas possible de déformer continûment une sphère en un tore. Pour définir précisément ce que signifie pour deux objets d'être topologiquement équivalents, il faut préciser quelles sont les transformations autorisées. Dans cette introduction, nous nous contenterons d'une image intuitive : on imagine que les objets sont faits en pâte à modeler et que les transformations autorisées consistent à déformer la pâte à modeler, mais sans la déchirer ni coller deux parties ensemble. Ainsi, une tasse à café a une anse, et correspond donc à une surface de genre 1, qui peut être déformée en un tore sans déchirure ni collage.

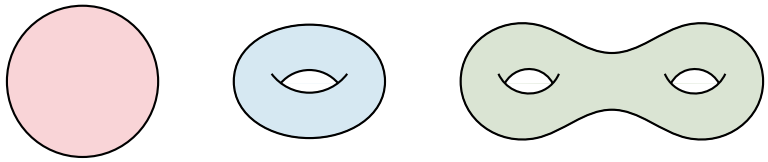

Figure 6.1: Genre de quelques surfaces à deux dimensions. Le genre g d'une surface fermée à deux dimensions compte essentiellement le nombre de "trous" (ou "anses") de la surface. Une sphère n'a pas de trou (genre 02), un tore a un trou (genre 1), etc. En fait, toute surface (variété à deux dimensions) fermée orientable est homéomorphe à une somme connexe de g tores. Le genre est relié par le théorème de Chern-Gauss-Bonnet à la caractéristique d'Euler de la surface $\chi = 2-2g$, un invariant homologique qui peut être calculé en intégrant la courbure locale de la surface.

Le caractère topologique des vortex leur assure une certaine robustesse (vis-à-vis des déformations continues du paramètre d'ordre), ce qui permet de les traiter comme des objets indépendants, qui se comportent comme des charges électriques – ce qui conduit à une analogie très fructueuse. Par exemple, comme on peut s'y attendre, deux vortex de charges opposées peuvent s'annihiler quand ils se rencontrent, et un vortex de charge +2 peut se scinder en deux vortex de charge +1, etc. Dans le cas des défauts, les méthodes topologiques servent à caractériser les différentes configurations d'une phase ordonnée donnée. La topologie peut aussi avoir le rôle très différent de distinguer différentes phases de la matière qui ont même symétrie, et qui ne peuvent donc pas être différenciées par un paramètre d'ordre. C'est le cas des phases topologiques de la matière comme l'effet Hall quantique, qui fait l'objet de la prochaine section.

1.1 L'effet Hall quantique

La découverte de l'effet Hall quantique par von Klitzing, Dorda et Pepper [KDP80] en 1980, puis de sa nature topologique par TKNN (Thouless, Kohmoto, Nightingale et den Nijs) [TKNN82] ainsi qu'Avron, Seiler et Simon [ASS83; Sim83] a donné l'essor à un nouveau champ d'étude, en matière condensée et au delà. L'effet Hall quantique a d'abord un intérêt fondamental, tant du point de vue théorique qu'expérimental : l'effet Hall quantique entier est le premier exemple d'une phase de la matière qui échappe au paradigme de Landau, puisqu'elle n'est pas associée à un paramètre d'ordre local ; il s'agit de plus d'une situation décrite par une théorie élégante, qui relie des constructions mathématiques assez modernes à des situations réalisables expérimentalement. D'autre part, l'effet Hall quantique entier présente un intérêt pratique pour la métrologie, puisqu'il permet une mesure très précise et reproductible de la constante fondamentale e^2/h (avec une incertitude relative inférieure à 10^{-9}), qui est utilisée comme référence de résistance électrique [WK11; JJ06]. Enfin, l'effet Hall quantique et ses dérivés (comme l'effet Hall quantique fractionnaire) sont désormais utilisés comme plateforme pour l'étude fondamentale de la mécanique quantique (en particulier de la décohérence) dans le champ de l'optique quantique électronique

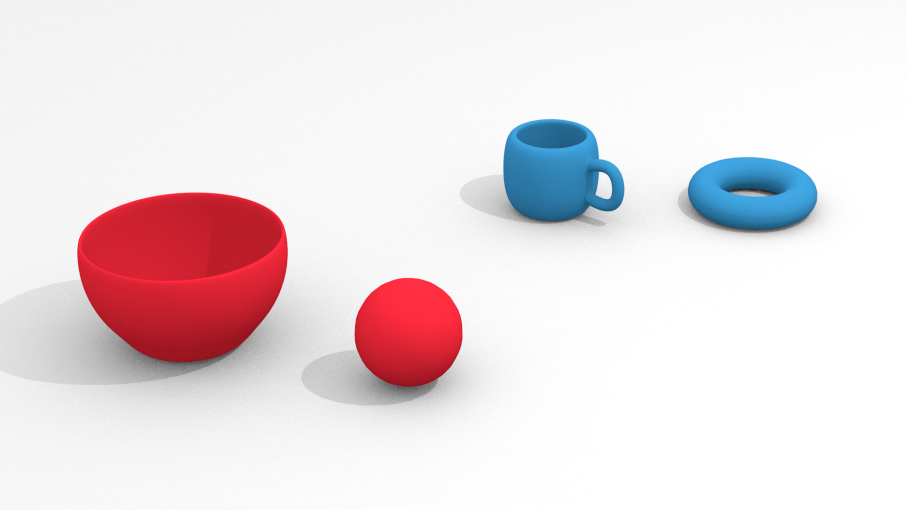

Figure 6.2: Topologie des surfaces à 2D. Un bol et une sphère ont comme genre $g = 0$. Une tasse et un tore ont comme genre $g = 1$.

[BFPB13], ainsi que pour développer le champ de l'informatique quantique [Kit03; NSSF08; JOPS10].

Commençons par rappeler ce qui se passe dans l'effet Hall "classique". Lorsqu'un gaz d'électrons bidimensionnel est soumis à un champ magnétique transverse B, la densité de courant J et le champ électrique E dans le plan sont reliés à la réponse linéaire par

$$J_\mu = \sigma_{\mu\nu} E_\nu \tag{6.1}$$

où σ est le tenseur de conductivité 2×2. Dans le cadre de la théorie semi-classique de Drude (voir e.g. [Pot07])

$$\sigma = \frac{\sigma_0}{1 + (\omega_c \tau)^2} \begin{pmatrix} 1 & \omega_c \tau \\ -\omega_c \tau & 1 \end{pmatrix} \tag{6.2}$$

où

$$\sigma_0 = \frac{n e^2 \tau}{m^*} \tag{6.3}$$

est la conductivité à champ magnétique nul et où

$$\omega_c = \frac{eB}{m^*} \tag{6.4}$$

est la pulsation cyclotron, proportionnelle au champ magnétique, n la densité électronique, τ un temps de relaxation (un temps caractéristique de la relaxation des électrons vers l'équilibre, principalement due aux processus de collision), m^* la masse effective des électrons et e la charge fondamentale. Quand le champ magnétique est assez fort ou le temps de relaxation assez grand pour que que $\omega_c \tau \gg 1$, les composantes diagonales σ_{xx} et σ_{yy} peuvent être négligées devant les composantes antidiagonales

$\sigma_{xy} = -\sigma_{yx}$; dans ce cas, la conductance de Hall est à peu près $\sigma_{xy} = \frac{e^2}{h}\,\nu$ où on a introduit le paramètre sans dimension $\nu = hn/eB$. Expérimentalement, les différentes composantes du tenseur de conductivité sont généralement mesurées avec une barre de Hall, comme représenté sur la figure 6.3, ce qui permet d'éviter des problèmes de résistance de contact, et de mesurer à la fois la conductance longitudinale et la conductance de Hall (à deux dimensions, les conductances et les conductivités sont reliées par un paramètre géométrique sans dimension, du moins quand le tenseur de conductivité est uniforme dans l'échantillon, qui se trouve être 1 dans le cas de la conductance de Hall [Goe11]).

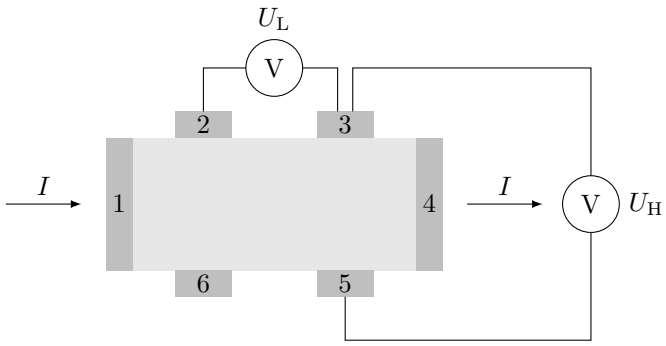

Figure 6.3: Dispositif de barre de Hall. Dans un dispositif de barre de Hall, on fait passer à travers l'échantillon un courant I par les terminaux 1 et 4. Pendant ce temps, on mesure la tension longitudinale U_L, par exemple entre les terminaux 2 et 3, ainsi que la tension transverse U_H, par exemple entre les terminaux 3 et 5. On obtient alors les résistances longitudinale et de Hall $R_\mathrm{L} = U_\mathrm{L}/I$ et $R_\mathrm{H} = U_\mathrm{H}/I$.

Un comportement surprenant appelé l'effet Hall quantique a lieu lorsqu'un gaz d'électrons faiblement désordonné est soumis à un champ magnétique intense à basse température (quand $\hbar\omega_\mathrm{c} \gg k_\mathrm{B}T$): en 1980, von Klitzing, Dorda et Pepper [KDP80] observèrent que la courbe de la conductance de Hall σ_{xy} en fonction de l'inverse du champ magnétique $1/B$ montre des plateaux, où la valeur de σ_{xy} est très précisément quantifiée en multiples entiers de e^2/h, c'est-à-dire que

$$\sigma_{xy} = \frac{e^2}{h}\,\tilde{\nu} \qquad \text{où } \tilde{\nu} \in \mathbb{Z}. \tag{6.5}$$

L'entier $\tilde{\nu}$ est la quantité sans dimension $\nu = hn/eB$ arrondie à l'entier le plus proche, et la conductance de Hall σ_{xy} saute d'un plateau à l'autre. Les transitions entre plateaux sont accompagnées d'un pic de conductance longitudinale σ_{xx}, qui est nulle ailleurs, comme représenté figure 6.4. Expérimentalement, on mesure généralement la résistivité de Hall ρ_{xy} ainsi que la résistivité longitudinale ρ_{xx}, composantes du tenseur de résistivité $\rho = \sigma^{-1}$. C'est par exemple le cas sur la figure 6.5. Pour relier ces deux points de vue, remarquons que tant que σ_{xy} n'est pas nulle (donc tant que $B \neq 0$), $\rho_{xx} = 0$ ssi $\sigma_{xx} = 0$. De plus, quand σ_{xx} (ou ρ_{xx}) s'annule, on a $\rho_{xy} = -1/\sigma_{xy}$ de sorte que si l'une des deux quantités est quantifiée, l'autre l'est aussi. La quantification de σ_{xy} est universelle : elle n'est pas affectée par la géométrie précise du système, ni par les impuretés ou le désordre ; et la même valeur, avec une

très grande précision, est obtenue dans divers systèmes comme les interfaces oxyde-semiconducteur dans les MOSFET, les hétérojonctions de semiconducteurs ou encore le graphène. Cette universalité et cette invariance vis-à-vis des perturbations laissent penser que la conductance de Hall quantifiée est reliée à un invariant topologique : c'est effectivement le cas, et la quantité $\tilde{\nu}$ est un invariant topologique du fondamental du système, le "premier nombre de Chern associé au projecteur de Fermi" (voir le chapitre 2).

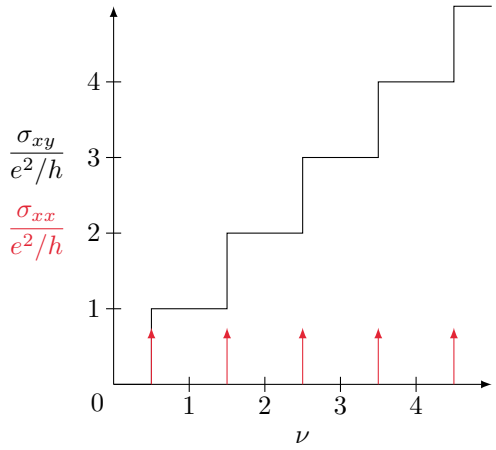

Figure 6.4: Image simplifiée de l'effet Hall quantique. Dans une image idéalisée, on observe des plateaux quantifiés de conductance de Hall autour des valeurs entières $\tilde{\nu} \in \mathbb{Z}$ du paramètre sans dimension $\nu = hn/eB$, sur lesquels la conductance de Hall est égale à $\tilde{\nu}e^2/h$. Une transition brutale a lieu aux valeurs demi-entières de ν. La conductivité longitudinale est nulle, à part au voisinage des transitions entre plateaux, où elle est très grande.

Pour décrire le gaz d'électrons bidimensionnel dans lequel à lieu l'effet Hall quantique entier (ou IQHE, pour *integer quantum Hall effect*), une description simplifiée qui néglige les effets des interactions est suffisante, et on se concentre donc sur le problème à une particule. Le hamiltonien de Landau décrivant un électron à deux dimensions et sous un champ magnétique B constant est

$$H = \frac{1}{2m^*}(P + eA)^2 = \frac{1}{2m^*}\Pi^2 \tag{6.6}$$

où P est l'opérateur impulsion, A est le potentiel vecteur, et où $\Pi = P + eA$. Ce hamiltonien peut être réécrit comme celui d'un oscillateur harmonique

$$H = \hbar\omega_{\mathrm{c}}\left(a^\dagger a + \frac{1}{2}\right) \quad \text{om} \quad a^\dagger = \frac{1}{\sqrt{2\hbar eB}}\left(\Pi_x + \mathrm{i}\Pi_y\right) \tag{6.7}$$

avec $[a, a^\dagger] = \mathrm{Id}$. Son spectre est donc

$$E_n = \hbar\omega_{\mathrm{c}}\left(n + \frac{1}{2}\right). \tag{6.8}$$

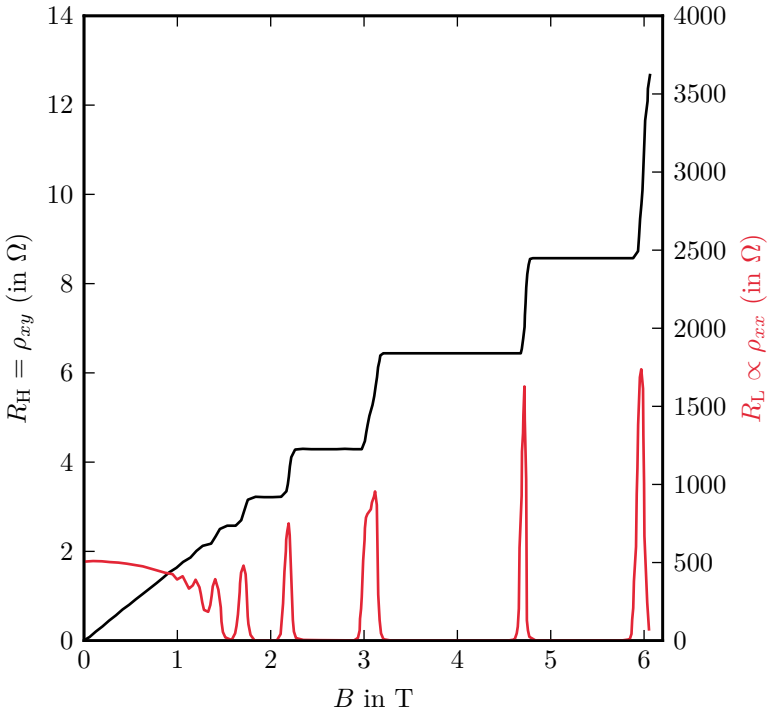

Figure 6.5: Résistance de Hall et résistance longitudinale dans l'effet Hall quantique. Courbes expérimentales de la résistance de Hall (en noir) et de la résistance longitudinale (en rouge) dans une hétérostructure de GaAs-AlGaAs en fonction du champ magnétique, à 8 mK. Adapté de [Kli86].

Chaque énergie E_n est fortement dégénérée, puisqu'il y a $N_A = A/(2\pi\ell_B^2)$ états d'énergie E_n dans une surface d'aire A, où $\ell_B = \sqrt{\hbar/eB}$ est la longueur magnétique. L'ensemble des états dégénérés d'énergie E_n est appelé le $n$ème niveau de Landau, ou la $n$ème bande de Landau lorsqu'elle est élargie par le désordre.

De par plusieurs aspects, les niveaux de Landau sont très proches des bandes d'énergie d'un cristal isolant : ils sont séparés les uns des autres par des gaps d'énergie, et contiennent un grand nombre d'états. Lorsque du désordre est présent, il est possible de placer le potentiel chimique dans un gap entre deux niveaux de Landau : dans cette situation, le système est similaire à un isolant de bande. Il s'agit néanmoins d'un isolant aux propriétés très particulières, ce qu'on peut illustrer à l'aide d'une description semi-classique (voir la figure 6.6) : sous un champ magnétique intense, les états d'un niveau de Landau dérivent le long d'équipotentielles du potentiel de confinement et de désordre. Dans le volume[(1)], le système est isolant : chaque électron est confiné sur une orbite fermée, et ne peut pas transporter de courant. Au bord,

[(1)] Je traduis l'anglais *bulk* par *volume* : ce terme sous-entend qu'on se situe loin des interfaces ou bords du système, dans une région où leur influence est négligeable.

par contre, les électrons peuvent se déplacer le long de l'interface, ce qui donne lieu à un mouvement global. En d'autres termes, au bord du système, le potentiel de confinement courbe les niveaux de Landau (dont la relation de dispersion de volume est plate), ce qui fait que les niveaux de Landau qui dans le volume du système sont sous le potentiel chimique sont forcés de le traverser près du bord. Il apparaît ainsi des états qui conduisent le courant, confinés près des bords de l'échantillon : les états de bord unidirectionnels. Le bord du système est donc un métal à une dimension. Les états de bord sont chiraux (ou unidirectionnels), c'est-à-dire qu'ils peuvent aller de la gauche vers la droite, par exemple, mais pas de la droite vers la gauche. Ce comportement chiral peut être expliqué dans une approche semi-classique en termes de sauts entre orbites cyclotron près du bord [Büt88a] (voir la figure 6.6). Une conséquence importante de cette propriété est qu'il n'y a pas d'états disponibles permettant la rétrodiffusion des électrons, même en présence d'impuretés : les états de bord peuvent être déformés lorsque le bord est rugueux, ou quand il y a des impuretés, mais ils se déplacent toujours dans la même direction, sans dissipation. L'existence de tels états chiraux robustes provient en dernière analyse de la topologie non-triviale des états de volume. Une bande d'énergie est un objet bien défini, décrit par un ensemble de relations de dispersion et par les états propres correspondants (ou si on se contente des informations essentielles, comme on va le voir plus tard, d'un domaine d'énergie et d'un projecteur spectral). En tant que tel, elle peut avoir une topologie non-triviale, contenue dans les états propres. De la même manière que les surfaces fermées ont un certain nombre d'anses g, une bande d'énergie peut avoir des propriétés topologiques, décrites (dans le cas présent) par leur premier nombre de Chern C_1. Une bande triviale, par exemple obtenue par un modèle de liaisons fortes avec des intégrales de saut tendant vers zéro, a un nombre de Chern nul. C'est aussi le cas des bandes d'énergie des matériaux usuels, comme l'air ou le vide. Au contraire, une bande de Landau a un nombre de Chern non nul. Cette propriété topologique est préservée tant que la bande est bien définie, c'est-à-dire séparée de toutes les autres bandes. Lorsqu'un gap se ferme et que deux bandes se touchent, elles peuvent échanger leurs propriétés topologiques : par exemple, deux (sous-)bandes avec des nombres de Chern opposés peuvent être transformées en deux bandes triviales lorsqu'elles se rencontrent (de manière à ce que le nombre de Chern total, pour l'ensemble des deux bandes, soit conservé). Tant que les bandes sont séparées les unes des autres, néanmoins, leurs propriétés topologiques sont laissées invariantes par les perturbations. En particulier, cela explique la robustesse des états de bord "topologiquement protégés". Dans le cas de l'effet Hall quantique, le nombre d'états de bord est donné par le nombre de bandes de Landau en dessous du niveau de Fermi ; en général, il est donné par le nombre de Chern de l'ensemble des bandes en dessous du niveau de Fermi. Dans les expériences de transport, le courant de Hall est transporté par les états de bord, chacun d'eux contribuant d'un facteur e^2/h à la conductance de Hall [Büt88a], ce qui implique que $\tilde{\nu} = C_1$ dans l'équation (6.5). La nature topologique de cette quantité explique que les plateaux de Hall soient si précisément quantifiés. (Je renvoie le lecteur aux revues [PKG90; DP08; CJOD99; Goe11; DPR06] pour plus de détails sur l'effet Hall quantique.)

L'effet Hall quantique est le premier exemple d'une famille de phénomènes appelés *isolants topologiques*, où des *états de bord topologiquement protégés* apparaissent au bord du système, à cause de la topologie non-triviale de ses bandes de volume. Ce

principe général est appelé la correspondance bord-volume : dès que le volume du système est non-trivial, des états de bord topologiquement protégés apparaissent au bord d'un échantillon de taille finie, et inversement, des états de bord topologiquement protégés indiquent une topologie non-triviale du volume du système[(2)].

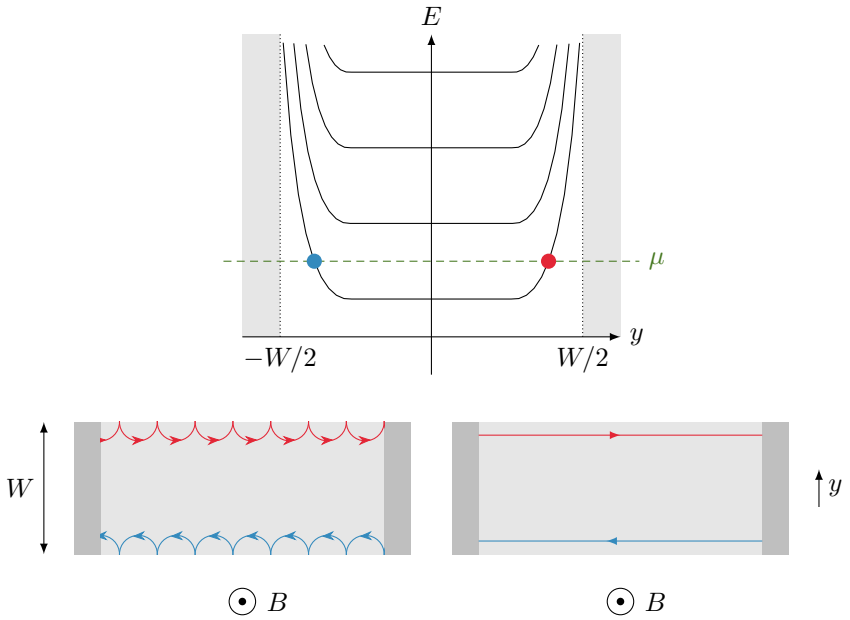

Figure 6.6: Orbites rebondissantes (*skipping orbits*) et états de bord. Un échantillon de taille finie peut être modélisé par un potentiel de confinement qui courbe les niveaux de Landau au voisinage du bord (ici en $y = \pm W/2$). Par conséquent, même si le système est un isolant dans son volume, et que le potentiel chimique est fixé entre deux niveaux de Landau, il y aura des états métalliques croisant le potentiel chimique près du bord (en bleu et rouge), et qui correspondent aux états de bord. Ces états de bord peuvent être représentés schématiquement comme des orbites cyclotron rebondissant sur les interfaces, ce qui conduit à un mouvement chiral. Les états de bord chiraux résultats, qui sont une propriété commune de l'IQHE et des isolants de Chern, sont représentés sur l'image de droite.

Un gaz d'électrons désordonné sous un champ magnétique intense a le défaut de ne pas facilement être décrit dans le cadre de la théorie de Bloch. D'une part, le champ magnétique nécessite de considérer une super-cellule unité (pour des valeurs rationnelles du flux magnétiques adimensionné), qui dépend de l'amplitude du champ; sous un très fort champ magnétique, il s'agit du problème de Harper-Hofstadter [Har55; Hof76], qui recèle des phénomènes remarquables, mais très complexes. D'autre part, un système désordonné n'a pas d'invariance par translation, et ne peut donc pas être

[(2)] En fait, lorsqu'une symétrie est nécessaire pour définir l'invariant de volume (voir plus loin), et que la dimension d'espace est adéquate, il est possible au système de briser la symétrie à l'interface plutôt que de former des états de bord à l'interface, une situation décrite en premier par Ezawa, Tanaka et Nagaosa [ETN13].

décrit par la théorie de Bloch. Or, le désordre joue un rôle essentiel dans l'effet Hall quantique : la description par la mécanique quantique d'un gaz d'électrons bidimensionnel sans aucun désordre prévoit simplement l'effet Hall classique usuel. Une compréhension cohérente de la nature topologique de l'effet Hall quantique nécessite de prendre en compte le désordre dès le début, et définir des invariants topologiques dans cette situation nécessite de recourir au cadre de la géométrie non-commutative [BEB94], un outil mathématique élégant, mais complexe conceptuellement et techniquement. Il est néanmoins possible de comprendre les propriétés clés de l'effet Hall quantique (et plus généralement des isolants topologiques) dans le cadre de la théorie des bandes. Haldane [Hal88] est le premier à avoir découvert un exemple de modèle implémenté sur réseau, sans flux magnétique net (ainsi la périodicité du réseau est maintenue, et la théorie de Bloch s'applique), qui montre les mêmes propriétés topologiques que l'effet Hall quantique. De tels modèles, désormais appelés isolants de Chern, sont plus faciles à étudier théoriquement. Cet avantage a permis une série de développements, parmi lesquels

– l'inclusion de symétries dans la description : les symétries ajoutent des contraintes qui permettent l'existence (ou non) de différentes classes de propriétés topologiques;
– l'extension à d'autres domaines de la physique : l'existence d'analogues de l'effet Hall quantique dans d'autres domaines a été discutée dès 1988 dans le cas de films hélium 3 par Volovik [Vol88a], puis en 2005 dans des cristaux photoniques par Haldane et Raghu [HR08; RH08]; on sait désormais que des analogues de l'effet Hall quantique (et de ses dérivés avec des symétries supplémentaires) sont envisageables dans tous les systèmes ondulatoires (optique, acoustique, mécanique, atomes froids, etc.);
– la possibilité d'induire des propriétés topologiques à travers des interactions [RQHZ08], de la dissipation [RL09; ZRPL15; DRBZ11; BBKR13; BD15; RLL16], ou un forçage extérieur (voir plus loin).

Cette liste n'a pas vocation à être complète, mais souligne les trois principales directions qui, à mon sens, s'entrecroisent dans cette thèse.

Le cadre de la théorie des bandes de Bloch topologique est le suivant : on associe à un système invariant par translation un hamiltonien de Bloch $H(k)$, où k est un réseau réciproque vivant dans la zone de Brillouin, qui est un tore puisque k n'est défini que modulo un vecteur du réseau réciproque. Le spectre de $H(k)$ fournit une structure de bande décrite par des niveaux d'énergie $E_i(k)$, qui peut avoir des gaps spectraux. Dans ce cas, un projecteur spectral associé à une famille de projecteurs $P(k)$ décrit les états propres de la bande située entre deux gaps. Par exemple, un hamiltonien de Bloch deux par deux a des états propres $\psi_\pm(k)$ d'énergies $E_\pm(k)$; si $E_+(k) > \mu > E_-(k)$, on définit $P_\pm(k) = |\psi_\pm(k)\rangle\langle\psi_\pm(k)|$. Il est possible d'associer des invariants topologiques (comme le premier nombre de Chern) à la famille de projecteurs P, et ces invariants ne changent pas quand H est modifié, tant que le gap ne se ferme pas.

Considérons désormais une interface entre deux isolants topologiquement inéquivalents : le système à gauche de l'interface est supposé trivial, alors que celui à droite est supposé non-trivial. Loin de l'interface, le système n'est en quelque sorte pas au courant de l'existence d'une interface : c'est donc un isolant de volume, qui peut être

décrit comme s'il était infini, et la théorie de Bloch (topologique) s'applique. Près de l'interface, cette description n'est plus forcément valide, mais acceptons provisoirement d'utiliser un hamiltonien de Bloch dépendant de la position, et plus particulièrement de la distance à l'interface : pour qu'il soit possible de passer d'un isolant trivial à un isolant non-trivial, il y a forcément un endroit près de l'interface où le gap se ferme (de sorte que les invariants topologiques ne peuvent pas y être définis), ce qui conduit à des états de bord métalliques. Il est possible de rendre cette description partiellement rigoureuse en utilisant des fonctions de Green, une méthode développée par Volovik [Vol88a] et étendue de manière significative par Gurarie et Essin [Gur11; EG11]. Cette méthode a aussi été étendue [RLBL13; NR15] au cas des phases topologiques dans des systèmes soumis à un forçage périodique (ou phases topologiques de Floquet).

1.2 Symétries et isolants topologiques

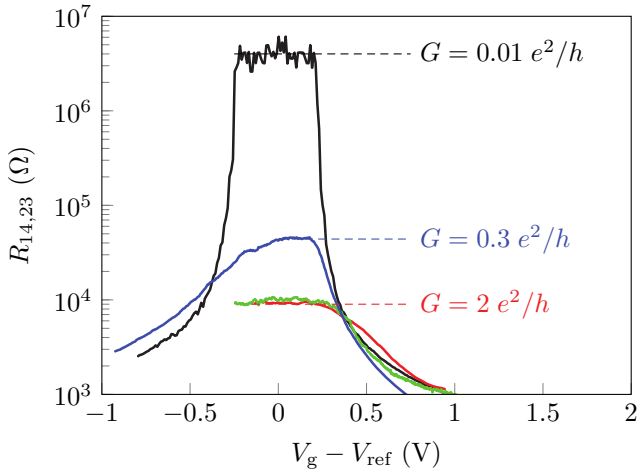

Figure 6.7: Signatures de transport des états de bord topologiques du QSHE dans des puits quantiques de HgTe. On trace la résistance quatre terminaux longitudinale $R_{14,23}$ en fonction de la tension de grille $V_g - V_{ref}$ dans un puits quantique de HgTe-CdTe trivial (courbe noire) et topologique (courbes roulge, verte et bleue) à 30 mK. Dans le cas topologique (lorsqu'il y a une inversion de bande), $R_{14,23}$ atteint une valeur quantifiée de 2 e^2/h, comme on l'attend d'après le formalisme de Landauer-Büttiker appliqué au transport par les états de bord (à part dans la courbe bleue, qui correspond à un échantillon de taille plus importante où la conductance est réduite par des processus inélastiques qui permettent de la rétrodiffusion. Dans la situation triviale (courbe noire), la résistance est très grande dans le gap : c'est le comportement qu'on attend pour un isolant usuel. Adapted from [KWBR07]. Reprinted with permission from AAAS.

L'étude de l'effet Hall quantique était un sous-domaine bien établi de la matière condensée lorsque furent publiés les articles de Kane et Mele en 2005 [KM05a; KM05b]. Ils proposèrent une "version invariante par renversement du temps" de

l'effet Hall quantique (la brisure de l'invariance par renversement du temps est un ingrédient essentiel de l'IQHE et des isolants de Chern), appelée "effet Hall quantique de spin" (QSHE, pour "quantum spin Hall effect"). Dans cet effet, les ingrédients essentiels sont une inversion de bande au voisinage d'un point de symétrie de la zone de Brillouin et un fort couplage spin-orbite, qui génère de manière effective un champ magnétique dépendant de l'impulsion et du spin. Un an plus tard, Bernevig, Hughes et Zhang [BHZ06] proposèrent un schéma de réalisation expérimentale dans des puits quantiques d'HgTe-CdTe, qui fut réalisé un an après par König et collaborateurs [KWBR07], dans le groupe de Molenkamp (voir figure 6.7). Fu, Kane et Mele [FKM07], Roy [Roy09], ainsi que Moore et Balents [MB07] découvrirent alors qu'une version à trois dimensions de cet isolant topologique invariant par renversement du temps était possible. Cette version fut rapidement observée expérimentalement dans du $Bi_{1-x}Sb_x$ par Hsieh et collaborateurs [HQWX08] dans le groupe d'Hasan, par des mesures de spectroscopie de photoémission angulairement résolue (ARPES). Ils observèrent la signature caractéristique d'états de surface : une relation de dispersion de Dirac pour les électrons de surface, à des énergies correspondant au gap de volume du matériau, comme prévu par la théorie des bandes topologique. D'autres matériaux ayant une topologie de Kane-Mele non-triviale en trois dimensions ont ensuite été découverts, parmi lesquels Bi_2Se_3; on reproduit à la figure 6.8 un spectre ARPES expérimental des états topologiques de surface de ce matériau, tiré de [XQHW09].

Dans un système électronique invariant par renversement du temps (TRI), il n'est pas possible d'avoir un isolant de Chern non-trivial. Le renversement du temps est représenté par un opérateur anti-unitaire Θ avec $\Theta^2 = -\mathrm{Id}$ pour les particules avec spin demi-entier. Dans un système invariant par renversement du temps, le hamiltonien de Bloch satisfait $\Theta H(k)\Theta^{-1} = H(-k)$, et ainsi chaque état propre $\psi(k)$ de $H(k)$ a un *partenaire de Kramers* $\Theta\psi(k)$ qui est état propre de $H(-k)$. Les contributions des partenaires de Kramers à la topologie d'un isolant de Chern sont opposées et se compensent mutuellement Il a été montré par Kane et Mele qu'il est néanmoins possible de contourner cette annulation en définissant un invariant plus fin, qui caractérise la topologie des systèmes invariants par renversement du temps. Pour comprendre la topologie de Kane-Mele, le plus simple est de s'intéresser à leur manifestation expérimentale la plus frappante, les états de bord. Alors que les isolants de Chern ont des états de bord chiraux caractéristiques, les isolants de Kane-Mele sont caractérisés par des états de bord hélicaux, qui sont essentiellement des paires de Kramers d'états de bord chiraux, avec des chiralités opposées (voir figure 6.9). Comme ces états de bord contra-propagatifs forment une paire de Kramers, la rétrodiffusion d'un état de bord vers son partenaire contra-propagatif n'est pas autorisée. Tant que l'invariance par renversement du temps (avec $\Theta^2 = -\mathrm{Id}$) n'est pas brisée, en dimensions d'espace $d = 2$ et $d = 3$, une quantité topologique appelée *l'invariant de Kane-Mele* $\mathrm{KM} \in \mathbb{Z}_2$ (associé à la bande de valence) peut être défini. En termes d'états de bord, cela signifie qu'une paire de Kramers d'états de bord est topologiquement distincte d'une absence complète d'états de bord, mais que deux paires de Kramers d'états de bord sont topologiquement équivalent à l'absence complète d'états de bord, puisque la rétrodiffusion est possible dans ce cas (c'est pourquoi $\mathrm{KM} \in \mathbb{Z}_2$). En fait, l'invariant de Kane-Mele peut être défini directement sans partir d'une situation où une composante du spin est conservée, et il est même possible de concevoir un modèle jouet où seuls des termes de saut ne conservant pas le spin sont présents, mais qui est malgré tout

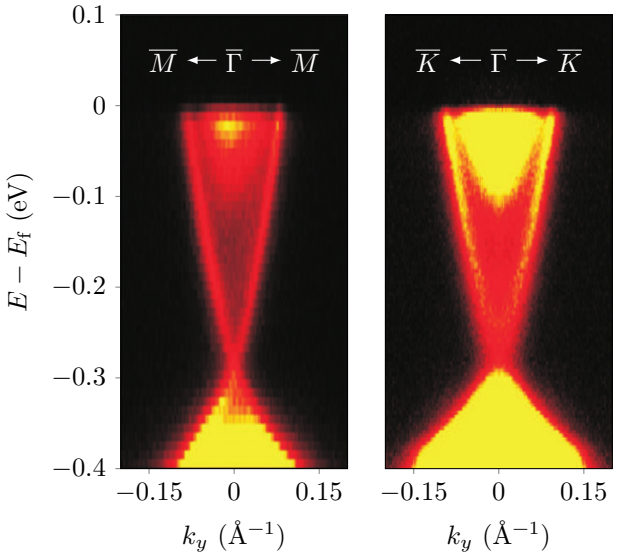

Figure 6.8: Signature en ARPES signature des états de surface topologiques dans Bi_2Se_3. Spectre ARPES de la relation de dispersion électronique de surface (à deux dimensions) de l'isolant topologique invariant par renversement du temps à trois dimensions Bi_2Se_3 (111) près du point Γ, le long des lignes $\overline{\Gamma}-\overline{M}$ (à gauche) et $\overline{\Gamma}-\overline{K}$ (à droite) de la zone de Brillouin de surface. Ces données démontrent l'existence d'états de surface avec une relation de dispersion linéaire dans le gap de volume de Bi_2Se_3. Adapted from [XQHW09]. Reprinted by permission from Macmillan Publishers Ltd, Nature Physics, copyright 2009.

invariance par renversement du temps, et topologiquement non-triviale du point de vue de la topologie de Kane-Mele.

Un exemple peut aider à illustrer ce qui a lieu dans un tel système : quand une projection du spin est conservée, il est possible d'associer des premiers nombres de Chern $C_{\uparrow\downarrow}$ à chaque espèce de spin. Dans un système invariant par renversement du temps $C_\uparrow = -C_\downarrow$. Lorsque $C_\uparrow = -C_\downarrow = 1$, chaque espèce de spin est dans une phase isolant de Chern, ce qui donne lieu, dans un échantillon fini, à une paire de Kramers composée d'un état de bord allant e.g. vers la droite pour les spins pointant vers le haut et d'un état allant vers la gauche pour les spins pointant vers le bas. Dans cette situation, l'invariant de Kane-Mele se simplifie en

$$\mathrm{KM} = \frac{C_\uparrow - C_\downarrow}{2} \text{ mod. } 2 = C_\uparrow \text{ mod. } 2. \tag{6.9}$$

Si l'on part de cette situation et qu'on allume des perturbations qui brisent la symétrie de rotation de spin, mais maintiennent l'invariance par renversement du temps, la composante de spin choisie n'est plus conservée. Ainsi, ni $C_\uparrow$ ni $C_\downarrow$ ne restent bien définis. Par contre, l'invariant de Kane-Mele KM reste bien défini et ne change pas tant que le gap séparant la bande de valence de la bande de conduction reste ouvert (et que l'invariance par renversement du temps est préservée).

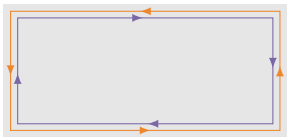

Figure 6.9: États de bord d'un isolant de Kane-Mele. Dans un isolant de Kane-Mele (aussi appelé QSHE), deux états de bord contra-propagatifs (dits hélicaux) forment une paire de Kramers, sur chaque interface. Par conséquent, la rétrodiffusion d'un état de bord vers son partenaire contra-propagatif n'est pas autorisée.

La découverte de Kane et Mele (ainsi que celle du graphene en 2004) a focalisé l'attention de la communauté de matière condensée sur la physique topologique, et un énorme nombre de résultats ont été produits (ou redécouverts ...) depuis (de bons articles de revue comprennent [Lud15; CTSR15; HK10; QZ11; BLD16]). Il a été compris que (i) il y a des systèmes analogues à l'effet Hall quantique dans des dimensions d'espace autres que $d = 2$ et (ii) que les symétries donnent lieu à des invariants topologiques différents et/ou plus fins, ce qui a conduit à décrire des phénomènes bien connus comme les parois de domaines du modèle de Su-Schrieffer-Heeger du polyacétylène [SSH79] ou les fermions de Majorana non appariés dans la chaîne de Kitaev [Kit01] dans le langage des isolants topologiques, ainsi que de concevoir et réaliser de nouveaux types d'isolants topologiques.

Une étape importante dans le sujet des isolants topologiques a été réalisée par Schnyder, Ryu, Furusaki et Ludwig [SRFL08; SRFL09; RSFL10] ainsi que Kitaev [Kit09], qui ont développé une classification des phases topologiques selon leurs symétries non-spatiales, appelée le "tableau périodique des isolants topologiques". L'idée principale est qu'il existe trois symétries fondamentales particulières, qui n'agissent que sur les degrés de liberté interne (c'est-à-dire localement dans l'espace) : le renversement du temps Θ, la conjugaison de charge C (aussi appelée symétrie particule-trou), et la symétrie chirale Γ (reliée à Θ et C par $\Gamma = \Theta C$ s'ils sont définis, éventuellement à une phase près). Le renversement du temps et la conjugaison de charge sont représentés par des opérateurs anti-unitaires dont le carré est $+\mathrm{Id}$ ou $-\mathrm{Id}$, alors que Γ est unitaire (mais n'est pas une symétrie implémentée unitairement, puisque Γ anticommute avec le hamiltonien). Il y a dix manières de combiner ces symétries potentielles d'un hamiltonien à une particule H, appelées des *classes de symétrie* (qui avaient déjà été découvertes par Altland et Zirnbauer dans le contexte des systèmes désordonnés [AZ97], et qui sont reliés aux espaces symétriques de Cartan). Par exemple, le hamiltonien peut n'avoir aucune symétrie : dans ce cas, on dit qu'il est dans la classe A, et c'est par exemple le cas de l'IQHE et des isolants de Chern. Il est aussi possible que H soit invariant par renversement du temps, avec un opérateur de renversement du temps dont le carré est $-\mathrm{Id}$, mais sans invariance par conjugaison de charge, ni par symétrie chirale : dans ce cas, H est dans la classe AII ; c'est le cas des isolants de Kane-Mele. Plusieurs approches ont été développées pour obtenir cette classification : Schnyder, Ryu, Furusaki et Ludwig [SRFL08; SRFL09; RSFL10] utilisent une méthode fondée sur la (ou l'absence de) localisation d'Anderson des états de Dirac apparaissant dans la description de basse énergie du bord d'un isolant topologique, alors que la description par la K-théorie développée

par Kitaev [Kit09] se concentre sur la classification des hamiltoniens de volume. Le fait que ces deux approches s'accordent n'est pas évident, et c'est en fait le cœur de la correspondance bord-volume. Un autre point de vue sur cette classification fondé sur les anomalies a émergé de l'étude de la réponse électromagnétique de l'effet Hall quantique, et plus généralement de l'étude de champs de jauge couplés aux isolants topologiques [RML12]. Les symétries spatiales/cristallographiques (qui sont unitairement réalisées) contraignent et enrichissent aussi les propriétés topologiques possibles, mais d'une manière moins robuste : la correspondance bord-volume n'est dans ce cas valable que lorsque les bords sont laissés invariants par les symétries pertinentes, au moins en moyenne. Malgré une intense activité, partiellement revue dans [CTSR15] (voir aussi les articles plus récents [WL16; SSG15; DL16]) une classification complète de ces phases topologiques plus fines n'est, à la connaissance de l'auteur, pas encore réalisée.

1.3 Phases topologiques en dehors de la physique du solide

La propagation d'ondes linéaire dans un milieu spatialement périodique est décrite dans le cadre de la théorie de Bloch par des relations de dispersion $\omega(k)$ qui s'organisent en une structure de bande, de la même manière que dans le cas d'électrons dans un cristal. Un tel système peut donc être caractérisé par des invariants topologiques, et supporter des états de bord topologiques dans un échantillon fini, à condition qu'il puisse y avoir des interférences entre les ondes, et que la structure de phases pertinente puisse être mise en place dans le milieu. Cela n'est pas une surprise dans la mesure où une topologie non-triviale se manifeste sous la forme de motifs particuliers de la phase géométrique, qui sont à l'origine des états de bord : les phases géométriques (phases de Pancharatnam–Berry [Pan56; Ber84] et angles de Hannay [Han85]) sont connus dans les systèmes classiques comme dans les systèmes quantiques [CJ04]. De telles propriétés ont été prédites (et souvent observées) dans des domaines très variés : dans des systèmes mécaniques [PP09; BJKP11; KL13; CUV14; VUG14; PCV15; SH15; NKRV15], des ondes acoustiques [YGSL15; KFMA15; FKA15; XMYS15], des ondes électromagnétiques, en particulier de la lumière visible et des micro-ondes [HR08; RH08; WCJS09; HDLT11; KMTK12; FYF12; RZPL13; HMFM13; LJS14; MGFV16; CJNM16], des systèmes opto-mécaniques [PBSM15], des gaz d'atomes froids [JMDL14; ALSA14; AALB13; MSKB13], des circuits électriques linéaires [NOSS15; AGJ15] et des réseaux de réactions (bio)chimiques [MV16]. Cet ensemble de travaux a eu une importance considérable, dans la mesure où il a permis de comprendre (et de confirmer expérimentalement) que les propriétés topologiques d'une structure de bande de Bloch et les états de bord associés sont des propriétés essentiellement ondulatoires, que l'on peut retrouver dans tous les domaines de la physique, ce qui a provoqué un intérêt considérable dans le domaine, des découvertes fondamentales passionnantes et des perspectives d'applications très prometteuses.

1.3.1 Ondes électromagnétiques: cristaux photoniques dans le domaine optique et micro-ondes

Une fructueuse analogie entre les systèmes optiques et électroniques [HL90; JJWM11] a émergé dans les années 80, en particulier après la conceptualisation de la notion de cristal photonique [Yab87; Joh87]. Les cristaux photoniques sont caractérisés par une structure de bande photonique, pouvant avoir des gaps (photoniques), de manière analogue aux systèmes électroniques. L'idée générale [JJWM11; NL14] est que les équations de Maxwell dynamiques peuvent être réécrites sous la forme d'une équation de Schrödinger

$$\mathrm{i}\partial_t \psi = M\psi \tag{6.10}$$

où l'opérateur de Maxwell M et le champ électromagnétique ψ sont définis par

$$\psi = \begin{pmatrix} E \\ H \end{pmatrix} \qquad \text{et} \qquad M = \begin{pmatrix} \varepsilon & 0 \\ 0 & \mu \end{pmatrix}^{-1} \begin{pmatrix} 0 & \mathrm{i}\,\mathrm{curl} \\ -\mathrm{i}\,\mathrm{curl} & 0 \end{pmatrix}. \tag{6.11}$$

Ici, E et H sont respectivement les champs électrique et magnétique mésoscopiques, ε et μ sont respectivement les tenseurs de permittivité diélectrique et de perméabilité magnétique locaux, qui décrivent la réponse du matériau dans lequel le champ électromagnétique se propage. Ils sont supposés être constants dans le temps, mais peuvent varier dans l'espace. Dans les milieux bi-anisotropes et bi-isotropes comme les milieux optiquement actifs, l'opérateur de Maxwell a aussi des composantes diagonales. En l'absence de sources, les deux autres équations de Maxwell donnent les contraintes $\mathrm{div}(\mu H) = 0$ et $\mathrm{div}(\varepsilon E) = 0$. En prenant le carré de l'équation de Maxwell-Schrödinger, on obtient l'équation d'onde du second ordre

$$(\partial_t^2 + M^2)\psi = 0 \tag{6.12}$$

où les évolutions des champs magnétique et électrique sont découplées. Dans un cristal photonique, la permittivité et la perméabilité $\varepsilon(x)$ et $\mu(x)$ varient périodiquement dans l'espace. La transformée de Fourier permet de décomposer l'opérateur de Maxwell M en une famille d'opérateurs de Bloch-Maxwell $M(k)$, où k est la quasi-impulsion, dont les valeurs propres donnent la relation de dispersion $\omega_n(k)$ du cristal photonique.

Haldane et Raghu [HR08; RH08] ont réalisé en 2005 qu'il est possible d'induire des propriétés topologiques dans un tel cristal photonique gappé si l'invariance par renversement du temps est brisée par effet Faraday dans un milieu gyromagnétique où μ n'est pas un tenseur symétrique[(3)]. Cette idée a été confirmée expérimentalement [WCJS09] par Wang, Chong, Joannopoulos et Soljačić, qui ont observé des modes électromagnétiques unidirectionnels protégés contre la rétrodiffusion dans un cristal photonique topologiquement non-trivial dans le régime des micro-ondes, réalisé à partir d'un réseau de bâtonnets cylindriques de ferrite de rayon de l'ordre du centimètre,

[(3)] Habituellement, la perméabilité et la permittivité sont des tenseurs symétriques. Néanmoins, sous un champ magnétique extérieur B_0, les tenseurs ϵ et μ peuvent ne pas être symétriques : dans ce cas, le milieu est dit *gyrotropique*. Le renversement du champ magnétique transpose les tenseurs, avec $\epsilon(-B_0) = \epsilon^T(B_0)$ et $\mu(-B_0) = \mu^T(B_0)$. Quand seul μ (resp. ε) est concerné, le matériau est dit *gyromagnétique* (resp. *gyroélectrique*).

soumis à un champ magnétique. À partir de mesures de diffusion utilisant deux antennes et un analyseur de réseau, dont le principe est essentiellement d'envoyer et de recevoir de la lumière micro-ondes pour mesurer la matrice de répartition (*scattering matrix*), ils ont montré l'existence de modes non-réciproques (chiraux) localisés près du bord, en accord avec les prédictions théoriques, voir figures 6.11 et 6.10. En ajoutant un obstacle métallique, ils ont aussi montré la robustesse de ces états de bord chiraux.

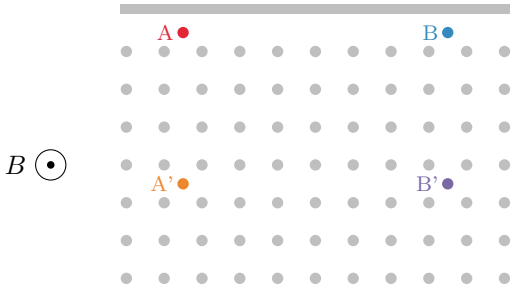

Figure 6.10: Cristal photonique avec un bord et des antennes de mesure. Le cristal photonique utilisé par [WCJS09] est composé de bâtonnets cylindriques ferrimagnétiques sous un champ magnétique. Une interface constituée d'un mur de métal joue le même rôle qu'une interface avec le vide dans un système électronique (de l'air ou du vide autoriseraient des pertes par radiation). Deux antennes sont utilisées pour mesurer la transmission directe et inverse de la lumière micro-onde dans le cristal photonique. Il est possible de sonder le volume (avec les antennes A' et B') ou les bords (avec les antennes A et B), voir figure 1.11. Ce dispositif a permis à Wang et collaborateurs [WCJS09] de démontrer l'existence de modes non-réciproques (chiraux) situés près du bord, en accord avec les prédictions théoriques.

Divers travaux théoriques et expérimentaux ont eu lieu à la suite de ces investigations ; une revue récente est [LJS14]. Du point de vue fondamental, la classification des isolants topologiques photoniques a été étudiée par De Nittis et Lein [NL14]. Les systèmes dans le domaine des micro-ondes comme celui utilisé par Wang et collaborateurs ont aussi été employés pour réaliser expérimentalement la fusion de cônes de Dirac [BKMM13] et pour observer des effets topologiques faibles [BKMM14] dans du graphène artificiel. Aux longueurs d'onde des micro-ondes, un analyseur de réseau peut permettre de sonder la phase des états propres, ce qui est particulièrement utile pour étudier les systèmes topologiques. Ce genre d'expérience de diffusion a été effectué par Hu et al. [HPWP15] dans un système de résonateurs optiques annulaires [LC13] qui peut être décrit comme un réseau orienté de diffusion [PC14; TD15] similaire au modèle de Chalker-Coddington [CC88; HC96]. Une autre branche de ce champ de recherche est particulièrement pertinent ici. Pour la lumière visible, les effets gyrotropiques sont généralement très petits, et une extension de la méthode utilisée par Wang et al. [WCJS09] semble hors d'atteinte expérimentale. Une possibilité pour passer outre cette difficulté a été proposée et réalisée expérimentalement par Rechtsman et collaborateurs [RZPL13], qui ont utilisé des guides d'onde en forme d'hélices arrangés en un réseau bidimensionnel pour réaliser un isolant topologique de Floquet à deux dimensions. Dans leur dispositif, la direction (spatiale) de propa-

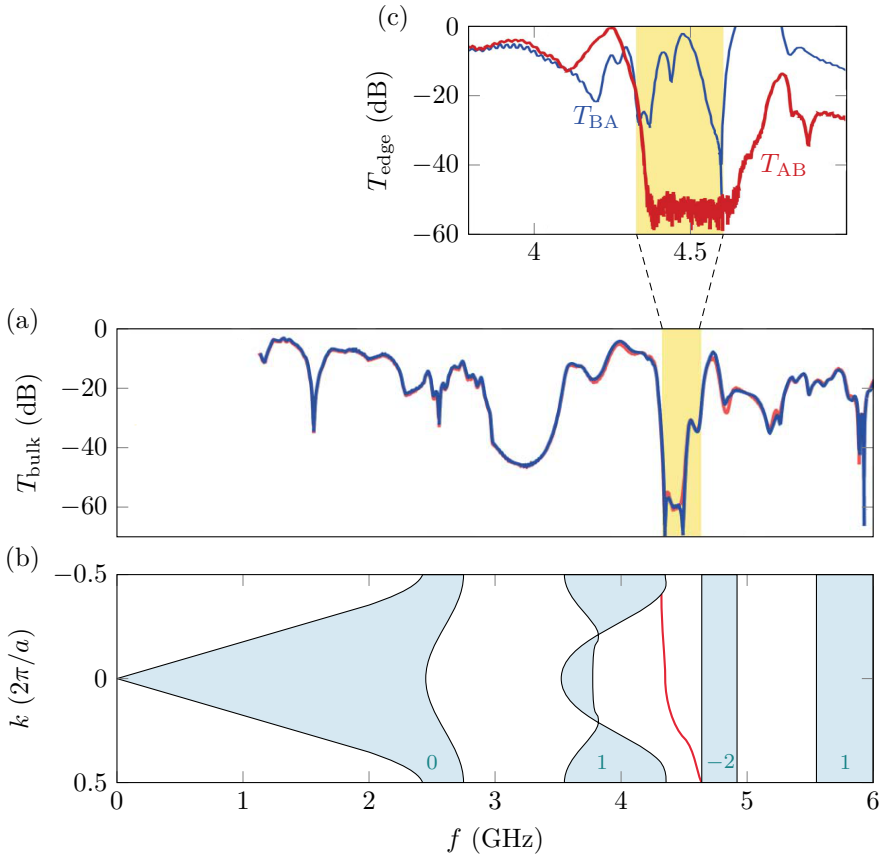

Figure 6.11: Signatures de diffusion des états de bord photoniques chiraux. La structure de bande photonique (projetée) pour les modes transverses magnétiques $f(k)$ du cristal photonique conçu par [WCJS09], dont l'allure est représentée en (b), présente des gaps topologiques, qui accueillent des états de bord topologiques (en rouge). Une signature de ces états de bord est obtenue par des mesures de coefficients de transmission : dans le volume (a), la transmission est réciproque : il n'y a pas de différence significative entre la transmission directe (en bleu) et indirecte (en rouge). (c) Au contraire, sur le bord, la transmission dans la direction inverse est nettement inférieure à la transmission dans la direction directe. Dans la structure de bande (b), les premiers nombres de Chern des bandes sont indiqué en bleu. Ils sont compatibles avec l'existence de l'état de bord rouge. Un état de bord supplémentaire devrait apparaître dans le gap séparant les deux bandes de plus haute fréquences, mais [WCJS09] expliquent que ces bandes ont des bords mal définis à cause d'une absorption importante à ces fréquences, due à la proximité avec la résonance ferromagnétique, ce qui explique sans doute que cet état de bord supplémentaire ne soit pas indiqué. Adapted from [WCJS09]. Reprinted by permission from Macmillan Publishers Ltd, Nature, copyright 2009.

gation de la lumière (dans les guides d'onde) ne joue pas le même rôle que les deux directions orthogonales, et il est commode de prendre cette particularité en compte pour simplifier les équations de Maxwell dynamiques. Les guides d'onde sont obtenus en illuminant un verre comme la silice avec des impulsions laser ultracourtes, qui modifient légèrement l'indice de réfraction, changeant sa valeur initiale n_0 en un indice dépendant de la position $n_0 + \delta n(x)$. Cette méthode permet de fabriquer des guides d'onde bien contrôlés pour la lumière visible. Dans l'approximation paraxiale où la lumière se propage essentiellement selon l'axe du guide d'onde z, l'équation de Helmholtz qui gouverne la partie spatiale ϕ d'un champ électromagnétique monochromatique $\psi(t, x) = \phi(x)\mathrm{e}^{-\mathrm{i}\omega t}$ à pulsation ω prend la forme

$$\mathrm{i}\partial_z \phi = -\frac{1}{2k_0}\nabla_\perp^2 \phi - \frac{k_0 \delta n}{n_0}\phi \tag{6.13}$$

où $\nabla_\perp = \partial_x^2 + \partial_y^2$, $k_0 = 2\pi n_0/\lambda$, et $\lambda = 2\pi c/\omega$ est la longueur d'onde dans le vide de la radiation. La propagation de la lumière le long du guide d'onde est similaire à une évolution dans le temps, où le temps t est remplacé par la distance z de propagation le long de l'axe du guide d'onde. L'équation de propagation est similaire à une équation de Schrödinger où l'indice optique dépendant de la position joue le rôle du potentiel (voir e.g. [Lon09; SN10] pour des détails). Par exemple, lorsque deux guides d'onde sont suffisamment proches l'un de l'autre, ils peuvent échanger de la lumière par couplage évanescent : ainsi, la lumière envoyée initialement dans un des guides d'onde oscille entre les deux guides au cours de sa propagation, de manière analogue aux oscillations de Rabi. Tant que les guides d'onde ne sont pas trop fortement couplés, il est ainsi possible de décrire un arrangement de guides d'onde parallèles par une théorie de couplage de modes analogue à une description de liaisons fortes en physique du solide (voir e.g. [YY06; SN10]). De plus, la forme en hélice des guides d'onde peut être prise en compte dans cette description comme une modulation périodique des paramètres de la théorie de couplage de modes/liaisons fortes dans la direction de propagation (voir e.g. [Lon09; SN10]). Les équations décrivant la propagation sont donc formellement équivalentes à l'équation d'évolution d'un hamiltonien de liaison fortes modulé périodiquement dans le temps. Une modulation sinusoïdale des guides d'onde imite l'interaction d'un électron avec un champ électrique linéairement polarisé. Les guides d'ondes en hélice utilisés par Rechtsman et collaborateurs correspondent à une polarisation circulaire, et ils ont comme attendu observé, pour des paramètres bien choisis, une propagation chirale de la lumière sur le bord du système, même en présence de défauts.

1.3.2 Ondes mécaniques : phonons dans des réseaux de billes et ressorts

Suite aux travaux de Prodan et collaborateurs [PP09; BJKP11] qui ont identifié des modes phonon topologiques dans des systèmes inspirés de la biologie, Kane et Lubensky [KL13] ont développé un cadre permettant de caractériser les propriétés topologiques des systèmes périodiques de billes et ressorts, en analogie avec les systèmes électroniques. En particulier, ils ont donné une formulation précise (du point de vue de la physique) sur la correspondance bord-volume dans les réseaux mécaniques. Dans ces réseaux mécaniques, des billes reliées les unes aux autres par des ressorts hookéens sont disposés périodiquement dans l'espace. Le spectre de phonons s'organise ainsi en bandes de Bloch $\omega_i(k)$, où k est la quasi-impulsion, et une bande de Bloch isolée

des autres par des gaps peut être topologiquement non-triviale. Le réseau mécanique possède deux types de degrés de liberté : les déplacements des billes, et les extensions des ressorts, définis dans les deux cas par rapport à une configuration d'équilibre. La relation géométrique entre les déplacements u_i et les extensions e_m est contenue dans la *matrice de rigidité* R définie par

$$e_m = R_{mi} u_i. \tag{6.14}$$

De même, la relation géométrique entre les tensions T_m des liens et les forces F_i s'appliquant sur les billes est contenue dans la *matrice d'équilibre* $Q \equiv R^T$ telle que

$$F_i = Q_{im} T_m. \tag{6.15}$$

Du point de vue de la dynamique, la tension T_m d'un lien hookéen est reliée à son extension par $T_m = -K_m e_m$, et la force F_i sur une bille est donnée par la loi de Newton $F_i = M_i \ddot{u}_i$. Quant toutes les raideurs et toutes les masses sont égales, $K_m = K$ et $M_i = M$, il est pratique de définir $\omega_0 = \sqrt{K/M}$, et l'équation du mouvement s'écrit

$$\mathrm{i}\frac{\mathrm{d}}{\mathrm{d}t}\psi = \mathcal{H}\psi \tag{6.16}$$

où

$$\mathcal{H} = \omega_0 \begin{pmatrix} 0 & Q \\ Q^T & 0 \end{pmatrix} \qquad \text{et} \qquad \psi = \begin{pmatrix} \dot{u} \\ -\mathrm{i}\omega_0 e \end{pmatrix}. \tag{6.17}$$

Encore une fois, la transformée de Fourier permet d'exploiter la périodicité spatiale du système, et on obtient une famille de hamiltoniens de Bloch matriciels $\mathcal{H}(k)$. Quand cette famille d'hamiltoniens de Bloch est gappée, les invariants topologiques peuvent être définis et calculés de la manière habituelle. Un gap à fréquence nulle dans le spectre d'excitation du système n'est possible que si le système est *isostatique*, c'est-à-dire quand le nombre de contraintes (dues aux liens) est égal au nombre de degrés de liberté des billes, et dans ce cas, une symétrie de structure (une symétrie chirale dans le langage des isolants topologiques) visible à la forme antidiagonale par blocs de $\mathcal{H}$ peut être utilisée pour protéger des phases topologiques. Une description hamiltonienne des systèmes mécaniques (topologiques) ne se limitant pas aux systèmes de billes et ressorts, ainsi qu'une classification des phases topologiques correspondantes (à fréquence nulle et finie) a récemment été développée par Süsstrunk et Huber [SH16] dans un article très clair.

Kane et Lubensky ont proposé un analogue mécanique du modèle deSu-Schrieffer-Heeger du polyacétylène, qui a été réalisé expérimentalement par Chen et al. [CUV14]. Mis à part aux points de transition, le volume du système est isolant, ce qui signifie qu'il n'y a pas de mode à fréquence nulle. Dans un système mécanique avec des liens de très grande raideur (par exemple si on remplace les ressorts par des tiges en plastique), aucun mouvement n'est possible. À l'interface entre deux isolants mécaniques topologiquement distincts, par contre, il existe un mode de fréquence nulle robuste, et le mouvement n'est possible qu'à travers ce mode de bord topologique (voir figure 6.12). Ici, le mouvement n'est pas infinitésimal, parce qu'un soliton couplé à la paroi de domaine séparant les deux phases topologiquement différentes peut se propager le long de la chaîne [CUV14; VUG14], un comportement proche de ce qu'on observe dans le polyacétylène [JR76].

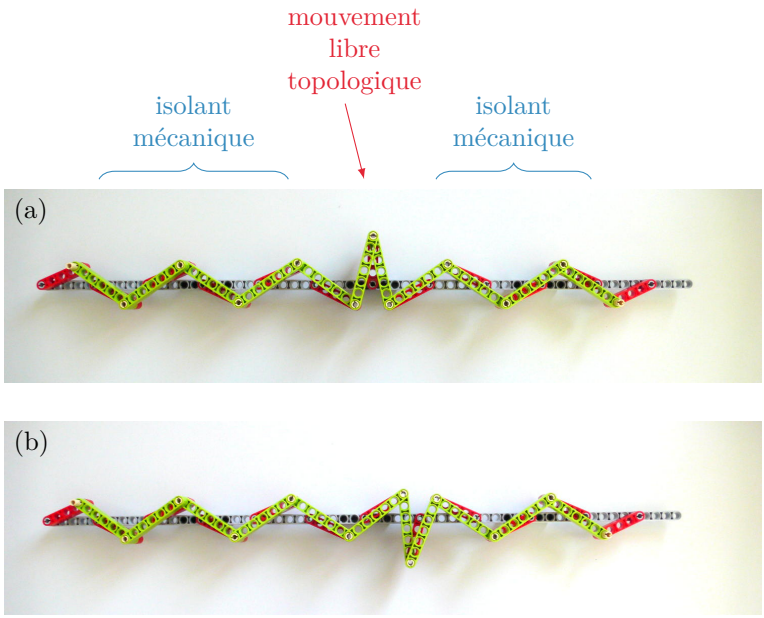

Figure 6.12: Isolant topologique mécanique en LEGO. Une version en LEGO du modèle SSH mécanique, conçue par Vitelli et al. [VUG14]. Les deux phases isolantes correspondent aux zones où les tiges rouges pointent vers la droite ou vers la gauche de leur point d'attache. Dans ces zones, aucun mouvement n'est possible (à fréquence nulle). À l'interface entre les deux phases topologiquement inéquivalentes, au contraire, il y a un degré de liberté à fréquence nulle, qui correspond à un mouvement libre. Si on pousse légèrement les tiges vertes ou rouges près de l'interface, la paroi de domaine peut se déplacer, e.g. de (a) à (b), et se propager tout le long du système.

Une autre réalisation expérimentale d'un système mécanique topologique est due à Nash et collaborateurs [NKRV15], qui ont utilisé un réseau de gyroscopes couplés pour créer un métamatériau bidimensionnel comportant des états de bord chiraux (un analogue du modèle de Haldane). J'invite le lecteur à aller voir leurs vidéos. Ici, encore une fois, un mouvement périodique dans le temps est utilisé pour induire des propriétés topologiques.

1.4 Induire des propriétés topologiques par un forçage périodique dans le temps

Nous avons déjà mentionné qu'une modulation périodique dans le temps (ou son équivalent en propagation paraxiale) peut être utilisé pour induire des propriétés topologiques dans les systèmes photoniques et mécaniques. Ces méthodes proviennent de la physique du solide, où il a été proposé de contrôler par la lumière les propriétés topologiques de systèmes électroniques, une idée qui se heurte à des difficultés expérimentales. L'idée d'induire une transition de phase topologique par une excitation périodique dans le temps, par exemple en éclairant par un laser une feuille de gra-

phène, a été proposée en 2009 par Oka et Aoki [OA09], qui ont rapidement été suivis par Inoue et Tanaka [IT10], puis Lindner, Refael et Galitski [LRG11] qui proposèrent un "isolant topologique de Floquet" où l'effet Hall quantique de spin est induit par la lumière. Des idées du même ordre avaient déjà été développées (du point de vue théorique) au début des années 2000 dans le domaine des atomes froids ; l'état du domaine de recherche en 2007 est revu dans l'article [LSAD07].

En première approximation, un hamiltonien (de Bloch) $H_0(k)$ soumis à une perturbation périodique dans le temps $W(t) = W(t+T)$ peut être remplacé par un "hamiltonien effectif" indépendant du temps, qui décrit la dynamique stroboscopique à long temps du système, après un nombre entier de périodes (i.e. aux temps nT, où $n \in \mathbb{Z}$). Pour une perturbation monochromatique

$$W(t) = W_1(k)\mathrm{e}^{\mathrm{i}\omega t} + W_{-1}(k)\mathrm{e}^{-\mathrm{i}\omega t} \tag{6.18}$$

ce hamiltonien effectif est, au premier ordre,

$$H^{\text{eff}}(k) = H_0(k) + \frac{1}{\omega}[W_1(k), W_{-1}(k)] + O\left(\frac{1}{\omega^2}\right). \tag{6.19}$$

En partant d'une phase critique avec des cônes de Dirac (comme le graphène), il est ainsi possible d'induire des propriétés topologiques à condition que le signe des masses aux différents points de Dirac puisse être contrôlé. C'est le cas du couplage avec une onde électromagnétique dans le graphène, qui induit des masses opposées dans les deux vallées [OA09; IT10]; de manière analogue, dans le dispositif utilisé par [RZPL13], les guides d'onde en hélice imitent justement le couplage avec de la lumière polarisée circulairement. Pour donner une idée de ce qui se passe, nous allons nous concentrer sur le hamiltonien de basse énergie au voisinage d'un seul cône de Dirac

$$H_0(q) = q_x\sigma_x + q_y\sigma_y \tag{6.20}$$

et prendre une perturbation simple, avec $W_1 = W/4\,(\sigma_x + \mathrm{i}\sigma_y)$ et $W_{-1} = W_1^\dagger$. On obtient

$$H^{\text{eff}}(q) = q_x\sigma_x + q_y\sigma_y + \frac{W^2}{\omega}\sigma_z + \text{termes d'ordre plus élevé.} \tag{6.21}$$

Il est ainsi possible de gapper le point de Dirac avec une masse dépendant de W. Dans le graphène, la perturbation correspondant à une lumière polarisée circulairement est W_1 ou $W_1^\dagger$, selon la vallée concernée, et les masses $\pm W^2/\omega$ dans les deux vallées sont donc bien opposées. Une perturbation plus simple, identique dans les deux vallées, peut aussi induire des propriétés topologiques, mais à un ordre plus haut en perturbation.

À première vue, le hamiltonien effectif indépendant du temps H^{eff} est suffisant pour comprendre la topologie de ces systèmes forcés périodiquement : le forçage peut conduire à un hamiltonien effectif H^{eff} non-trivial à partir d'un hamiltonien non-perturbé H_0 trivial. Le sens ce hamiltonien effectif doit cependant être précisé. Dans un système forcé, l'énergie n'est plus conservée, puisqu'elle peut être échangée avec le champ excitateur. Néanmoins, la périodicité temporelle du forçage assure que l'énergie n'est échangée que par quanta de $\hbar\omega$ (où ω est la pulsation de forçage), et la quantité

$$\varepsilon = E \bmod \hbar\omega \tag{6.22}$$

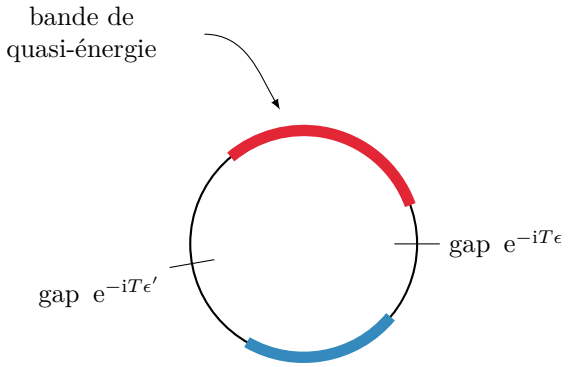

Figure 6.13: Un spectre de quasi-énergie. Le spectre de l'opérateur unitaire d'évolution après une période $U(T)$ est appelé spectre de quasi-énergie, et il s'organise sur le cercle unité $U(1)$. Comme dans le cas des systèmes statiques, le spectre de quasi-énergie d'un cristal est composé de bandes (dans cet exemple, il y a deux bandes, une en bleu et une en rouge), séparées par des gaps.

appelée *quasi-énergie* reste conservée. Ainsi, un système forcé périodiquement est caractérisé par son spectre de quasi-énergie (et les états propres correspondants) à la place d'un spectre d'énergie. Ce spectre de quasi-énergie apparaît comme le spectre du hamiltonien effectif H^{eff} ou, à une exponentielle près, comme le spectre sur le cercle de l'opérateur d'évolution après une période $U(T) = e^{-iTH^{\text{eff}}}$, qu'on appelle souvent l'opérateur de Floquet. Par suite, les quasi-énergies sont essentiellement des phases, c'est-à-dire des quantités périodiques, qui vivent sur un cercle, comme on le montre figure 6.13. L'opérateur de Floquet $U(T)$ est bien défini, mais le hamiltonien effectif n'est pas défini de manière unique : un choix de branche pour le logarithme complexe est nécessaire. La périodicité des quasi-énergies peut sembler inoffensive. À la place de bandes de quasi-énergie dans le spectre du hamiltonien, des bandes de quasi-énergie apparaissent dans le spectre de l'opérateur de Floquet $U(T)$, et on pourrait espérer décrire la topologie des systèmes forcés périodiquement de la même manière que pour les systèmes statiques, à travers la topologie des bandes de quasi-énergie. Il se trouve que ces phases hors d'équilibre ont une topologie plus riche que les phases d'équilibre : un système où tous les invariants de bande s'annulent peut tout de même avoir des propriétés topologiques non-triviales, dans des situations appelées des phases topologiques "anomales".

Ces propriétés particulières des systèmes forcés périodiquement ont été remarquées par Kitagawa et al. [KBRD10], puis rapidement observées dans des expériences dans le domaine optique [KBFR12]) et comprises en 2013 par Rudner, Lindner, Berg, et Levin [RLBL13]. Ces auteurs ont développé un nouveau cadre technique pour décrire complètement les propriétés topologiques d'une évolution unitaire dans un système à deux dimensions d'espace, soumis à une excitation périodique dans le temps, et sans symétrie particulière, qui permet de rendre compte correctement de l'existence d'états de bord chiraux au bord d'un échantillon fini. La raison de la particularité de ces phases anomales est la périodicité du spectre de quasi-énergie. Dans un système

à l'équilibre avec deux bandes d'énergie, il peut y avoir des états de bord dans le gap de volume situé (en énergie) entre les deux bandes[4]. Dans un système de Floquet avec deux bandes de quasi-énergie, il y a *deux* gaps de volume, et chacun d'eux peut accueillir des états de bord dans un système fini, comme on le voit sur la figure 6.14. Bien entendu, cette observation se généralise à plus que deux bandes. Dans les systèmes fermioniques, la périodicité de la quasi-énergie souligne la question du remplissage thermodynamique des bandes de quasi-énergie : il n'y a pas de "bas de bande" où commencer le remplissage. Il n'est donc pas raisonnable de s'attendre à un comportement indépendant du champ excitateur et des bains et réservoirs auxquels le système est relié.

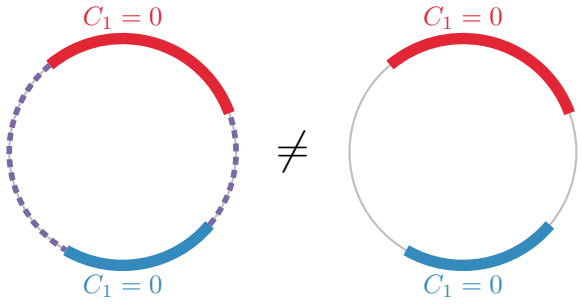

Figure 6.14: Systèmes trivial et topologique anomal. Les spectres de quasi-énergie de deux systèmes avec des bords, qui ont la même structure de bande de volume (bandes bleue et rouge) mais ont des différentes propriétés topologiques de volume, qui se manifestent par des relations de dispersion au bord différentes (en tirets violets). Malgré cette différence, les deux systèmes ont les mêmes invariants de bande de volume (les premiers nombres de Chern C_1), qui ne sont pas suffisants pour pleinement caractériser le système [RLBL13].

La méthode développée par Rudner et al. [RLBL13] consiste à définir des *invariants de gap* qui sont directement reliés (égaux) au nombre d'états de bord (comptés algébriquement avec chiralité) qui rempliraient le gap de volume concerné dans un système avec des bords. Ce point de vue est particulièrement bien adapté aux situations où il est possible de sonder la réponse du système à quasi-énergie fixée, par exemple lors d'expériences de diffusion (*scattering*), sans qu'il soit nécessaire d'avoir un remplissage particulier des états. C'est le cas dans plusieurs systèmes classiques (une belle expérience dans des cristaux photoniques peut être trouvée dans [SLIY15]). Au contraire, les phases topologiques sont généralement comprises à travers la topologie de l'état fondamental, un point de vue très fructueux qui a été étendu aux phases en interaction comme l'effet Hall quantique fractionnaire, et a conduit à la notion d'*ordre topologique*, introduite par Xiao-Gang Wen [Wen90]. Un bon nombre

[4] Pour traiter les deux situations sur le même pied, on peut considérer qu'un hamiltonien constant est en fait périodique dans le temps, avec une période T assez petite pour que $T\sigma(H) \subset]-\pi, \pi[$, c'est-à dire quelle que la structure de bande enroulée sur le cercle ne s'enroule pas sur elle-même.i.e. so that the band structure laid on the circle does not overlap with itself. Dans cette situation, les "gaps d'énergie" allant du haut de la bande de conduction à $+\infty$ et du bas de la bande de valence à $-\infty$ correspondent au gap de quasi-énergie autour de $e^{\pm i\pi} = -1$, qui ne peut par conséquent pas supporter d'état de bord.

de développements ont eu lieu dans cette direction, en particulier pour classer les phases topologiques protégées par symétrie (SPT, pour *symmetry protected topological phases*, une formalisation particulière de ce qu'on appelle *isolant topologique* ici) à travers l'état fondamental de hamiltoniens gappés, par des méthodes de cohomologie des groupes [CGLW13; GW14; CGLW12; Wit16]. Dans le cas des systèmes forcés périodiquement topologiques, plusieurs raisons laissent penser que cette description pourrait ne pas être entièrement pertinente : (i) dans les phases anomales, les invariants topologiques associés à une bande sont toujours nuls, mais le système manifeste néanmoins ses propriétés topologiques par l'apparition d'états de bord dans un système fini ; (ii) le fondamental n'est pas bien défini, puisque le remplissage des bandes de Floquet n'est pas univoque, et dépend fortement des détails du couplage avec l'environnement.

L'idée d'induire des propriétés topologiques à travers un forçage périodique, et par suite, les propriétés particulières des phases topologiques de Floquet, sont bien entendu intéressantes du point de vue fondamental. Au delà de cet intérêt fondamental, les phases topologiques de Floquet offrent un moyen commode de réaliser des phases topologiques en dehors du domaine de la physique du solide. Dans les atomes froids, l'idée d'utiliser des réseaux optiques modulés périodiquement dans le temps pour contrôler les paramètres de saut est bien établie, et je renvoie le lecteur aux revues récentes [Hol15; GD14] pour plus de détails. En particulier, contrôler les amplitudes tunnel permet de créer des champs de jauge artificiels [HTCÖ12]. Une application évidente d'une telle méthode est la simulation d'isolants topologiques : mentionnons les réalisations expérimentales du modèle de Haldane [JMDL14] et du hamiltonien de Harper-Hofstadter [ALSA14; AALB13; MSKB13]). De manière plus ou moins indépendante, comme on l'a vu, les mêmes concepts ont aussi été utilisées pour concevoir et réaliser des phases topologiques (i) dans des systèmes mécaniques, expérimentalement avec un réseau de gyroscopes reliés par des ressorts [NKRV15], et théoriquement avec des gyroscopes [WLB15] et dans un référentiel en rotation [WLZ15; KH15], ainsi que (ii) avec de la lumière [KBFR12; RZPL13], dans un dispositif où l'évolution périodique en temps est remplacé par une modulation périodique dans la $(d+1)$ème dimension d'espace selon laquelle la propagation a lieu. Tous comptes faits, je considère que les systèmes forcés périodiquement (et les champs de jauge artificiels correspondants) sont un outil important pour étendre la notion d'isolant topologique en dehors du cadre où elle a été initialement découverte.

Enfin, le cadre développé pour l'étude des phases topologiques des systèmes forcés périodiquement, qui peut aussi être appliqué aux systèmes à l'équilibre, pourrait servir comme plateforme pour une meilleure compréhension des phases topologiques. Par exemple, les états de bord d'une phase anomale sont (ou du moins semblent être) de la même nature que les états de bord topologiques habituels. Pourtant, les systèmes anomaux ne sont pas caractérisés par des invariants de bande : cet écart au comportement habituel pourrait servir d'outil pour comprendre les limites des caractérisations connues des états topologiques, et de les étendre d'une manière mieux adaptée aux systèmes hors matière condensée.

1.4.1 Phases topologiques de Floquet dans les systèmes électroniques

La réalisation expérimentale d'états de Floquet topologiques dans le cadre de la matière condensée électronique pose un certain nombre de défis, qui n'ont pas encore tous été résolus. La théorie de Floquet est une approche de haute fréquence, qui a du sens lorsque le forçage est rapide par rapport aux échelles de temps caractéristiques du système non-perturbé. Dans ce régime de très haute fréquence, le système ressent essentiellement un potentiel effectif statique. La limite opposée est celle d'un forçage adiabatique très lent, pendant lequel l'état du système suit les états propres instantanés du hamiltonien dépendant du temps. Si l'on part d'une limite de très haute fréquence, le régime où des comportements intéressants peuvent être observés est typiquement atteint lorsque la fréquence de forçage devient comparable aux échelles de temps naturelles du système non-perturbé. Néanmoins, plusieurs difficultés apparaissent lorsque la fréquence est "trop basse" : premièrement, à basse fréquence, les bandes d'énergie non-perturbées s'enroulent un grand nombre de fois sur le cercle, et obtenir un gap de taille raisonnable semble difficile. À encore plus basse fréquence, le spectre de quasi-énergie n'a plus vraiment de sens, les séries perturbatives ne sont plus pertinentes, et la théorie de Floquet n'est plus d'aucune aide. Ainsi, pour avoir des résultats intéressants et pourvus de sens, la largeur de bande doit être comparable à (ou du moins de l'ordre de) la fréquence d'excitation. Par exemple, la largeur de bande du graphène est de l'ordre de $6t$ où $t \approx 3\,\mathrm{eV}$, et on peut donc s'attendre à ce que l'ordre de grandeur de l'amplitude du rayonnement nécessaire soit dans la gamme de l'ultraviolet lointain, avec $f \sim 6t/h \sim 1 \times 10^{15}\,\mathrm{Hz}$. Un tel rayonnement ionisant va endommager le système. Le problème est encore pire lorsqu'on souhaite obtenir un gap de taille raisonnable dans le spectre de Floquet : une très forte intensité lumineuse est nécessaire à ces fréquences, qu'on pourrait imaginer obtenir avec un laser. Si l'effet de la lumière est pris en compte par couplage minimal $p \to p - eA$ dans un hamiltonien de Dirac $H(p) = v_\mathrm{F} p \cdot \sigma$, le gap est de l'ordre de [CPRT11]

$$\Delta \sim \frac{\alpha v_\mathrm{F}^2 I}{\omega^3} \tag{6.23}$$

où $I \sim c\,\varepsilon_0\,\omega^2 A^2$ est l'intensité du faisceau laser, en $\mathrm{W \cdot m^{-2}}$ (voir e.g. [Pas16]), et $\alpha \approx 1/137$ est la constante de structure fine. Avec la pulsation estimée $\omega \sim 1 \times 10^{16}\,\mathrm{rad \cdot s^{-1}}$, un gap de $10\,\mathrm{meV}$ nécessiterait $I \sim 1 \times 10^{17}\,\mathrm{W \cdot m^{-2}}$ avec $v_\mathrm{F} \sim 1 \times 10^6\,\mathrm{m \cdot s^{-1}}$ dans le graphène. Une si forte intensité laser risque d'avoir un effet délétère sur la stabilité de la feuille de graphène, ne serait-ce que par chauffage. Plusieurs propositions ont des estimations légèrement plus optimistes de la pulsation et de l'intensité laser nécessaires [CPRT11; UPTB14; PUBT14; QGS16], mais qui restent néanmoins pour l'instant hors de portée expérimentale . Malgré ces ordres de grandeur décevants, tout espoir n'est pas perdu, puisque des états de Floquet ont été détectés sans ambiguïté dans le groupe de Gedik par Mahmood et collaborateurs [MCAG16] (à la suite de précédents travaux [WSJG13]), qui ont utilisé des expériences de pompe-sonde associées à des méthodes de spectroscopie de photoémission résolue en angle et en temps (Tr-ARPES) sur les états de surface de l'isolant topologique Bi_2Se_3 pour induire des états de Floquet avec la lumière de pompe, puis les observer avec la lumière de sonde. En particulier, ils ont pu distinguer la contribution des états de Volkov (qui sont dans ce cas les états de Floquet des électrons libres en dehors de l'échantillon, mais près de sa surface) et les états de Bloch-Floquet du cristal, voir

figure 6.15. Pour donner un ordre de grandeur, la lumière de pompe utilisée pour induire les états de Floquet est dans la gamme infrarouge, avec $\omega \sim 10^{14}\,\mathrm{Hz}$ et $I \sim 10^{12}\,\mathrm{W}^2 \cdot \mathrm{m}^{-1}$. Même si ces travaux sont encore loin de la réalisation expérimentale de phases topologiques de Floquet, ils sont particulièrement prometteurs, et démontrent qu'il est effectivement possible d'induire des états de Floquet dans un cristal, au moins pour de courtes durées (environ une picoseconde).

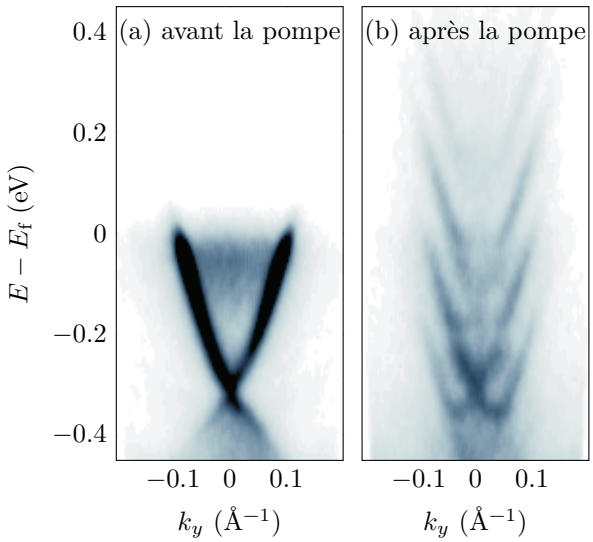

Figure 6.15: Signature en Tr-ARPES signature des états de Bloch-Floquet. Spectres d'ARPES résolue en temps issus de [MCAG16], montrant des états de Bloch-Floquet. (a) Avant l'excitation de forte amplitude, l'ARPES permet d'observer un cône de Dirac à la surface de Bi_2Se_3 ainsi que de bandes de volume. (b) Après que la pompe ait excité l'échantillon, plusieurs "répliques" (ou "bandes latérales") du cône de Dirac original sont observées dans le spectre d'ARPES résolue en temps, translatés en énergie de multiples de $\hbar\omega \simeq 0.16\,\mathrm{eV}$, où ω est la pulsation de la lumière de pompe. Des croisements évités peuvent être observés entre les bandes latérales de Floquet. Dans ce spectre, il y a un mélange de contributions des états de Floquet et des états de Volkov (qui, seuls, conduisent essentiellement à la même signature), mais Mahmood et al. ont réussi à prouver expérimentalement que les états de Bloch-Floquet states existent bel et bien dans le cristal. Adapted from [MCAG16]. Reprinted by permission from Macmillan Publishers Ltd, Nature Physics, copyright 2016.

Même quand (si ?) les difficultés à réaliser des états de Floquet topologiques dans le cadre de la matière condensée électronique seront surmontées, il sera nécessaire de résoudre ou d'éviter le problème du remplissage des bandes de quasi-énergie. Dans un tel système hors d'équilibre, une source de dissipation est essentielle pour espérer atteindre un état stationnaire hors d'équilibre pouvant être décrit par une évolution effective unitaire[TOA09; BDP15; DOM14; DOM15], puisque le champ excitateur agit comme source d'énergie. Une question importante, dans ce contexte, est celle du remplissage de la structure de bandes dans le régime stationnaire [SBLR15; INC15; LDM14], puisque les observables à long temps, comme les propriétés de transport ou

de réponse sont déterminées par l'état stationnaire.

Dans la suite, nous allons supposer qu'un état stationnaire est atteint, et nous n'allons pas nous concentrer sur la thermodynamique (le remplissage), mais plutôt sur la structure dynamique (l'opérateur d'évolution et le hamiltonien effectif) du système. Cela n'est pas un problème, puisque les propriétés topologiques de la structure de bande sont indépendantes de son remplissage. Dans ce cadre, nous allons cependant éviter d'utiliser le mot "isolant" (en particulier dans "isolant de Floquet") pour se référer à un système gappé, du moins tant que le remplissage des bandes de quasi-énergie n'est pas précisé.

2 But de ce travail

2.1 Topologie des systèmes soumis à une excitation périodique dans le temps

Les premières propositions visant à induire des états topologiques par un forçage périodique dans le temps ont été conçues dans une situation sans aucune symétrie (dans la classe A) par Oka et Aoki [OA09] ainsi qu'Inoue et Tanaka [IT10] (des idées du même ordre étaient aussi présentes dans la littérature des atomes froids, en particulier pour réaliser des champs de jauge artificiels). Un an après, Lindner, Refael et Galitski [LRG11] ont proposé une idée similaire pour des systèmes fermioniques invariants par renversement du temps (dans la classe AII, comme les isolants de Kane-Mele). La même année, Jiang et collaborateurs [JKAA11] ont proposé d'utiliser un forçage périodique pour induire des fermions de Majorana dans une chaîne 1D avec symétrie particule-trou (dans la classe D). En même temps, Kitagawa et collaborateurs [KRBD10; KBRD10] faisaient un premier pas vers une classification topologique des systèmes forcés périodiquement. Une avancée majeure a été faite par Rudner, Lindner, Berg, et Levin en 2013 [RLBL13], qui ont réalisé que les invariants caractérisant la topologie des systèmes à l'équilibre ne sont pas suffisants pour entièrement caractériser les systèmes forcés périodiquement, et ont développé une méthode permettant de décrire de manière satisfaisante la topologie des systèmes à deux dimensions sans aucune symétrie (dans la classe A. Au vu de l'importance des symétries dans les systèmes topologiques, il est crucial de généraliser cette méthode aux autres classes de symétrie. En utilisant des méthodes différentes, Asbóth, Tarasinski et Delplace [ATD14] ont défini un invariant pour les systèmes chiraux à une dimension forcés périodiquement (dans la classe AIII, comme le modèle SSH). Un des objectifs de cette thèse était de définir un tel invariant pour les systèmes avec invariants par un renversement du temps fermionique (dans la classe AII, comme les isolants de Kane-Mele), un but qui a été atteint en utilisant le cadre de Rudner et collaborateurs. J'ai aussi réinterprété les résultats de Asbóth et al. dans ce même cadre, et étendu la définition des invariants de Floquet à toutes les dimensions d'espace pour les classes complexes (A et AIII). L'objet principal de cette approche est l'opérateur d'évolution unitaire $U(t,k)$. Lorsque le spectre de l'opérateur de Floquet $U(T,k)$ (le spectre de quasi-énergie) possède des gaps, il est possible de définir des versions périodisées de l'opérateur d'évolution $V_\varepsilon(t,k) = V_\varepsilon(t+T,k)$, qui dépendent de manière cruciale du choix du gap

ε dans le spectre de quasi-énergie. Dans la classe A, la théorie de l'homotopie permet de définir un invariant topologique de volume à partir de l'application unitaire V_ε: son enroulement (ou degré)

$$W_\varepsilon[U] = \deg(V_\varepsilon) \in \mathbb{Z} \tag{6.24}$$

qui compte le nombre d'états de bord chiraux dans le gap de volume ε qui apparaissent dans un échantillon de taille finie [RLBL13]. Il s'agit d'un **invariant de gap**, par opposition e.g. aux invariants de Chern, qui sont des **invariants de bande**, en ce qu'ils caractérisent les bandes de (quasi-)énergie. Il y a une relation entre ces invariants : la différence entre les W dans deux gaps différents donne le nombre de Chern de la bande de quasi-énergie située entre les deux gaps,

$$W_{\varepsilon'}[U] - W_\varepsilon[U] = C_1[P_{\varepsilon,\varepsilon'}]. \tag{6.25}$$

J'ai étendu cette définition à toutes les dimensions paires d, où le $(d/2)$-ème invariant de Chern apparaît [Fru16]. Dans la classe AII, où le renversement du temps $\Theta^2 = -\mathrm{Id}$ est présent, c'est-à-dire quand

$$\Theta H(t,k)\Theta^{-1} = H(-t,-k) \tag{6.26}$$

l'invariant $W_\varepsilon[U]$ est toujours nul à deux dimensions, un comportement similaire à celui du premier nombre de Chern dans cette situation. Cependant, en dimensions $d = 2, 3$, il est possible de définir un nouvel invariant

$$K_\varepsilon[U] \in \mathbb{Z}_2 \tag{6.27}$$

qui compte les états de bord hélicaux dans le gap de volume ε qui apparaissent dans un échantillon de taille finie [CDFG15b]. C'est une quantité à valeurs dans $\mathbb{Z}_2$, comme l'invariant de Kane-Mele. De manière analogue au cas précédent, la différence entre les K de deux gaps donne l'invariant de Kane-Mele de la bande correspondante

$$K_{\varepsilon'}[U] - K_\varepsilon[U] = \mathrm{KM}[P_{\varepsilon,\varepsilon'}]. \tag{6.28}$$

Dans la classe AIII, quand la symétrie chirale est présente, c'est-à-dire que

$$\Gamma H(t,k)\Gamma^{-1} = H(-t,k) \tag{6.29}$$

il y a une contrainte sur les *gaps chiraux* $\varepsilon = 0$ et π (appelés aussi *gaps réels*), qui implique l'annulation de $W_{0/\pi}[U]$ en dimension paire. Dans toutes les dimensions impaires, W n'est pas défini, mais il est possible de définir des invariants de gap chiraux pour les gap chiraux,

$$G_\varepsilon[U] \in \mathbb{Z} \qquad (\varepsilon = 0 \text{ ou } \pi) \tag{6.30}$$

et encore une fois, leur différence donne l'invariant de bande chiral usuel [Fru16].

Je conjecture que cette structure est générale, et se retrouve pour toutes les classes de Cartan-Altland-Zirnbauer. Tous les isolants (ou supraconducteurs) topologiques connus devraient pouvoir être caractérisés par des invariants de gap, qui s'étendent naturellement aux systèmes de Floquet. Les travaux de Nathan et Rudner [NR15]

ainsi que de Roy et Harper [RH16] sont des indices allant dans ce sens. Dans le chapitre 4 de cette thèse, je montre que les invariants de volume W et G caractérisent toutes les classes $\mathbb{Z}$ (et $2/ZZ$) du tableau périodique des isolants topologiques ; en particulier, les contraintes auxquelles les symétries anti-unitaires soumettent ces invariants permettent de retrouver une grande partie du tableau périodique (à l'exception, en fait, des invariants $\mathbb{Z}_2$).

Il serait particulièrement intéressant d'observer des états de Floquet topologiques dans un contexte de physique du solide. Comme je l'ai déjà mentionné, c'est aussi un défi expérimental. En matière condensée électronique, les mesures de transport constituent une manière naturelle de sonder les états topologiques, comme par exemple dans le cas des effets Hall quantiques [Büt88a] ainsi que des isolants de Kane-Mele [RBBM09; Büt09]. On s'attend à observer l'analogue d'une quantification de la conductance dans les systèmes soumis à un forçage périodique, même s'il n'est pas forcément évident que cette quantification devrait toujours avoir lieu. Le transport dans des systèmes forcés périodiquement a déjà été étudié théoriquement dans diverses configurations [KOBF11; GFAA11; KS13; TPBU14; FP16]. J'ai utilisé des simulations numériques résolues en temps pour étudier les propriétés de transport d'états topologiques de Floquet. On observe comme attendu que la conductance différentielle moyenne est quantifiée dans un gap de volume topologique [FDWW16], dans une situation où le transport reste balistique et où la dissipation est principalement due au couplage avec les contacts métalliques. De plus, la conductance à trois terminaux permet de sonder la nature chirale des états de bord.

3 Organisation de la thèse et publications associées

Durant ma thèse, j'ai contribué à plusieurs articles publiés dans des revues à comité de lecture.

1. *An Introduction to Topological Insulators*,
Michel Fruchart, David Carpentier
Comptes Rendus Physique 14 (2013) 779-815
doi:10.1016/j.crhy.2013.09.013, arXiv:1310.0255
Cet article de revue a pour but de fournir une introduction simple et autosuffisante aux isolants topologiques de Chern et de Kane-Mele.

2. *Parallel Transport and Band Theory in Crystals*,
Michel Fruchart, David Carpentier, Krzysztof Gawędzki
EPL 106, 60002 (2014)
doi:10.1209/0295-5075/106/60002, arXiv:1403.2836
Dans les cristaux sur des réseaux qui ne sont pas de Bravais, la définition du hamiltonien de Bloch matriciel n'est pas unique : il y a plusieurs manières inéquivalentes de représenter l'opérateur hamiltonien comme une matrice dépendant de k. De manière similaire (mais indépendante), il y a plusieurs choix inéquivalents de *transport parallèle*, et donc de *courbures* de Berry. C'est surprenant, parce que la courbure de Berry (au contraire de la connexion de Berry) est invariante de jauge, et est donc généralement considérée comme une quantité physique. Dans cet article, nous montrons qu'il existe une courbure de Berry "canonique" qui ne dépend

pas du choix du domaine fondamental (ou cellule unité) utilisé pour décrire le cristal, qui est directement reliée à l'opérateur position, et qui respecte les symétries du cristal. Il est remarquable que cette courbure de Berry canonique ne soit *pas* périodique dans l'espace réciproque. Comme ce sujet n'est relié qu'indirectement aux travaux développés dans cette thèse, je ne l'exposerai pas en détail.

3. *Topological index for periodically driven time-reversal invariant 2D systems*,
David Carpentier, Pierre Delplace, Michel Fruchart, Krzysztof Gawędzki
Phys. Rev. Lett. 114, 106806 (2015)
doi:10.1103/PhysRevLett.114.106806, arXiv:1407.7747
Cet article définit un invariant topologique pour les systèmes forcés périodiquement invariants par un renversement du temps fermionique (dans la classe AII), en deux dimensions, c'est-à-dire une extension de l'invariant de Kane-Mele aux systèmes de Floquet. Son contenu est discuté en détail dans la section 3.4 du chapitre 4, page 152.

4. *Construction and properties of a topological index for periodically driven time-reversal invariant 2D crystals*,
David Carpentier, Pierre Delplace, Michel Fruchart, Krzysztof Gawędzki, Clément Tauber
Nuclear Physics B 896 (2015) 779-834
doi:10.1016/j.nuclphysb.2015.05.009, arXiv:1503.04157
Cet article détaille les preuves des résultats exposés dans l'article précédent. Pour éviter une répétition inutile de sujets techniques, je n'inclurai pas son contenu dans cette thèse, et le lecteur recherchant des preuves ou des détails techniques sur la construction de l'indice K est invité à ce référer à cet article.

5. *Probing (topological) Floquet states through DC transport*,
Michel Fruchart, Pierre Delplace, Joseph Weston, Xavier Waintal, David Carpentier
Physica E 75 (2016) 287-294
doi:10.1016/j.physe.2015.09.035, arXiv:1507.00152
Les mesures de transport sont la méthode usuelle pour sonder les états de bord topologiques. Dans cet article, nous utilisons des simulations numériques résolues en temps pour sonder les propriétés de transport d'états de Floquet (topologiques) dans un régime où nous nous attendons à comprendre les résultats, dans le but de préparer le terrain pour des explorations plus hasardeuses. Malgré des résultats encourageants, il s'avère que même ce régime simple n'est pas complètement compris. Ce sujet est discuté en détails dans le chapitre 5, page 165.

6. *Complex classes of periodically driven topological lattice systems*,
Michel Fruchart, Phys. Rev. B 93, 115429 (2016)
doi:10.1103/PhysRevB.93.115429, arXiv:1511.06755. Cet article étend des travaux précédents pour rassembler dans un même cadre unifié les invariants topologiques connus pour les classes CAZ complexes A et AIII, et étend leurs définitions à toutes les dimensions d'espace. En particulier, un invariant topologique pour les systèmes de Floquet chiraux à trois dimensions est défini. Le contenu de cet article est discuté en détail dans les sections 3.2 et 3.3 du chapitre 4, respectivement aux pages 126 et 143.

7. Anomalous topological directed scattering networks
Pierre Delplace, Michel Fruchart, Clément Tauber

en préparation.
Les réseaux orientés de diffusion comme le modèle de Chalker-Coddington [CC88; HC96] sont décrits par des opérateurs d'évolution exprimés en termes de matrices de diffusion. Chong et collaborateurs [PC14] ont identifié une réalisation "statique" de systèmes de Floquet, et plus précisément de "marches quantiques à temps discrets" (DTQW). En particulier, ils ont été les premiers à observer expérimentalement des phases de Floquet topologiques anomales (où tous les invariants de bandes sont nuls), dans des systèmes de ce type [HPWP15; GGSY16]. Cet article est dédié à l'équivalence entre deux points de vue assez différents sur ces systèmes. Dans la formulation de Ho et Chalker [HC96] apparaissent à la fois l'opérateur d'évolution à une étape du réseau orienté et un opérateur d'évolution à deux étapes qui fournit la formulation de type Floquet/DTQW utilisée par Chong et collaborateurs. Le premier point de vue s'occupe de l'ensemble des degrés de liberté, et la nature orientée du réseau se traduit par une "contrainte de structure" qui est à l'origine de la possibilité d'une topologie non-triviale. Le second point de vue, qui ne garde que la moitié des degrés de liberté pour adhérer plus fermement à l'analogie avec une évolution à temps discret, est rendu possible par cette contrainte de structure. En plus de la contrainte de structure, toujours présente, on identifie aussi une (pseudo-)symétrie sans équivalent dans les systèmes hamiltoniens, qui est associée à une rotation des quasi-énergies. Cette symétrie peut forcer les invariants de bande (le premier nombre de Chern) à s'annuler, malgré un brisure explicite de l'invariance par renversement du temps. Cet article est en préparation au moment de l'écriture de cette thèse.

Cette thèse est organisée comme suit.

- Une introduction générale (dont vous êtes en train de lire la version française) commence à la page 3.
- Un chapitre assez technique 2, débutant à la page 33, expose rapidement la topologie des fibrés vectoriels.
- Le chapitre 3, qui commence à la page 57, fait une revue des isolants topologiques d'équilibre usuels, et de leur classification.
- Le chapitre 4, commençant à la page 109 est le cœur de cette thèse, et est dédié à la topologie des systèmes forcés périodiquement/de Floquet, en particulier en présence de symétries.
- Enfin, le chapitre 5 qui commence à la page 165 est une autre partie importante de ce travail, et est dédié aux signatures de transport des états de Floquet (en particulier topologiques).
- Une version française de l'introduction générale (que vous êtes en train de lire) commence à la page 199.

Bibliography

[AALB13]
M. Aidelsburger, M. Atala, M. Lohse, J. T. Barreiro, B. Paredes, and I. Bloch. "Realization of the Hofstadter Hamiltonian with Ultracold Atoms in Optical Lattices". In: *Phys. Rev. Lett.* 111.18 (Oct. 2013)
DOI: 10.1103/physrevlett.111.185301.

[ADHW11]
A. R. Akhmerov, J. P. Dahlhaus, F. Hassler, M. Wimmer, and C. W. J. Beenakker. "Quantized Conductance at the Majorana Phase Transition in a Disordered Superconducting Wire". In: *Phys. Rev. Lett.* 106.5 (Jan. 2011)
DOI: 10.1103/physrevlett.106.057001.

[Adl69]
Stephen L. Adler. "Axial-Vector Vertex in Spinor Electrodynamics". In: *Phys. Rev.* 177.5 (Jan. 1969), pp. 2426–2438
DOI: 10.1103/physrev.177.2426.

[AGJ15]
Victor V. Albert, Leonid I. Glazman, and Liang Jiang. "Topological Properties of Linear Circuit Lattices". In: *Phys. Rev. Lett.* 114.17 (Apr. 2015)
DOI: 10.1103/physrevlett.114.173902.

[AI98]
J.A. de Azcárraga and J.M. Izquierdo. *Lie Groups, Lie Algebras, Cohomology and Some Applications in Physics*. Cambridge Monographs on Mathematical Physics. Cambridge University Press, 1998. ISBN: 9780521597005.

[ALSA14]
M. Aidelsburger, M. Lohse, C. Schweizer, M. Atala, J. T. Barreiro, S. Nascimbène, N. R. Cooper, I. Bloch, and N. Goldman. "Measuring the Chern number of Hofstadter bands with ultracold bosonic atoms". In: *Nat Phys* 11.2 (Dec. 2014), pp. 162–166
DOI: 10.1038/nphys3171.

[AM06]
Liliana Arrachea and Michael Moskalets. "Relation between scattering-matrix and Keldysh formalisms for quantum transport driven by time-periodic fields". In: *Phys. Rev. B* 74.24 (Dec. 2006)
DOI: 10.1103/physrevb.74.245322.

[AO13]
János K. Asbóth and Hideaki Obuse. "Bulk-boundary correspondence for chiral sym-

metric quantum walks". In: *Phys. Rev. B* 88.12 (Sept. 2013)
DOI: 10.1103/physrevb.88.121406.

[Asb12]
J. K. Asbóth. "Symmetries, topological phases, and bound states in the one-dimensional quantum walk". In: *Phys. Rev. B* 86.19 (Nov. 2012)
DOI: 10.1103/physrevb.86.195414.

[ASS83]
J. E. Avron, R. Seiler, and B. Simon. "Homotopy and Quantization in Condensed Matter Physics". In: *Phys. Rev. Lett.* 51.1 (July 1983), pp. 51–53
DOI: 10.1103/physrevlett.51.51.

[ASSS89]
J. E. Avron, L. Sadun, J. Segert, and B. Simon. "Chern numbers, quaternions, and Berry's phases in Fermi systems". In: *Communications in Mathematical Physics* 124.4 (Dec. 1989), pp. 595–627
DOI: 10.1007/bf01218452. URL: http://projecteuclid.org/euclid.cmp/1104179297.

[ASV12]
Julio Cesar Avila, Hermann Schulz-Baldes, and Carlos Villegas-Blas. "Topological Invariants of Edge States for Periodic Two-Dimensional Models". In: *Mathematical Physics, Analysis and Geometry* 16.2 (Oct. 2012), pp. 137–170
DOI: 10.1007/s11040-012-9123-9.

[ATD14]
J. K. Asbóth, B. Tarasinski, and P. Delplace. "Chiral symmetry and bulk-boundary correspondence in periodically driven one-dimensional systems". In: *Phys. Rev. B* 90.12 (Sept. 2014)
DOI: 10.1103/physrevb.90.125143.

[Ati66]
Michael Francis Atiyah. "K-theory and reality". In: *The Quarterly Journal of Mathematics* 17.1 (1966), pp. 367–386
DOI: 10.1093/qmath/17.1.367.

[AZ97]
Alexander Altland and Martin R. Zirnbauer. "Nonstandard symmetry classes in mesoscopic normal-superconducting hybrid structures". In: *Phys. Rev. B* 55.2 (Jan. 1997), pp. 1142–1161
DOI: 10.1103/physrevb.55.1142.

[BBKR13]
C-E Bardyn, M A Baranov, C V Kraus, E Rico, A İmamoğlu, P Zoller, and S Diehl. "Topology by dissipation". In: *New Journal of Physics* 15.8 (Aug. 2013), p. 085001
DOI: 10.1088/1367-2630/15/8/085001.

[BCM92]
Dionys Baeriswyl, David K. Campbell, and Sumit Mazumdar. "Conjugated Conducting Polymers". In: ed. by Helmut G. Kiess. Springer Berlin Heidelberg, 1992. ISBN: 978-3-642-46731-8
DOI: 10.1007/978-3-642-46729-5.

[BCR15]
C. Bourne, A. L. Carey, and A. Rennie. "A noncommutative framework for topological insulators". In: (Sept. 2015)
arXiv: 1509.07210.

[BD15]
Jan Carl Budich and Sebastian Diehl. "Topology of density matrices". In: *Phys. Rev. B* 91.16 (Apr. 2015)
DOI: 10.1103/physrevb.91.165140.

[BDP15]
Marin Bukov, Luca D'Alessio, and Anatoli Polkovnikov. "Universal high-frequency behavior of periodically driven systems: from dynamical stabilization to Floquet engineering". In: *Advances in Physics* 64.2 (Mar. 2015), pp. 139–226
DOI: 10.1080/00018732.2015.1055918.

[BEB94]
J. Bellissard, A. van Elst, and H. Schulz- Baldes. "The noncommutative geometry of the quantum Hall effect". In: *J. Math. Phys.* 35.10 (1994), p. 5373
DOI: 10.1063/1.530758.

[Bee97]
C. W. J. Beenakker. "Random-matrix theory of quantum transport". In: *Reviews of Modern Physics* 69.3 (July 1997), pp. 731–808
DOI: 10.1103/revmodphys.69.731.

[Ber84]
M. V. Berry. "Quantal Phase Factors Accompanying Adiabatic Changes". In: *Proceedings of the Royal Society A: Mathematical, Physical and Engineering Sciences* 392.1802 (Mar. 1984), pp. 45–57
DOI: 10.1098/rspa.1984.0023.

[Bernevig]
B. Andrei Bernevig and Taylor L. Hughes. *Topological Insulators and Topological Superconductors*. Princeton University Press, Apr. 2013. ISBN: 9780691151755.

[BFKP15]
A. J. Bestwick, E. J. Fox, Xufeng Kou, Lei Pan, Kang L. Wang, and D. Goldhaber-Gordon. "Precise Quantization of the Anomalous Hall Effect near Zero Magnetic Field". In: *Phys. Rev. Lett.* 114.18 (May 2015)
DOI: 10.1103/physrevlett.114.187201.

[BFPB13]
Erwann Bocquillon, Vincent Freulon, François D. Parmentier, Jean-Marc Berroir, Bernard Plaçais, Claire Wahl, Jérome Rech, Thibaut Jonckheere, Thierry Martin, Charles Grenier, Dario Ferraro, Pascal Degiovanni, and Gwendal Fève. "Electron quantum optics in ballistic chiral conductors". In: *Annalen der Physik* 526.1-2 (Dec. 2013), pp. 1–30
DOI: 10.1002/andp.201300181.

[BH89]
H. P. Breuer and M. Holthaus. "Adiabatic processes in the ionization of highly excited hydrogen atoms". In: *Zeitschrift für Physik D Atoms, Molecules and Clusters* 11.1 (Mar. 1989), pp. 1–14
DOI: 10.1007/bf01436579.

[BHZ06]
B. A. Bernevig, T. L. Hughes, and S.-C. Zhang. "Quantum Spin Hall Effect and Topological Phase Transition in HgTe Quantum Wells". In: *Science* 314.5806 (Dec. 2006), pp. 1757–1761
DOI: 10.1126/science.1133734.

[BILP85]
M. Büttiker, Y. Imry, R. Landauer, and S. Pinhas. "Generalized many-channel conductance formula with application to small rings". In: *Phys. Rev. B* 31.10 (May 1985), pp. 6207–6215
DOI: 10.1103/physrevb.31.6207.

[BJ69]
J. S. Bell and R. Jackiw. "A PCAC puzzle: $\pi 0 \to \gamma\gamma$ in the σ-model". In: *Il Nuovo Cimento A* 60.1 (Mar. 1969), pp. 47–61
DOI: 10.1007/bf02823296.

[BJKP11]
Nina Berg, Kira Joel, Miriam Koolyk, and Emil Prodan. "Topological phonon modes in filamentary structures". In: *Physical Review E* 83.2 (Feb. 2011)
DOI: 10.1103/physreve.83.021913.

[BKMM13]
Matthieu Bellec, Ulrich Kuhl, Gilles Montambaux, and Fabrice Mortessagne. "Topological Transition of Dirac Points in a Microwave Experiment". In: *Phys. Rev. Lett.* 110.3 (Jan. 2013)
DOI: 10.1103/physrevlett.110.033902.

[BKMM14]
Matthieu Bellec, Ulrich Kuhl, Gilles Montambaux, and Fabrice Mortessagne. "Manipulation of edge states in microwave artificial graphene". In: *New Journal of Physics* 16.11 (Nov. 2014), p. 113023
DOI: 10.1088/1367-2630/16/11/113023.

[BKR16]
Chris Bourne, Johannes Kellendonk, and Adam Rennie. *The K-theoretic bulk-edge correspondence for topological insulators*. 2016. arXiv: 1604.02337.

[BLD16]
A. Bansil, H. Lin, and T. Das. "Colloquium: Topological Band Theory". In: (Mar. 2016)
arXiv: 1603.03576.

[Blo29]
Felix Bloch. "Über die Quantenmechanik der Elektronen in Kristallgittern". In: *Zeitschrift für Physik* 52.7-8 (July 1929), pp. 555–600
DOI: 10.1007/bf01339455.

[Blo62]
E.I. Blount. "Formalisms of band theory". In: *Solid State Physics*. Ed. by F. Seitz and D. Turnbull. Vol. 13. Academic Press, 1962, pp. 305–373.

[BM09]
Cristina Bena and Gilles Montambaux. "Remarks on the tight-binding model of graphene". In: *New J. Phys.* 11 (9 2009), p. 095003
DOI: 10.1088/1367-2630/11/9/095003. arXiv: 0712.0765.

[BS78]
R. Bott and J. R. Seeley. "Some remarks on the paper of Callias: "Axial anomalies and index theorems on open spaces"". In: *Comm. Math. Phys.* 62 (1978), pp. 235–245
DOI: 10.1007/BF01202526. URL: http://projecteuclid.org/euclid.cmp/1103904396.

[Büt09]
M. Büttiker. "Edge-State Physics Without Magnetic Fields". In: *Science* 325.5938 (July 2009), pp. 278–279
DOI: 10.1126/science.1177157.

[Büt86]
M. Büttiker. "Four-Terminal Phase-Coherent Conductance". In: *Phys. Rev. Lett.* 57.14 (Oct. 1986), pp. 1761–1764
DOI: 10.1103/physrevlett.57.1761.

[Büt88a]
M. Büttiker. "Absence of backscattering in the quantum Hall effect in multiprobe conductors". In: *Phys. Rev. B* 38.14 (Nov. 1988), pp. 9375–9389
DOI: 10.1103/PhysRevB.38.9375.

[Büt88b]
M. Büttiker. "Symmetry of electrical conduction". In: *IBM Journal of Research and Development* 32.3 (May 1988), pp. 317–334
DOI: 10.1147/rd.323.0317.

[CC88]
J T Chalker and P D Coddington. “Percolation, quantum tunnelling and the integer Hall effect”. In: *J. Phys. C: Solid State Phys.* 21.14 (May 1988), pp. 2665–2679
DOI: 10.1088/0022-3719/21/14/008.

[CCB15]
M. D. Caio, N. R. Cooper, and M. J. Bhaseen. “Quantum Quenches in Chern Insulators”. In: *Phys. Rev. Lett.* 115.23 (Dec. 2015)
DOI: 10.1103/physrevlett.115.236403.

[CDFG15a]
D. Carpentier, P. Delplace, M. Fruchart, K. Gawędzki, and C. Tauber. “Construction and properties of a topological index for periodically driven time-reversal invariant 2D crystals”. In: *Nuclear Physics B* 896 (July 2015), pp. 779–834
DOI: 10.1016/j.nuclphysb.2015.05.009.

[CDFG15b]
David Carpentier, Pierre Delplace, Michel Fruchart, and Krzysztof Gawędzki. “Topological Index for Periodically Driven Time-Reversal Invariant 2D Systems”. In: *Phys. Rev. Lett.* 114.10 (Mar. 2015)
DOI: 10.1103/physrevlett.114.106806.

[CGLW12]
X. Chen, Z.-C. Gu, Z.-X. Liu, and X.-G. Wen. “Symmetry-Protected Topological Orders in Interacting Bosonic Systems”. In: *Science* 338.6114 (Dec. 2012), pp. 1604–1606
DOI: 10.1126/science.1227224.

[CGLW13]
Xie Chen, Zheng-Cheng Gu, Zheng-Xin Liu, and Xiao-Gang Wen. “Symmetry protected topological orders and the group cohomology of their symmetry group”. In: *Phys. Rev. B* 87.15 (Apr. 2013)
DOI: 10.1103/physrevb.87.155114.

[CGPN09]
A. H. Castro Neto, F. Guinea, N. M. R. Peres, K. S. Novoselov, and A. K. Geim. “The electronic properties of graphene”. In: *Rev. Mod. Phys.* 81 (1 Jan. 2009), pp. 109–162
DOI: 10.1103/RevModPhys.81.109.

[CH85]
C.G. Callan and J.A. Harvey. “Anomalies and fermion zero modes on strings and domain walls”. In: *Nuclear Physics B* 250.1-4 (Jan. 1985), pp. 427–436
DOI: 10.1016/0550-3213(85)90489-4.

[CJ04]
Dariusz Chruściński and Andrzej Jamiołkowski. *Geometric Phases in Classical and Quantum Mechanics (Progress in Mathematical Physics)*. 2004th ed. Birkhäuser, June 2004. ISBN: 9780817642822.

[CJNM16]
Xiaojun Cheng, Camille Jouvaud, Xiang Ni, S. Hossein Mousavi, Azriel Z. Genack, and Alexander B. Khanikaev. "Robust reconfigurable electromagnetic pathways within a photonic topological insulator". In: *Nature Materials* 15.5 (Feb. 2016), pp. 542–548
DOI: 10.1038/nmat4573.

[CJOD99]
A. Comtet, T. Jolicœur, S. Ouvry, and F. David, eds. *Aspects topologiques de la physique en basse dimension. Topological aspects of low dimensional systems – École d'été de physique des Houches, session XXXIV (1999)*. Springer Berlin Heidelberg, 1999. ISBN: 978-3-540-66909-8
DOI: 10.1007/3-540-46637-1.

[CPRT11]
Herna'n L. Calvo, Horacio M. Pastawski, Stephan Roche, and Luis E. F. Foa Torres. "Tuning laser-induced band gaps in graphene". In: *Appl. Phys. Lett.* 98.23 (2011), p. 232103
DOI: 10.1063/1.3597412.

[CT04]
Shih-I Chu and Dmitry A. Telnov. "Beyond the Floquet theorem: generalized Floquet formalisms and quasienergy methods for atomic and molecular multiphoton processes in intense laser fields". In: *Physics Reports* 390.1-2 (Feb. 2004), pp. 1–131
DOI: 10.1016/j.physrep.2003.10.001.

[CTSR15]
C.-K. Chiu, J. C. Y. Teo, A. P. Schnyder, and S. Ryu. "Classification of topological quantum matter with symmetries". In: *ArXiv e-prints* (May 2015)
arXiv: 1505.03535.

[CUV14]
Bryan Gin-ge Chen, Nitin Upadhyaya, and Vincenzo Vitelli. "Nonlinear conduction via solitons in a topological mechanical insulator". In: *Proceedings of the National Academy of Sciences* 111.36 (Aug. 2014), pp. 13004–13009
DOI: 10.1073/pnas.1405969111.

[CYR13]
Ching-Kai Chiu, Hong Yao, and Shinsei Ryu. "Classification of topological insulators and superconductors in the presence of reflection symmetry". In: *Phys. Rev. B* 88.7 (Aug. 2013)
DOI: 10.1103/physrevb.88.075142.

[CZFS13]
C.-Z. Chang, J. Zhang, X. Feng, J. Shen, Z. Zhang, M. Guo, K. Li, Y. Ou, P. Wei, L.-L. Wang, Z.-Q. Ji, Y. Feng, S. Ji, X. Chen, J. Jia, X. Dai, Z. Fang, S.-C. Zhang, K. He, Y. Wang, L. Lu, X.-C. Ma, and Q.-K. Xue. "Experimental Observation of the Quantum Anomalous Hall Effect in a Magnetic Topological Insulator". In: *Science*

340.6129 (Mar. 2013), pp. 167–170
DOI: 10.1126/science.1234414.

[CZKZ15]
Cui-Zu Chang, Weiwei Zhao, Duk Y. Kim, Haijun Zhang, Badih A. Assaf, Don Heiman, Shou-Cheng Zhang, Chaoxing Liu, Moses H. W. Chan, and Jagadeesh S. Moodera. "High-precision realization of robust quantum anomalous Hall state in a hard ferromagnetic topological insulator". In: *Nature Materials* 14.5 (Mar. 2015), pp. 473–477
DOI: 10.1038/nmat4204.

[DFN85]
B.A. Dubrovin, A.T. Fomenko, and S.P. Novikov. *Modern Geometry Methods and Applications: Part II: The Geometry and Topology of Manifolds*. 1985th ed. Springer, Aug. 1985. ISBN: 9780387961620.

[DGP13]
Pierre Delplace, Álvaro Gómez-León, and Gloria Platero. "Merging of Dirac points and Floquet topological transitions in ac-driven graphene". In: *Phys. Rev. B* 88.24 (Dec. 2013)
DOI: 10.1103/physrevb.88.245422.

[DK16]
C. Dutreix and M. I. Katsnelson. "Friedel oscillations at the surfaces of rhombohedral N -layer graphene". In: *Phys. Rev. B* 93.3 (Jan. 2016)
DOI: 10.1103/physrevb.93.035413.

[DL16]
Xiao-Yu Dong and Chao-Xing Liu. "Classification of topological crystalline insulators based on representation theory". In: *Phys. Rev. B* 93.4 (Jan. 2016)
DOI: 10.1103/physrevb.93.045429.

[DOM14]
Hossein Dehghani, Takashi Oka, and Aditi Mitra. "Dissipative Floquet topological systems". In: *Phys. Rev. B* 90.19 (Nov. 2014)
DOI: 10.1103/physrevb.90.195429.

[DOM15]
Hossein Dehghani, Takashi Oka, and Aditi Mitra. "Out-of-equilibrium electrons and the Hall conductance of a Floquet topological insulator". In: *Phys. Rev. B* 91.15 (Apr. 2015)
DOI: 10.1103/physrevb.91.155422.

[DP08]
S. Das Sarma and A. Pinczuk. *Perspectives in Quantum Hall Effects: Novel Quantum Liquids in Low-Dimensional Semiconductor Structures*. Wiley, 2008. ISBN: 9783527617265.

[DPR06]
B. Douçot, V. Pasquier, and V. Rivasseau, eds. *The Quantum Hall Effect: Poincaré*

Seminar 2004. Progress in Mathematical Physics. Birkhäuser Basel, 2006. ISBN: 9783764373931
DOI: 10.1007/3-7643-7393-8. URL: http://www.bourbaphy.fr/novembre2004.html.

[DRBZ11]
Sebastian Diehl, Enrique Rico, Mikhail A. Baranov, and Peter Zoller. "Topology by dissipation in atomic quantum wires". In: *Nat Phys* 7.12 (Oct. 2011), pp. 971–977
DOI: 10.1038/nphys2106.

[DSPA16]
V. Dziom, A. Shuvaev, A. Pimenov, G. V. Astakhov, C. Ames, K. Bendias, J. Böttcher, G. Tkachov, E. M. Hankiewicz, C. Brüne, H Buhmann, and L. W. Molenkamp. *Observation of the universal magnetoelectric effect in a 3D topological insulator*. 2016. arXiv: 1603.05482.

[DSV11]
Wade DeGottardi, Diptiman Sen, and Smitha Vishveshwara. "Topological phases, Majorana modes and quench dynamics in a spin ladder system". In: *New Journal of Physics* 13.6 (June 2011), p. 065028
DOI: 10.1088/1367-2630/13/6/065028.

[DWD14]
D.-L. Deng, S.-T. Wang, and L.-M. Duan. "Systematic construction of tight-binding Hamiltonians for topological insulators and superconductors". In: *Phys. Rev. B* 89.7 (Feb. 2014)
DOI: 10.1103/physrevb.89.075126.

[EA15]
Jonathan M. Edge and János K. Asbóth. "Localization, delocalization, and topological transitions in disordered two-dimensional quantum walks". In: *Phys. Rev. B* 91.10 (Mar. 2015)
DOI: 10.1103/physrevb.91.104202.

[EBPB15]
G. Engelhardt, M. Benito, G. Platero, and T. Brandes. "Topological instabilities in ac-driven bosonic systems". In: (Dec. 2015)
arXiv: 1512.07653.

[EG02]
P. Elbau and G. M. Graf. In: *Commun Math Phys* 229.3 (Sept. 2002), pp. 415–432
DOI: 10.1007/s00220-002-0698-z.

[EG11]
Andrew M. Essin and Victor Gurarie. "Bulk-boundary correspondence of topological insulators from their respective Green's functions". In: *Phys. Rev. B* 84.12 (Sept. 2011)
DOI: 10.1103/physrevb.84.125132.

[EGH80]
Tohru Eguchi, Peter B. Gilkey, and Andrew J. Hanson. "Gravitation, gauge theories and differential geometry". In: *Physics Reports* 66.6 (Dec. 1980), pp. 213–393
DOI: 10.1016/0370-1573(80)90130-1.

[EMV09]
Andrew M. Essin, Joel E. Moore, and David Vanderbilt. "Magnetoelectric Polarizability and Axion Electrodynamics in Crystalline Insulators". In: *Phys. Rev. Lett.* 102.14 (Apr. 2009)
DOI: 10.1103/physrevlett.102.146805.

[EN16]
Dominic V. Else and Chetan Nayak. "Classification of topological phases in periodically driven interacting systems". In: *Phys. Rev. B* 93.20 (May 2016)
DOI: 10.1103/physrevb.93.201103.

[ETN13]
Motohiko Ezawa, Yukio Tanaka, and Naoto Nagaosa. "Topological Phase Transition without Gap Closing". In: *Sci. Rep.* 3 (Sept. 2013)
DOI: 10.1038/srep02790.

[FCG14]
Michel Fruchart, David Carpentier, and Krzysztof Gawędzki. "Parallel transport and band theory in crystals". In: *EPL* 106.6 (June 2014), p. 60002
DOI: 10.1209/0295-5075/106/60002.

[FDWW16]
M. Fruchart, P. Delplace, J. Weston, X. Waintal, and D. Carpentier. "Probing (topological) Floquet states through DC transport". In: *Physica E: Low-dimensional Systems and Nanostructures* 75 (Jan. 2016), pp. 287–294
DOI: 10.1016/j.physe.2015.09.035.

[FGDY14]
Matthew S. Foster, Victor Gurarie, Maxim Dzero, and Emil A. Yuzbashyan. "Quench-Induced Floquet Topological p -Wave Superfluids". In: *Phys. Rev. Lett.* 113.7 (Aug. 2014)
DOI: 10.1103/physrevlett.113.076403.

[FH07]
Takahiro Fukui and Yasuhiro Hatsugai. "Quantum Spin Hall Effect in Three Dimensional Materials: Lattice Computation of Z 2 Topological Invariants and Its Application to Bi and Sb". In: *Journal of the Physical Society of Japan* 76.5 (May 2007), p. 053702
DOI: 10.1143/jpsj.76.053702.

[FHA12]
I. C. Fulga, F. Hassler, and A. R. Akhmerov. "Scattering theory of topological insu-

lators and superconductors". In: *Phys. Rev. B* 85.16 (Apr. 2012)
DOI: 10.1103/physrevb.85.165409.

[FHAB11]
I. C. Fulga, F. Hassler, A. R. Akhmerov, and C. W. J. Beenakker. "Scattering formula for the topological quantum number of a disordered multimode wire". In: *Phys. Rev. B* 83.15 (Apr. 2011)
DOI: 10.1103/physrevb.83.155429.

[FHS05]
Takahiro Fukui, Yasuhiro Hatsugai, and Hiroshi Suzuki. "Chern Numbers in Discretized Brillouin Zone: Efficient Method of Computing (Spin) Hall Conductances". In: *Journal of the Physical Society of Japan* 74.6 (June 2005), pp. 1674–1677
DOI: 10.1143/jpsj.74.1674.

[FK06]
Liang Fu and C. L. Kane. "Time reversal polarization and a Z 2 adiabatic spin pump". In: *Phys. Rev. B* 74.19 (Nov. 2006)
DOI: 10.1103/physrevb.74.195312.

[FKA15]
R. Fleury, A. Khanikaev, and A. Alu. "Floquet Topological Insulators for Sound". In: (Nov. 2015)
arXiv: 1511.08427.

[FKM07]
Liang Fu, C. L. Kane, and E. J. Mele. "Topological Insulators in Three Dimensions". In: *Phys. Rev. Lett.* 98.10 (Mar. 2007)
DOI: 10.1103/physrevlett.98.106803.

[FL81]
Daniel S. Fisher and Patrick A. Lee. "Relation between conductivity and transmission matrix". In: *Phys. Rev. B* 23.12 (June 1981), pp. 6851–6854
DOI: 10.1103/physrevb.23.6851.

[Flo83]
Gaston Floquet. "Sur les équations différentielles linéaires à coefficients périodiques." In: *Annales scientifiques de l'École Normale Supérieure* Sér. 2, 12.1-2 (1883), pp. 47–88
URL: http://www.numdam.org/item?id=ASENS_1883_2_12__47_0.

[FM13]
Daniel S. Freed and Gregory W. Moore. "Twisted Equivariant Matter". In: *Ann. Henri Poincaré* 14.8 (Mar. 2013), pp. 1927–2023
DOI: 10.1007/s00023-013-0236-x.

[FM16]
I. C. Fulga and M. Maksymenko. "Scattering matrix invariants of Floquet topological

insulators". In: *Phys. Rev. B* 93.7 (Feb. 2016)
DOI: 10.1103/physrevb.93.075405.

[FMP16]
Domenico Fiorenza, Domenico Monaco, and Gianluca Panati. "Z_2 Invariants of Topological Insulators as Geometric Obstructions". In: *Commun. Math. Phys.* (Jan. 2016)
DOI: 10.1007/s00220-015-2552-0.

[FP15]
Aaron Farrell and T. Pereg-Barnea. "Photon-Inhibited Topological Transport in Quantum Well Heterostructures". In: *Phys. Rev. Lett.* 115.10 (Sept. 2015)
DOI: 10.1103/physrevlett.115.106403.

[FP16]
Aaron Farrell and T. Pereg-Barnea. "Edge-state transport in Floquet topological insulators". In: *Phys. Rev. B* 93.4 (Jan. 2016)
DOI: 10.1103/physrevb.93.045121.

[FPGM10]
J. N. Fuchs, F. Piéchon, M. O. Goerbig, and G. Montambaux. "Topological Berry phase and semiclassical quantization of cyclotron orbits for two dimensional electrons in coupled band models". In: *Eur. Phys. J. B* 77 (2010), pp. 351–362
DOI: 10.1140/epjb/e2010-00259-2. arXiv: 1006.5632.

[Fru16]
Michel Fruchart. "Complex classes of periodically driven topological lattice systems". In: *Phys. Rev. B* 93.11 (Mar. 2016)
DOI: 10.1103/physrevb.93.115429.

[FSWS84]
M. H. Friedman, J. B. Sokoloff, A. Widom, and Y. N. Srivastava. "Chiral Anomaly and the Rational Quantization of the Hall Conductance". In: *Phys. Rev. Lett.* 52.18 (Apr. 1984), pp. 1587–1589
DOI: 10.1103/physrevlett.52.1587.

[Fu11]
Liang Fu. "Topological Crystalline Insulators". In: *Phys. Rev. Lett.* 106.10 (Mar. 2011)
DOI: 10.1103/physrevlett.106.106802.

[FYF12]
Kejie Fang, Zongfu Yu, and Shanhui Fan. "Realizing effective magnetic field for photons by controlling the phase of dynamic modulation". In: *Nature Photonics* 6.11 (Oct. 2012), pp. 782–787
DOI: 10.1038/nphoton.2012.236.

[Gan15]
Yuval Gannot. *Effects of Disorder on a 1-D Floquet Symmetry Protected Topological Phase*. 2015. arXiv: 1512.04190.

[Gaw15]
Krzysztof Gawędzki. "Bundle gerbes for topological insulators". In: (Dec. 2015) arXiv: 1512.01028.

[GBL08]
Timothy Gowers, June Barrow-Green, and Imre Leader, eds. *The Princeton Companion to Mathematics*. First Edition. Princeton University Press, Sept. 2008. ISBN: 9780691118802.

[GD14]
N. Goldman and J. Dalibard. "Periodically Driven Quantum Systems: Effective Hamiltonians and Engineered Gauge Fields". In: *Phys. Rev. X* 4.3 (Aug. 2014) DOI: 10.1103/physrevx.4.031027.

[GD15]
Balázs Gulácsi and Balázs Dóra. "From Floquet to Dicke: Quantum Spin Hall Insulator Interacting with Quantum Light". In: *Phys. Rev. Lett.* 115.16 (Oct. 2015) DOI: 10.1103/physrevlett.115.160402.

[GDP14]
Álvaro Gómez-León, Pierre Delplace, and Gloria Platero. "Engineering anomalous quantum Hall plateaus and antichiral states with ac fields". In: *Phys. Rev. B* 89.20 (May 2014) DOI: 10.1103/physrevb.89.205408.

[Get93]
Ezra Getzler. "The odd chern character in cyclic homology and spectral flow". In: *Topology* 32.3 (July 1993), pp. 489–507 DOI: 10.1016/0040-9383(93)90002-d.

[GFAA11]
Zhenghao Gu, H. A. Fertig, Daniel P. Arovas, and Assa Auerbach. "Floquet Spectrum and Transport through an Irradiated Graphene Ribbon". In: *Phys. Rev. Lett.* 107.21 (Nov. 2011) DOI: 10.1103/physrevlett.107.216601.

[GGN15]
A. G. Grushin, Á. Gómez-León, and T. Neupert. "Reply to "Comment on 'Floquet Fractional Chern Insulators"'". In: (Mar. 2015) arXiv: 1503.02580.

[GGSY16]
Fei Gao, Zhen Gao, Xihang Shi, Zhaoju Yang, Xiao Lin, Hongyi Xu, John D. Joannopoulos, Marin Soljačić, Hongsheng Chen, Ling Lu, Yidong Chong, and Baile Zhang. "Probing topological protection using a designer surface plasmon structure".

In: *Nature Communications* 7 (May 2016), p. 11619
DOI: 10.1038/ncomms11619.

[GM10]
Víctor A. Gopar and Rafael A. Molina. "Controlling conductance statistics of quantum wires by driving ac fields". In: *Phys. Rev. B* 81.19 (May 2010)
DOI: 10.1103/physrevb.81.195415.

[Goe11]
M. O. Goerbig. "Quantum Hall Effects". In: *Ultracold Gases and Quantum Information: Lecture Notes of the Les Houches Summer School in Singapore: Volume 91, July 2009*. Ed. by C. Miniatura, L.C. Kwek, and M. Ducloy. Lecture Notes of the Les Houches Summer School vol. 91. OUP Oxford, 2011. ISBN: 9780199603657
arXiv: 0909.1998.

[GP13a]
A. Gómez-León and G. Platero. "Floquet-Bloch Theory and Topology in Periodically Driven Lattices". In: *Phys. Rev. Lett.* 110.20 (May 2013)
DOI: 10.1103/PhysRevLett.110.200403.

[GP13b]
Gian Michele Graf and Marcello Porta. "Bulk-Edge Correspondence for Two-Dimensional Topological Insulators". In: *Commun. Math. Phys.* 324.3 (Oct. 2013), pp. 851–895
DOI: 10.1007/s00220-013-1819-6.

[GTB16]
Y. Gerasimenko, B. Tarasinski, and C. W. J. Beenakker. "Attractor-repeller pair of topological zero modes in a nonlinear quantum walk". In: *Phys. Rev. A* 93.2 (Feb. 2016)
DOI: 10.1103/physreva.93.022329. URL: http://dx.doi.org/10.1103/PhysRevA.93.022329.

[Gur11]
V. Gurarie. "Single-particle Green's functions and interacting topological insulators". In: *Phys. Rev. B* 83.8 (Feb. 2011)
DOI: 10.1103/physrevb.83.085426.

[GW14]
Zheng-Cheng Gu and Xiao-Gang Wen. "Symmetry-protected topological orders for interacting fermions: Fermionic topological nonlinear σ-models and a special group supercohomology theory". In: *Phys. Rev. B* 90.11 (Sept. 2014)
DOI: 10.1103/physrevb.90.115141.

[GWAW14]
Christoph W Groth, Michael Wimmer, Anton R Akhmerov, and Xavier Waintal. "Kwant: a software package for quantum transport". In: *New Journal of Physics* 16.6 (June 2014), p. 063065
DOI: 10.1088/1367-2630/16/6/063065.

[GWSH14]
Benoit Gaury, Joseph Weston, Matthieu Santin, Manuel Houzet, Christoph Groth, and Xavier Waintal. “Numerical simulations of time-resolved quantum electronics”. In: *Physics Reports* 534.1 (Jan. 2014), pp. 1–37
DOI: 10.1016/j.physrep.2013.09.001.

[Hal88]
F. D. M. Haldane. “Model for a Quantum Hall Effect without Landau Levels: Condensed-Matter Realization of the "Parity Anomaly"”. In: *Phys. Rev. Lett.* 61.18 (Oct. 1988), pp. 2015–2018
DOI: 10.1103/physrevlett.61.2015.

[Han85]
J H Hannay. “Angle variable holonomy in adiabatic excursion of an integrable Hamiltonian”. In: *J. Phys. A: Math. Gen.* 18.2 (Feb. 1985), pp. 221–230
DOI: 10.1088/0305-4470/18/2/011.

[Har55]
P G Harper. “Single Band Motion of Conduction Electrons in a Uniform Magnetic Field”. In: *Proc. Phys. Soc. A* 68.10 (Oct. 1955), pp. 874–878
DOI: 10.1088/0370-1298/68/10/304.

[Hat03a]
Allen Hatcher. *Algebraic Topology*. 2003. ISBN: 9780521795401
URL: https://www.math.cornell.edu/~hatcher/AT/ATpage.html.

[Hat03b]
Allen Hatcher. *Vector bundles and K-theory*. 2003
URL: http://www.math.cornell.edu/~hatcher/VBKT/VBpage.html.

[Hat11]
Y Hatsugai. “Topological aspect of graphene physics”. In: *J. Phys.: Conf. Ser.* 334 (Dec. 2011), p. 012004
DOI: 10.1088/1742-6596/334/1/012004.

[Hat93a]
Yasuhiro Hatsugai. “Chern number and edge states in the integer quantum Hall effect”. In: *Phys. Rev. Lett.* 71.22 (Nov. 1993), pp. 3697–3700
DOI: 10.1103/physrevlett.71.3697.

[Hat93b]
Yasuhiro Hatsugai. “Edge states in the integer quantum Hall effect and the Riemann surface of the Bloch function”. In: *Phys. Rev. B* 48.16 (Oct. 1993), pp. 11851–11862
DOI: 10.1103/physrevb.48.11851.

[HC96]
C.-M. Ho and J. T. Chalker. “Models for the integer quantum Hall effect: The network model, the Dirac equation, and a tight-binding Hamiltonian”. In: *Phys.*

Rev. B 54.12 (Sept. 1996), pp. 8708–8713
DOI: 10.1103/physrevb.54.8708.

[HDLT11]
Mohammad Hafezi, Eugene A. Demler, Mikhail D. Lukin, and Jacob M. Taylor. "Robust optical delay lines with topological protection". In: *Nat Phys* 7.11 (Aug. 2011), pp. 907–912
DOI: 10.1038/nphys2063.

[Hil86]
G. W. Hill. "On the part of the motion of the lunar perigee which is a function of the mean motions of the sun and moon". In: *Acta Mathematica* 8.1 (Dec. 1886), pp. 1–36
DOI: 10.1007/bf02417081.

[HK10]
M. Z. Hasan and C. L. Kane. "Colloquium : Topological insulators". In: *Reviews of Modern Physics* 82.4 (Nov. 2010), pp. 3045–3067
DOI: 10.1103/revmodphys.82.3045.

[HKA16]
Yakir Hadad, Alexander B. Khanikaev, and Andrea Alù. "Self-induced topological transitions and edge states supported by nonlinear staggered potentials". In: *Phys. Rev. B* 93.15 (Apr. 2016)
DOI: 10.1103/physrevb.93.155112.

[HKSS88]
A. J. Heeger, S. Kivelson, J. R. Schrieffer, and W. -P. Su. "Solitons in conducting polymers". In: *Reviews of Modern Physics* 60.3 (July 1988), pp. 781–850
DOI: 10.1103/revmodphys.60.781.

[HL90]
Willem van Haeringen and Daan Lenstra, eds. *Analogies in Optics and Micro Electronics*. Springer Science, 1990. ISBN: 978-94-010-7400-1
DOI: 10.1007/978-94-009-2009-5.

[HMFM13]
M. Hafezi, S. Mittal, J. Fan, A. Migdall, and J. M. Taylor. "Imaging topological edge states in silicon photonics". In: *Nature Photonics* 7.12 (Oct. 2013), pp. 1001–1005
DOI: 10.1038/nphoton.2013.274.

[HMT16]
K. C. Hannabuss, V. Mathai, and G. C. Thiang. "T-duality simplifies bulk-boundary correspondence: the general case". In: *ArXiv e-prints* (Feb. 2016)
arXiv: 1603.00116.

[Hof76]
Douglas R. Hofstadter. "Energy levels and wave functions of Bloch electrons in rational and irrational magnetic fields". In: *Phys. Rev. B* 14.6 (Sept. 1976), pp. 2239–

2249
DOI: 10.1103/physrevb.14.2239.

[Hol15]
Martin Holthaus. "Floquet engineering with quasienergy bands of periodically driven optical lattices". In: *J. Phys. B: At. Mol. Opt. Phys.* 49.1 (Nov. 2015), p. 013001
DOI: 10.1088/0953-4075/49/1/013001.

[HPWP15]
Wenchao Hu, Jason C. Pillay, Kan Wu, Michael Pasek, Perry Ping Shum, and Y. D. Chong. "Measurement of a Topological Edge Invariant in a Microwave Network". In: *Phys. Rev. X* 5.1 (Feb. 2015)
DOI: 10.1103/physrevx.5.011012.

[HQWX08]
D. Hsieh, D. Qian, L. Wray, Y. Xia, Y. S. Hor, R. J. Cava, and M. Z. Hasan. "A topological Dirac insulator in a quantum spin Hall phase". In: *Nature* 452.7190 (Apr. 2008), pp. 970–974
DOI: 10.1038/nature06843.

[HR08]
F. D. M. Haldane and S. Raghu. "Possible Realization of Directional Optical Waveguides in Photonic Crystals with Broken Time-Reversal Symmetry". In: *Phys. Rev. Lett.* 100.1 (Jan. 2008)
DOI: 10.1103/physrevlett.100.013904.

[HTCÖ12]
Philipp Hauke, Olivier Tieleman, Alessio Celi, Christoph Ölschläger, Juliette Simonet, Julian Struck, Malte Weinberg, Patrick Windpassinger, Klaus Sengstock, Maciej Lewenstein, and André Eckardt. "Non-Abelian Gauge Fields and Topological Insulators in Shaken Optical Lattices". In: *Phys. Rev. Lett.* 109.14 (Oct. 2012)
DOI: 10.1103/physrevlett.109.145301.

[Hus93]
Dale Husemöller. *Fibre Bundles (Graduate Texts in Mathematics) (v. 20)*. 3rd. Springer, Dec. 1993. ISBN: 9780387940878.

[INC15]
Thomas Iadecola, Titus Neupert, and Claudio Chamon. "Occupation of topological Floquet bands in open systems". In: *Phys. Rev. B* 91.23 (June 2015)
DOI: 10.1103/physrevb.91.235133.

[Ish84]
K. Ishikawa. "Chiral Anomaly and Quantized Hall Effect". In: *Phys. Rev. Lett.* 53.17 (Oct. 1984), pp. 1615–1618
DOI: 10.1103/physrevlett.53.1615.

[IT10]
Jun-ichi Inoue and Akihiro Tanaka. "Photoinduced Transition between Conventional

and Topological Insulators in Two-Dimensional Electronic Systems". In: *Phys. Rev. Lett.* 105.1 (June 2010)
DOI: 10.1103/physrevlett.105.017401.

[Jac84]
R. Jackiw. "Fractional charge and zero modes for planar systems in a magnetic field". In: *Physical Review D* 29.10 (May 1984), pp. 2375–2377
DOI: 10.1103/physrevd.29.2375.

[JJ06]
B. Jeckelmann and B. Jeanneret. In: *The Quantum Hall Effect: Poincaré Seminar 2004*. Ed. by B. Douçot, V. Pasquier, and V. Rivasseau. Progress in Mathematical Physics. Birkhäuser Basel, 2006. Chap. The Quantum Hall Effect as an Electrical Resistance Standard, pp. 55–131. ISBN: 9783764373931
DOI: 10.1007/3-7643-7393-8. URL: http://www.bourbaphy.fr/novembre2004.html.

[JJWM11]
J.D. Joannopoulos, S.G. Johnson, J.N. Winn, and R.D. Meade. *Photonic Crystals: Molding the Flow of Light (Second Edition)*. Princeton University Press, 2011. ISBN: 9781400828241.

[JKAA11]
Liang Jiang, Takuya Kitagawa, Jason Alicea, A. R. Akhmerov, David Pekker, Gil Refael, J. Ignacio Cirac, Eugene Demler, Mikhail D. Lukin, and Peter Zoller. "Majorana Fermions in Equilibrium and in Driven Cold-Atom Quantum Wires". In: *Phys. Rev. Lett.* 106.22 (June 2011)
DOI: 10.1103/physrevlett.106.220402.

[JMDL14]
Gregor Jotzu, Michael Messer, Rémi Desbuquois, Martin Lebrat, Thomas Uehlinger, Daniel Greif, and Tilman Esslinger. "Experimental realization of the topological Haldane model with ultracold fermions". In: *Nature* 515.7526 (Nov. 2014), pp. 237–240
DOI: 10.1038/nature13915.

[Joh87]
Sajeev John. "Strong localization of photons in certain disordered dielectric superlattices". In: *Phys. Rev. Lett.* 58.23 (June 1987), pp. 2486–2489
DOI: 10.1103/physrevlett.58.2486.

[JOPS10]
Jesper Jacobsen, Stephane Ouvry, Vincent Pasquier, Didina Serban, and Leticia Cugliandolo, eds. *Exact methods in low-dimensional statistical physics and quantum computing – École d'été de physique des Houches, session LXXXIX (2008)*. Oxford: Oxford University Press, 2010. ISBN: 9780199574612.

[JR76]
R. Jackiw and C. Rebbi. "Solitons with fermion number ½". In: *Physical Review D* 13.12 (June 1976), pp. 3398–3409
DOI: 10.1103/physrevd.13.3398.

[JWM94]
Antti-Pekka Jauho, Ned S. Wingreen, and Yigal Meir. "Time-dependent transport in interacting and noninteracting resonant-tunneling systems". In: *Phys. Rev. B* 50.8 (Aug. 1994), pp. 5528–5544
DOI: 10.1103/physrevb.50.5528.

[Kap92]
David B. Kaplan. "A method for simulating chiral fermions on the lattice". In: *Physics Letters B* 288.3-4 (Aug. 1992), pp. 342–347
DOI: 10.1016/0370-2693(92)91112-m.

[Kar08]
Max Karoubi. *K-Theory: An Introduction (Classics in Mathematics)*. 2008th ed. Springer, Nov. 2008. ISBN: 9783540798897.

[KBFR12]
T. Kitagawa, M. A. Broome, A. Fedrizzi, M. S. Rudner, E. Berg, I. Kassal, A. Aspuru-Guzik, E. Demler, and A. G. White. "Observation of topologically protected bound states in photonic quantum walks". In: *Nature Communications* 3, 882 (June 2012), p. 882
DOI: 10.1038/ncomms1872. arXiv: 1105.5334.

[KBRD10]
Takuya Kitagawa, Erez Berg, Mark Rudner, and Eugene Demler. "Topological characterization of periodically driven quantum systems". In: *Phys. Rev. B* 82.23 (Dec. 2010)
DOI: 10.1103/physrevb.82.235114.

[KDP80]
K. v. Klitzing, G. Dorda, and M. Pepper. "New Method for High-Accuracy Determination of the Fine-Structure Constant Based on Quantized Hall Resistance". In: *Phys. Rev. Lett.* 45.6 (Aug. 1980), pp. 494–497
DOI: 10.1103/physrevlett.45.494.

[Kel15]
Johannes Kellendonk. *On the C*-algebraic approach to topological phases for insulators*. 2015. arXiv: 1509.06271.

[KFMA15]
Alexander B. Khanikaev, Romain Fleury, S. Hossein Mousavi, and Andrea Alù. "Topologically robust sound propagation in an angular-momentum-biased graphene-like resonator lattice". In: *Nature Communications* 6 (Oct. 2015), p. 8260
DOI: 10.1038/ncomms9260.

[KFS14]
Arijit Kundu, H. A. Fertig, and Babak Seradjeh. "Effective Theory of Floquet Topological Transitions". In: *Phys. Rev. Lett.* 113.23 (Dec. 2014)
DOI: 10.1103/physrevlett.113.236803.

[KG15]
Ricardo Kennedy and Charles Guggenheim. "Homotopy theory of strong and weak topological insulators". In: *Phys. Rev. B* 91.24 (June 2015)
DOI: 10.1103/physrevb.91.245148.

[KH15]
Toshikaze Kariyado and Yasuhiro Hatsugai. "Manipulation of Dirac Cones in Mechanical Graphene". In: *Sci. Rep.* 5 (Dec. 2015), p. 18107
DOI: 10.1038/srep18107.

[Kha16]
A. F. Kharshiladze. *Article on 'Chern number' in the Encyclopedia of Mathematics, Online Version*. 2016. URL: http://www.encyclopediaofmath.org/index.php?title=Chern_number&oldid=13675 (visited on 04/19/2016).

[Kit01]
A Yu Kitaev. "Unpaired Majorana fermions in quantum wires". In: *Physics-Uspekhi* 44.10S (Oct. 2001), pp. 131–136
DOI: 10.1070/1063-7869/44/10s/s29.

[Kit03]
A. Yu. Kitaev. "Fault-tolerant quantum computation by anyons". In: *Annals of Physics* 303.1 (Jan. 2003), pp. 2–30
DOI: 10.1016/s0003-4916(02)00018-0.

[Kit09]
A. Kitaev. "Periodic table for topological insulators and superconductors". In: *AIP Conference Proceedings* 1134.1 (2009), pp. 22–30
DOI: 10.1063/1.3149495.

[Kit87]
Charles Kittel. *Quantum Theory of Solids*. 2nd ed. Wiley, Apr. 1987. ISBN: 9780471624127.

[KL13]
C. L. Kane and T. C. Lubensky. "Topological boundary modes in isostatic lattices". In: *Nat Phys* 10.1 (Dec. 2013), pp. 39–45
DOI: 10.1038/nphys2835.

[KLH05]
Sigmund Kohler, Jörg Lehmann, and Peter Hänggi. "Driven quantum transport on the nanoscale". In: *Physics Reports* 406.6 (Feb. 2005), pp. 379–443
DOI: 10.1016/j.physrep.2004.11.002.

[Kli86]
Klaus von Klitzing. “The quantized Hall effect”. In: *Reviews of Modern Physics* 58.3 (July 1986), pp. 519–531
DOI: 10.1103/revmodphys.58.519.

[KM05a]
C. L. Kane and E. J. Mele. “Quantum Spin Hall Effect in Graphene”. In: *Phys. Rev. Lett.* 95.22 (Nov. 2005)
DOI: 10.1103/physrevlett.95.226801.

[KM05b]
C. L. Kane and E. J. Mele. “Z_2 Topological Order and the Quantum Spin Hall Effect”. In: *Phys. Rev. Lett.* 95.14 (Sept. 2005)
DOI: 10.1103/physrevlett.95.146802.

[KMTK12]
Alexander B. Khanikaev, S. Hossein Mousavi, Wang-Kong Tse, Mehdi Kargarian, Allan H. MacDonald, and Gennady Shvets. “Photonic topological insulators”. In: *Nature Materials* 12.3 (Dec. 2012), pp. 233–239
DOI: 10.1038/nmat3520.

[KOBF11]
Takuya Kitagawa, Takashi Oka, Arne Brataas, Liang Fu, and Eugene Demler. “Transport properties of nonequilibrium systems under the application of light: Photoinduced quantum Hall insulators without Landau levels”. In: *Phys. Rev. B* 84.23 (Dec. 2011)
DOI: 10.1103/physrevb.84.235108.

[KOD12]
Takuya Kitagawa, Takashi Oka, and Eugene Demler. “Photo control of transport properties in a disordered wire: Average conductance, conductance statistics, and time-reversal symmetry”. In: *Annals of Physics* 327.7 (July 2012), pp. 1868–1889
DOI: 10.1016/j.aop.2012.02.012.

[KRBD10]
Takuya Kitagawa, Mark S. Rudner, Erez Berg, and Eugene Demler. “Exploring topological phases with quantum walks”. In: *Phys. Rev. A* 82.3 (Sept. 2010)
DOI: 10.1103/physreva.82.033429.

[KRS02]
Johannes Kellendonk, Thomas Richter, and Hermann Schulz-Baldes. “Edge current channels and Chern numbers in the integer quantum Hall effect”. In: *Reviews in Mathematical Physics* 14.01 (Jan. 2002), pp. 87–119
DOI: 10.1142/s0129055x02001107.

[KS04]
Johannes Kellendonk and Hermann Schulz-Baldes. “Quantization of edge currents for continuous magnetic operators”. In: *Journal of Functional Analysis* 209.2 (Apr.

2004), pp. 388–413
DOI: 10.1016/s0022-1236(03)00174-5.

[KS13]
Arijit Kundu and Babak Seradjeh. "Transport Signatures of Floquet Majorana Fermions in Driven Topological Superconductors". In: *Phys. Rev. Lett.* 111.13 (Sept. 2013)
DOI: 10.1103/physrevlett.111.136402.

[KS16a]
C. W. von Keyserlingk and S. L. Sondhi. *1D Many-body localized Floquet systems II: Symmetry-Broken phases*. 2016. arXiv: 1602.06949.

[KS16b]
C. W. von Keyserlingk and S. L. Sondhi. *Phase Structure of 1d Interacting Floquet Systems I: Abelian SPTs*. 2016. arXiv: 1602.02157.

[KSSV14]
G. Kells, D. Sen, J. K. Slingerland, and S. Vishveshwara. "Topological blocking in quantum quench dynamics". In: *Phys. Rev. B* 89.23 (June 2014)
DOI: 10.1103/physrevb.89.235130.

[Kuc93]
P.A. Kuchment. *Floquet Theory for Partial Differential Equations (Operator Theory: Advances and Applications)*. 1993rd ed. Birkhäuser, July 1993. ISBN: 9783764329013.

[KWBR07]
M. König, S. Wiedmann, C. Brüne, A. Roth, H. Buhmann, L. W. Molenkamp, X.-L. Qi, and S.-C. Zhang. "Quantum Spin Hall Insulator State in HgTe Quantum Wells". In: *Science* 318.5851 (Nov. 2007), pp. 766–770
DOI: 10.1126/science.1148047.

[KZ15]
R. Kennedy and M. R. Zirnbauer. "Bott Periodicity for Z_2 Symmetric Ground States of Gapped Free-Fermion Systems". In: *Commun. Math. Phys.* (Nov. 2015)
DOI: 10.1007/s00220-015-2512-8.

[Lan57]
R. Landauer. "Spatial Variation of Currents and Fields Due to Localized Scatterers in Metallic Conduction". In: *IBM Journal of Research and Development* 1.3 (July 1957), pp. 223–231
DOI: 10.1147/rd.13.0223.

[Lan70]
Rolf Landauer. "Electrical resistance of disordered one-dimensional lattices". In: *Philosophical Magazine* 21.172 (Apr. 1970), pp. 863–867
DOI: 10.1080/14786437008238472.

[LAT15]
V. Dal Lago, M. Atala, and L. E. F. Foa Torres. "Floquet topological transitions in

a driven one-dimensional topological insulator". In: *Phys. Rev. A* 92.2 (Aug. 2015) DOI: 10.1103/physreva.92.023624.

[Lau81]
R. B. Laughlin. "Quantized Hall conductivity in two dimensions". In: *Phys. Rev. B* 23.10 (May 1981), pp. 5632–5633
DOI: 10.1103/physrevb.23.5632.

[LC13]
G. Q. Liang and Y. D. Chong. "Optical Resonator Analog of a Two-Dimensional Topological Insulator". In: *Phys. Rev. Lett.* 110.20 (May 2013)
DOI: 10.1103/physrevlett.110.203904.

[LC16]
Daniel Leykam and Y. D. Chong. *Edge Solitons in Nonlinear Photonic Topological Insulators*. 2016. arXiv: 1605.09501.

[LDM14]
Achilleas Lazarides, Arnab Das, and Roderich Moessner. "Equilibrium states of generic quantum systems subject to periodic driving". In: *Physical Review E* 90.1 (July 2014)
DOI: 10.1103/physreve.90.012110.

[Le 12]
Michel Le Bellac. *Quantum Physics*. Cambridge University Press, Jan. 2012. ISBN: 9781107602762.

[Lee16]
Tony E. Lee. "Anomalous Edge State in a Non-Hermitian Lattice". In: *Phys. Rev. Lett.* 116.13 (Apr. 2016)
DOI: 10.1103/physrevlett.116.133903.

[LFM15]
Lih-King Lim, Jean-Noël Fuchs, and Gilles Montambaux. "Geometry of Bloch states probed by Stückelberg interferometry". In: *Phys. Rev. A* 92.6 (Dec. 2015)
DOI: 10.1103/physreva.92.063627.

[LJS14]
Ling Lu, John D. Joannopoulos, and Marin Soljačić. "Topological photonics". In: *Nature Photonics* 8.11 (Oct. 2014), pp. 821–829
DOI: 10.1038/nphoton.2014.248.

[Lon09]
S. Longhi. "Quantum-optical analogies using photonic structures". In: *Laser & Photonics Review* 3.3 (Apr. 2009), pp. 243–261
DOI: 10.1002/lpor.200810055.

[LPRS13]
Yaakov Lumer, Yonatan Plotnik, Mikael C. Rechtsman, and Mordechai Segev. "Self-

Localized States in Photonic Topological Insulators". In: *Phys. Rev. Lett.* 111.24 (Dec. 2013)
DOI: 10.1103/physrevlett.111.243905.

[LRG11]
Netanel H. Lindner, Gil Refael, and Victor Galitski. "Floquet topological insulator in semiconductor quantum wells". In: *Nat Phys* 7.6 (Mar. 2011), pp. 490–495
DOI: 10.1038/nphys1926.

[LSAD07]
Maciej Lewenstein, Anna Sanpera, Veronica Ahufinger, Bogdan Damski, Aditi Sen(De), and Ujjwal Sen. "Ultracold atomic gases in optical lattices: mimicking condensed matter physics and beyond". In: *Advances in Physics* 56.2 (Mar. 2007), pp. 243–379
DOI: 10.1080/00018730701223200.

[Lud15]
Andreas W W Ludwig. "Topological phases: classification of topological insulators and superconductors of non-interacting fermions, and beyond". In: *Phys. Scr.* T168 (Dec. 2015), p. 014001
DOI: 10.1088/0031-8949/2015/t168/014001.

[Lya96]
A. M. Lyapunov. "Sur une série relative a la théorie des équations différentielles linéaires à coeficients périodiques". In: *Comptes Rendus Acad. Sci. Paris* 123.26 (1896), pp. 1248–1252
URL: http://gallica.bnf.fr/ark:/12148/bpt6k30799/f1248.item.

[Lya99]
A. M. Lyapunov. "Sur une équation transcendante et les équations différentielles linéaires du second ordre à coefficients périodiques". In: *Comptes Rendus Acad. Sci. Paris* 128 (1899), pp. 1085–1088
URL: http://gallica.bnf.fr/ark:/12148/bpt6k30841/f1085.item.

[Mar15]
Michael P. Marder. *Condensed Matter Physics*. 2nd ed. Wiley, Jan. 2015. ISBN: 9780470617984.

[MB02]
M. Moskalets and M. Büttiker. "Floquet scattering theory of quantum pumps". In: *Phys. Rev. B* 66.20 (Nov. 2002)
DOI: 10.1103/physrevb.66.205320.

[MB07]
J. E. Moore and L. Balents. "Topological invariants of time-reversal-invariant band structures". In: *Phys. Rev. B* 75.12 (Mar. 2007)
DOI: 10.1103/physrevb.75.121306.

[MCAG16]
Fahad Mahmood, Ching-Kit Chan, Zhanybek Alpichshev, Dillon Gardner, Young

Lee, Patrick A. Lee, and Nuh Gedik. “Selective scattering between Floquet–Bloch and Volkov states in a topological insulator”. In: *Nat Phys* (Jan. 2016)
DOI: 10.1038/nphys3609.

[Mer79]
N. D. Mermin. “The topological theory of defects in ordered media”. In: *Reviews of Modern Physics* 51.3 (July 1979), pp. 591–648
DOI: 10.1103/revmodphys.51.591.

[MGFV16]
Sunil Mittal, Sriram Ganeshan, Jingyun Fan, Abolhassan Vaezi, and Mohammad Hafezi. “Measurement of topological invariants in a 2D photonic system”. In: *Nature Photonics* 10.3 (Feb. 2016), pp. 180–183
DOI: 10.1038/nphoton.2016.10.

[Mor13]
René Moreau. *L’air et l’eau : Alizés, cyclones, Gulf Stream, tsunamis et tant d’autres curiosités naturelles*. EDP SCIENCES, Mar. 2013. ISBN: 9782759808281.

[MRW08]
Joel E. Moore, Ying Ran, and Xiao-Gang Wen. “Topological Surface States in Three-Dimensional Magnetic Insulators”. In: *Phys. Rev. Lett.* 101.18 (Oct. 2008)
DOI: 10.1103/physrevlett.101.186805.

[MS74]
John Milnor and James D. Stasheff. *Characteristic Classes. (AM-76)*. First Edition. Princeton University Press, Aug. 1974. ISBN: 9780691081229.

[MSKB13]
Hirokazu Miyake, Georgios A. Siviloglou, Colin J. Kennedy, William Cody Burton, and Wolfgang Ketterle. “Realizing the Harper Hamiltonian with Laser-Assisted Tunneling in Optical Lattices”. In: *Phys. Rev. Lett.* 111.18 (Oct. 2013)
DOI: 10.1103/physrevlett.111.185302.

[MSVA16]
Sebabrata Mukherjee, Alexander Spracklen, Manuel Valiente, Erika Andersson, Patrik Öhberg, Nathan Goldman, and Robert R. Thomson. *Experimental observation of anomalous topological edge modes in a slowly-driven photonic lattice*. 2016. arXiv: 1604.05612.

[MT15a]
V. Mathai and G. C. Thiang. “T-duality simplifies bulk-boundary correspondence”. In: *ArXiv e-prints* (May 2015)
arXiv: 1505.05250.

[MT15b]
Varghese Mathai and Guo Chuan Thiang. “T-duality of topological insulators”. In: *Journal of Physics A: Mathematical and Theoretical* 48.42 (Sept. 2015), 42FT02
DOI: 10.1088/1751-8113/48/42/42ft02.

[MV16]
Arvind Murugan and Suriyanarayanan Vaikuntanathan. *Topologically protected modes in non-equilibrium stochastic systems*. 2016. arXiv: 1605.08407.

[MZNS16]
Lukas J. Maczewsky, Julia M. Zeuner, Stefan Nolte, and Alexander Szameit. *Observation of photonic anomalous Floquet Topological Insulators*. 2016. arXiv: 1605.03877.

[NG15a]
Giuseppe De Nittis and Kiyonori Gomi. *Chiral vector bundles: A geometric model for class AIII topological quantum systems*. 2015. arXiv: 1504.04863.

[NG15b]
Giuseppe De Nittis and Kiyonori Gomi. "Classification of "Quaternionic" Bloch-Bundles: Topological Quantum Systems of Type AII". In: *Commun. Math. Phys.* 339.1 (June 2015), pp. 1–55
DOI: 10.1007/s00220-015-2390-0. arXiv: 1404.5804.

[NG16]
Giuseppe De Nittis and Kiyonori Gomi. "Topological nature of Fu-Kane-Mele invariants". In: (Mar. 2016)
arXiv: 1603.09421.

[NKRV15]
Lisa M. Nash, Dustin Kleckner, Alismari Read, Vincenzo Vitelli, Ari M. Turner, and William T. M. Irvine. "Topological mechanics of gyroscopic metamaterials". In: *Proceedings of the National Academy of Sciences* 112.47 (Nov. 2015), pp. 14495–14500
DOI: 10.1073/pnas.1507413112.

[NL14]
Giuseppe De Nittis and Max Lein. "On the role of symmetries in the theory of photonic crystals". In: *Annals of Physics* 350 (Nov. 2014), pp. 568–587
DOI: 10.1016/j.aop.2014.07.032.

[NN81a]
H.B. Nielsen and M. Ninomiya. "A no-go theorem for regularizing chiral fermions". In: *Physics Letters B* 105.2-3 (Oct. 1981), pp. 219–223
DOI: 10.1016/0370-2693(81)91026-1.

[NN81b]
H.B. Nielsen and M. Ninomiya. "Absence of neutrinos on a lattice: (I). Proof by homotopy theory". In: *Nuclear Physics B* 185.1 (July 1981), pp. 20–40
DOI: 10.1016/0550-3213(81)90361-8.

[NN81c]
H.B. Nielsen and M. Ninomiya. "Absence of neutrinos on a lattice: (II). Intuitive

topological proof". In: *Nuclear Physics B* 193.1 (Dec. 1981), pp. 173–194
DOI: 10.1016/0550-3213(81)90524-1.

[NN83]
H.B. Nielsen and Masao Ninomiya. "The Adler-Bell-Jackiw anomaly and Weyl fermions in a crystal". In: *Physics Letters B* 130.6 (Nov. 1983), pp. 389–396
DOI: 10.1016/0370-2693(83)91529-0.

[NOSS15]
Jia Ningyuan, Clai Owens, Ariel Sommer, David Schuster, and Jonathan Simon. "Time- and Site-Resolved Dynamics in a Topological Circuit". In: *Phys. Rev. X* 5.2 (June 2015)
DOI: 10.1103/physrevx.5.021031.

[Nov07]
Kostya Novoselov. "Graphene: Mind the gap". In: *Nature Materials* 6.10 (Oct. 2007), pp. 720–721
DOI: 10.1038/nmat2006.

[NR15]
Frederik Nathan and Mark S Rudner. "Topological singularities and the general classification of Floquet–Bloch systems". In: *New Journal of Physics* 17.12 (Dec. 2015), p. 125014
DOI: 10.1088/1367-2630/17/12/125014.

[NS14]
Giuseppe De Nittis and Hermann Schulz-Baldes. "Spectral Flows Associated to Flux Tubes". In: *Ann. Henri Poincaré* 17.1 (Dec. 2014), pp. 1–35
DOI: 10.1007/s00023-014-0394-5.

[NS83]
A. J. Niemi and G. W. Semenoff. "Axial-Anomaly-Induced Fermion Fractionization and Effective Gauge-Theory Actions in Odd-Dimensional Space-Times". In: *Phys. Rev. Lett.* 51.23 (Dec. 1983), pp. 2077–2080
DOI: 10.1103/physrevlett.51.2077.

[NSSF08]
Chetan Nayak, Steven H. Simon, Ady Stern, Michael Freedman, and Sankar Das Sarma. "Non-Abelian anyons and topological quantum computation". In: *Reviews of Modern Physics* 80.3 (Sept. 2008), pp. 1083–1159
DOI: 10.1103/revmodphys.80.1083.

[OA09]
Takashi Oka and Hideo Aoki. "Photovoltaic Hall effect in graphene". In: *Phys. Rev. B* 79.8 (Feb. 2009)
DOI: 10.1103/physrevb.79.081406.

[PA04]
Gloria Platero and Ramón Aguado. "Photon-assisted transport in semiconductor

nanostructures". In: *Physics Reports* 395.1-2 (May 2004), pp. 1–157
DOI: 10.1016/j.physrep.2004.01.004.

[Pan56]
S. Pancharatnam. "Generalized theory of interference, and its applications". In: *Proceedings of the Indian Academy of Sciences - Section A* 44.5 (Nov. 1956), pp. 247–262
DOI: 10.1007/BF03046050.

[Par08]
Efton Park. *Complex Topological K-Theory (Cambridge Studies in Advanced Mathematics)*. 1st ed. Cambridge University Press, Mar. 2008. ISBN: 9780521856348.

[Pas16]
R. Paschotta. *Article on 'optical intensity' in the Encyclopedia of Laser Physics and Technology, Online Version*. 2016. URL: https://www.rp-photonics.com/optical_intensity.html (visited on 03/07/2016).

[PBSM15]
V. Peano, C. Brendel, M. Schmidt, and F. Marquardt. "Topological Phases of Sound and Light". In: *Phys. Rev. X* 5.3 (July 2015)
DOI: 10.1103/physrevx.5.031011.

[PC14]
Michael Pasek and Y. D. Chong. "Network models of photonic Floquet topological insulators". In: *Phys. Rev. B* 89.7 (Feb. 2014)
DOI: 10.1103/physrevb.89.075113.

[PCV15]
Jayson Paulose, Bryan Gin-ge Chen, and Vincenzo Vitelli. "Topological modes bound to dislocations in mechanical metamaterials". In: *Nat Phys* 11.2 (Jan. 2015), pp. 153–156
DOI: 10.1038/nphys3185.

[PKG90]
R.E. Prange, K. Klitzing, and S.M. Girvin. *The Quantum Hall Effect*. 2nd ed. Graduate Texts in Contemporary Physics. Springer New York, 1990. ISBN: 9781468404999.

[PM93]
Uri Peskin and Nimrod Moiseyev. "The solution of the time-dependent Schrödinger equation by the (t, t') method: Theory, computational algorithm and applications". In: *The Journal of Chemical Physics* 99.6 (1993), p. 4590
DOI: 10.1063/1.466058.

[PMV16]
Andrew C. Potter, Takahiro Morimoto, and Ashvin Vishwanath. *Topological classification of interacting 1D Floquet phases*. 2016. arXiv: 1602.05194.

[Pot07]
Noëlle Pottier. *Physique statistique hors d'équilibre: Processus irréversibles linéaires*. EDP Sciences, June 2007. ISBN: 9782868839343.

[PP09]
Emil Prodan and Camelia Prodan. "Topological Phonon Modes and Their Role in Dynamic Instability of Microtubules". In: *Phys. Rev. Lett.* 103.24 (Dec. 2009) DOI: 10.1103/physrevlett.103.248101.

[PRSH13]
Yonatan Plotnik, Mikael C. Rechtsman, Daohong Song, Matthias Heinrich, Julia M. Zeuner, Stefan Nolte, Yaakov Lumer, Natalia Malkova, Jingjun Xu, Alexander Szameit, Zhigang Chen, and Mordechai Segev. "Observation of unconventional edge states in 'photonic graphene'". In: *Nature Materials* 13.1 (Nov. 2013), pp. 57–62 DOI: 10.1038/nmat3783.

[PS16]
Emil Prodan and Hermann Schulz-Baldes. *Bulk and Boundary Invariants for Complex Topological Insulators*. Springer International Publishing, 2016 DOI: 10.1007/978-3-319-29351-6.

[PST03]
Gianluca Panati, Herbert Spohn, and Stefan Teufel. "Effective Dynamics for Bloch Electrons: Peierls Substitution and Beyond". In: *Communications in Mathematical Physics* 242.3 (Nov. 2003), pp. 547–578 DOI: 10.1007/s00220-003-0950-1.

[PUBT14]
P. M. Perez-Piskunow, Gonzalo Usaj, C. A. Balseiro, and L. E. F. Foa Torres. "Floquet chiral edge states in graphene". In: *Phys. Rev. B* 89.12 (Mar. 2014) DOI: 10.1103/physrevb.89.121401.

[QGS16]
A Quelle, M O Goerbig, and C Morais Smith. "Bandwidth-resonant Floquet states in honeycomb optical lattices". In: *New Journal of Physics* 18.1 (Jan. 2016), p. 015006 DOI: 10.1088/1367-2630/18/1/015006.

[QHZ08]
Xiao-Liang Qi, Taylor L. Hughes, and Shou-Cheng Zhang. "Topological field theory of time-reversal invariant insulators". In: *Phys. Rev. B* 78.19 (Nov. 2008) DOI: 10.1103/physrevb.78.195424.

[QLZZ09]
X.-L. Qi, R. Li, J. Zang, and S.-C. Zhang. "Inducing a Magnetic Monopole with Topological Surface States". In: *Science* 323.5918 (Feb. 2009), pp. 1184–1187 DOI: 10.1126/science.1167747.

[QZ11]
Xiao-Liang Qi and Shou-Cheng Zhang. "Topological insulators and superconduc-

tors". In: *Reviews of Modern Physics* 83.4 (Oct. 2011), pp. 1057–1110
DOI: 10.1103/revmodphys.83.1057.

[RA15]
Tibor Rakovszky and János K. Asbóth. "Localization, delocalization, and topological phase transitions in the one-dimensional split-step quantum walk". In: *Phys. Rev. A* 92.5 (Nov. 2015)
DOI: 10.1103/physreva.92.052311.

[RBBM09]
A. Roth, C. Brune, H. Buhmann, L. W. Molenkamp, J. Maciejko, X.-L. Qi, and S.-C. Zhang. "Nonlocal Transport in the Quantum Spin Hall State". In: *Science* 325.5938 (July 2009), pp. 294–297
DOI: 10.1126/science.1174736.

[Red84a]
A. N. Redlich. "Gauge Noninvariance and Parity Nonconservation of Three-Dimensional Fermions". In: *Phys. Rev. Lett.* 52.1 (Jan. 1984), pp. 18–21
DOI: 10.1103/physrevlett.52.18.

[Red84b]
A. N. Redlich. "Parity violation and gauge noninvariance of the effective gauge field action in three dimensions". In: *Physical Review D* 29.10 (May 1984), pp. 2366–2374
DOI: 10.1103/physrevd.29.2366.

[RGF03]
Saar Rahav, Ido Gilary, and Shmuel Fishman. "Effective Hamiltonians for periodically driven systems". In: *Phys. Rev. A* 68.1 (July 2003)
DOI: 10.1103/physreva.68.013820.

[RH08]
S. Raghu and F. D. M. Haldane. "Analogs of quantum-Hall-effect edge states in photonic crystals". In: *Phys. Rev. A* 78.3 (Sept. 2008)
DOI: 10.1103/physreva.78.033834.

[RH16]
Rahul Roy and Fenner Harper. "Periodic Table for Floquet Topological Insulators". In: *ArXiv e-prints* (Mar. 2016)
arXiv: 1603.06944.

[RL09]
M. S. Rudner and L. S. Levitov. "Topological Transition in a Non-Hermitian Quantum Walk". In: *Phys. Rev. Lett.* 102.6 (Feb. 2009)
DOI: 10.1103/physrevlett.102.065703.

[RLBL13]
Mark S. Rudner, Netanel H. Lindner, Erez Berg, and Michael Levin. "Anomalous Edge States and the Bulk-Edge Correspondence for Periodically Driven Two-

Dimensional Systems". In: *Phys. Rev. X* 3.3 (July 2013)
DOI: 10.1103/physrevx.3.031005.

[RLL00]
M. Rørdam, F. Larsen, and N. Laustsen. *An Introduction to K-Theory for C*-Algebras*. An Introduction to K-theory for C*-algebras. Cambridge University Press, 2000. ISBN: 9780521789448.

[RLL16]
Mark S. Rudner, Michael Levin, and Leonid S. Levitov. *Survival, decay, and topological protection in non-Hermitian quantum transport*. 2016. arXiv: 1605.07652.

[RML12]
Shinsei Ryu, Joel E. Moore, and Andreas W. W. Ludwig. "Electromagnetic and gravitational responses and anomalies in topological insulators and superconductors". In: *Phys. Rev. B* 85.4 (Jan. 2012)
DOI: 10.1103/physrevb.85.045104.

[Roy09]
Rahul Roy. "Topological phases and the quantum spin Hall effect in three dimensions". In: *Phys. Rev. B* 79.19 (May 2009)
DOI: 10.1103/physrevb.79.195322.

[RQHZ08]
S. Raghu, Xiao-Liang Qi, C. Honerkamp, and Shou-Cheng Zhang. "Topological Mott Insulators". In: *Phys. Rev. Lett.* 100.15 (Apr. 2008)
DOI: 10.1103/physrevlett.100.156401.

[RS78]
Michael Reed and Barry Simon. *Methods of Modern Mathematical Physics IV: Analysis of Operators*. 4th ed. Academic Press, May 1978. ISBN: 9780125850049.

[RSFL10]
Shinsei Ryu, Andreas P Schnyder, Akira Furusaki, and Andreas W W Ludwig. "Topological insulators and superconductors: tenfold way and dimensional hierarchy". In: *New Journal of Physics* 12.6 (June 2010), p. 065010
DOI: 10.1088/1367-2630/12/6/065010.

[RZPL13]
Mikael C. Rechtsman, Julia M. Zeuner, Yonatan Plotnik, Yaakov Lumer, Daniel Podolsky, Felix Dreisow, Stefan Nolte, Mordechai Segev, and Alexander Szameit. "Photonic Floquet topological insulators". In: *Nature* 496.7444 (Apr. 2013), pp. 196–200
DOI: 10.1038/nature12066.

[Sak93]
J. J. Sakurai. *Modern Quantum Mechanics*. 1st ed. Addison Wesley, Sept. 1993. ISBN: 9780201539295.

[Sam73]
Hideo Sambe. “Steady States and Quasienergies of a Quantum-Mechanical System in an Oscillating Field”. In: *Phys. Rev. A* 7.6 (June 1973), pp. 2203–2213
DOI: 10.1103/physreva.7.2203.

[SBLR15]
Karthik I. Seetharam, Charles-Edouard Bardyn, Netanel H. Lindner, Mark S. Rudner, and Gil Refael. “Controlled Population of Floquet-Bloch States via Coupling to Bose and Fermi Baths”. In: *Phys. Rev. X* 5.4 (Dec. 2015)
DOI: 10.1103/physrevx.5.041050.

[Sem84]
Gordon W. Semenoff. “Condensed-Matter Simulation of a Three-Dimensional Anomaly”. In: *Phys. Rev. Lett.* 53 (26 Dec. 1984), pp. 2449–2452
DOI: 10.1103/PhysRevLett.53.2449.

[SH15]
R. Süsstrunk and S. D. Huber. “Observation of phononic helical edge states in a mechanical topological insulator”. In: *Science* 349.6243 (July 2015), pp. 47–50
DOI: 10.1126/science.aab0239.

[SH16]
R. Süsstrunk and S. D. Huber. “Classification of topological phonons in linear mechanical metamaterials”. In: (Apr. 2016)
arXiv: 1604.01033.

[Shi65]
Jon H. Shirley. “Solution of the Schrödinger Equation with a Hamiltonian Periodic in Time”. In: *Phys. Rev.* 138.4B (May 1965), B979–B987
DOI: 10.1103/physrev.138.b979.

[Sim83]
Barry Simon. “Holonomy, the Quantum Adiabatic Theorem, and Berry’s Phase”. In: *Phys. Rev. Lett.* 51.24 (Dec. 1983), pp. 2167–2170
DOI: 10.1103/physrevlett.51.2167.

[SKR99]
Hermann Schulz-Baldes, Johannes Kellendonk, and Thomas Richter. “Simultaneous quantization of edge and bulk Hall conductivity”. In: *J. Phys. A: Math. Gen.* 33.2 (Dec. 1999), pp. L27–L32
DOI: 10.1088/0305-4470/33/2/102.

[SKRG08]
G. Stefanucci, S. Kurth, A. Rubio, and E. K. U. Gross. “Time-dependent approach to electron pumping in open quantum systems”. In: *Phys. Rev. B* 77.7 (Feb. 2008)
DOI: 10.1103/physrevb.77.075339.

[SLIY15]
Scott A. Skirlo, Ling Lu, Yuichi Igarashi, Qinghui Yan, John Joannopoulos, and

Marin Soljačić. “Experimental Observation of Large Chern Numbers in Photonic Crystals”. In: *Phys. Rev. Lett.* 115.25 (Dec. 2015)
DOI: 10.1103/physrevlett.115.253901.

[SN10]
Alexander Szameit and Stefan Nolte. “Discrete optics in femtosecond-laser-written photonic structures”. In: *J. Phys. B: At. Mol. Opt. Phys.* 43.16 (July 2010), p. 163001
DOI: 10.1088/0953-4075/43/16/163001.

[SOPC16]
Grazia Salerno, Tomoki Ozawa, Hannah M. Price, and Iacopo Carusotto. “Floquet topological system based on frequency-modulated classical coupled harmonic oscillators”. In: *Phys. Rev. B* 93.8 (Feb. 2016)
DOI: 10.1103/physrevb.93.085105.

[Spa94]
Edwin H. Spanier. *Algebraic Topology*. 3rd ed. Springer, Dec. 1994. ISBN: 9780387944265.

[SPFK12]
Doru Sticlet, Frederic Piéchon, Jean-Noël Fuchs, Pavel Kalugin, and Pascal Simon. “Geometrical engineering of a two-band Chern insulator in two dimensions with arbitrary topological index”. In: *Phys. Rev. B* 85.16 (Apr. 2012)
DOI: 10.1103/physrevb.85.165456.

[SRFL08]
Andreas P. Schnyder, Shinsei Ryu, Akira Furusaki, and Andreas W. W. Ludwig. “Classification of topological insulators and superconductors in three spatial dimensions”. In: *Phys. Rev. B* 78.19 (Nov. 2008)
DOI: 10.1103/physrevb.78.195125.

[SRFL09]
Andreas P. Schnyder, Shinsei Ryu, Akira Furusaki, and Andreas W. W. Ludwig. “Classification of Topological Insulators and Superconductors”. In: *AIP Conference Proceedings* 1134.1 (2009), pp. 10–21
DOI: 10.1063/1.3149481.

[SSG15]
K. Shiozaki, M. Sato, and K. Gomi. “Topology of nonsymmorphic crystalline insulators and superconductors”. In: *ArXiv e-prints* (Nov. 2015)
arXiv: 1511.01463.

[SSH79]
W. P. Su, J. R. Schrieffer, and A. J. Heeger. “Solitons in Polyacetylene”. In: *Phys. Rev. Lett.* 42.25 (June 1979), pp. 1698–1701
DOI: 10.1103/physrevlett.42.1698.

[Ste51]
Norman Steenrod. *The Topology of Fibre Bundles. (PMS-14)*. 1999th ed. Princeton University Press, Apr. 1951. ISBN: 9780691005485.

[SV11]
Alexey A. Soluyanov and David Vanderbilt. "Computing topological invariants without inversion symmetry". In: *Phys. Rev. B* 83.23 (June 2011)
DOI: 10.1103/physrevb.83.235401.

[SWSH06]
D. N. Sheng, Z. Y. Weng, L. Sheng, and F. D. M. Haldane. "Quantum Spin-Hall Effect and Topologically Invariant Chern Numbers". In: *Phys. Rev. Lett.* 97.3 (July 2006)
DOI: 10.1103/physrevlett.97.036808.

[TAD14]
B. Tarasinski, J. K. Asbóth, and J. P. Dahlhaus. "Scattering theory of topological phases in discrete-time quantum walks". In: *Phys. Rev. A* 89.4 (Apr. 2014)
DOI: 10.1103/physreva.89.042327.

[Tau15]
Clément Tauber. "Three applications of a geometric approach to conformal field theory". PhD thesis. École normale supérieure de Lyon, Dec. 2015
URL: https://tel.archives-ouvertes.fr/tel-01247290.

[TBRR16]
Paraj Titum, Erez Berg, Mark S. Rudner, Gil Refael, and Netanel H. Lindner. "Anomalous Floquet-Anderson Insulator as a Nonadiabatic Quantized Charge Pump". In: *Phys. Rev. X* 6.2 (May 2016)
DOI: 10.1103/physrevx.6.021013.

[TD15]
Clément Tauber and Pierre Delplace. "Topological edge states in two-gap unitary systems: a transfer matrix approach". In: *New Journal of Physics* 17.11 (Nov. 2015), p. 115008
DOI: 10.1088/1367-2630/17/11/115008.

[TG63]
P. K. Tien and J. P. Gordon. "Multiphoton Process Observed in the Interaction of Microwave Fields with the Tunneling between Superconductor Films". In: *Phys. Rev.* 129.2 (Jan. 1963), pp. 647–651
DOI: 10.1103/physrev.129.647.

[Thi15a]
Guo Chuan Thiang. "On the K-Theoretic Classification of Topological Phases of Matter". In: *Ann. Henri Poincaré* 17.4 (May 2015), pp. 757–794
DOI: 10.1007/s00023-015-0418-9.

[Thi15b]
Guo Chuan Thiang. "Topological phases: Isomorphism, homotopy and K-theory". In: *International Journal of Geometric Methods in Modern Physics* 12.09 (Oct. 2015),

p. 1550098
DOI: 10.1142/s021988781550098x.

[Tho83]
D. J. Thouless. "Quantization of particle transport". In: *Phys. Rev. B* 27.10 (May 1983), pp. 6083–6087
DOI: 10.1103/physrevb.27.6083.

[TKNN82]
D. J. Thouless, M. Kohmoto, M. P. Nightingale, and M. den Nijs. "Quantized Hall Conductance in a Two-Dimensional Periodic Potential". In: *Phys. Rev. Lett.* 49.6 (Aug. 1982), pp. 405–408
DOI: 10.1103/physrevlett.49.405.

[TLRR15]
Paraj Titum, Netanel H. Lindner, Mikael C. Rechtsman, and Gil Refael. "Disorder-Induced Floquet Topological Insulators". In: *Phys. Rev. Lett.* 114.5 (Feb. 2015)
DOI: 10.1103/physrevlett.114.056801.

[TOA09]
Naoto Tsuji, Takashi Oka, and Hideo Aoki. "Nonequilibrium Steady State of Photoexcited Correlated Electrons in the Presence of Dissipation". In: *Phys. Rev. Lett.* 103.4 (July 2009)
DOI: 10.1103/physrevlett.103.047403.

[TPBU14]
L. E. F. Foa Torres, P. M. Perez-Piskunow, C. A. Balseiro, and Gonzalo Usaj. "Multiterminal Conductance of a Floquet Topological Insulator". In: *Phys. Rev. Lett.* 113.26 (Dec. 2014)
DOI: 10.1103/physrevlett.113.266801.

[TWZ13]
Thomas Tradler, Scott O. Wilson, and Mahmoud Zeinalian. "An elementary differential extension of odd K-theory." In: *Journal of K-theory: K-theory and its Applications to Algebra, Geometry, and Topology* 12.02 (Apr. 2013), pp. 331–361
DOI: 10.1017/is013002018jkt218. arXiv: 1211.4477.

[Uni13]
The Univalent Foundations Program. *Homotopy Type Theory: Univalent Foundations of Mathematics*. Institute for Advanced Study, 2013
URL: https://homotopytypetheory.org/book.

[UPTB14]
Gonzalo Usaj, P. M. Perez-Piskunow, L. E. F. Foa Torres, and C. A. Balseiro. "Irradiated graphene as a tunable Floquet topological insulator". In: *Phys. Rev. B* 90.11 (Sept. 2014)
DOI: 10.1103/physrevb.90.115423.

[Ver16]
Alberto D. Verga. *Edge states in a two-dimensional quantum walk with disorder.* 2016. arXiv: 1606.00613.

[Vie09]
David Viennot. "Geometric phases in adiabatic Floquet theory, Abelian gerbes and Cheon's anholonomy". In: *Journal of Physics A: Mathematical and Theoretical* 42.39 (Sept. 2009), p. 395302
DOI: 10.1088/1751-8113/42/39/395302.

[Vol85]
Pankratov O. A. Volkov B. A. "Two-dimensional massless electrons in an inverted contact". In: *Sov. Phys. JETP Letters* 42.4 (Aug. 1985), p. 178
URL: http://www.jetpletters.ac.ru/ps/1420/article_21570.shtml.

[Vol88a]
G. E. Volovik. "An analog of the quantum Hall effect in a superfluid ^{3}He film". In: *Sov. Phys. JETP* 67.9 (Sept. 1988), p. 1804
URL: http://www.jetp.ac.ru/cgi-bin/e/index/e/67/9/p1804?a=list.

[Vol88b]
G. E. Volovik. "Quantized hall effect in superfluid helium-3 film". In: *Physics Letters A* 128.5 (Apr. 1988), pp. 277–279
DOI: 10.1016/0375-9601(88)90373-8.

[VPM16]
Albert Verdeny, Joaquim Puig, and Florian Mintert. *Quasi-periodically driven quantum systems.* 2016. arXiv: 1603.03923.

[VRM14a]
O. Viyuela, A. Rivas, and M. A. Martin-Delgado. "Two-Dimensional Density-Matrix Topological Fermionic Phases: Topological Uhlmann Numbers". In: *Phys. Rev. Lett.* 113.7 (Aug. 2014)
DOI: 10.1103/physrevlett.113.076408.

[VRM14b]
O. Viyuela, A. Rivas, and M. A. Martin-Delgado. "Uhlmann Phase as a Topological Measure for One-Dimensional Fermion Systems". In: *Phys. Rev. Lett.* 112.13 (Apr. 2014)
DOI: 10.1103/physrevlett.112.130401.

[VRM15]
O Viyuela, A Rivas, and M A Martin-Delgado. "Symmetry-protected topological phases at finite temperature". In: *2D Mater.* 2.3 (June 2015), p. 034006
DOI: 10.1088/2053-1583/2/3/034006.

[VUG14]
V. Vitelli, N. Upadhyaya, and B. Gin-ge Chen. "Topological mechanisms as classical

spinor fields". In: *ArXiv e-prints* (July 2014)
arXiv: 1407.2890.

[Wal47]
P. R. Wallace. "The Band Theory of Graphite". In: *Phys. Rev.* 71.9 (May 1947), pp. 622–634
DOI: 10.1103/physrev.71.622.

[WCJS09]
Zheng Wang, Yidong Chong, J. D. Joannopoulos, and Marin Soljačić. "Observation of unidirectional backscattering-immune topological electromagnetic states". In: *Nature* 461.7265 (Oct. 2009), pp. 772–775
DOI: 10.1038/nature08293.

[WDMS15]
S.-T. Wang, D.-L. Deng, Joel E. Moore, Kai Sun, and L.-M. Duan. "Quantized electromagnetic response of three-dimensional chiral topological insulators". In: *Phys. Rev. B* 91.3 (Jan. 2015)
DOI: 10.1103/physrevb.91.035108.

[Wen90]
Xiao-Gang Wen. "Topological orders in rigid states". In: *Int. J. Mod. Phys. B* 04.02 (Feb. 1990), pp. 239–271
DOI: 10.1142/s0217979290000139.

[Wit16]
Edward Witten. "Fermion path integrals and topological phases". In: *Reviews of Modern Physics* 88.3 (July 2016)
DOI: 10.1103/revmodphys.88.035001.

[WK11]
J. Weis and K. von Klitzing. "Metrology and microscopic picture of the integer quantum Hall effect". In: *Philosophical Transactions of the Royal Society A: Mathematical, Physical and Engineering Sciences* 369.1953 (Sept. 2011), pp. 3954–3974
DOI: 10.1098/rsta.2011.0198.

[WL16]
Qing-Ze Wang and Chao-Xing Liu. "Topological nonsymmorphic crystalline superconductors". In: *Phys. Rev. B* 93.2 (Jan. 2016)
DOI: 10.1103/physrevb.93.020505.

[WLB15]
Pai Wang, Ling Lu, and Katia Bertoldi. "Topological Phononic Crystals with One-Way Elastic Edge Waves". In: *Phys. Rev. Lett.* 115.10 (Sept. 2015)
DOI: 10.1103/physrevlett.115.104302.

[WLZ15]
Yao-Ting Wang, Pi-Gang Luan, and Shuang Zhang. "Coriolis force induced topological order for classical mechanical vibrations". In: *New Journal of Physics* 17.7 (July

2015), p. 073031
DOI: 10.1088/1367-2630/17/7/073031.

[WSJG13]
Y. H. Wang, H. Steinberg, P. Jarillo-Herrero, and N. Gedik. "Observation of Floquet-Bloch States on the Surface of a Topological Insulator". In: *Science* 342.6157 (Oct. 2013), pp. 453–457
DOI: 10.1126/science.1239834.

[WW13]
Juven Wang and Xiao-Gang Wen. *A Lattice Non-Perturbative Hamiltonian Construction of 1+1D Anomaly-Free Chiral Fermions and Bosons - on the equivalence of the anomaly matching conditions and the boundary fully gapping rules*. 2013. arXiv: 1307.7480.

[WW16a]
Joseph Weston and Xavier Waintal. "Linear-scaling source-sink algorithm for simulating time-resolved quantum transport and superconductivity". In: *Phys. Rev. B* 93.13 (Apr. 2016)
DOI: 10.1103/physrevb.93.134506.

[WW16b]
Joseph Weston and Xavier Waintal. *Towards Realistic Time-Resolved Simulations of Quantum Devices*. 2016. arXiv: 1604.01198.

[WY75]
Tai Tsun Wu and Chen Ning Yang. "Concept of nonintegrable phase factors and global formulation of gauge fields". In: *Physical Review D* 12.12 (Dec. 1975), pp. 3845–3857
DOI: 10.1103/physrevd.12.3845.

[XMYS15]
Meng Xiao, Guancong Ma, Zhiyu Yang, Ping Sheng, Z. Q. Zhang, and C. T. Chan. "Geometric phase and band inversion in periodic acoustic systems". In: *Nat Phys* 11.3 (Feb. 2015), pp. 240–244
DOI: 10.1038/nphys3228.

[XQHW09]
Y. Xia, D. Qian, D. Hsieh, L. Wray, A. Pal, H. Lin, A. Bansil, D. Grauer, Y. S. Hor, R. J. Cava, and M. Z. Hasan. "Observation of a large-gap topological-insulator class with a single Dirac cone on the surface". In: *Nat Phys* 5.6 (May 2009), pp. 398–402
DOI: 10.1038/nphys1274.

[XYFW10]
Di Xiao, Yugui Yao, Wanxiang Feng, Jun Wen, Wenguang Zhu, Xing-Qiu Chen, G. Malcolm Stocks, and Zhenyu Zhang. "Half-Heusler Compounds as a New Class of Three-Dimensional Topological Insulators". In: *Phys. Rev. Lett.* 105.9 (Aug. 2010)
DOI: 10.1103/physrevlett.105.096404.

[Yab87]
Eli Yablonovitch. “Inhibited Spontaneous Emission in Solid-State Physics and Electronics”. In: *Phys. Rev. Lett.* 58.20 (May 1987), pp. 2059–2062
DOI: 10.1103/physrevlett.58.2059.

[YGSL15]
Zhaoju Yang, Fei Gao, Xihang Shi, Xiao Lin, Zhen Gao, Yidong Chong, and Baile Zhang. “Topological Acoustics”. In: *Phys. Rev. Lett.* 114.11 (Mar. 2015)
DOI: 10.1103/physrevlett.114.114301.

[YMN07]
Wang Yao, A. H. MacDonald, and Qian Niu. “Optical Control of Topological Quantum Transport in Semiconductors”. In: *Phys. Rev. Lett.* 99.4 (July 2007)
DOI: 10.1103/physrevlett.99.047401.

[YY06]
Amnon Yariv and Pochi Yeh. *Photonics: Optical Electronics in Modern Communications (The Oxford Series in Electrical and Computer Engineering)*. 6th ed. Oxford University Press, Jan. 2006. ISBN: 9780195179460.

[Zak68]
J. Zak. “Dynamics of Electrons in Solids in External Fields”. In: *Phys. Rev.* 168.3 (Apr. 1968), pp. 686–695
DOI: 10.1103/physrev.168.686.

[Zak89]
J. Zak. “Berry’s phase for energy bands in solids”. In: *Phys. Rev. Lett.* 62.23 (June 1989), pp. 2747–2750
DOI: 10.1103/physrevlett.62.2747.

[Zel67]
Iakov Borissovitch Zel’dovich. “The Quasienergy of a Quantum-mechanical System Subjected to a Periodic Action”. In: *Sov. Phys. JETP* 24.5 (May 1967), p. 1006
URL: http://www.jetp.ac.ru/cgi-bin/e/index/e/24/5/p1006?a=list.

[ZGFF07]
S. Y. Zhou, G.-H. Gweon, A. V. Fedorov, P. N. First, W. A. de Heer, D.-H. Lee, F. Guinea, A. H. Castro Neto, and A. Lanzara. “Substrate-induced bandgap opening in epitaxial graphene”. In: *Nature Materials* 6.10 (Sept. 2007), pp. 770–775
DOI: 10.1038/nmat2003.

[Zim79]
J. M. Ziman. *Principles of the Theory of Solids*. 2nd ed. Cambridge University Press, Nov. 1979. ISBN: 9780521297332.

[Zir10]
Martin R. Zirnbauer. “Oxford Handbook of Random Matrix Theory”. In: ed. by Gernot Akemann, Jinho Baik, and Philippe Di Francesco. Oxford: Oxford University

Press, 2010. Chap. Symmetry Classes
arXiv: 1001.0722.

[ZRPL15]
Julia M. Zeuner, Mikael C. Rechtsman, Yonatan Plotnik, Yaakov Lumer, Stefan Nolte, Mark S. Rudner, Mordechai Segev, and Alexander Szameit. "Observation of a Topological Transition in the Bulk of a Non-Hermitian System". In: *Phys. Rev. Lett.* 115.4 (July 2015)
DOI: 10.1103/physrevlett.115.040402.

Table of Contents